Flow-Enhanced Detection of Biological Pathogens using Piezoelectric Microcantilever Arrays

A Thesis

Submitted to the Faculty

of

Drexel University

by

John-Paul McGovern

in partial fulfillment of the

requirements for the degree

of

Doctor of Philosophy

September 2008

Dedication

This dissertation, and, indeed, all of my endeavors for the rest of my days on this earth, are and will be dedicated, with love, to the soul and memory of my Mother,

Christine C. McGovern

(March 6, 1952 - July 8, 2008)

Without her selfless love, guidance and prayers, not only would the achievement of this degree be impossible, but similarly, all previous and subsequent personal accomplishments. My hope and goal for myself is that I am able to adequately honor her memory from this point forward in all of my choices, acts and deeds.

Acknowledgments

I would like to thank my advisors, Drs. Wei-Heng and Wan Y. Shih for five years of guidance, advice and discussion. I cannot quantify the knowledge and experience I have gained. I'd also like to thank my examination committee members for their time and input, as well as members of the Ceramics Sensors and Processing Group; specifically, Joe Capobianco, Dr. Huidong Li, Hakki Yegingil, Bernie Zhu, Jose Bermudez and Dr. Qiang Zhao for their friendship, moral and technical support over the past five years.

I'd also like to humbly express my complete gratitude to my Mother, Father and Sister for their love, caring, encouragement and support (spiritual, emotional, intellectual, physical, and yes, financial) during my entire life.

Also, I'd like to acknowledge my soon-to-be wife, Marisa, for her love, friendship, devotion, encouragement, support, laughter, proofreading, collating, and her sticking with a poor grad student like me for the past years.

Finally, I'd like to acknowledge the most important help I've received through my entire life – that from our Lord.

Surely, I have omitted some names that should be mentioned and for this I apologize. If you are one of these individuals, I highly encourage you to inform me of this mistake.

Table of Contents

List of Tables

List of Figures

Abstract

Flow-Enhanced Detection of Biological Pathogens using Piezoelectric Microcantilever Arrays
John-Paul McGovern
Wan Y. Shih, Ph.D. and Wei-Heng Shih, Ph.D.

The piezoelectric microcantilever sensor (PEMS) is an all-electrical resonant oscillator biosensor system capable of in-situ and label-free detection. Immobilized receptors on the sensor surface enable real-time electrical measurement of the resonance frequency shift due to the binding of target antigens to the surface. With silane-based insulation methods and bifunctional linker antibody immobilization schemes, it is well-suited for applications in sensitive, specific detection of biological pathogens with limits of detection on the order of relevant lethal infectious dosage concentrations. Initial PEMS implementation demonstrated biodetection of *Bacillus anthracis* (BA) spores at a concentration of just 36 total spores in 0.8 mL of liquid. While these results are exciting, concerns that cross reactivity between the antibody and closely related species of the target pathogens cast doubts on the usefulness of any antibody-based assays in terms of the specificity of pathogen detection.

The goal of this dissertation is to develop the PEMS biosensor as a viable antibody-based assay for in-situ, label-free, water-borne pathogen detection with better limits of detection than current antibody-based methods as well as high sensitivity and specificity, by exploring array PEMS detection and specificity augmentation by engineered fluidics. In the detection of BA spores, controlled fluid flow experiments in an 8 mm wide flow channel at flow rates ranging from 0 to 14 mL/min led to a determination of optimal flow rates for discriminatory detection of BA spores among

close cousins: *B. cereus* (BC), *B. thuringiensis* (BT) and *B. subtilis* (BS). It is shown that the detection signal of all such spores first increased with an increasing flow rate. The detection signals of BC, BT and BS eventually diminished with the increasing flow rate as the force of the flow overcame the interaction force of the BC, BT, and BS spores with the sensor surface. The optimal flow rate was determined to be 14 mL/min at which detection signals of BC, BT, and BS all fell to within the noise level of the sensor, while the detection BA was still nearly optimal. As a result, it was deduced that the interaction forces of BC, BT, and BS were about 100 pN.

Design and implementation of array sensing systems enabled real-time simultaneous redundant biosensor assays and concurrent background determination by a reference PEMS. By virtue of this advance in PEMS technology, successful real-time detection of just 10 BA spores/mL was achieved and step-wise, single *Cryptosporidium parvum* (CP) oocyst detection at 0.1 oocysts/mL was accomplished with resonance frequency step-wise shifts of 290 Hz and signal to noise ratios greater than 5 per instance of oocyst detection. It was found that, in a 19 mm wide flow channel, optimal single oocyst detection efficiency was achieved at 2 mL/min, while optimal discrimination of CP from *C. muris* (CM) oocysts was achieved at 5 mL/min. At this flow rate the detection signal of CP was close to optimal with a signal to noise ratio of 5 per step-wise shift and that of CM was close to the noise level. The interaction forces of CP and CM oocysts with the biosensor surfaces were deduced to be 110 and 70 pN, respectively.

CHAPTER 1:INTRODUCTION, MOTIVATION AND GOALS

1.1 Biodetection and Biosensors

Biodetection can be defined as the determination of the presence of biological entities in a given sample or space. Clearly, however, the types of biological entities as well as the methods for determining their presence can be, and indeed are, widely varied. In this dissertation, the types of biodetection to be reviewed, studied and developed are chiefly concerned with determining the presence of biological pathogens, *i.e.* biological entities that are harmful to humans. The presence of these pathogens will be determined by means of readily quantifiable properties. Such properties may be the directly observed presence of the actual biological pathogen by means of microscope visualization, or may be some property associated with the presence of said antigens such as mass, extracted DNA or colonies grown from the original antigens of interest.

Whatever the antigen or biological entity of interest, a biosensor is defined as any device that uses specific biochemical reactions, immunosystems, etc, to detect chemical or biological compounds by electrical, thermal or optical signals.[1] The most sophisticated biosensor could be a push-button device engineered to give a basic 'yes' or 'no' answer concerning the presence of the biological entity of interest, or it could be something considerably more complicated requiring extensive user intervention and interpretation of results. These two far ends of the biosensor continuum, if you will, each have their own advantages as well as their own shortcomings.

The literature review presented in Chapters 2 and 3 will aim to elucidate the function, strong-points and shortcomings of some of the more prominent biosensors in

use, both commercially and in academic research. The Piezoelectric Microcantilever Sensor (PEMS) and PEMS array system will then be presented in Chapter 3 and demonstrated as a versatile and robust biosensor capable of real-time, *in situ*, direct, label-free, continuous, specific and selective detection of biological pathogens.

1.2 Biological Pathogens

A pathogen is any agent of disease, while a biological pathogen is an agent of disease of biological origin, such as an infectious organism like a virus or bacteria.[2] As recently as December 2006, fifteen fast food restaurants in the Philadelphia area were temporarily closed as a result of the biological pathogen *Escherichia coli* (commonly known as *E. coli*) found in food products.[3] Then, even more recent still, Princeton University's Dining Services was confirmed to have exposed more than a dozen students to *Salmonella* in May of 2008. [4] Cases such as these are certainly abnormal occurrences, but they do serve to illustrate that the safety we take for granted in modern food-processing methods is not foolproof. Thus, the need is identified for technologies and biosensor systems to be used for monitoring the possible presence of biological pathens in foodstuffs.

Some of the more prominent biological pathogens in today's public awareness are bacteria such as *E. coli*, *Bacillus anthracis* (commonly known as anthrax) and *Salmonella typhimurium* and *Salmonella Enteritidis* (usually collectively referred to as 'Salmonella'). *Bacillus anthracis* is listed in the United States Centers for Disease Control and Prevention's (CDC) Category A of Bioterrorism Agents and Diseases, while *Salmonella* and *E. coli* are listed in Category B.[5] Catergory A bioterrorism agents are regarded by the CDC as 'easily disseminated,' 'result in high mortality rates,' 'might cause public

panic and social disruption,' and require special action for public health preparedness.' Category B bioterrorism agents are deemed 'moderately easy to disseminate,' 'result moderate morbidity rates and low mortality rates,' and 'require enhanced disease surveillance.' Regardless of their location on the CDC's list of bioterrorism agents, control and prevention of exposure to these pathogens by the public citizenry is of utmost importance to most governments around the globe. In order to achieve such prevention of exposure and to minimize the number of individuals exposed once a bioterrorism attack has occurred, highly specific, rapid, real-time detection of such biological pathogens among the plethora of non-pathogenic organisms and particulate matter in air and water supplies is a critical need.

In this dissertation, the piezoelectric microcantilever sensor (PEMS) will be utilized as this tool for improved detection of biological pathogens. The two main model pathogen systems to be studied are *Bacillus anthracis* and *Cryptosporidium*.

1.2.1 *BACILLUS ANTHRACIS*

Bacillus anthracis (BA) is a Gram positive, spore-forming bacterium that has gained widespread notoriety – or perhaps, infamy – as a result of its recent use in bioterrorism attacks on United States soil. As mentioned above, it is listed in the CDC's Category A list of bioterrorism agents, partly due to its ability to remain viable in harsh environments for long periods of time. For instance, BA spores can remain viable in air or soil environments for over a decade, but then begin to germinate in just minutes upon attaining proper growth conditions in a host organism.[6]

Despite BA's ability to quickly begin reproduction upon finding a suitable host, such as the human respiratory system, current CDC-approved positive identification

techniques involve collecting spores from air or water by filtration, culturing the spores on growth media for a period of several hours to more than a day, then staining for the vegetative cells and visually identifying them under a microscope.[7] Clearly, this is a time-consuming endeavor, while in the event of a bioterrorist attack, early detection of BA is of the utmost importance when human or animal exposure is a possibility.

To reduce the time required for positive detection of BA spores in a public airspace, a host of academic and industrial research has been focused on more innovative detection methodologies. These methods range from tried and true biological procedures such as ELISA (Enzyme Linked ImmunoSorbent Assay) and PCR (Polymerase Chain Reaction) to technologies with more 'real-time' detection capabilities such as Fiber Optic, Surface Plasmon Resonance (SPR), Quartz Crystal Microbalance (QCM), and Microsphere Immunoassay sensors.[7-13] However, the best real-time performance of BA spore detection by these systems is 10^3 spores/mL.

The lethal dose of BA spores for 50% of the population (LD_{50}) is estimated to be exactly on this order of magnitude, at four to eight thousand spores.[14] However, it has been further shown that the LD_5 of BA spores could be as low as 14 spores and the LD_1 as low as just one spore.[14] With such high mortality rates (1 in 100) for such low numbers of spores, clearly biodetection of BA spores in much lower concentrations that currently available in real-time is desirable.

1.2.2 *CRYPTOSPORIDIUM*

Unlike BA, *Cryptosporidium* is a biological pathogen that has not had widespread, high-profile press coverage or notoriety. First identified as a parasite in mice in 1907,[15,16] *Cryptosporidium* is now recognized as a potential cause of widespread

severe gastroenteritis and infirmity in humans,[17] as well as death in individuals with deficient immune systems,[18] such as arises from AIDS and chemotherapies. At least 16 species of *Cryptosporidium* have been identified.[19] Some species survive only in particular host animals, while other species are more zoonotic in nature.[20] *C. meleagridis, C. felis, C. canis* and *C. suis* have all been identified as having caused at least one case of cryptosporidiosis in humans. However, it is the highly zoonotic species *C. parvum* and the human-specific *C. hominis* that are responsible for the vast majority of parasitic infections of the human gastrointestinal tract.[21]

The life cycle of *Cryptosporidium* is complicated in nature and is comprised of many different stages of growth and reproduction. Figure 1-1(a)[22], below, illustrates this lifecycle. The thick-walled, hardy oocyst is the stage that, when shed from a host animal by excretion, is capable of surviving in the soil, surface- and drinking-waters.[20] This oocyst contains four sporozoites, which are the infective agent upon re-entry to a sufficient host. Once an oocyst is consumed by a host animal from its environment, and once this oocyst reaches the intestinal tract of the host animal, the oocyst opens and the sporozoites infect the intestinal tissue of the host. This process of the oocyst opening and releasing the sporozoites is captured by Scanning Electron Microscopy (SEM) in Figure 1-1(b)[22]. Once implanted in the intestinal walls of the host, these sporozoites then mature into trophozoites which then progress into later stages of growth and reproduction to ultimately produce new oocysts which are again shed from the host into the environment.[20]

(a)

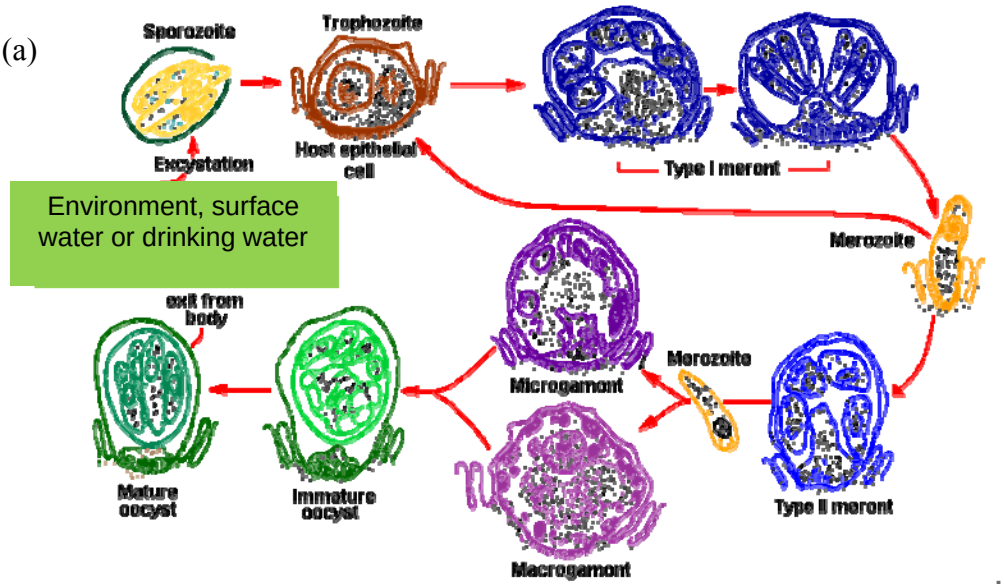

(b)

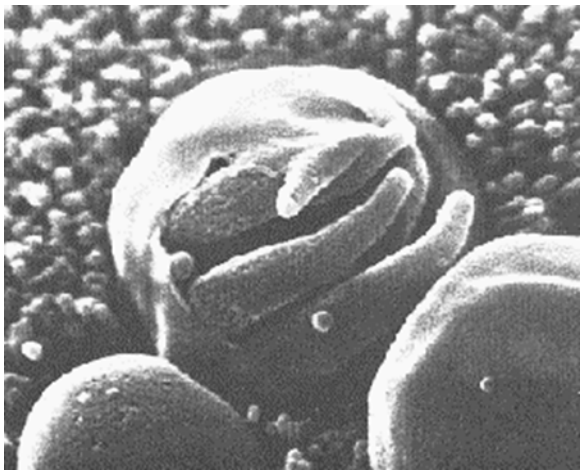

Figure 1-1: (a) Life cyle of Cryptosporidium (b) Scanning Electron Micrograph of sporozoites exiting an oocyst

It has long been known that C*ryptosporidium* oocysts are prevalent in surface waters such as streams, ponds, lakes and rivers. Once shed from its host, *Cryptosporidium* oocysts can remain viable and infectious for several months in both salt and fresh water.[23] However, as illustrated by the massive 1994 cryptosporidosis outbreak in Milwaukee, Wisconsin, which infected over 400,000 people[17], utility water treatment plants can be largely ineffective in the removal of *Cryptosporidium* oocysts from the

drinking water supply even in developed countries.[24] This ineffectiveness stems from the resistance of the oocyst to the antiseptic chlorination procedures[25] currently practiced in water treatment plants. Progressive methods such as micro-pore filtering and UV irradiation have been demonstrated to be effective in oocyst removal from surface water[20,24], but the issues of verifying remediation effectiveness and oocyst enumeration influent and effluent to such systems still remain.

Since *Cryptosporidium* can only effectively reproduce in the intestines of its host organism, it is impossible to use traditional cell culture colony growth techniques[26] to verify the presence, or lack thereof, of oocysts in a water sample.[20] At present, the only United States Environmental Protection Agency (EPA)-approved method for detection and enumeration of *Cryptosporidium* oocysts in drinking water involves filtration of large volumes of water, followed by collection of the filtrate, re-suspension and incubation with anti-*Cryptosporidium*-functionalized magnetic beads.[27] Once conjugated to an oocyst, a magnet is used to separate the complex from the suspension and the resulting analyte is then fluorescently stained for analysis and enumeration by optical microscopy. This method is provided by the US EPA and is widely regarded by practitioners as time- and expertise-intensive, and as such, is highly expensive.

For years, the search has been on for improved methods of C*ryptosporidium* enumeration and detection that allow for more cost-effective, reliable, real-time, *in situ* monitoring of drinking water. With the inability to culture *Cryptosporidium*, PCR is a natural choice for sensitive detection as just a single oocyst is needed for nucleic acid amplification and organism identification. Indeed, PCR has been used successfully in laboratory settings,[28,29] but due to its high cost per assay, its use has remained limited in

deployed applications, *i.e*. at the point of detection in utility water treatment plants.[30] Also, the issue of detection time is only partially improved as filtration of the analyte water is still required prior to PCR amplification.[31]

In hopes of improving this detection time and possibly providing point of detection functionality, surface plasmon resonance (SPR) has been used for label-free, real-time detection of *Cryptosporidium parvum*. However, while providing vastly improved detection times (on the order of tens of minutes), the lowest detection level achieved without the use of signal amplification by labeling was just 1 x 10^6 oocysts.[31]

With the "detection limit of biosensor [sic] for detecting pathogens" the "most important criteria in monitoring the quality of water in environmental fields,"[31] and with the US EPA requiring further remediation of drinking water containing more than just one *Cryptosporidium* oocyst per 13 liters[32], clearly, the need is identified for real-time, label-free, highly sensitivity methodologies capable of lower detection limits than cited above. The PEMS has been amply demonstrated for label-free, real-time, *in situ*, continuous monitoring in biodetection applications,[33-35] and recent advances in array multiplexing[36] make it ideal for the detection of waterborne pathogens such as *Cryptosporidium*.

1.3 Piezoelectric Microcantilever Sensors (PEMS) for Real-Time Biodetection

The PEMS is a cantilever resonator system that is electrically induced to vibrate by means of its piezoelectric layer. As dictated by the geometry of the particular PEMS used, the cantilever will resonate at given frequencies. This resonance can then be detected electrically, through the same electrical connections used for actuation, and shifts in resonance can be attributed to the detection of biological pathogen by specific

receptors immobilized on the sensor's surface. As theoretical and experimental analysis in this dissertation will show, miniaturization of PEMS biosensors necessarily leads to more sensitive detection, and can enable extremely low limits of detection.

Biological pathogen detection sensitivity levels for PEMS have been demonstrated on the order of 10^{-13} g/Hz,[35] or in terms of the limit of detection of biological cells: as few as just tens of *Bacillus anthracis* spores have been detected[34,35]. Effective, sensitive detection of *E. coli*,[33] *Salmonella*[37-39] and cancer marker proteins[40] has also been demonstrated. This high level of sensitivity has been attained by combining advanced sensor insulation[33,40] and analyte fluid flow engineering[34] with the theoretically predicted exponential increases in sensitivity associated with PEMS miniaturization.[41] Motivated by the need for an effective and reliable, *in situ*, real-time biosensor, this dissertation will focus upon two areas associated with increasing the detection abilities of the PEMS system.

First, the precise control of the fluid flow conditions of the biological pathogen analyte suspension will be engineered to increase the limits of detection and degree of selectivity from other biological species with which pathogens are detected. Additionally, the implementation of several, identical PEMS cantilevers for simultaneous, redundant monitoring and background determination of the analyte suspension will be engineered to increase the confidence with which the presence of pathogens can be detected in very low concentrations.

1.3.1 Fluid Flow Engineering

The necessity for fluid flow engineering arises from two basic physical phenomena: particle interaction length scales and particle settling. First, since specific

detection of biological antigens will be accomplished by functionalizing the surface of our PEMS with antibody molecules, the pathogen of interest must come sufficiently close to the sensor surface for interactions between the two to take place. This distance is known to be on the order of 10 μm to 10 nm, with the longer range interactions resulting from electrostatic forces and the middle and shorter range interactions resulting from van der Waals forces and molecular steric repulsions.[42-44]

Consider the example of biological pathogens one micron in diameter (about the size of a BA spore) in aqueous suspension at a concentration of 1000 per mL in a total volume of one milliliter. Assuming that these pathogens are well-dispersed and not agglomerated, each pathogen is, on average, 1 mm away from the immediately surrounding pathogens. Likewise, while a very few pathogens might be less than a millimeter away from a biosensor inserted into this suspension, the vast majority of pathogens will be much greater than 1 mm away from the sensor surface. Regardless of the specificity of the antibody on the surface of the biosensor, diffusion will not be sufficient to deliver more than just a very few pathogens to this surface for detection. If the limit of detection of this biosensor is on the order of 100 pathogens, accurate detection may never take place.

To make matters even worse, under the effect of gravity, cellular biological pathogens will also experience significant Stokes Settling over the period of time that detection is to occur. *Cryptosporidium* oocysts have been shown to settle at a rate of 2 μm per minute or 0.1 mm per hour,[45] while anthrax spores settle at about half this rate.[46] When even the most rapid biosensor detection times of fifteen minutes to an hour are

considered, settling at such rates will thus, appreciably decrease the concentration of pathogens in the vicinity of biosensor.

Considering these basic needs to improve upon diffusion-based delivery of analyte to the sensor surface and also counteract the effects of settling on local analyte concentrations near the sensor surface, a significant part of this dissertation will focus upon the implementation of analyte fluid flow. In addition to this goal of improving the practical limit of detection the PEMS to be used, more advanced fluidics engineering methods will be explored and employed with the goal of enhancing the natural specificity of the antibody-functionalized PEMS biosensor.

1.3.2 ARRAY PEMS

As mentioned above, a second focus in the development of a more effective PEMS-based biosensor system will be the implementation of a true, real-time array of piezoelectric cantilevers. A PEMS array system will allow for multiple simultaneous biodetection assays, as well as concurrent monitoring of a reference PEMS to continuously check for non-specific or 'false positive' detection. Such real-time redundancy of detection will allow for more confidence in the correctness of the PEMS biosensor results, or in statistical terms, better detection 'sensitivity' and 'specificity,'[47] without the need to wait for additional, subsequent confirmatory assays.

While array biodetection is quite obviously a desirable goal to pursue, many obstacles to effective implementation exist. Thus, at present, no other biodetection platform has effectively implemented real-time array detection while also attaining the low limits of detection required for biological pathogen monitoring. Such obstacles to array implementation include: fabrication of identical biosensors to facilitate direct

comparison of results; true multiplexed monitoring of the biosensor array such that real-time biodetection is not compromised; and effective miniaturization of the fabricated array so as to not require additional volumes of analyte and/or to sacrifice the inherent sensitivity of the biosensor.

These, and other hindrances to array development, were overcome during the engineering and design iterations that have lead to the successful PEMS array detection demonstrations to be detailed herein. Figure 1-2, below, is an optical micrograph of a nine-cantilever PEMS array that was developed and fabricated by this author along this path to effective PEMS array implementation for biodetection.

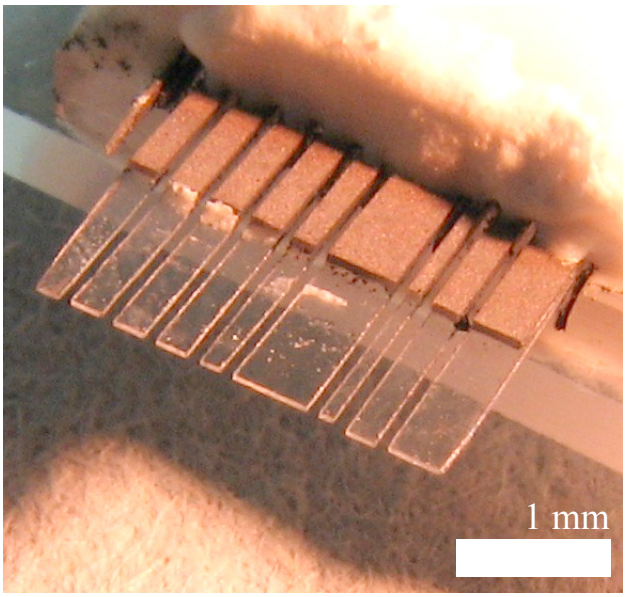

Figure 1-2: A nine-cantilever PEMS array

1.4 Chapter Summary

A multitude of biosensors and biodetection methodologies are available to academic researchers as well as corporations and governments requiring real-time biological

pathogen monitoring of airspaces, water sources and foodstuffs. As will be reviewed and elucidated in coming chapters, however, no single embodiment of these methodologies is capable of the low limits of detection required by real-world applications while also possessing rapid, real-time means of detection. As such, this dissertation will present the PEMS biosensor as a solution to this technological shortcoming.

Building upon previous theoretical work and initial demonstrations of single instances of this robust biosensor for pathogen detection, a main goal of this work will be to attain the low limit of detection levels for BA and *Cryptosporidium* required for useful real-world applications. These limits of detection are on the order of one to ten spores for BA[14] and on the order of less than one *Cryptosporidium* oocyst per mL of water.[32] Ancillary, but also interrelated goals in this work will involve the use of engineered analyte fluid flow and the development and implementation of real-time PEMS biosensor arrays to improve upon the statistical sensitivity and specificity with which these low limits of detection are achieved.

CHAPTER 2: LITERATURE REVIEW

2.1 Categories of Biosensors and Biodetection

The methodologies of biodetection and the biosensors used to perform such biodetection can vary greatly from one to another. In surveying the entire field of biodetection and biosensors it is useful to make a distinction between sensors and methodologies that require hands-on laboratory procedures as opposed to sensors that are more automated and rapid in nature. For simplicity, biodetection methodologies requiring trained laboratory technicians to perform analysis steps and interpret results will be referred to 'Laboratory Techniques,' while biodetection systems that are automated and rapid will be referred to as 'Real-time Biosensors.' Certainly, the distinction being made here begins to blur where certain laboratory techniques become more advanced and automated while perhaps some real-time techniques remain in such an early stage of development that they require extensive preparation and interpretation of results much like a laboratory technique might. Nonetheless, the reader will hopefully agree with the utility of this distinction.

2.2 Laboratory Biodetection Techniques

The laboratory techniques for biodetection to be discussed here include methods that share the common need for some sort of filtration or pre-concentration step prior to the actual detection or identification of the biological species of interest.

2.2.1 Filtration and Colony Growth

Perhaps the most basic form of biological pathogen detection is the method of filtration, followed by colony growth on an appropriate growth medium.[48,49] In such a

procedure, the particular space to be monitored is first filtered to capture any particulate matter than may be present. The 'space to be monitored' could be a sample of drinking or river water for example, or could be the airspace of a public transportation center. Typically, this filtration will be performed for a sufficiently long period of time to ensure capture of the analyte of interest if it were present. Additionally, the filter used must be of an appropriate pore size to allow unwanted smaller particles to pass through while successfully entraining the analyte of interest.[50]

While in some cases, this filtration could conceivably be performed in a few minutes, generally, hours or even days are required to ensure that a complete representative sample of the space being monitored is taken. Following this filtration step, transportation to the laboratory for analysis of the filtrate is required. Once arrived at the laboratory, the filter is first eluted. If there is an appropriate solvent for the filter itself that is known to not damage the analyte of interest, the analyte may be eluted in this manner. Otherwise, a suitable suspension medium for the analyte is passed through the filter in the reverse direction as was used for the original filtration step. The elution is then captured and typically re-concentrated by means of centrifugation. The product of this re-concentration is then spread, or 'plated' on a laboratory dish coated with appropriate growth medium for the pathogen of interest.

After allowing the potential pathogens on these plates to grow for a sufficient amount of time, a trained laboratory technician can then visually identify the presence or absence of the pathogen of interest. The length of time needed for sufficient growth and multiplication of the bacterial pathogen can range from hours to days and is dependent upon the particular pathogen in question.[48,51] Complications and shortcomings of this

process arise when identification of a specific species is necessary if the presence of other closely-related species is possible. In such situations a sophisticated and specific growth medium must be identified and additional steps after the growth of the colony may be required. Such is the case in the identification of BA by colony growth techniques.[52] Figure 2-1, below is an image published by the CDC[53] to aid in the identification of BA by means of colony growth.

Figure 2-1: Cultured *Bacillus anthracis* colonies

While filtration and colony growth techniques are obviously quite labor and time-intensive, they do possess the advantage of possible single-cell sensitivity for identification of bacterial pathogens. As long as just one pathogen is captured by the initial filtration, eluted and applied to a growth plate, a colony can form and be identified. Thus this methodology is highly sensitive, though not real-time and also not quantitative.

2.2.2 ENZYME-LINKED IMMUNOSORBENT ASSAY (ELISA)

ELISA is a common laboratory technique used to identify the presence of just about any antigen for which an antibody, antibody fragment[54] or synthetic receptor[54] can be found or produced. An antibody is a protein that is produced as a recognition protein generated by animals to just about any foreign substance that might enter the body.[55] Antibodies, or more precisely, immunoglobulins are classified into several different isotypes based on their structure and function. The most commonly studied type of immunoglobulin is Immunoglobulin G, or IgG. Figure 2-2(a) is a schematic representation of an IgG molecule[56] while Figure 2-2(b) is a model a crystallized IgG molecule[57] where the blue regions in (a) and top left and right in (b) represent the binding domains of the protein. In the schematic representation, we see that each IgG protein contains two antigen binding sites and these sites reside in the variable region of the protein. The constant region of the IgG molecule is just that – it remains constant among IgG antibodies from a particular species while their binding sites can vary widely. An antibody fragment is a synthetic receptor produced by mimicking and synthetically reconstructing just the binding site of an antibody. Clearly, these synthetic receptors, called antibody fragments or single chain variable fragments (scFv) are much smaller in size than the entire IgG molecule. Typical IgG molecules are approximately 150 kDa (or 150,000 atomic mass units), while scFv molecules can be just tens of kDa in size.

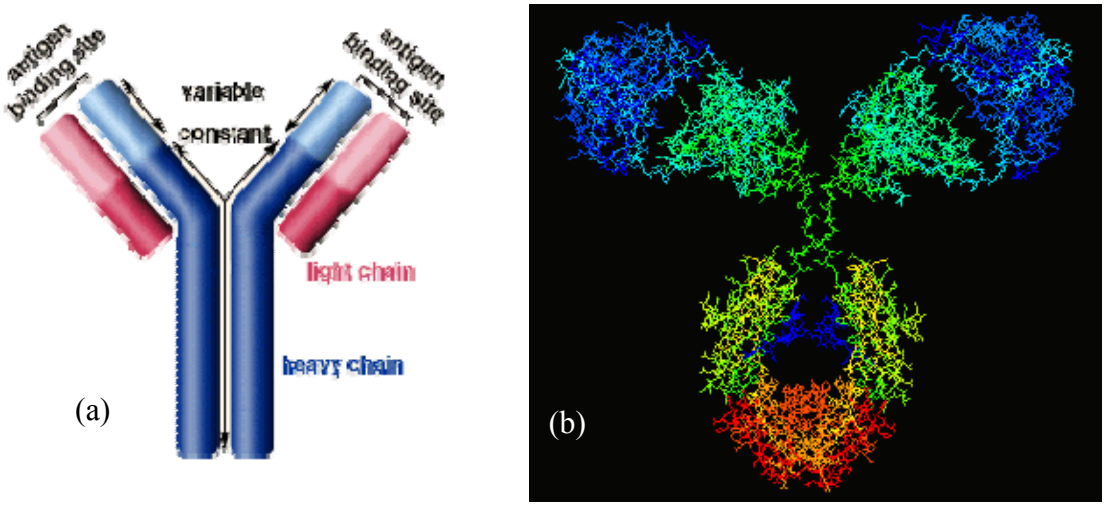

Figure 2-2: (a) Schematic representation of an IgG molecule. (b) a stick-model simulated rendering of an IgG molecule.

In addition to IgG antibodies, there are IgA, IgD, IgE, and IgM isotopes of immunoglobulin. Types IgD and IgE are largely similar to IgG in structure, but differ in where they are produced in the body and what role they serve in the overall immune response. IgA, however, is a dimer structure of IgG connected at the base of the heavy chains, *i.e.* it is symmetric about this connection and contains a total of four functional antigen binding sites. IgM molecules are pentamers of the standard Y structure of IgG, IgD and IgE. The five units of this pentamer are again, joined at the base of the heavy chains, leaving all ten binding sites available for antigen recognition. This pentamer structure also means that IgM molecules are five times (~800 kDa) more massive than IgG.

The basic principle of ELISA is that the presence of an antigen can be determined by allowing the conjugation of a labeled antibody (or synthetic receptor, *etc*) to the antigen. This receptor must be labeled so that its presence after washing can be

determined by some measurable quantity, typically optical, *i.e.* fluorescence, color change, *etc*. Also, concurrent control experiments are important in ELISA since quantification of such optical properties and subsequent back-calculation to quantities of antigen present in unknown samples are inherently difficult. At best, ELISA is referred to as 'semi-quantitative.'[34]

Several different ELISA methods exist and each possess their own advantages and disadvantages. The most basic ELISA method is sometimes referred to as 'indirect' ELISA. In this assay, the final analysis involves the determination of the presence or absence of a labeled antibody specific only for the heavy chain region of the antibody to the pathogen of interest.[55] First, in this method, the unknown sample is diluted from its stock solution into several different dilutions. Typically, dilutions from 1:2 to 1:10 are made and these dilutions are then, in turn diluted again so that including the stock sample, dilutions of 1:1, 1:2, 1:4, through perhaps 1:64 now exist. A few microliters of each of these dilutions are then applied to the wells of a multi-well plate, usually a ninety six well plate, as shown in Figure 2-3. The highest concentration (*i.e.* 1:1 sample) is deposited in row A, as labeled in the figure with decreasing concentrations of sample occupying increasing alphabetic positions in the same column. For consistency and to keep results organized, column one is usually reserved for the control (or known or standard) dilutions, if available, with column two beginning the unknown or experimental samples. Additional dilutions of the first unknown sample would then carry over into column three, or additional unknown experimental dilutions would be added to subsequent columns.

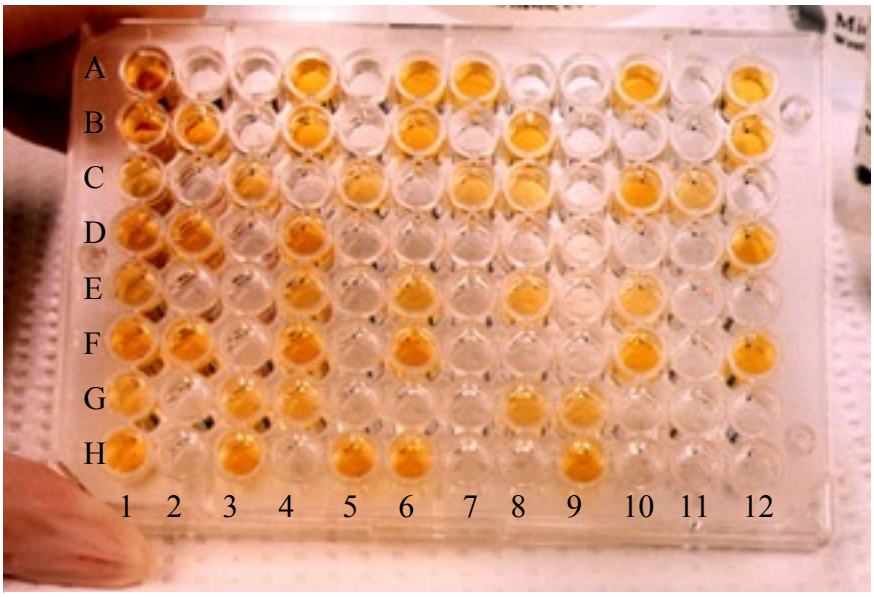

Figure 2-3: Ninety-six well ELISA plate

Once all desired known and experimental dilutions are deposited into wells, the analyte (proteins or cells) in the samples is allowed to 'fix,' or adhere to the surface of the wells. This can be accomplished at room temperature or at a controlled temperature and atmospheric conditions and for a specified amount of time, all according to the protocols of the particular experiment. Following this period of time, a blocking solution is added to all the wells. This is typically Bovine Serum Albumin (BSA) in a high concentration. BSA will adhere to any uncovered areas of the well itself, but not adhere to the biological cells or proteins of interest. The entire 96-well plate is then washed with an appropriate buffer so that any excess BSA is washed away as well as any unbound analyte.

The 'detection antibody' or 'detection receptor' solution is then added to all wells of the washed plate. This antibody is specific for the analyte of interest in the

experimental (as well as control) samples. It could be a monoclonal antibody specific for a particular epitope on the cell or protein of interest; a polycolonal antibody for a variety of protein or cell epitopes; or a synthetic receptor of engineered specificity. Whatever the case, this detection receptor is incubated for a prescribed period of time to allow conjugation with any analyte previously adhered to the well walls. The plate is then washed again and the labeled 'secondary antibody' solution is added to all wells. This labeled secondary antibody is specific for the type of the detection receptor. That is, if the detection receptor was an IgG antibody specific for the analyte of interest, the secondary antibody would recognize and conjugate to the constant region, or heavy chain of the IgG detection antibody. The entire plate is rinsed again, to remove excess secondary antibody and the remaining presence of this secondary antibody is probed by means of testing for its label. Again, this label could fluoresce a particular color when exposed to a particular wavelength of light, it could cause the particular well to change color in ambient light, as in Figure 2-3, or it could perform some other distinguishable function.

Whatever this function, it is then the job of the laboratory technician to determine the presence or absence of the analyte tested for in all experimental wells. Using the example in Figure 2-3, the technician would conclude that the analyte tested for was present in wells B2, D2, C3, etc, while not present in wells A2, E2, A3, etc.

With this method of ELISA being the most basic, newer methodologies continue to be developed to improve the performance and reliability of the test. Two additional types of ELISA to be discussed here are the 'Sandwich ELISA' and the 'Competitive ELISA.' The sandwich ELISA is quite similar to indirect ELISA except that an

additional antibody is used. This additional antibody, called the 'capture antibody' is adsorbed to the wells of the ELISA plate before all other steps. Then, BSA is used to block any regions of the plate that may remain uncovered by this capture antibody. The plate is then rinsed, then the same steps as in the indirect ELISA method are performed. In this way, the unknown samples added to the well after the capture antibody and BSA blocking are effectively filtered for the analyte of interest in that any cell or protein that is not conjugated to the capture antibody is washed away upon rinsing.[55,58]

The 'Competitive ELISA' method is a bit more distinct from the indirect and sandwich methods. In this method, control amounts of the antigen of interest are added to the wells of the ELISA plate and then blocked and rinsed. Then, separately, unlabeled primary antibody for the antigen of interest is incubated in a tube with the dilutions of the unknown samples. These antibody/antigen samples are then added to the antigen coated wells of the ELISA plate. The plate is then washed and the secondary antibody is added and the plate is examined by the technician.

This incubation of the primary antibody with the unknown samples allows the antibody in solution to conjugate to the antigen in solution. Then, when this solution of [possibly] antigen-antibody conjugates, free antigen and free antibody are added to the wells of the plate, only free antibody can bind to the antigen already deposited in the wells. Thus after rinsing and addition of secondary antibody, the wells with the highest fluorescence (or color change, etc.) will be from the incubated unknown samples that contained the lowest amount of antigen. The wells with the lowest fluorescence will correspond to the incubated unknown samples that contained the highest amount of unknown sample.[55,58]

Whatever the method of ELISA used, the test outcome of wells B2, D2, C3, etc, and wells A2, E2, A3, etc., in Figure 2-3 are quite clear cut. However, wells such as C8 and C11 are less so. There is some color in these wells, but exactly how does this compare to the other wells, or the standards in column one? To answer this question, automated plate readers have been developed to help quantify the amount of color, or fluorescence present in each well as compared to the standards.[59] However, quantification of the amount of analyte present can only be applicable to the particular plate being studied at the time. Claims to comparisons of ELISA experiments performed previous or subsequent to a particular experiment can only be qualitative in nature since the amounts of reagents added to and rinsed from the wells in each step cannot be precisely know from experiment to experiment. Hence, the term 'semi-quantitative' is used when referring to ELISA, and it is inherently difficult to define limits of detection or cells/mL sensitivity values for these related techniques. However, detection levels as low as 10^3 bacterial cells/mL have been reported recently in literature[60,61].

2.2.3 POLYMERASE CHAIN REACTION (PCR)

PCR is a DNA amplification method that allows specific identification of biological antigens in a sample down to the level of just a single antigen. However, the drawback is that the method is not real-time and is usually performed in a laboratory by trained personal.

PCR was first conceived in 1971,[62] first proven in practice in 1983[63] and perfected for extensive use in 1988.[64] Since this time, it has seen explosive use and development as a nearly-indispensible laboratory tool for molecular biologists. The basic idea behind PCR is the ability to identify the presence or absence of a biological

organism by amplifying (or copying) a known section of its DNA in such high numbers that simple agarose gel electrophoresis can confirm the presence of the known section of DNA.[65]

This known section of DNA is referred to as the 'ampilcon' or 'amplimer' and special single stranded DNA 'primers' are needed to begin the reaction. These primers are short fragments of single stranded DNA that are complementary to the beginning and end of the amplicon sought after. Amplicon lengths are usually about 10 to 40 kilo-basepairs (kbp) long while the primers used are generally about 20 bp long.[65] First, when PCR is used for biodetection, the sample to be tested must first be acquired. This is usually accomplished by filtering the medium to be monitored, in the same way as precedes biodetection by colony growth (Section 2.2.1, above). However, since, in the case of PCR, as long as the DNA of the sought-after antigen is intact, only one instance of the antigen need be present in the sample.

Once filtration of the monitored medium is carried out, the sample is transported to the PCR lab. Here, the sample is eluted from the filter and any cells contained in the elution are lysed to release their genetic material. To this mixture of genetic material and whatever else may be present in the elution, the sample primers for the amplicon of interest, a DNA polymerase enzyme, as well as an excess of single DNA bases (or deoxynucleotiside triphosphates) are added. This entire reaction mixture is then heated to 94-96^{o}C for a period of up to ten minutes. This heat-and-hold step causes the double-stranded DNA genetic material from the lysed cell in the elution to 'melt' or denature into single strands. The reaction mixture is then allowed to cool to 50-65 ^{o}C, where it is held for about 30 seconds in order to allow the primers to hybridize with the single-

stranded DNA. Due to the inherent specificity of DNA hybridization, effectively designed primers will only hybridize to the amplicon. After this hybridization step, the temperature is raised to 70-80 ^{o}C and held for anywhere from ten minutes to several hours depending on the length of the amplicon. During this step, the DNA polymerase uses the free single DNA bases in solution to complete the formation of the complimentary DNA amplicon begun by the binding of the primers in the previous step. When the polymerase reaches the primer for the end of the amplicon, replication stops and the polymerase releases from the newly formed double-stranded DNA molecule.

Once this step is complete, the temperature is again raised to 94-96^{o}C to being the melt-hybridize-replicate process again. These alternating steps of heating and cooling are repeated as desired. In each cycle, the amount of amplicon in the solution is doubled, such that the concentration of the amplicon grows according to 2^n where n is the number of thermal cycles performed. However, as either enzyme activity begins to wane or the number of free DNA bases available for amplicon extension are consumed, the rate at which new strands are produced begins to diminish. At this point, either new reagents need to be added, or the amplification is complete. In the most basic PCR techniques, once amplification is completed, the resulting mixture of genetic material is analyzed by gel electrophoresis for the presence of the amplicon for which the primers were specific.[65]

To further improve the performance of this most basic form of PCR, nested-PCR was developed.[66] Much as its name suggests, this method involves two separate runs of PCR. In the first run, a set of primers is chosen to amplify a relatively long amplicon, as described above. Once this amplification is carried out, a second set of primers is added

with their target amplicon being a smaller section of DNA within the first amplicon. In this manner, the precision of PCR is improved for samples in which only small amounts of analyte DNA were first available.

Another advance in PCR technology is the development of real-time PCR[67], also known as 'quantitative PCR.' In real-time PCR (not to be confused with RT-PCR, Reverse Transcription PCR, which is used for measuring RNA activity), a molecule that fluoresces only when bound to double-stranded DNA is added to the reaction mixture. With this addition, and by using a photo-detector to compare the amount of fluorescence in the reaction mixture at the end of each hybridization cycle to a control standard, it is possible to determine how the amplification is progressing in real-time.

With this method, the need to perform gel electrophoresis after amplification is abrogated as the increasing fluorescence (or lack thereof) of the reaction mixture after each cycle is directly related to the presence of the original amplicon (or lack thereof). Clearly, this improvement over standard PCR techniques greatly diminishes the length of time needed to complete a biodetection assay. Still, at least four hours are needed for completion of a biodetection assay when using real-time PCR.[20]

Despite the length of time needed for assay, PCR techniques are quite popular for detection of biological pathogens. Since, *Cryptosporidium* oocysts cannot be cultured,[20] PCR is a natural choice for surveillance of its presence in drinking and surface waters. Yet more advanced than the methods described above, PCR-restriction fragment length polymorphism (PCR-RFLP) has been used to specifically identify the species of *Cryptosporidium* found in raw surface water and wastewater.[29] PCR-RFLP focuses on a particular section of rRNA in the trophozoites of the *Cryptosporidium* oocyst that is

common to mutations among different species and species subtypes. By analyzing possible *Cryptosporidium* samples in this way, the exact species can be identified.[20,29] And since, it is a PCR technique being used, only one *Cryptosporidium* oocyst need be present in the sample. Again, though, the time required to perform these experiments is typically about a half of a day and the equipment needed for such advanced techniques is quite pricey, from $5,000 to $100,000.[20]

PCR has also been applied to the detection of BA. Recently, positive detection of just one BA spore has been reported by real-time PCR in a time of approximately 100 minutes, 'excluding time needed for sample processing.'[12] To be sure, this time is impressive for PCR-based biodetection, but the filtration, transportation and laboratory prep work for 'sample processing could take just as long as, if not longer than, the time required for final identification.

2.2.4 EPA METHOD 1623

As discussed in Section 1.2.2, the hardy oocyst stage of the *Cryptosporidium* lifecycle, the stage that is potentially found in waste-, surface- and drinking water, cannot be cultured for growth and colony identification outside of a host organism.[20] Thus, either surface antigen/antibody techniques or PCR methods must be applied. While PCR does provide attractive sensitivity results, its high cost of equipment needed for assay and somewhat lengthy detection times, leave room for improvement. To address the first issue – the high cost of equipment – the EPA has developed and sanctioned a method that can be performed in just about any biological lab.

This method, known as EPA Method 1623 is provided for detection and identification of *Cryptosporidium* and *Giardia* in surface and drinking waters, but can be

used for identification of these species in just about any sample type. This method stems from EPA Method 1622 , which was originally released in 1999, solely for the detection of *Cryptosporidium.* Upon further testing and the addition of methods for *Giardia* detection, Method 1623, for the detection of both *Cryptosporidium* and *Giardia,* was released in 2001 and has been revised several times leading up to its current embodiment, released in December of 2005.[27]

As with all biodetection methods discussed thus far, the first step of EPA Method 1623 is the filtration of the water to be tested. The official protocol specifies the manufacturers and types of filters acceptable for this step and also the amount of water that should be filtered through each type of filter. This amount of water required for filtration is between 10 and 50 liters, depending on the model of filter used. Once filtration is complete, the filter must then be stored on site according to specific protocols, then transported (again, by specific temperature protocols) to the lab for the completion of the test. Once arrived at the lab, the filter is eluted and the particulate matter of the elution is collected and separated by means of centrifugation.

The resulting pellet is then re-suspended in water and immuno-magnetic separation (IMS) beads are used to separate any *Cryptosporidium* oocysts present in the sample from other particles in the elution. These IMS beads are simply tiny magnetic beads that are functionalized with antibody specific to the surface of *Cryptosporidium* oocysts. Once added to the resulting particle re-suspension, these IMS beads are allowed conjugate to a *Cryptosporidium* oocysts in the solution and then a magnet is used to physically pull the conjugated oocysts away from extraneous particulate matter in the sample. Once separated in this way, the IMS beads are released from the oocysts and the

oocysts are identified by direct microscopic observation after staining. The stain used is 4',6-diamidino-2-phenylindole (DAPI) and it imparts a green glow to the oocyst outer coat while also staining the four nuclei of the trophozoites internal to the oocyst a bright blue. Figure 2-4 is an example of a *Cryptosporidium* oocyst after DAPI staining[68].

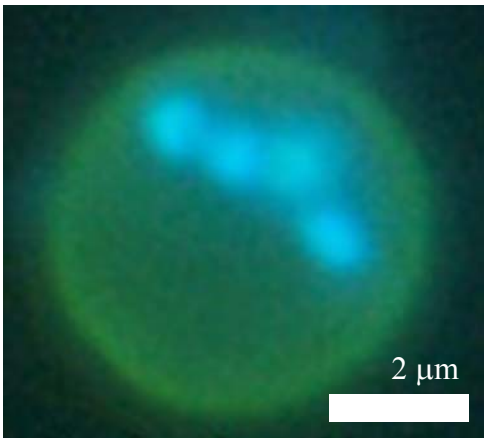

Figure 2-4: DAPI stained *Cryptospordium* oocyst

Finally, for a positive identification of *Cryptosporidium* in a given sample, at least three oocysts must be identified by this DAPI staining, as well as by Differential Interference Contrast (DIC) microscopy for internal and external structure. Figure 2-5 is an example of an oocyst as viewed by DIC microscopy.[68] The oocyst wall and three individual sporozoites are indicated by arrows.

Figure 2-5: *Cryptosporidium* oocyst as imaged by DIC microscopy

The concentration sensitivity of method 1623 has not been discussed in literature or by the EPA, but the time needed for detection of *Cryptosporidium* oocysts is quite lengthy, as deduced by the precise protocols of the method. After completion of filtration and transportation of the filter or filtrate to the laboratory, final results are not obtained until at least eight hours after initiation of testing procedures.

2.3 Real-time Biosensors

The biosensor technologies and methodologies reviewed thus far all required initial filtration of the medium to be monitored before information about the presence or absence of an antigen of interest is obtained. In the following discussion, biosensors that are capable of monitoring the presence of antigen in real-time will be discussed. To be sure, the detection level sensitivities of these methods could be improved by some pre-concentration of sample, such as by filtering, but the important point to remember is that this pre-filtration is not a requirement as it was in the preceding discussion. A real-time biosensor is a sensor that is capable of simply performing passive biodetection without the need for pre-concentration or constant attention of laboratory personal for preparation

of samples and interpretation of results. Once a real-time biosensor is set to monitoring, it will continue to monitor *ad infinitum*, until it is stopped by a user.

2.3.1 QUARTZ CRYSTAL MICROBALANCE (QCM)

At present, the QCM is perhaps the most widely studied and used piezoelectric biosensor. This widespread use and notoriety is due mainly to its simplicity and ease of implementation. Studied extensively by G. Sauerbrey in the 1950's, the theoretical mass detection sensitivity of the QCM is given by his now famous equation[69]:

$$\frac{\Delta f}{\Delta m} = \frac{-2f_0^2}{A\sqrt{\rho_q \mu_q}} \qquad (2.1)$$

where *(Δf/Δm)* is the resonant frequency shift of the QCM per change in mass adhered to the sensor surface, f_0 is the inherent resonant frequency of the QCM, A is the active oscillating area of the QCM (as defined by the electrodes), ρ_q is the density of quartz (2.65 g/cm^3), and μ_q is the Shear modulus of quartz (2.95 x 10^{11} g/cm·s^2). From this equation, calculating the theoretical mass detection sensitivity is trivial, provided the resonant frequency of the oscillator is well known. This can be determined experimentally, simply by performing a frequency scan of an AC voltage on the QCM and finding the minimum(s) in electrical impedance of the system. Or, this resonant frequency can be estimated theoretically, by the equation[70]:

$$f_0 = \frac{1}{2t}\sqrt{\frac{E_q}{\rho_q}} \qquad (2.2)$$

where t is the thickness of the QCM, E_q is the Young's Modulus of quartz (71.7 GPa), and again, ρ_q is the density of quartz.

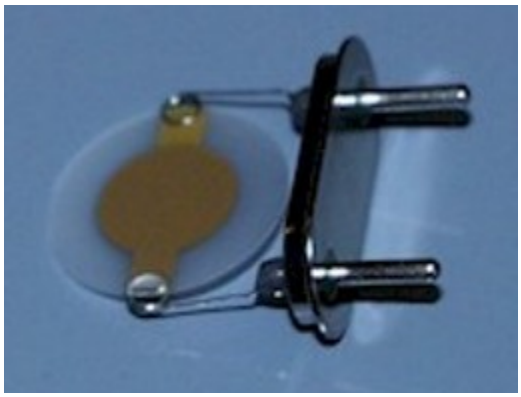

Figure 2-6: A 10 MHz QCM

In practice, the QCM is used for measuring very small masses adhered to one of its electrodes. When this mass adheres, the resonant frequency of vibration of the QCM will decrease (hence, the negative term) according to equation (2.1). This phenomenon in itself, is clearly quite useful when precise determination of the amount of a thin layer deposited on a surface is needed.[33,40] However, when the QCM is functionalized with an antibody (or other receptor) for a specific antigen, it becomes a powerful real-time biodetection tool.[71-73] It has been demonstrated for detection of *E. coli*[71], *Salmonella*[72] and BA[74]. However, commercially available 10 MHz QCMs, as shown in Figure 2-6,[75] are limited in sensitivity to about 10^5 biological cells, as shown both experimentally and theoretically.[71,72,76] As a result, methods of detection amplification have been developed to bring this sensitivity down to levels nearing 100 cells/mL.[71] This amplification, though, removes the real-time nature of the sensor as the amplification material needs to be conjugated to the analyte of interest after its initial immobilization on the sensor surface, much like ELISA. In situations such as this, detection times are lengthened to

over 1.5 hrs when direct detection by QCM (albeit at much higher concentrations) can be accomplished in under thirty minutes.[71]

In an effort to avoid such amplification strategies which require additional steps and lengthen detection time, higher frequency, and thus more sensitive[69] versions of the QCM have been produced. However, these microbalances often require specific atmospheres such as supercritical carbon dioxide, in which the actual detection step must be performed in order to avoid excessive damping that would arise from detection in liquid.[77] Thusly, this method of biodetection is rendered not-real-time once again.

2.3.2 Surface Plasmon Resonance(SPR)

SPR is a relatively new technology that has gained widespread acclaim for its high level of sensitivity and genuine real-time biodetection capabilities. The Biacore system and its many available models is the most well-known commercial embodiment of SPR technology and boasts the ability to perform automated, real-time kinetics analysis of protein-protein interactions on its 'sensorchip' platform.[78] Of course, this comes with a hefty price-tag[79], but it is often deemed indispensible when determination of protein interactions is imperative.

The term surface plasmon resonance refers to a phenomenon that occurs when light is incident upon a thin metallic film, usually gold at a thickness of 40 nm. At a small range of angles, near the critical angle of reflection, the incident light is not reflected by the metallic film, but rather absorbed and transformed into resonant electron oscillations in the film. These electronic oscillations are referred to as a surface plasmon and this plasmon propagates along the surface of the metallic film. Resulting from this surface plasmon is an evanescent field that extends into the space on the side of the

metallic film opposite the incident light. The refractive index of this space directly affects the surface plasmon generation, and thus the angle of incidence at which the plasmon and evanescent field are formed.[80,81]

The utility of this phenomenon is put into practice by coating one side of a triangular prism with the thin metallic layer. One side of this layer is thus available for biological immobilization while the side of the layer contacting the prism is available for illumination by light from inside the prism. The angle of incidence of this light is incremented and recorded and the reflectance intensity is measured by a photodetector to precisely locate the angle at which the surface plasmon is generated and all incident light is absorbed. This angle is recorded for the condition when only the antibody or biological receptor is immobilized on the metallic layer. Then, as antigen is presented to the antibody on the metallic surface and conjugation occurs, the refractive index of the space adjacent to the metallic film changes and thus, the critical angle for the incident light on the metallic layer changes. This change in angle is quantified by the photodetector and the amount of antigen bound to the surface can then be calculated.[79-81] When this process is automated, as in the case of the Biacore system, once the sensor surface is appropriately prepared, binding of the antigen can be monitored in real-time. Figure 2-7 is a schematic representation of a typical SPR biodetection setup, where a flow channel is used to deliver the analyte solution to the detection side of the metallic coating.

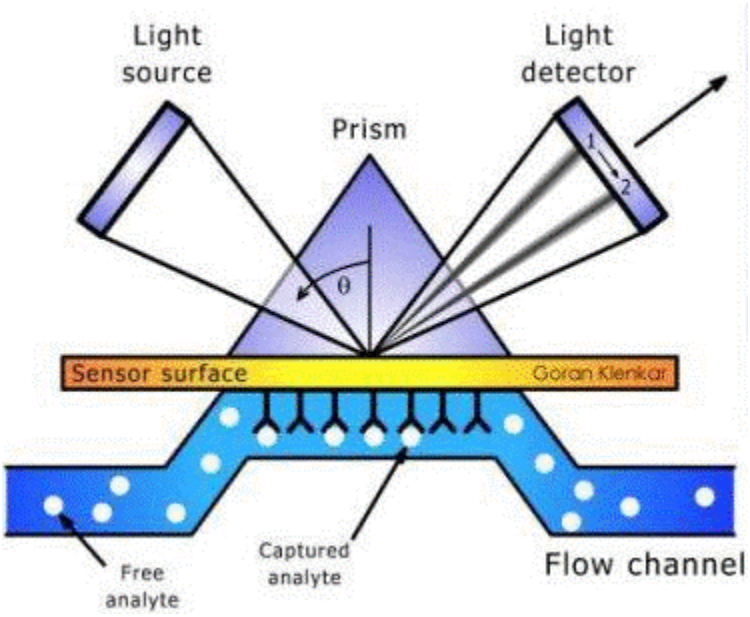

Figure 2-7: Schematic of SPR biodetection

Though SPR is indeed highly sensitive and well-suited for detection and probing of protein interactions at the sensor surface,[82-84] only moderate success has been demonstrated in the detection of biological cells. This arises from the fact that SPR is inherently adept at characterizing small changes in refractive index of the entire space adjacent to its sensor surface. However, when only a few biological cells bind to the sensor surface, the refractive index of this space is changed only in the immediate region of binding while the refractive index of the bulk of the sensor surface remains unchanged. Thus, in studies of SPR's direct, real-time detection capabilities of a variety of biological cells, sensitivities of only 10^6 *Cryptosporidium* oocysts/mL[31] and 10^4 to 10^5 cells/mL of *Salmonella typhimurium,*[85] *E. coli,*[86] *Bacillus* spores[79] and other bacterial pathogens[79,86] have been achieved.

So, SPR, while decidedly real-time in its detection capabilities, has not been demonstrated in published literature for the degree of sensitive detection needed for real-time pathogen monitoring of airspaces and water.

2.3.3 Fiber Optic

Originally developed for the transmission of information by total internal reflection of light over long distances, optical fibers have found utility as biosensors since the early-1990's.[87,88] Fiber optic biosensors are similar to SPR biosensing technologies in that they use the evanescent field generated by the propagation of light along a fiber to sense changes in the refractive index near the surface of the fiber, which are, in turn, used to deduce the presence of biological entities.[87,89,90] However, the cladding on standard communications optical fibers is too thick for sufficient penetration of the evanescent field into the surrounding medium. As such, this cladding layer is typically stripped from the fiber in the area to be used for biodetection and/or a taper is introduced in order to enhance the evanescent field magnitude as well as its penetration into the surrounding medium.[87,90,91]

Once fabricated, as with all truly real-time biosensors, the optical fiber must be coated with a receptor layer for the antigen to be detected. Again, these receptors are typically antibodies or antibody fragments. Immobilization of such receptors is accomplished in a variety of ways, with the most common being covalent immobilization[91] or biotin-avidin conjugation.[92-95]

In the simplest embodiment of a fiber optic biosensor, once functionalized, analyte molecules or cells are presented to the fiber optic sensor surface and allowed to conjugate to the antibody immobilized on the surface. This conjugation gives rise to a

change in refractive index of the surrounding medium of the fiber, which leads to greater absorbance of the evanescent field and a resulting decrease in transmission of the light source along the optical fiber. When the wavelength of the light is properly tuned to maximize this effect, a photo-detector at the far end of the fiber can record this change. This method of fiber optic biodetection directly quantifies the analytes adhering to the surface of the fiber in real-time. However, detection sensitivities using this method are not sufficient for biological pathogen monitoring and enhancements of fiber optic detection methods have been developed and widely studied and improved.[87,90,93,94]

The fluorescent sandwich assay is the most common method for fiber optic biodetection now in use and verily, has demonstrated impressive limits of detection. As early as 1999, this method has demonstrated detection of approximately 30 cells/mL of *E. coli* and *Salmonella typhimurium* in seeded samples of ground beef.[96] More recently, a detection limit of 10^3 *E. coli* cells/mL has been reported,[94] and the detection of *Bacillus anthracis* has been demonstrated at 3×10^5 spores/mL.[13] Even more impressively, the detection of just one *E. coli* cells/mL has been reported, but this occurred only after four hours of 'enrichment,' or cell culture[94].

Clearly, this four hour period of enrichment renders the protocol decidedly not-real-time, but some methods of fiber optic fluorescent sandwich assay do approach real-time status even though they are rendered 'indirect' by the requirement of a second labeled antibody in their detection protocol.

In the fluorescent sandwich assay, much like ELISA sandwich methods, first a capture antibody is immobilized on the fiber surface. Then, the analyte solution is presented to the sensor surface for antibody-antigen conjugation if the antigen is present

in the analyte solution. Finally, a fluorescently-labeled secondary antibody is added and allowed to conjugate to the antigen that has been captured by the antibody on the sensor surface. The utility of performing this detection on the fiber optic platform is that the label on the secondary antibody is specifically chosen to fluoresce upon the exposure to the evanescent field generated by the light passing through the optical fiber. A portion of this fluorescence then enters the optical fiber and can be read by the system's photodetector. By appropriately choosing and tuning the fluorescence molecule and wavelength of light used, the performance of this system is optimized.[87,88,91,94,95,97] Figure 2-8[90] is a schematic representation of the various steps of a fiber optic fluorescent sandwich assay.

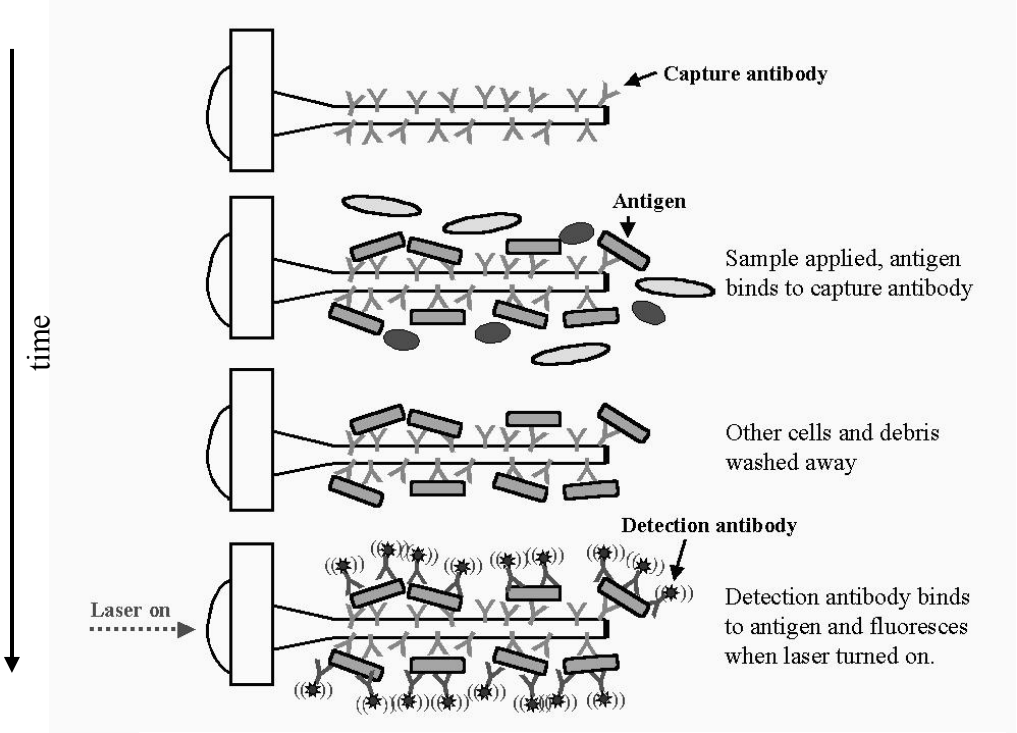

Figure 2-8: Schematic of fiber optic fluorescent sandwich assay

Alternatively, this labeled, secondary antibody can be incubated with the sample solution prior to exposure to the optical fiber.[93] However, in this case, care must be taken to not block the binding sites for the detection antibody on the sensor surface with the secondary antibody. Typically, different monoclonal antibodies are used in this arrangement, or a monoclonal secondary antibody and a polyclonal detection antibody can be used.

Whatever the methodology used for enhancement of the fiber optic biosensor by means of the sandwich assay, this enhancement comes at a price. As alluded to previously, that price is the compromising of the real-time nature of the assay. That is, this requirement of either addition of the labeled secondary antibody, or pre-incubation with this labeled antibody requires time to perform in addition to the actual capture and quantification of the presence of antigen. It should be noted that the time required for this extra step can be as little as five minutes[90], and thus is acceptable in many applications. Additionally, as will be discussed in Section 2.5.3, the addition of this labeled, secondary antibody can be automated, and thus streamlined with the whole of the detection process.

2.3.4 Laser-monitored Microcantilever Biosensors

The last major category of biosensors to be treated herein resides in the broad category of cantilever biosensors. This category of cantilever biosensors can be further sub-classified into families of cantilevers that are monitored for antigen binding by means of a laser focused on the tip of the cantilever, and cantilevers that are electrically self-exciting and self-sensing by means of a piezoelectric element incorporated into the sensor's construction. We will discuss cantilever biosensors that are monitored by laser

in this section and focus in more depth on piezoelectric cantilever biosensors in the aptly named Chapter 3: Piezoelectric Cantilever Biosensors.

Laser monitored cantilever biosensors are generally micro-machined by photolithography techniques from silicon,[98,99] silicon nitride,[100] silicon oxide[101] or other MEMS-friendly materials.[99,101] These cantilevers can be as small as a few nanometers thick, hundreds of nanometers wide and just a few microns long. Similar to the previous real-time biosensors discussed, these cantilever biosensors are first functionalized with an antigen receptor such as an antibody or synthetic receptor. This immobilization can be achieved by direct covalent linkage methods,[100] or biotin-avidin conjugation.[102] Once functionalized, the analyte solution is presented to the cantilever sensor and a determination of binding to the sensor is made.

As the title of this section suggests, a laser is always used to determine this binding, but the manner in which this determination is made can vary quite widely. One method of antigen binding determination involves functionalizing just one side of such a microcantilever sensor. The tip of the cantilever is monitored by laser for displacement of its tip due to bending induced by an increase in surface stress on the functionalized side of the cantilever when antigen conjugates to the immobilized antibody.[100,103] Figure 2-9[100] schematically represents this type of detection. It should be noted that this determination of binding must be performed *in situ* as it is the change in position of the tip with time that is measured by the laser.

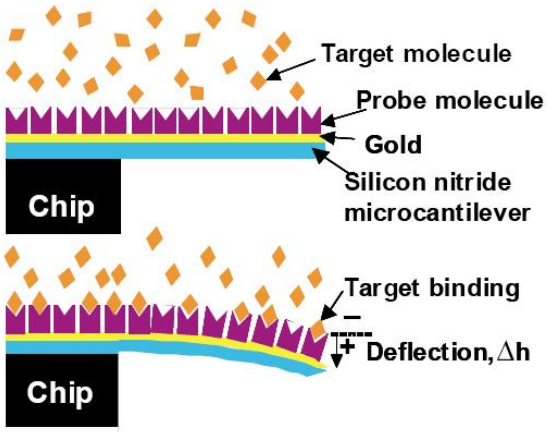

Figure 2-9: Detection schematic of static deflection detection method for laser monitored cantilever

A second method of biodetection using laser monitored microcantilevers is to monitor the resonance frequency of vibration of the cantilever and deduce the amount of antigen that adheres to the surface of the cantilever by recording the change in this resonance frequency. This type of monitoring can once again, be performed real-time, *in situ* as detection progresses,[104] or since it is a change in resonance frequency that is monitored in this case, a baseline frequency can be recorded in air (or vacuum), and then the resonance frequency can be recorded again after detection has taken place.[98,105-107] This before-and-after method of monitoring is decidedly not-real-time, but it can allow for greater sensitivities of detection when the quality factor (Q) of these passively vibrating sensors can approach unity as it does in liquid.[9] The Q value is a quantitative way to evaluate the 'monitorability' of a peak. The sharper a given peak, the higher its Q value will be and the easier such a peak is to monitor. Q is calculated by the equation:

$$Q = \frac{f_r}{w_{(1/2 max)}} \tag{2.3}$$

Where f_r is the monitored resonance frequency peak position of the cantilever and $w_{(½max)}$ is the full width at half of the maximum height of the resonant peak.

Sensitivities with this low Q, before-and-after method of antigen monitoring are impressive, indeed, as single cell detection has been achieved[108]. In this instance of detection, a silicon microcantilever with a Q of 24 in air was used to detect a single *E. coli* cell on its tip. The Q of such a cantilever would be expected to diminish to less than one if dipped in water.[9] However, the real-time potential of these laser monitored microcantilever biosensors is sacrificed by employing this detection method. When real-time detection of cellular biological pathogen is performed using laser monitored microcantilever biosensors, the most sensitive detections reported have been on the order of 10^3 *Bacillus* spores/mL[98,109] in approximately one hour.

2.4 Statistical Methodologies for Biodetection Tests

Previous to this point, the discussion of various biosensor platforms has focused on the methodology of detection, as well as the particular sensor's ability to detect small amounts of the pathogen of interest. Units of cells/mL, spores/mL, and oocyst/mL have been used in discussing the limit of detection or 'sensitivity' of a particular sensor. While benchmarks such as limits of detection have been claimed to be the most important aspect of biosensor development[31] there are additional statistical performance characteristics of such sensors that are equally, if not more, important. These statistical characteristics of a sensor reveal how the sensor performs under a wide range of conditions and circumstances.

To illustrate how such statistical analysis is performed, an example of a hypothetical real-time biosensor will be developed. Consider the situation where a biosensor platform is actively and continuously monitoring an airspace for presence of the bioterrorism agent *Bacillus anthracis* in real-time.

2.4.1 Types of Test Outcomes

Whatever the type of this biosensor platform, there are two test outcomes that are of the most interest to the general public and emergency response teams alike: positive or negative. That is, was there a bioterrorism attack where *Bacillus anthracis* was released or was there not? Certainly, in the event of an actual attack, the amount of *Bacillus anthracis* that was released into the air is of interest, but considering the fact that just one *Bacillus anthracis* spore is capable of reaching the lungs of an individual, colonizing and causing death,[110] the priority of quantification of spores released is subjugated to the need to know with the utmost certainty whether or not spores have been released.

In the case of our hypothetical biosensor, we will further assume that our biosensor is fitted with a filter to capture particulate matter that has passed through the biosensor. When anthrax is detected and evacuation and remediation procedures are effected, this filter is collected and taken to a biological laboratory facility for confirmation of the actual presence of *Bacillus anthracis* spores by additional methods such as colony growth, PCR, etc. If these additional tests come back positive, then the original detection by our hypothetical biosensor is confirmed and we call this a 'True Positive' detection[47]. That is, our sensor's positive detection was confirmed by an additional 'gold standard' method.

However, if additional test methods found that there were, in fact, no *Bacillus anthracis* spores present when our hypothetical real-time biosensor sounded the alarm, we refer to this false alarm detection as a 'False Positive' detection[47]. In this case, the alarm was sounded, the airspace being monitored was presumably cordoned off and anyone present in the space at the time was treated for exposure to inhalation *Bacillus anthracis*. Clearly, large sums of government money were spent, there was likely much anguish on the part of those treated for exposure and their loved ones and likely some costly medical supplies and equipment were misappropriated.

Consider a third scenario where it protocol that the particulate filter in our real-time continuously monitoring biosensor must be changed every two weeks. It is further protocol to send this used filter to a biological laboratory for testing of what might have been captured over the past two weeks. If, upon testing, it is found that *Bacillus anthracis* was, indeed, captured some time during the past two weeks, but that the real-time biosensor missed the detection of this bioterrorism agent, we would refer to this missed detection as a 'False Negative,'[47] *i.e.*, detection should have taken place, but it was falsely identified as a 'safe' situation for the passersby in this space. Clearly, this is a terrible occurrence as we have no idea when, over the past two weeks this attack occurred, and thus, we have no idea which passersby might have been affected by this attack. As such, upon realization of this false negative event, a broadcast announcement that anyone who passed through the monitored airspace over the past two weeks was potentially exposed to inhalation *Bacillus anthracis* and they should proceed immediately to a hospital, lest they die!

In a more pleasant situation to imagine, picture now that this filter, upon removal from the biosensor device and testing in the off-site laboratory is found to contain just dust and benign bacteria common to airspaces where people commonly sneeze and cough without covering their nose and mouth. In this case, our real-time biosensor has indicated that there has been no airborne release of *Bacillus anthracis* and this result has been confirmed by our gold standard test(s). We refer to this happy occasion as a 'True Negative'[47].

2.4.2 Statistical Sensitivity

In order to give a true picture of the utility of our biosensor, a statistician would keep track of a very many of these two week periods and fill in the data in a table similar to Table 2-1.[111]

Table 2-1: Possible categorized statistical outcomes of biosensor tests

	Filter Culture Results ('Gold Standard' Test)		
Biosensor Test Results	**BA attack (+)**	**No BA (-)**	**Totals**
BA attack (+)	TP	FP	
No BA (-)	FN	TN	
Totals			

In this table, the initials TP, FP, FN and TN stand for true positive, false positive, false negative and true negative, respectively. If, over the course of fifty weeks of testing (twenty five total tests) all real-time biosensor readouts were recorded, as well as the laboratory results of the filter culture growth tests, and these results were compiled, the table would appear something like Table 2-2.

Table 2-2: Statistical outcomes of hypothetical biosensor test

	Filter Culture Results ('Gold Standard' Test)		
Biosensor Test Results	**BA attack (+)**	**No BA (-)**	**Totals**
BA attack (+)	1	2	*3*
No BA (-)	0	22	*22*
Totals	*1*	*24*	*25*

In examining Table 2-2 we see that over the course of the 50 week period, there were three times where the alarm was sounded by our real-time biosensor presumably resulting in the space being evacuated and people were treated for *Bacillus anthracis* exposure, etc. However, upon filter delivery to the laboratory, only one of these three cases was confirmed as an actual bioterrorism attack. It is certainly an unfortunate occurrence that the public was alarmed and remediation procedures were effected, but we can also see that our biosensor system did not miss the one real bioterrorism attack. That is, whenever our biosensor did not respond, this lack of response was confirmed correct by the filter culture test at the end of the two weeks. We refer to this correctness of response to instances where detection should have occurred as 'Sensitivity.' Using the nomenclature for possible test outcomes developed above, equation (4.16) details this calculation[47]:

$$Sensitivity = \frac{TP}{TP + FN} \tag{2.4}$$

In layman's terms, sensitivity is the number of correct positive detections relative to all the instances where detections were should have occurred.

2.4.3 Statistical Specificity

While sensitivity quantifies the ability of a particular detection scheme to correctly identify instances where a positive response should occur, 'Specificity' refers to

how accurately our biosensor reports positive detection events, *i.e.* of the total amount of non-attacks, what percentage were correctly identified. Equation (2.5) details this calculation of specificity[47]:

$$Specificity = \frac{TN}{TN + FP} \tag{2.5}$$

2.4.4 Statistical Results

If we go ahead and do the calculations for sensitivity and specificity for the trials run by our hypothetical biosensor we find that we have a sensitivity of 100% and a specificity of 92%. These high levels of sensitivity and specific are quite encouraging, but still, we see that there were two false alarms given by our biosensor. Certainly, it is better to have a false alarm than to miss an instance of attack, but we must bear in mind two things here: First, this total sample size (n=25) is small by statistics standards. Second, the number of total positive detection events available for study is smaller still. These two points shed some light on the subject as to why it takes so long for government agencies to approve new drugs and validate new medical diagnostic tools. However, in the case of a biosensor such as we have considered here, the testing of the device can clearly not be performed while the public's health is at risk. Thus, extensive and expensive testing must be performed in laboratory conditions before any real world tests can be run. Furthermore, it is of the utmost importance that, when designing a biosensor for field deployment, all efforts must be made to maximize both sensitivity and specificity. That is to say, instances of false positive and false negative both must be minimized.

2.5 Array Biosensors

Thus far, the discussion of biosensors has been focused simply on the method of detection of a single such instance of the particular type of sensor. In the case of real-time biosensors discussed above, this single sensor is indeed a powerful bioassay tool, but when performing tests upon which treatment of possibly gravely ill individuals or populations will be based, it is of the utmost importance that the results being obtained are absolutely correct[11]. Or in the statistical terms just developed, the numbers of false negatives and false positives must be kept to an absolute minimum if not at zero. As such, it is only logical that multiple trials of the same test be performed before a conclusive answer can be given with confidence. If these multiple tests are to be performed on the same equipment, however, then once again the real-time nature of the assay is lost. Hence, the need for parallel processing is identified.

The easiest way to achieve this parallel processing is simply to purchase or build several identical entire pieces of equipment and perform the multiple assays needed simultaneously. However, it is more economical (and often more advantageous in other ways as well) to build the original biosensor with a multiplexed detection array that shares as much of the equipment needed for function as possible. For example, in the case of SPR biodetection, if by mirrors and computer control, the laser and photo-detector used to perform bioanalysis on the metallic layer can be shared among multiple different prism units, then the entire cost of the multiplexed PCR detection apparatus can be reduced while still retaining the ability for multiplexed detection.

In addition to this cost-benefit of having integrated, multiplexed biosensor platforms, the overall accuracy of detection can also be improved by having multiple

sensors online simultaneously. Consider again, the situation where our hypothetical biosensor platform is actively and continuously monitoring an airspace for presence of the bioterrorism agent *Bacillus anthracis*. If it is known that the false positive rate is two out of three, or 66.7%, then the addition of, not only simultaneous redundant sensors for *Bacillus anthracis* spores, but also reference sensors could help improve results. For example, if it known that these false positives can arise from the presence of simple dust particles in the air, then a reference sensor included in the system to check for dust in the air could inform the system not to respond when both the sensor(s) specific for *Bacillus anthracis* spores and the reference dust sensor read positive. The system would only sound the alarm when the *Bacillus anthracis* spores sensor(s) respond and the dust sensor remains unresponsive. This is only a trivial solution and it perhaps creates more problems than it solves, in that, if a bioterrorist knew how the system worked, he could simply flood the airspace with dust and *Bacillus anthracis* spores and simply fool the system into not responding.

A more sophisticated solution to this issue may include a secondary detection method whenever a positive response is attained by the *Bacillus anthracis* spores biosensor. This would sacrifice some degree of real-time detection, but would also not leave the two week period of unknowingness in such cases. Clearly, the design and implementation of such sensors is not trivial. Forthcoming sections will detail some initial reports concerning attempts at array biosensor development and implementation.

2.5.1 QCM ARRAYS

While not demonstrated for monitoring of airborne or waterborne pathogens, detection of proteins[112,113] and cancer marker cells[114] have been demonstrated and

published recently using two different QCM array systems. The first of these systems employed a 2 x 5 array of standard 10 MHz QCM modules.[112,113] In the detections of human IgE[113] and human chorionic gonadotropin[112] described, the coefficient of variability (CV) of frequency shifts between sensors was near 10% for most assays, but as high as 13% in some instances. This represents good reproducibility between sensors, however, as with single QCM detections, the mg/mL sensitivities to these proteins was modest. Five mg/mL of antibody produced resonant frequency shifts of only a few hundred hertz and no lower concentration detections were reported.

The second published demonstration of QCM array capabilities reported development of a 2 x 2 array of 9 MHz QCM probes[114], but little detail was given about the sensitivity capabilities of the resulting sensor array. In this study, surface antigens of acute leukemia leukocytes were detected by the QCM array. Monoclonal antibodies to the different antigens were immobilized on the various sensors of the QCM array. It appears that reasonable specificity was achieved in the experimental results presented, but no quantitative analysis was performed, thus comparisons to other systems are difficult.

2.5.2 Surface Plasmon Resonance Arrays

Just last year, a completely self-contained SPR array system was developed and demonstrated for detection of viruses, proteins, *Francisella tularensis* cells and *Bacillus subtilis* spores[79]. This system was based on the Spreeta 2000 SPR chip developed by Texas Instruments and is called Surface Plasmon Instrumentation for Rapid Identification of Toxins or SPIRIT. It boasts eight three-channel Spreeta 2000 chips (24 channels total) and measures 28 x 22 x 13 cm while weighing in at three kilograms.

In the experimental work described, six of the eight Spreeta chips were immobilized with a different antibody for a different pathogen, while two chips remained open for reference measurements. Upon presentation with the two cellular pathogens, concentrations of 10^4 *F. tularensis* cells/mL and 9 x 10^4 *Bacillus subtilis* spores/mL were successfully detected. However, the detection procedures used involved an amplification step after initial direct detection. This amplification step only required an additional ten minutes however.

2.5.3 Fiber Optic Arrays

The RAPTOR system, developed by Research International (Monroe, WA) is the most advanced and studied fiber optic array biosensor system on the market or in research today.[92,97,115-117] This system employs a four-channel fiber optic array system that is capable of performing analysis from air sampling to results reporting and interpretation completely autonomously. However, it is the Fluorescent Sandwich Assay that is used for detection of pathogens, so some degree of real-time monitoring capabilities are sacrificed with the need for the additional labeling step. But, as mentioned previously, only five to ten extra minutes of time are needed for this step. In detection procedures, each of the four channels can be immobilized with a different detection antibody[92], but in the studies presented, all four channels are immobilized with the same antibody to provide for redundant assays of the same antigen. Cells per mL sensitivities of this system were reported at 10^4 *Bacillus globigii* spores and 10^5 *Bacillus anthracis* spores while the statistical sensitivity of *Bacillus anthracis* spore detection was reported at 100% (specificity was not reported)[92]. Since this work, improved antibody immobilization techniques have lead to positive detections of 10^3 *Listeria monocytogenes*

cells/mL[117] as well as 10^4 *Salmonella Typhimurium* cells/mL[115]. Considering only the injection of sample over the surface of the array detection system, detection times for these experiments were as short at fifteen minutes. Regardless of the labeling steps needed to achieve this detection, this rapidity of results is impressive and the fastest reported to date by any biodetection system.

2.5.4 Multiplexed Microsphere Immunoassay Systems

Yet another type of array detection system is the multiplexed microsphere immunoassay. This is a fully automated system produced and tested by the Army Research Laboratories (ARL). The system involves array detection of up to 100 different biological analytes using antibody functionalized microbeads, followed by PCR confirmation of positive microbead test results.[118,119] Clearly, this is a sophisticated system.

This refrigerator sized detection system performs continuous detection of airspaces first by entraining airborne particulate matter in liquid by means of a wetted wall cyclone, similar to the SASS2000[120] (Research International, Monroe, WA). This liquid sample is then transferred hourly to the immunoassay stage of automated testing. Here, any antigen present in the sample is presented with a mixture of antibody-functionalized microspheres as well as fluorescent detector antibodies. This mixture provides for a sandwich assay similar to those used in ELISA, SPR and optical fiber techniques. Each functionalized microsphere/detector antibody pair has a specific color associated with its fluorescence such that when the antigen of interest is present, the resulting sandwich complex fluoresces and this particular wavelength intensity increase is recorded by a photo-detector as a ‘level 1’ detection event.

Following this detection, the system automatically makes contact with an off-site monitoring station for initiation of appropriate reaction procedures and also begins its automated internal PCR confirmation of the immunoassay test results.[118] The positive sample is transferred to the PCR section of the machinery, appropriate PCR reagents and primers are added and confirmation is made (or refuted) of the original detection. Concentration sensitivities and times of PCR confirmation were not discussed, but graphical evidence showed that it typically took one to two microsphere assay cycles (or one to two hours) to detect the presence of an experimentally released antigen such as *Bacillus globigii* or *Yersinia pestis*.[118]

2.5.5 Laser-monitored Microcantilever Biosensor Arrays

As discussed in Section 2.3.4, MEMS microfabriaction techniques lend themselves readily to the production of micron-scale cantilever biosensors. Taking further advantage of these techniques, it is trivial to make several to many cantilevers simultaneously arranged in the layout of an array.[98,103,105] With such arrays produced commercially and readily available for purchase,[121] several identical biosensor platforms are thus, available for simultaneous, multiplexed detection of biological antigens with the ability for redundant detection as well as comparison to a reference sensor(s) while the assay is in progress. However, the requirement of laser-monitoring of each individual cantilever remains. Thus, in order to achieve true real-time array detection, each cantilever in the array must have its own dedicated laser in order to monitor the resonance frequency (or bending) of the cantilever as time elapses. However, published literature has only presented such a setup for the measurement of DNA hybridization,[103] rather than actual detection of biological cells, spores or oocysts. Current literature presenting bacillus

spore detection using laser-monitored microcantilever arrays shows only data monitored on only one cantilever at a time, rather than simultaneously.[98]

Thus, while single biological cell detection has been achieved using laser-monitored microcantilevers only when monitoring the resonance frequency of the sensor in-vacuum conditions before and after cell adhesion,[108] and while real-time detection of lone laser-monitored microcantilevers has demonstrated a sensitivity of 10^3 *Bacillus* spores/mL[98,109], no laser-monitored microcantilever array system has been demonstrated for real-time biological detection.

2.6 Literature Review Summary and Research Aims

In this survey of current biosensor technology and methodology performance, an overarching theme is that the highest levels of sensitivity to biological pathogens were attained using methods that are most certainly not real-time in nature.

.

Table 2-3, below, summarizes the sensitivities and time frames needed for such detections that were discussed in this chapter. Here, we see that methods such as colony growth, PCR and laser monitored cantilevers (when their resonant frequency is monitored in vacuum before and after detection) are capable of single biological pathogen detection. However, the time frames needed for such methodologies is always in the range of hours and usually requires additional time for pre-concentration before the actual detection is performed. Additionally, such techniques require trained laboratory personnel to carry out the required protocols and to interpret results. Thus, these methodologies, while indeed highly sensitive, do not lend themselves to on-site, real-time monitoring or to applications where results are needed in times less than one hour.

In contrast, methodologies with true real-time potential, such as QCM, SPR, Fiber Optic and Microcantilever sensor systems have presented lowest limits of detection in the range of 10^3 pathogens/mL in time frames on the order of thirty minutes. This time frame is more suited for real-time monitoring of a waterway or airspace, as multiple assays can be run in just one hour's time. Additionally, the mechanisms of detection in these methodologies further lend themselves to automated sensor operation where detection algorithms can be executed by a portable computing system, and results can be telemetrically sent to centralized monitoring facilities. Furthermore, these real-time systems have the potential and have been demonstrated for (though to varying degrees of effectiveness) multiplexed array implementation such that statistical sensitivities and specificities of system can be improved while still retaining the ability for real-time monitoring.

Table 2-3: Performance Summary of Current Biosensor Technologies

Sensor Methodology	Lowest Detectable Pathogen Concentration	Detection Time	Notes
Colony Growth	1	filtration time + hours to days	not possible for cryptosporidium
ELISA	10^3 bacterial cells/mL	filtration time + 1 hr+	only 'semi-quantitative'
PCR	1	filtration time + 1.5 hrs+	
EPA Method 1623	N/P	filtration time + 8 hrs+	laboratory and experience intensive
QCM	10^5 bacterial cells/mL 100 bacterial cells/mL	30 min 1.5 hrs+	100 cells/mL uses labeled amplification
SPR	10^6 *Cryptosporidium* oocysts/mL 10^4 bacterial cells/mL 10^4 *Bacillus* spores/mL	~30 min	better suited for protein detection
Fiber Optic	10^3 *E. coli* cells/mL 3 x 10^5 *B. anthracis* spores/mL	~30 min	uses a secondary labeled antibody, but only adds 5 min to detection time
Laser-Monitored Microcantilever	1 *E. coli* cell 10^3 *Bacillus* spores/mL	hours 1 hr	single cell detection achieved using non-real-time vacuum monitoring method
QCM Array	N/P	N/A	
SPR Array	9 x 10^4 *Bacillus* spores/mL 10^4 *F. tularensis* cells/mL	~40 min	indirect amplification of direct detection used
Fiber Optic Array	10^4 *B. globigii* spores/mL 10^5 *B. anthracis* spores/mL 10^3 *L. monocytogenes* cells/mL	~15m min	statistical sensitivity of *B. anthracis* detection = 100%
Multiplexed Microsphere Immunoassay	N/P	1-2 hrs	uses PCR confirmation of initial microsphere immunoassay
Laser-Monitored Cantilever Array	10^3 *Bacillus* spores/mL	1 hr	no real-time array detection published

Notes: N/A = not applicable N/P = not published

While we are not always making one to one comparisons in this survey, *i.e.* the sensitivity of one method may be cited for the detection of *E. coli* cells, while for another the most sensitive detection cited might be for *Bacillus* spores, comparisons between

such similarly sized organic entities remains useful. Provided antibody is available for functionalization of a sensor, one would not expect the lowest detectable concentration to differ more than an order of magnitude for similarly sized biological entities. Indeed, this is born out in the noted sensitivities of Fiber Optic and SPR sensors.

2.6.1 Research Aims

With the current state of the art of real-time biodetection on the order of 10^3 biological pathogens/mL, the aim of this research dissertation is to better this sensitivity while also implementing true, real-time, multiplexed array detection for simultaneous detection and confirmation of the presence of biological pathogens. In order to accomplish this aim, the sensor platform to be surveyed, studied and engineered is that of the PEMS. As mentioned briefly in Section 2.3.4, PEMS differ from laser-monitored microcantilever sensors in that their actuation and detection is completely electrical. Thus, as will be discussed in greater depth in "Chapter 3: Piezoelectric Cantilever Biosensors," Q factors of resonant frequencies can remain sufficiently high in liquid environments and the need for laser monitoring of resonant frequencies is abrogated. These factors, coupled with the already impressive limits of detection and detection times for this type of sensor make it an ideal candidate for further lowering detectable concentrations of biological pathogens in real-time. Upon explanation of piezoelectric cantilever background and fundamentals in the next chapter, the specific goals and aims of the research to be accomplished using said sensor will be presented.

CHAPTER 3: PIEZOELECTRIC CANTILEVER BIOSENSORS SENSITIVITIES AND LITERATURE REVIEW

In the field of cantilever biosensors, beyond microcantilever biosensors that are monitored by laser, lie piezoelectric cantilever sensors. Piezoelectric cantilever (and microcantilever) sensors share many common attributes with silicon and other laser-monitored cantilever sensors, such as the capability for real-time, *in situ* detection of biological pathogens by means of induced resonant frequency change. However, in the case of piezoelectric cantilever sensors, this *in situ* monitoring is made easier and more effective by all electrical actuation and detection and the resulting ability to retain high Q factors (as in equation (2.3)) in liquid. Whereas, the Q of a laser-monitored silicon microcantilever can degrade from approximately thirty in air to less than two in water,[9] Q values of piezoelectric microcantilevers have been demonstrated to decrease from approximately 150 to only seventy nine upon submersion in aqueous solution.[35] This enhancement of Q values arises from the fact that piezoelectric biosensors are actively excited by the piezoelectric layer that makes up all or most of the length of the cantilever. In contrast, laser-monitored cantilevers are actuated only at the base of the cantilever. Thus, submersion in a more viscous liquid necessarily leads to significant damping, whereas in the case of piezoelectric cantilevers, as long as they are properly insulated, they are continually driven electrically to vibrate by the full length of the piezoelectric layer regardless of the surrounding medium. Additionally, the all-electrical activation and detection abilities of piezoelectric microcantilever sensors make them ideal candidates for array multiplexing.

3.1 Theoretical and Practical Sensitivities

3.1.1 Modes of vibration: Flexural and Length Modes

When discussing the mechanical resonance of a piezoelectric cantilever, it is important to make a distinction as to which type of resonance is being studied. The most often discussed (whether explicitly or implicitly) mode of resonance of any type of cantilever (be it a piezoelectric or nonpiezoelectric cantilever) structure is more precisely known as flexural resonance. Flexural resonance is the vibration of a cantilever in much the same manner as a diving board vibrates after the diver makes his/her dive. For this mode of vibration, the clamping of at least one end of the cantilever is a requirement. Figure 3-1, below, depicts the first mode of flexural resonance vibration schematically, where the grey dashed lines indicate the alternating upward and downward oscillations of the cantilever. Higher mode resonance vibrations occur when the length of the cantilever is equal to a multiple of the wavelength of vibration, and nodes, or points of zero-displacement, occur along the length of the cantilever during vibration.

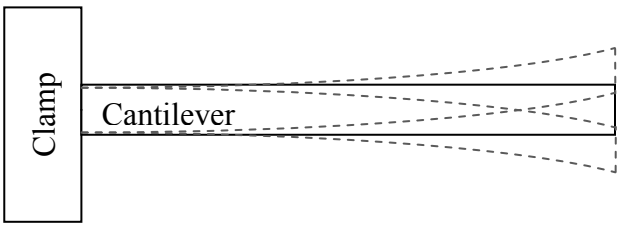

Figure 3-1: Side view of a flexurally vibrating cantilever

In contrast to this type of vibration, length and width mode vibrations also occur in piezoelectric cantilever structures. This vibrational mode is somewhat more abstract

than flexural vibration. One might liken this type of non-flexural vibration to the to-and-fro 'wiggling' of a free standing mold of Jell-O© mold when poked. This type of vibration can be either expansion-and-contraction of the piezoelectric material or shear oscillations as occur in QCM sensors. In more geometric terms, expansion and contraction of piezoelectric materials occur when opposite faces of the material move toward and away from each other, as if the whole piece were breathing. This can occur in the direction of the width, length or thickness of the cantilever. The 'length' and 'width' modes of this type of vibration are depicted schematically in Figure 3-2(a). Shear occurs when all opposite faces of a rectangle remain parallel, but the corner angles deviate from 90 degrees, changing the rectangle to a rhombus, as depicted in Figure 3-2(b), below.

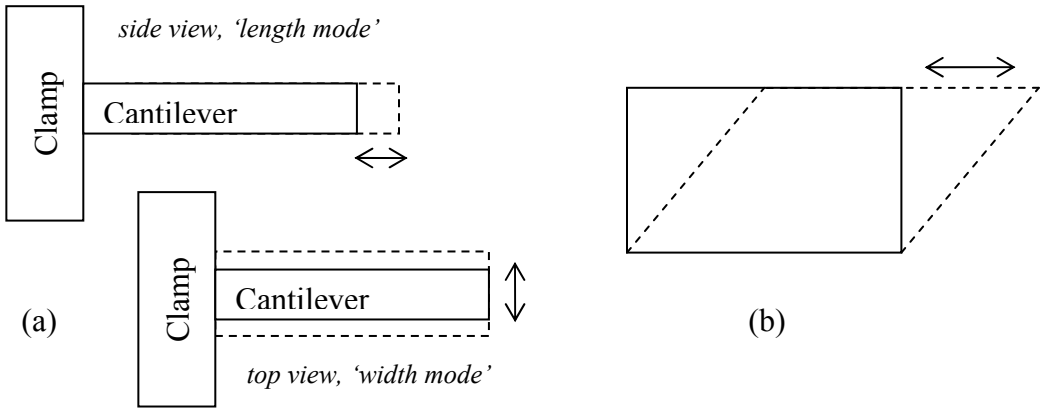

Figure 3-2: 2D views of a length and with mode deformations (a) length and width 'breathing' modes and (b) shear mode

Shear type of vibration is the primary mode of vibration for a QCM sensor, and as such, the QCM is alternately known as an STM resonator, or Shear Thickness Mode resonator. The exact type of vibration that occurs in piezoelectric cantilevers, *i.e.* breathing or shear, is currently under investigation, but an analysis will be presented later

in Chapter 4 that indicates that breathing is the most likely mode of non-flexural vibration in the cantilevers fabricated herein.

3.1.2 Flexural-Mode Piezoelectric Cantilever Sensitivities

Piezoelectric cantilevers can be fabricated in a variety of shapes and sizes, but there are three categories into which such cantilevers can be classified. A unimorph bilayer cantilever (henceforth simply, 'unimorph cantilever') is composed of equal dimensions, as depicted in Figure 3-3(a), below. A bimorph cantilever consists of piezoelectric layer bound to a nonpiezoelectric layer that protrudes past the edge of the piezoelectric layer, as shown in Figure 3-3(c). A freestanding piezoelectric cantilever, also referred to as a 'PZT-only' cantilever consists of just one layer of piezoelectric material without a nonpiezoelectric layer, as shown in Figure 3-3(b).

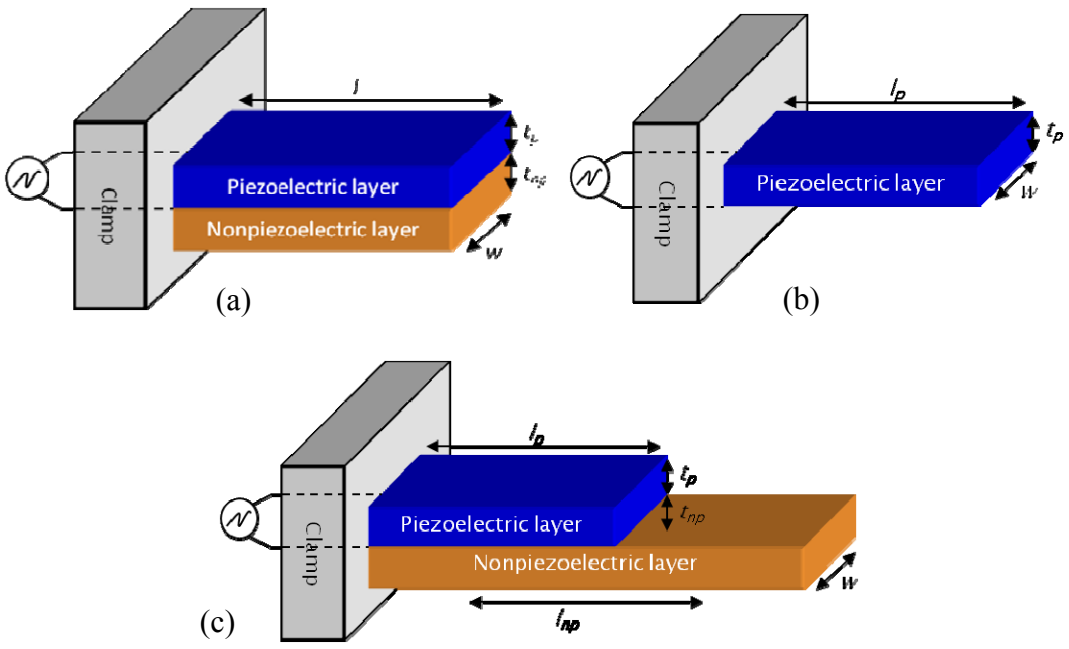

Figure 3-3: Schematic representations of standard piezoelectric cantilevers. (a) a unimorph bilayer cantilever (b) a freestanding piezoelectric cantilever (c) a bimorph cantilever

Similar in form to the equation for a simple harmonic oscillator, the flexural resonance, f_r, of a unimorph cantilever sensor is given by the equation:

$$f_r = \frac{\nu_i^2}{2\pi}\sqrt{\frac{K}{M_e}} \tag{3.1}$$

where v^2_i is the ith mode eigen value of vibration, $M_e=0.236mwl$ is the effective mass of the cantilever, where w is the width, l is the length of the cantilever and m is the mass per unit area of the cantilever, given by the equation:

$$m = \rho_p t_p + \rho_{np} t_{np} \tag{3.2}$$

where ρ and t are the density and thickness, respectively, of the material of interest and the subscripts p and np denote the material as piezoelectric and nonpiezoelectric in this equation and all following equations. The term, K, in equation (3.1) is the spring constant of the cantilever given by:

$$K = \frac{3Dw}{l^3} \tag{3.3}$$

where D is the bending modulus of the cantilever and is given by:

$$D = \frac{E_p^2 t_p^4 + E_{np}^2 t_{np}^4 + 2E_p E_{np} t_p t_{np}(2t_p^2 + 2t_{np}^2 + 3t_p t_{np}}{12(E_p t_p + E_{np} t_{np})} \tag{3.4}$$

where E is the Young's Modulus of the piezo- and nonpiezoelectric materials .[122]

Considering this definition of the resonance frequency of vibration, f_r, the mass detection sensitivity of a unimorph cantilever sensor is given by the equation[122]:

$$\frac{\Delta f}{\Delta m} = -\frac{f_r}{2M_e} = -\frac{\nu_i^2}{4\pi}\sqrt{\frac{K}{M_e^3}} = -\frac{\nu_i^2}{4\pi}\sqrt{\frac{K}{((0.236)mwl)^3}} \tag{3.5}$$

or equivalently:

$$\frac{\Delta f}{\Delta m} = -\frac{\nu_i^2}{4\pi(0.236)mwl^3}\sqrt{\frac{3D}{(0.236)m}} \tag{3.6}$$

where ($\Delta f/\Delta m$) is the change in resonant frequency that occurs due to the addition of a small mass to the surface of the sensor. The negative sign appears since the addition of a small mass to the system will necessarily induce a resonance frequency shift to a lower value.

When it comes to calculating the theoretical mass detection sensitivity of a bimorph piezoelectric microcantilever, rather than a unimorph cantilever (see Figure 3-3), the boundary conditions between the nonpiezoelectric tip and the piezoelectric/nonpiezoelectric base section of the cantilever must be considered as well as those conditions at the clamp and free end in order to accurately describe the harmonics of the cantilever system. The reader is directed to an extremely in-depth treatment of this subject in a dissertation by Zuyan Shen,[122] but briefly, here, the effective mass of a bimorph vibrating beam can be written as:

$$M_e = \frac{1}{h_0^2}\int m(x)\big(h(x)\big)^2 dx \tag{3.7}$$

where h(x) is the vertical displacement of the cantilever at a distance x from the clamp.

With this more flexible (no pun intended) definition of M_e, equation (3.5) can be rewritten as:

$$\left(\frac{\Delta f(x)}{\Delta m}\right)_I = -\frac{\nu_i^2}{4\pi}\frac{h_0^2}{\left(m_I w\int_{-l_I}^{0} h^2(x)dx + m_{II} w\int_0^{l_{II}} h^2(x)dx\right)}\sqrt{\frac{K}{m_I}} \tag{3.8}$$

for the mass sensitivity in the piezoelectric-nonpiezoelectric bilayer region of the cantilever closest to the clamp. In the protruding nonpiezoelectric tip region of the cantilever, the sensitivity is calculated as:

$$\left(\frac{\Delta f(x)}{\Delta m}\right)_{II} = -\frac{v_i^2}{4\pi}\frac{h_0^2}{\left(m_I w\int_{-l_I}^{0} h^2(x)dx + m_{II} w\int_{0}^{l_{II}} h^2(x)dx\right)}\sqrt{\frac{K_{II}}{m_{II}}} \qquad (3.9)$$

where the subscripts *I* and *II*, in equations (3.8) and (3.9), denote values pertaining to the piezoelectric-nonpiezoelectric bilayer region closest to the clamp and the nonpiezoelectric tip region of the cantilever, respectively and illustrated in Figure 3-3(c), and where the value of *x=0* is point along the cantilever where this transition occurs.

In putting this mass detection sensitivity into practice, Shen[122] observed that, for the first flexural resonant frequency peak, frequency shift sensitivity enhancements of up to 1.4 times can be expected when the nonpiezoelectric layer is made to protrude past the tip of the piezoelectric layer by 60% of the length of the piezoelectric layer – as compared to a cantilever of the same nonpiezoelectric layer length with no tip. Further theoretical investigations showed that frequency shift sensitivity enhancements approaching seven times can be achieved for higher harmonic resonances.[122]

Whether considering a cantilever with a tip or without, the preceding analysis focuses primarily on the addition of a mass to the cantilever system and the resultant change in resonant frequency as a result of this mass change. However, evidence has shown that a change in resonant frequency of the cantilever can also occur due to a change in spring constant of the cantilever as a result of analyte binding to the sensor surface.[123-127] In detection of protein on a functionalized piezoelectric cantilever sensor, a proposed theory is that the addition of this layer of detected protein changes the surface

stress of the sensor and thus induces a frequency shift up to two orders of magnitude larger than that predicted by just mass additional alone.[35,123]

Furthermore, recent work has indicated that in addition to this possible surface stress effect, detection of mass on the surface of the sensor can actually lead to changes in the Young's Modulus of the piezoelectric material in the cantilever.[128,129] In this experimental work, separately, both a DC bias of the piezoelectric material as well as detection of humidity of the cantilever's environment were shown to induce a change in the spring constant (*K*, in the preceding equations) as a function of Young's Modulus change according to yet another mathematical representation of the cantilevers spring constant[129]:

$$K = \frac{E_{eff} t^3}{4l^3} \tag{3.10}$$

where E_{eff}, the effective Young's Modulus is:

$$E_{eff} = \frac{E_p^2 t_p^4 + E_n^2 t_n^4 + 2E_p E_n t_p t_n (2t_p^2 + 2t_n^2 + 3t_p t_n)}{(E_p t_p + E_n t_n)(t_p + t_n)^3} \tag{3.11}$$

Thus, considering that the Young's Modulus of the piezoelectric layer (*Ep*) can vary under conditions of imposed electric field or an applied stress, clearly this can induce a frequency shift in the piezoelectric cantilever itself.[127,130]

Whether the mechanism for frequency shift enhancement be a change in the spring constant of the cantilever due to an applied surface stress, or an actual change in Young's Modulus of the piezoelectric material in the cantilever, enhancements of two orders of magnitude greater than the detection sensitivity predicted by mass addition alone have been observed and reported by multiple researchers.[35,126-129] These

enhancements have all been observed in piezoelectric microcantilevers and have been shown to be a function of the cantilevers' size, specifically its length.

3.1.3 Cantilever Design Criteria for Maximizing Sensitivity

The above discussion concerning the sensitivities of piezoelectric cantilevers applies to cantilevers of any size and shape, but even a cursory examination of these sensitivity equations leads the astute engineer to establish several basic design criteria. If the goal of your piezoelectric biosensor is to detect biological pathogens in the lowest possible concentrations while maintaining high levels of statistical sensitivity and specificity, you will want to: 1) maximize your resonant frequency shift relative to the mass adhered to the sensor, 2) maximize your signal to noise ratios for such shifts and 3) minimize nonspecific interactions of your intended analyte with your sensor and flow system surfaces (so as to avoid false positive and false negative detection events). While points 2 and 3 will be discussed in subsequent chapters, the design criteria pertaining to point 1, follows directly from equations (3.5), (3.6), (3.8) and (3.9) for flexural resonance sensitivities. Considering the simpler unimorph cantilever design of the flexural resonance case, we can distill equation (3.6) down to the following relationship of geometrical properties:

$$\frac{\Delta f}{\Delta m} \propto \frac{1}{w l^3} \tag{3.12}$$

From this relationship we find that, in order to optimize our cantilever's sensitivity for flexural resonance detection we want to: (1) make the cantilever as short as possible; (2) make the cantilever as light as possible; (3) make it as narrow as possible; (4) make it as stiff (in terms of bending modulus) as possible. And with the cubic enhancement in

sensitivity from decreasing the length of the cantilever, this is logically the most important area to focus upon.

3.2 Experimental Piezoelectric Cantilever Sensitivities and Limits of Detection

3.2.1 Microfabricated Piezoelectric Biosensors

With length being the most important factor concerning sensitivity, microfabrication of piezoelectric biosensors has become a popular area of research in recent years. Such fabrication of sensors is inherently difficult due to the harsh chemicals and environments used in MEMS processes[99] to achieve the many layers needed for proper function of the cantilever. As such, much attention has been given to the fabrication of these sensors at the expense of actual biological pathogen detection.[123,131] Figure 3-4[132] details just the structural complexity inherent in creating these piezoelectric microcantilevers. Even this does not do justice to the process complexity needed to achieve each individual layer.

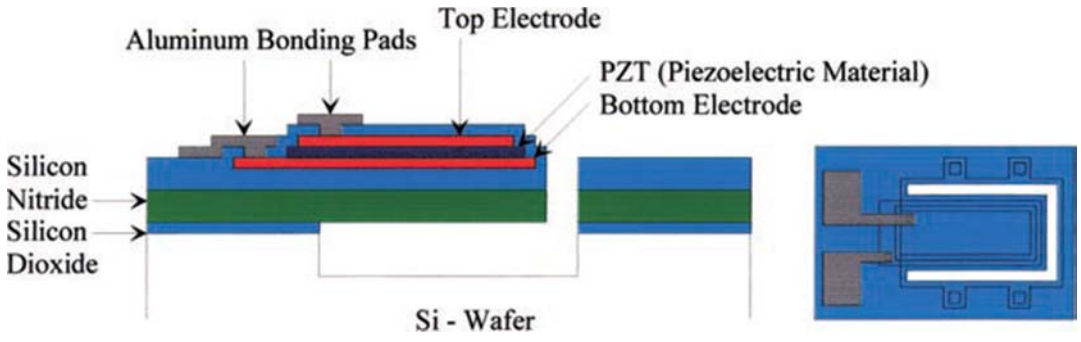

Figure 3-4: Cross-sectional schematic of microfabricated PZT cantilever

Nonetheless, some impressive detection has been demonstrated in recent years. Detection of Prostate Specific Antigen (PSA), a marker protein for prostate cancer, has been achieved at levels of 10 pg/mL using a PZT microcantilever fabricated by MEMS methodologies.[123,133] However, since this microcantilever was not electrically insulated, real-time detection was sacrificed. After antibody functionalization, the microcantilever was monitored for a baseline resonant frequency position in air under controlled humidity conditions, then immersed in the PSA solution for a period of 1 hr, rinsed, dried and then monitored for a frequency shift in the same controlled humidity conditions.[123]

In another demonstration of a microfabricated piezoelectric microcantilever used in a biological detection application, the cantilever shown in Figure 3-5[131], is used to detect the presence of a DNA sequence and a protein in solution.

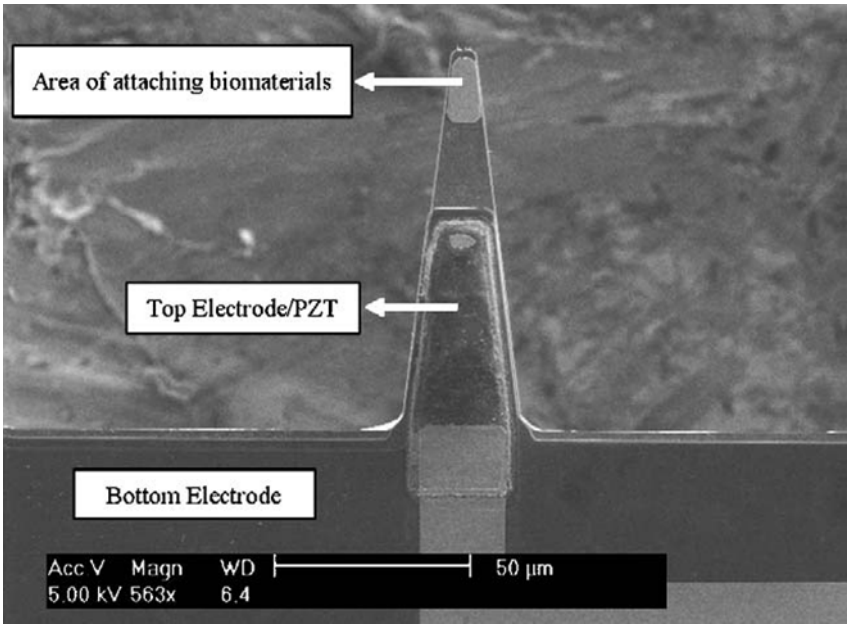

Figure 3-5: A microfabricated PZT cantilever used for biodetection

In this work, the concentrations of detected DNA and protein were not discussed, nor was the actual method of quantifying the frequency shift resultant from analyte adhesion. That is, it was not described whether real-time detection was performed or if it was simply a before-and-after measurement of resonance frequency shift that was carried out. Regardless of this, it is interesting to point out that, should Q values remain high enough, the cantilever shown in Figure 3-5 would be capable of continuous, real-time biosensing without the need for electrical insulation. This would be possible if just the tip, or 'area of attaching biomaterials,' in Figure 3-5 were dipped into the analyte liquid and the 'top electrode/PZT,' remained clear of the analyte solution, such as is depicted in Figure 3-6[131].

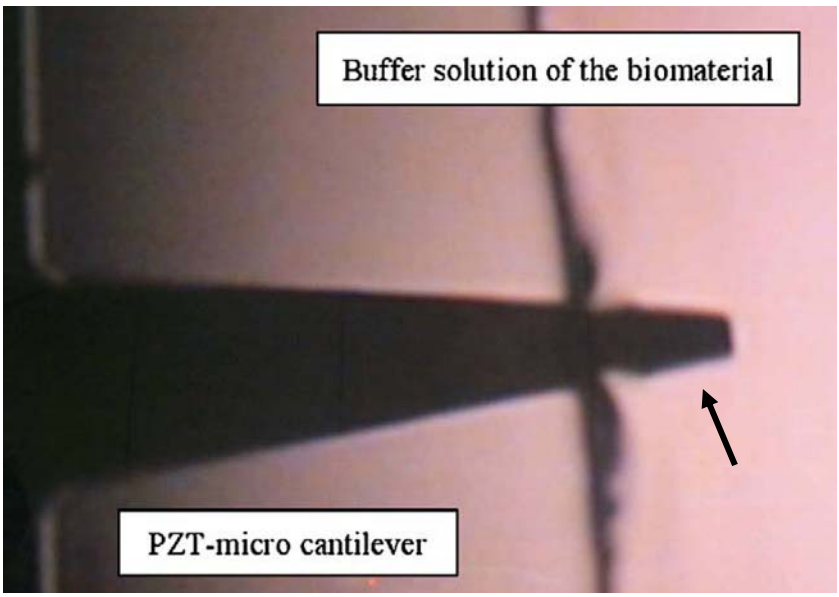

Figure 3-6: Tip of microfabricated PZT cantilever dipped in analyte solution (indicated by arrow)

However, the dipping of the tip of such a small cantilever is certainly not trivial as the meniscus of the analyte solution would tend to cover the entirety of the cantilever. This accurate dipping would be especially difficult if real-time monitoring were to be performed over an extended period of time (*i.e.* fifteen minutes or more), as aqueous solution levels have been shown to change significantly in this time frame.[38]

3.2.2 Piezoelectric Cantilever Biosensors

In an effort to simplify cantilever construction, as well as to lessen the damping effects that an insulation layer may impose on a smaller microcantilever sensor, some researchers have chosen to improve upon and optimize what we might term 'macro' or millimeter-sized cantilever sensors. That is, the use of sensors that are on the order of several millimeters long and approximately 1 mm wide[134] has been demonstrated for detection of biological pathogens. In several instances of protein detection, a bimorph cantilever was constructed such that the nonpiezoelectric tip was available for immobilization of antibody and dipping into solution while not necessitating dipping, and thus insulation, of the electrodes on the piezoelectric layer.[135,136] In more sophisticated detection of biological antigens, two different insulation schemes were employed on sensors to serve as insulating layers for piezoelectric electrodes upon complete submersion in liquid. The first of these schemes involved coating the PZT in polyurethane while the second method utilized SU-8 photoresist (MicroChem, Newton, MA) as an insulating layer.[137]

This insulation and real-time monitoring allowed for detection of *E. coli* cells in concentrations of 100 cells/mL in a volume of 70 mL in about thirty minutes.[137] This value represents the lowest limit of biological pathogen detection achieved by these

millimeter-sized cantilevers. In other work, though the insulation method was not described, detections of 700 *Streptococcus* cells/mL[138] and 300 BA spores/mL[139] were achieved.

While these limits of detection do improve upon the levels achieved by the methodologies reviewed in Chapter 2, the original pioneering theoretical work in this field of macro- or milli- piezoelectric cantilevers by the Shih and Shih group, as well as some of their more recent advances in this field have even further lowered the limits of detection for biological pathogens. The theory behind much of the piezoelectric cantilever biosensors in use today, and discussed above in Section 3.1.2, was originally developed theoretically in the last few years of the 20th Century,[140,141] and initially demonstrated in practice in 2001.[41,142] In this work,[41] a piezoelectric unimorph cantilever of sensitivity $\Delta f / \Delta m = 3.2 \times 10^5$ Hz/g was demonstrated, and predictions of lengths needed for sensitivities relevant to protein, DNA and biological cell detections were made. The predicted sensitivity and length needed for biological cell detection were 4×10^{-7} g/Hz and 3 mm, respectively. This prediction was indeed born out in very early work by the present author. *Salmonella typhimurium* cells were successfully detected in 15 min using a 3 mm long piezoelectric cantilever with an experimentally determined mass sensitivity of 0.1 ng/Hz, or 1×10^{-10} g/Hz.[37]

In more recent work by the Shih group, bimorph PZT-glass PEMS, with sensitivities of 5×10^{-11} g/Hz, have been used to successfully detect *S. typhimurium* cells in concentrations as low as 10^3 cells/mL.[38,39] However, moving beyond the simple, hand-glued PZT-glass cantilevers discussed so far in this section, the Shih group, has demonstrated the use of Lead Magnesium Niobate-Lead Titanate (PMN-PT) free-

standing tapes[143] to create PEMS that do not involve microfabrication techniques, yet are markedly more sensitive than the macro- and milli- cantilever biosensors discussed above. This increased sensitivity arises from a thickness effect enhancement in the piezoelectric properties of the PMN-PT when cast at thicknesses approaching the grain size of the piezoelectric, *i.e.* 8 to 20 microns.[143] Utilizing this effect, and a novel insulation scheme to be discussed in depth in Chapter 4, Capobianco, *et al*, have demonstrated detection of just 100 *E. coli* cells in a volume of less than one milliliter and a sensor mass sensitivity of 3×10^{-12} g/Hz.[33] Furthermore, using a similar PMN-PT PEMS, shown in Figure 3-7, below, the present author, *et al*, has demonstrated the detection of just thirty six total BA spores in 0.8 mL of liquid (45 spores/mL), with a mass detection sensitivity of 2×10^{-13} g/Hz.[35]

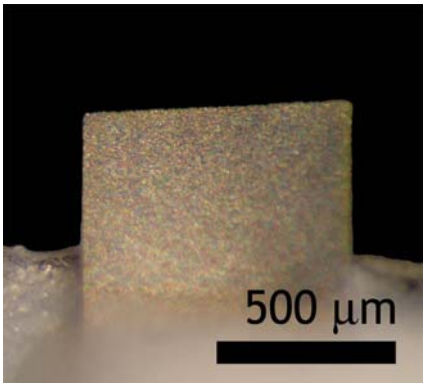

Figure 3-7: PMN-PT PEMS used for successful real-time, *in* situ detection of just 36 BA spores

This represents the lowest published limit of detection by any real-time biosensor to date and this detection will be discussed in depth in Chapter 5.

3.2.3 MICROCANTILEVER BIOSENSOR ARRAYS

With the highly sensitive, real-time detection capabilities of the piezoelectric cantilever biosensors discussed in this chapter, it is only logical to multiplex these sensors into array systems in order to achieve better statistical sensitivity and specificity of detection. Though array biosensors have been implemented to varying degrees, as discussed in Section 2.5, none of these detection technologies have realized both the limits of detection and detection times required for true real-time, sensitive detection. Aside from QCM arrays, which are quite far from the limits of detection needed for biological pathogen monitoring, all array systems discussed previously are optical in nature. In the case of these methods, such as SPR, Fiber Optic, and Laser-monitored microcantilevers, the impediment to array multiplexing is due, at least in part, to the need for either a separate optical system or laser for each instance of biosensor in the array, or complicated optics and mirrors to 'switch' the monitoring system between sensors in a rapid manner.

Similar to the QCM, which is all-electric in its actuation and detection, the much more sensitive piezoelectric cantilever biosensor can be multiplexed simply by building several identical sensors and connecting them electronically through a switching system. Such a switching system allows each cantilever to be electrically interrogated for presence of biological pathogen on its surface individually. This 'scanning' of each sensor can be very rapid, such that ten or more cantilevers can be scanned within just a minute's time. While these switching systems are inexpensive and while piezoelectric cantilever biosensor systems have been demonstrated for detection of biological pathogens in extremely low limits of detection, the implementation of such array systems

has yet to be achieved.

In the case of microfabricated piezoelectric biosensors, as discussed in Section 3.2.1, the array itself has been constructed, as it is relatively easy to do so with MEMS methodologies. However, owing to the lack of an effective, non-damping insulation method, actual real-time, *in situ,* sensitive detection is the shortcoming of these sensors. In the case of millimeter-sized cantilevers as discussed in Section 3.2.2, real-time, *in situ*, detection with low limits of detection have been achieved, but it is an inability to effectively produce the actual arrays of cantilevers that has prevented implementation of multiplexed piezoelectric cantilever biosensors thus far. This shortcoming is largely due to the fact that such millimeter-sized piezoelectric cantilevers are handmade by the researcher in an on-demand basis, and thus, reproducibility of cantilever dimensions and resulting resonance spectra is inherently difficult.

3.3 Summary and Research Goals

3.3.1 Chapter Summary

As detailed above, based on equation (3.12), the primary objective of an engineer aiming to design a highly sensitive piezoelectric cantilever sensor should be to reduce the length of the cantilever as much as possible. Of course, there are practical limitations of this mantra in that a cantilever that is shorter than it is thick will hardly vibrate at all and be utterly useless for detection. Thus, while shortening the length of the cantilever is the primary goal, this goal, in turn, necessitates other miniaturizations in terms of width and thickness.

In the case of microfabricated piezoelectric microcantilever biosensors, impressively small and precisely fabricated cantilevers have been produced and

characterized, however, it is a common theme that continuously monitored, real-time detection has not been demonstrated. Two possible (and possibly interrelated) major factors for this shortcoming in application are: 1) the lack of electrical insulation which would enable complete submersion of the microcantilever in the analyte solution; and 2) possible damping of the cantilevers' resonant peaks upon either insulation, submersion in aqueous solution, or both.

Conventionally fabricated piezoelectric cantilever biosensors, such as the PEMS do not suffer from these shortcomings as robust insulation has been achieved for use in water and PBS solutions and Q values have been demonstrated to remain sufficiently high in these environments. However, their 'macro' or 'milli' sizes necessarily sacrifice some degree of sensitivity. Nonetheless, detections of less than 50 BA spores/mL have been achieved using PEMS that were fabricated without MEMS methodologies.

3.3.2 Research Goals

With PEMS biosensors representing the best of real-time, *in situ* biosensor with low limits of detection, and high promise of multiplexing, the specific aims of this Research Dissertation are as follows:

1. As discussed in Chapter 1, flow can be used to deliver samples in dilute concentration to the biosensor surface. A major aim of this dissertation will be to optimize this fluid flow to improve the limits of detection of the piezoelectric microcantilever sensor, and also to study statistical sensitivity and specificity of such sensors as a function of the flow rates and speeds of the analyte solution over the surface of the sensor. The theoretical and practical engineering considerations

concerning fluid flow analysis and optimization will be discussed in depth beginning in Chapter 4.

2. As discussed in Section 3.1, the design and construction of cantilevers possessing higher frequency resonance peaks as a result of engineered geometries will be studied with the goal of improving biological pathogen limits of detection. Theoretical consideration will be given to possible length and width mode resonance peaks occurring higher than 300 kHz and these peaks will be explored for use in detection.
3. Per the benefits identified in Chapters 2 and 3, a major focus of this work will be to engineer, build, test and re-engineer an effective PEMS array system that retains or improves upon the low limit of detection capabilities of individual PEMS sensors, while also enabling true, multiplexed, real-time, *in situ* array detection. Such an array will allow for real-time redundancy of detection as well as real-time quantification of detection background. By utilizing these real-time capabilities of the array, resulting statistical sensitivity and specificity enhancements will be studied in relation to detection of *Bacillus anthracis* and *Cryptosporidium parvum* as model systems for PEMS detection.

CHAPTER 4: SENSOR AND FLOW SYSTEM DESIGN, FABRICATION, AND MATERIALS CONSIDERATIONS

4.1 Sensor Design and Fabrication

Whether the piezoelectric sensor to be constructed be a PMN-PT based sensor or a PZT based sensor; a piezoelectric/glass sensor or a freestanding piezoelectric shear-mode sensor; a unimorph or a bimorph sensor; a single cantilever or an array of cantilevers, many of the design and construction aspects remain common to all types of fabrication. Generally speaking, first the piezoelectric material to be used is cut to the desired size. Next, if it is to be a piezoelectric/glass cantilever to be constructed, the piezoelectric material is bonded to the glass via non-conducting epoxy. Then, wire leads are attached to the electrodes of the piezoelectric material. This assembly is then potted in a non-conductive epoxy with the desired cantilever length protruding from the epoxy and the wire leads used for electrical connection protruding from the rear end of the epoxy. Once the epoxy cures, a functioning cantilever exists. In order to use this cantilever in biodetection applications, it should then be insulated and have extended wire leads attached to the existing leads to meet the demands of the application.

Figure 3-3 schematically illustrates the various piezoelectric cantilever embodiments fabricated, studied and used for detection in this body of research. In all three types of cantilevers, the 'piezoelectric layer' denotes the material that will perform the actuation and detection of the vibration of the cantilever. This material will be either PZT or PMN-PT in the research presented here, while the 'nonpiezoelectric layer' in (a) and (c) represent the layer of glass that can be bonded to the piezoelectric layer. This

layer could also be a metal such as stainless steel or titanium, but in this work, will be exclusively glass. The lengths of the piezoelectric and nonpiezoelectric layers are termed l_p and l_{np}, respectively, while the widths and thicknesses of the two layers (when applicable) are denoted by w and t. Additionally, the clamp is indicated in the figure and it also encapsulates and protects the posterior end of the cantilever, as well as the wire leads that are attached to electrodes of the piezoelectric layer. These wire leads are illustrated schematically by the dashed lines inside the clamp, and are also shown to be schematically connected to an alternating current (AC) voltage source that drives the cantilever during detection.

4.1.1 Lead Zirconate Titanate (PZT) Based Sensors

As mentioned above, the piezoelectric layer in the various cantilever embodiments can be either PZT or PMN-PT. When PZT is the material of choice, it can be procured from PiezoSystems, Inc. (Cambridge, MA) in their 5H4E formulation with a thickness of 127 μm (0.005 inches). These sheets are factory sputtered with nickel electrodes to which electrical leads can be soldered.

4.1.1.1 PZT/Glass Sensors

Typically, for PZT/glass sensors, the bimorph geometry shown in Figure 3-3(c) is used. Fabricating a cantilever with a nonpiezoelectric tip is straightforward when prefabricated PZT is used and constructing a cantilever in this way has distinct advantages when it comes to mass detection sensitivities. As detailed above in Section 3.1, depending on the length and thickness of the cantilever constructed, when the nonpiezoelectric layer is made to protrude past the tip of the piezoelectric layer by 60%

of the length of the piezoelectric layer, mass detection sensitivity enhancements of up to 1.4 times better than similar-sized unimorph cantilevers can be expected.[122]

To construct a cantilever in this way, first, the PZT layer of the cantilever-to-be is cut from the bulk sheet with a diamond pen or razor blade. For most biodetection applications, sensor widths of less than 2 mm are desired, while widths under 500 μm are ideal for highly sensitive applications. The length of this PZT layer is dictated by the application. The edges of this cut piece are carefully sanded such that all edges are smooth, parallel and square. The glass layer is then cut in a similar fashion, with identical width and a length dictated by the desired tip protrusion length. As mentioned above, these glass and PZT layers are bonded with non-conductive epoxy (Hysol 1C, Loctite Corporation, Rocky Hill, CT), clamped and allowed to cure for 24 hrs.

Once the epoxy has cured, copper wire is soldered to the top and bottom electrodes of the PZT piece. Stranded wire thinner or equal to 22 gauge (AWG) is used in this process and the wire is typically trimmed so that just one strand is used to bond to the PZT layer. This method is used to reduce breakage of the cantilever prior to potting, as a result of the fragility of the PZT layer. Once soldered, these connections are potted in Hysol 1C, as previous, such that the protruding cantilever is of the desired length. Care must be taken to ensure that the clamped edge of the cantilever is straight and free of excess glue and that the cantilever does not shift or sag in the epoxy before it is cured. Sagging of the cantilever and a resulting non-orthogonal clamped edge of the cantilever can, and necessarily does, lead to poorly functioning cantilevers with poor resonance spectra and peaks characterized by low Q values.

After the potting epoxy has again cured, the cantilever is tested for function. Minor imperfections in the clamped edge can often be remedied by additional epoxy after potting, but major flaws in the clamp can fatal to proper function. Once any further adjustments are made to the clamp and allowed to cure, if only the tip of the cantilever is to be dipped into the detection solution,[34,37-39] it is ready for use. If it is required that the entire cantilever be dipped into the solution, it is then insulated at this point in time according to the protocols in Section 4.2. Insulation is, by far, the desired choice at this point as issues of dipping depth[38] and humidity[39] are made moot. However, effective insulation methodologies[33,40] were only recently developed and thus, dipping was a necessity at times.

Figure 4-1[37] displays a typical phase angle *vs.* frequency spectrum of a hand-made, bimorph PZT cantilever. Some aspects of this spectrum common to all cantilever spectra are: the resonance peaks, in this case near 20, 60 and 165 kHz; the baseline of the spectrum, with its proximity to -90^{o} indicating good capacitance away from resonance; and the good overall heights of the peaks, with all exceeding 10^{o} in height in this instance. Since this is a PZT-glass cantilever designed to resonate in the flexural mode, the peaks observed all occur below 200 kHz, while no further peaks are observed at higher frequencies.

Also shown in this figure inset is the behavior of a detection peak of this particular sensor. We see that, in air the peak occurs at a higher frequency, while, upon dipping of the tip into liquid, the peak shifts to lower values. Then, during detection, the peak continues to shift downward as biological pathogens (in this case *Salmonella typhimurium*) are detected. Notice too, that in this case of tip-only dipping of the

bimorph cantilever, the Q factor of the detection peak decreases only by a value of one upon dipping, from 46 to 45, as opposed to the decrease from 25 to 1 in the case of silicon microcantilevers.[9]

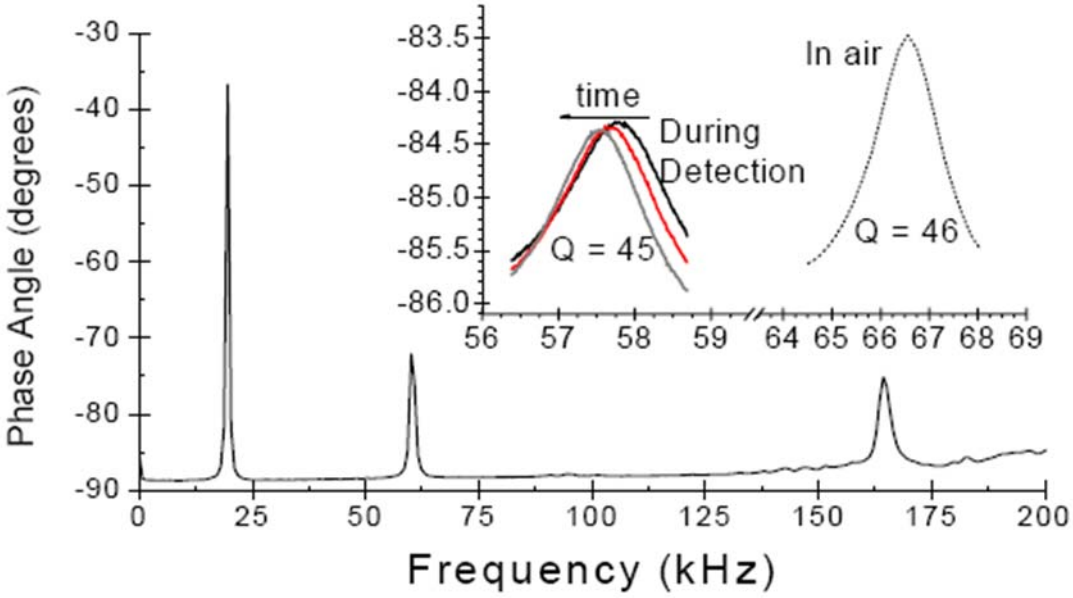

Figure 4-1: Phase angle versus frequency spectrum of a PZT bimorph cantilever. Inset: detection peak in air and during aqueous detection

4.1.1.2 PZT-only Sensors

PZT-only biosensors, as constructed by this author, resonate in the length and width modes as described in Section 3.1. As will be discussed in Chapter 6, the conception of developing PZT-only PEMS led directly from the observation of new, higher frequency peaks found useful for detection, in PZT-glass PEMS arrays fabricated using wire saw cutting. These PZT-only cantilevers can be assembled in single instances in a very similar fashion to PZT-glass cantilevers, save the bonding of the PZT piece to the glass layer. That is, the PZT can cut by diamond pen or razor blade, sanded on all

four edges, then has wire leads soldered to its electrodes, is potted in epoxy and is then function tested. Alternatively, PZT-only PEMS can be fabricated by wire-saw cutting, instead of diamond pen cutting and sanding. This technique allows for more precision in the fabrication process and also allows for the fabrication of much more narrow PEMS in either single or array format. Regardless of the method of production, however, since these cantilevers are comprised solely of PZT, they must necessarily be insulated to facilitate *in situ*, real-time monitoring of biological pathogens in aqueous solutions. Please see Section 4.2 regarding possible insulation techniques.

While the derivation for the flexural resonance frequency of vibration of a piezoelectric cantilever, as reviewed in Section 3.1.2, necessarily involves the calculations of bending moduli and eigen values, which can often only be solved numerically, the derivation of length and width mode resonances are markedly simpler. Whereas, in flexural mode vibration, the entire cantilever vibrates as a wave, in length and width mode vibrations, the waveform of vibration is internal to the cantilever itself. In other words, vibrational resonance occurs when the wavelength of vibration (or a fraction or multiple thereof) coincides with either: the length, width or thickness of the cantilever itself.

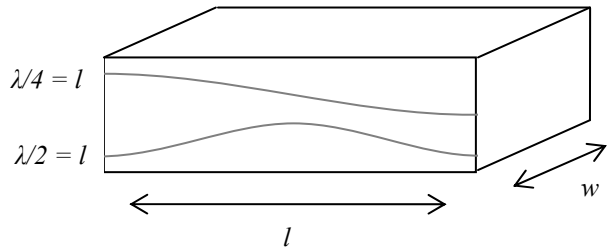

Figure 4-2: Schematic representation of resonant length mode oscillations

Figure 4-2, above illustrates how waveforms of vibration occur in length mode resonances. Such resonance occurs when two nodes of vibration coincide with the ends of a cantilever, shown here as the quarter wavelength, *λ/4*, and half wavelength, *λ/2*. However, for length mode oscillations since one end of the cantilever is clamped, an additional vibrational mode is available, that of the quarter wavelength, *λ/4*. With this knowledge, all that needs to be determined in addition to these geometric dimensional values is the propagation speed of a wave in the piezoelectric medium. For the case of extensional vibration length and width modes of vibration, as shown schematically in Figure 3-2(a) this is calculate using the Young's Modulus, *E*, of the piezoelectric and the equation[144]:

$$c = \sqrt{\frac{E}{\rho}} \tag{4.1}$$

where *c* is the wave propagation speed in the medium, and *ρ* is the density of the medium. If it were shear mode vibrations that were occurring in our piezoelectric material, *E*, in equation (4.1) would be replaced by the Shear Modulus, usually abbreviated, *G*.

With knowledge of this speed of propagation, the length and width mode resonance frequencies in the piezoelectric medium are given by:

$$f_r = n\frac{c}{4l} = n\frac{\sqrt{\frac{E}{\rho}}}{4l} \tag{4.2}$$

and

$$f_r = n\frac{c}{2w} = n\frac{\sqrt{\frac{E}{\rho}}}{2w} \tag{4.3}$$

where *l* and *w* are the length and width of the cantilever, respectively and *n*=1, 2, 3 etc. for higher harmonic resonances. The factors of ¼ and ½ in the equations allows for the fractional harmonics of the fundamental wavelength.

To illustrate and validate this theory, consider the cantilever pictured in Figure 6-9. This PZT-only cantilever is 375 microns in width and 1.9 mm long. Table 4-1 presents selected length and width mode resonances that would be expected from such a cantilever according to equations (4.2) and (4.3).

Table 4-1: Calculated Length and Width Mode Resonances

		Resonance Modes (MHz)									
	Dimension (mm)	¼ f_r	½ f_r	f_r	$\frac{3f_r}{2}$	$2f_r$	$3f_r$	$6f_r$	$8.5f_r$	$9.5f_r$	$11f_r$
Length Mode	1.9	0.39	0.79	1.58	2.37	3.15	4.73	9.46	13.4	14.9	17.3
Width Mode	0.375	N/A	3.99	7.99	12.0	15.9	23.9	47.9	67.9	75.9	87.9

If we compare these calculated values to the spectrum of an actual cantilever constructed to these specifications, we find good agreement between the predicted and experimental location of resonance peaks. In Figure 4-1, the spectrum obtained from such a cantilever is plotted as the solid line, while the dashed vertical lines indicate the calculated positions of length mode resonances and the dotted vertical lines mark the positions of calculated width mode resonances.

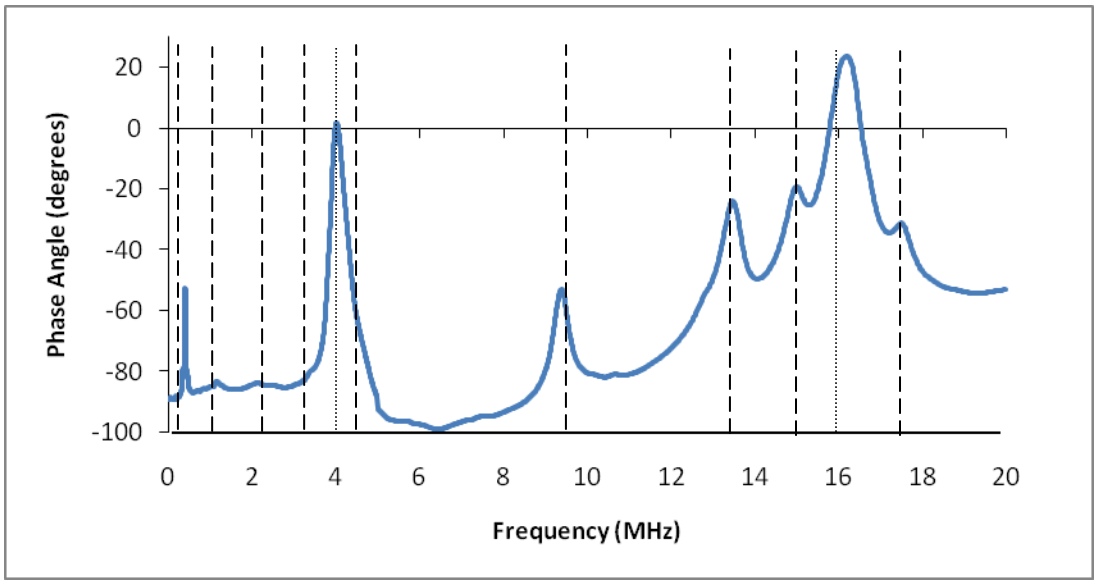

Figure 4-3: Resonance spectrum of 375 µm wide x 2 mm long PZT-only cantilever. Dashed vertical lines indicate calculated positions of length mode resonances Dotted vertical lines indicate positions of calculated width mode resonances.

From a comparison of Table 4-1 and Figure 4-3, we see that excellent agreement is found between the predicted length and width mode locations and experimentally determined resonances in such a cantilever. Specifically: A length mode peak was predicted at 0.39 MHz and was observed at 0.40 MHz. A width mode peak was predicted at 3.99 MHz and was observed at this value. Length mode peaks of lesser amplitude are observed between these values and higher harmonic length mode peaks are predicted and observed near 10 MHz and above. A width mode peak was predicted at 15.9 MHz and a strong peak was observed only slightly higher. Additionally, and interestingly, a length mode peak was predicted to occur at 4.7 MHz, and although the base of a strong peak at 4 MHz occludes this position, the asymmetry in this peak indicates that the 4.7 MHz peak is likely convoluted within this peak. Also, an interesting note is that the two highest intensity peaks are width mode peaks at $f_r/2$ and

$2f_r$. These peaks are 82 and 78° in amplitude, respectively, while all observed length mode peaks ($f_r/4$, $6f_r$ and $8.5f_r$) are between 28 and 32° above their local baselines. The reason for this observation is unclear at present.

This comparison of equations (4.2) and (4.3) with experimentally determined cantilever resonances validates the analysis of higher frequency peaks in piezoelectric cantilevers as length and width mode vibrations. Furthermore, the fact that the use of the Young's Modulus, (E_{PZT} = 60 GPa at room temperature)[145], in equation (4.1), validates the theory and that using the Shear Modulus (G_{PZT} = 40 GPa at room temperature)[145] does not correctly predict the locations of length and width mode peaks indicates that these vibrational modes are extensional or 'breathing' rather than shear in nature. In Chapters 5 and 6, extensive use of such resonance peaks will made in the detection of *Bacillus anthracis* and *Cryptosporidium*.

4.1.2 Lead Magnesium Niobate – Lead Titanate (PMN-PT) Based Sensors

As initially described in Chapter 3, the Shih and Shih group have pioneered formulation and process techniques to enable free-standing tape-casting of PMN-PMT on the order of tens of microns thick.[143] Free-standing piezoelectric tape such as this can then be metalized and made into a cantilever biosensor with superior detection sensitivities.[35] However, the thickness of the resultant tape, as compared with commercial PZT (as thin as 8 μm for PMN-PT as compared to 127 μm for PZT) requires more advanced processing and handling techniques due to its increased fragility. This free-standing tape must have electrodes deposited on its top and bottom surfaces for electrical actuation and detection. Also, the non-piezoelectric layer must be deposited onto one of these electrodes in order for flexural resonance to be realized. Additionally,

an insulation method must be used since the small size and unimorph nature of the resulting cantilever necessitate complete submersion in the analyte suspension.

While MEMS technology is not required to produce these PMN-PT microcantilever biosensors, inspiration is taken from such processes in order to effectively produce these cantilevers in as high a yield as possible. Namely, with the first step being to deposit thin electrodes upon the free-standing tape surfaces, it is common practice to deposit the electrode material onto just one surface first. This enables subsequent electro-plating techniques to be performed prior to dicing of the PMN-PT tape. If both sides of the tape were electroded prior to electroplating of the non-piezoelectric layer, it would be impossible to prevent the plating metal from covering both sides of the electrode-covered tape.

As such, to create a PMN-PT cantilever, first a 30 nm thick nickel layer with a 15–30 nm thick chromium bonding layer is first deposited on one side of the PMN-PT freestanding film by evaporation (E-gun Evaporator, Semicore Equipment, Livermore, CA) in order to form the first electrode. A tin layer is then electroplated onto this nickel surface at a rate of 0.5 mm/min using tin sulfate as the plating solution. This tin layer then serves as the nonpiezoelectric layer of the final unimorph cantilever and its thickness is chosen based on the thickness of the PMN-PT. For 22 and 8 μm thick PMN-PT-based cantilevers to be used for detection of *Bacillus anthracis* spore in Chapter 5, tin thicknesses of 20 and 6 μm were used, respectively. A 150 nm thick platinum on a 10 nm thick titanium adhesion layer is then evaporated onto the other face of the film to form the other electrode. Thusly, the tin non-piezoelectric layer is confined to only one side of the PMN-PT tape.

Following these deposition processes, the PMN-Pt/Sn bilayer is then embedded in wax and cut into the cantilever shape with a wire saw (Princeton Scientific Precision Wire-saw WS-22, Princeton, NJ). Gold wires are attached to the top and bottom electrodes using conductive glue (XCE 3104XL, Emerson and Cuming Company, Billerica, MA) for electrical connection. The PMN-PT/Sn strips are finally glued to a glass slide or a plastic substrate with epoxy (Hysol 1C, Loctite Corporation, Rocky Hill, CT) and embedded in epoxy as shown in Figure 3-7 to form the microcantilever geometry and electrically insulate the gold wires. Sections 4.2.1 and 4.3.2will detail the insulation and functionalization methods, respectively, that allow for use of this sensor as a biological pathogen detector.

4.1.3 Cantilever Biosensor Arrays

The preceding sections explain how various embodiments of single piezoelectric cantilever biosensors can be fabricated. As discussed in Section 3.2.3, though, the natural next-step for these biosensors is integration into a true multiplexed array platform for continuous, real-time, *in situ* detection of pathogens with simultaneous confirmation of detection and determination of false positives by complementary cantilever biosensors. Much of this author's time and effort been focused on this goal during the past years. With the platform of the single piezoelectric cantilever biosensor having been well tested and characterized, the goal was to engineer effective fabrication techniques such that multiple cantilevers can be produced with nearly identical geometries and resulting resonance spectra.

While the simplest piezoelectric cantilever biosensor array is comprised simply of more than one individually fabricated single biosensor, this process of array production

necessarily consumes the time required to produce each individual cantilever separately and then situate them in the flow chamber. Additionally, even the most experienced cantilever-makers have great difficulty producing consistently geometrically identical cantilevers. As such, the approach of this author sought to combine several common fabrication steps into one and reserve much of the tedious cutting processes until near the end of processing. This has the effect of speeding the production of such arrays as well as precisely controlling the geometrical dimensions of the final cantilevers produced. While this array fabrication procedure has gone through many iterations and improvements, the procedure which follows represents the current, and best known method for piezoelectric cantilever array production.

For construction of an array of PZT-glass cantilevers, this method begins with the bonding of a PZT layer to a glass layer to form a PZT-glass bilayer, much the same as the first step of single PZT-glass cantilever construction. However, this bilayer can be quite a bit wider than in standard single-cantilever construction as multiple adjacent cantilevers will eventually be cut from this blank by means of a precision wire-saw (Princeton Scientific Precision Wire-saw WS-22, Princeton, NJ). Additionally, copper foil (25μ m thick, Alfa-Aesar, Ward Hill, MA) of similar width as the PZT layer is bonded to the nickel electrodes of the PZT prior to cutting of the array to allow for subsequent attachment of longer wire leads to each cantilever. For PZT-only and PMN-PT cantilevers, the procedure is adjusted accordingly.

Regardless of the type of array, first, the desired final cantilever array to be constructed is sketched. This enables the fabricator to determine what size parts for the assembly will be needed. Figure 4-4, below is an example of one such sketch.

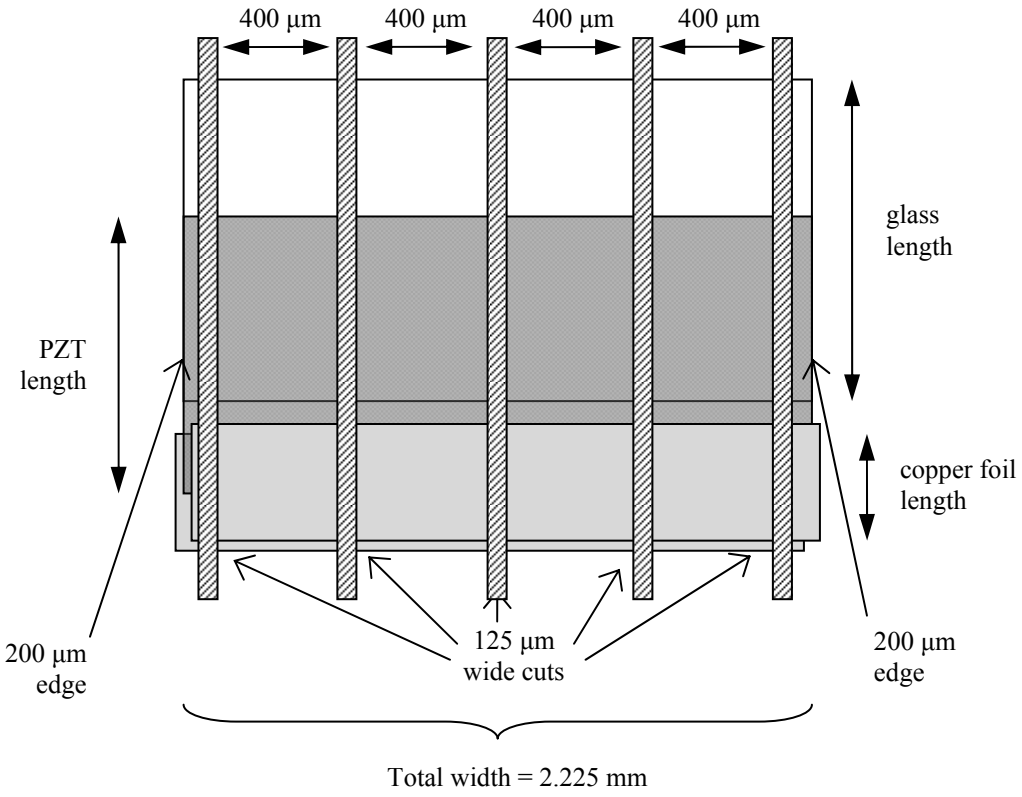

Figure 4-4: Pre-fabrication cantilever array sketch

This fabrication plan will yield a cantilever array comprised of four, 400 µm wide PZT-glass bimorph cantilevers. Once this sketch and appropriate calculations are made, the widths of the PZT, glass and two pieces of copper foil needed for fabrication are determined. These pieces are cut and the PZT layer is glued to the glass layer as in Section 4.1.1.1. One piece of copper foil is then soldered to the top electrode of the PZT and one piece is soldered to the bottom electrode. In early methods of array construction, conductive glue, as in Section 4.1.2, was used to bond these foil layers to the PZT electrodes, but it was later determined that significantly better electrical connections were attained by taking the time and effort to neatly and continuously solder the edge of the

copper foil along the width of the PZT electrode. This improvement led to markedly lowered baselines of the resonance spectra – *i.e.* away from resonance, the entire system became more capacitive (a characteristic of the PZT itself) and less resistive (indicating poor connections in the system) in nature. Figure 4-5 shows a side-view schematic of the final glass/PZT/copper foil soldered assembly prior to cutting.

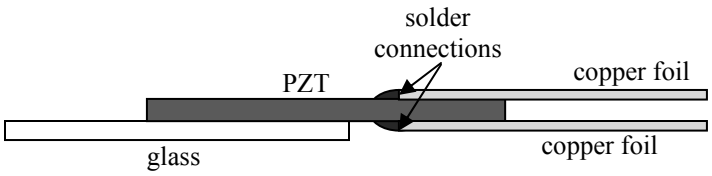

Figure 4-5: Side view of cantilever array prior to wire-saw cutting

Once this PZT-glass-copper-foil assembly is completed, its bottom side (*i.e.* with the glass layer down) is embedded in non-conductive epoxy onto a glass or plastic substrate (as required by the application). Care is taken such that the desired protrusion of the PZT-glass bimorph is made over the edge of the substrate, similar to the setting of the clamp in Section 4.1.1.1. In this way, the common length of the cantilevers is defined, but the top surface of the PZT-glass-copper-foil assembly is still available for cutting by the wire saw. Once this epoxy is cured, the entire assembly is embedded in wax and mounted upon a cutting stage mounting block for the wire saw. Once the wax is cooled, the sample is mounted in the saw and the manual micrometer is used to position the wax-covered PZT-glass-copper-foil assembly under the wire at the appropriate position for the first cut, as indicated in the sketch.

According to this example pre-fabrication array sketch, the widths of the PZT, glass, and other layers needed for construction will be approximately 2.3 mm. This

dimension allows for the production of four 400 μm wide cantilevers, while also accounting for the width of each cut to be made (~125 μm) and some waste material at the edges of the end cantilevers. This waste material results from the fact that it is impractical to make a completely perfect starting PZT-glass bilayer and also allows for a bit more error than usual in the parallel- and square-ness of this starting bilayer as these edges will be cut off with by the wire-saw. The production process is, thus, speeded by this edge allowance.

As for the 125 μm allowance for each cut: this stems from the fact that 100 μm thick tungsten wire has been determined as the most effective for cutting these cantilever arrays and also from the fact that the cuts resulting from this wire-saw are typically 25% wider than the particular wire used. This is because the actual cutting is accomplished by the back-and-forth motion of silicon carbide particles that make up the cutting slurry.[146] The oscillations of the wire simply provide the motion and energy for these particles to wear away and remove material in the sample being cut; thus the final cut with is wider than the actual width of the wire itself.

With the positions of the cuts to be made in the PZT-glass-copper-foil assembly laid out in Figure 4-4, the only remaining dimensional variable is the depth of the cut to be made. While difficult to control, this dimension is critical as the cuts must be sufficiently deep in order to mechanically and electrically separate each cantilever in the array, but cuts that are too deep will lead to additional fabrication effort and time. This additional effort arises in the form of having to connect individual wires to each individual ground lead on each cantilever if cuts are made clear through the bottom copper foil layer of the assembly. If the wire saw cuts are made such that at least some

section of the bottom copper foil layer remains connected, while the cantilevers protruding over the edge of the glass substrate are completely cut through, it is possibly to use a common ground lead for all of the cantilevers in the array. This greatly reduces the tediousness and time required for some of the final assembly steps of the array.

However, with the wax that secures the assembly during cutting obscuring the fabricator's determination of the depth of this cut, several practical methodologies have been developed by this author. First when mounting the PZT-glass-copper-foil assembly onto the wire saw mounting stage, ensure that the edge of the assembly that will become the cantilevers is elevated slightly, while the edge of the assembly that is comprised of the back ends of the copper foil is accordingly, relatively depressed. This will ensure that the cantilevers are cut through before the bottom copper foil layer. Also, it is critical that the top layer of copper foil be separate by wax from contact with the bottom layer of copper foil. By effecting this mounting technique, and by leaving a small section of the top layer of copper foil uncovered by wax along its entire width, a handheld digital electronic multi-meter can be used to determine when cuts have been made sufficiently deep.

This is accomplished by setting the multi-meter to its 'conductivity beep test,' or equivalent. With the multi-meter in this mode, the wire saw is stopped and the probes of the multi-meter are touched to the copper foil on either side of the cut being made. If the multi-meter indicates conductivity between its two probes, it is concluded that the cut has not been made completely through the top piece of copper foil, the top electrode of the PZT and the solder connecting the two. The saw is then restarted and allowed to continue cutting. After a period of time, the saw is stopped again and the same test is

performed. Once the multi-meter indicates that there is no conductivity between the two sides of the cut, it is concluded that the cut is sufficiently deep. Furthermore, if the original mounting angle of the sample, as described above, is correct, it will also be the case that the wire has cut completely through the protruding PZT-glass bilayer. Thus, the micrometer on the saw is adjusted so that the wire is aligned with the desired position for the next cut.

After all cuts are made, the sample is demounted from saw, and acetone is used to dissolve the wax fixing the sample to the wire saw mounting block. Once this cut PZT-glass-copper-foil assembly is freed from the wax, a piece of ribbon wire is cut and stripped for use as final leads to the electronic monitoring equipment. If the correct depth of cuts were made, this ribbon wire should contain wires for the number of cantilevers cut, plus one for the common ground lead - e.g. five wires would be needed in the case of an array fashioned after of our example sketch. This ribbon wire is then epoxied in place behind the cut PZT-glass-copper-foil assembly, and once the epoxy has cured, soldered connections are made to the bottom piece of copper foil for the ground wire and to each individual copper tab connected to each cantilever.

In Figure 4-6, we see an example of a PZT-glass cantilever array at this stage of construction. To be sure, these fine solder connections are tedious, but practice and patience make the job bearable. Notice that the copper tabs are bent upward to facilitate the solder connections. With these electrical connections made, the cantilever should be capable of resonance upon testing with an impedance analyzer (Agilent 4294A, Agilent, Palo Alto, CA). The ground lead is connected to one terminal of the impedance analyzer and each cantilever lead is sequentially connected to the other terminal for function

testing. If any cantilever resonance spectra are found to be nonexistent or of poor quality, it is possible at this point to de- and then re-solder the connections just made, and also to ensure that no copper tabs are shorting to ground or to each other.

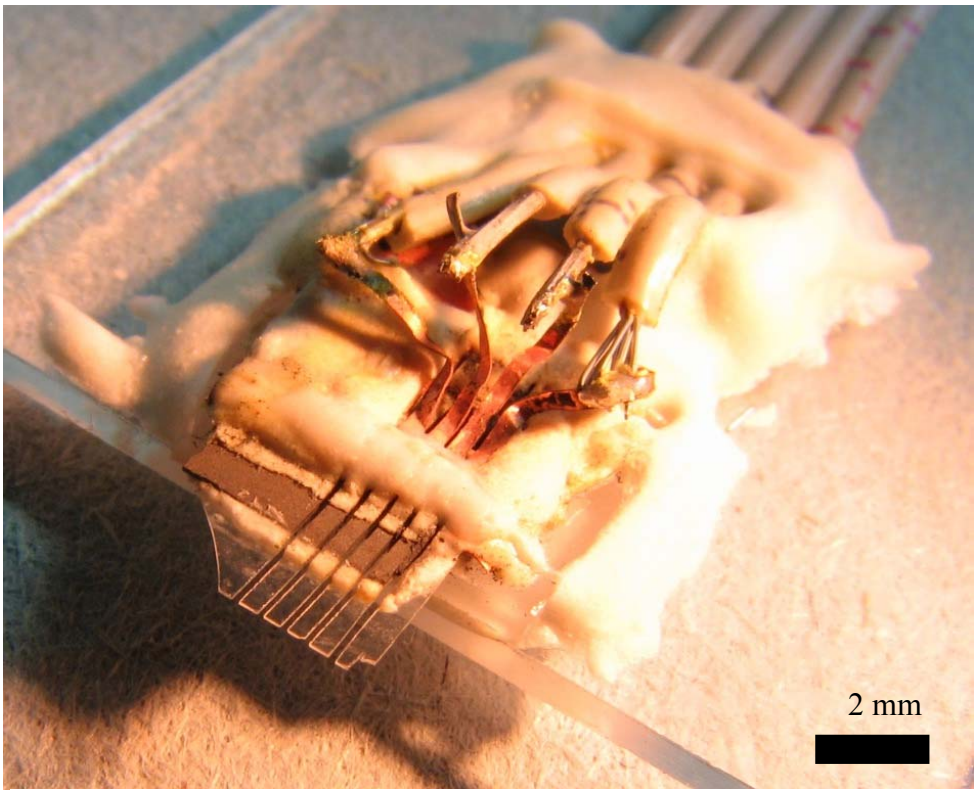

Figure 4-6: PZT-glass array after wire saw cutting and attachment of ribbon wire leads

Once the resonance spectra of the array are deemed acceptable, the copper tab – ribbon wire connections are potted in epoxy and allowed to cure. This prevents corrosion of the copper and solder connection that would occur in and near aqueous environments. Once the epoxy is cured, this new cantilever array is ready for insulation.

First, though, a brief word regarding the width of cantilevers in arrays constructed as described above: The width of 400 μm for each cantilever in the array is a width

determined to be the narrowest width that can consistently be cut while still retaining good cantilever yield and function. From equation (3.12) we recall that minimizing the width of our cantilever to be built will improve the detection sensitivity of the cantilever. As such, we desire to make the cantilevers in our array as narrow as possible. The arrow in Figure 4-7, below indicates the smallest cantilever successfully cut by a wire saw that did not break during cutting and actually possessed a resonance spectra upon testing. This cantilever was 150 μm in width. However, after insulation procedures, the cantilever no longer functioned. Many additional attempts at cantilevers of such widths as well as 200, 300 and 350 μm widths have been unsuccessful. As such, 400 μm is the standard width for cantilevers in these arrays – it represents the best blend of sensitivity and consistency of yield.

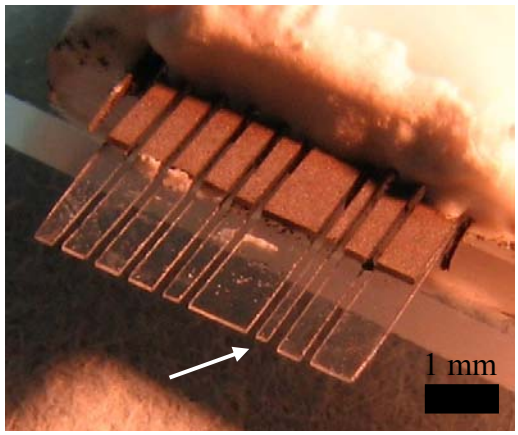

Figure 4-7: PEMS array with narrowest (150 micron) functioning cantilever cut to date

4.2 Sensor Insulation

As discussed above, for any piezoelectric biosensor to be fully submerged in the analyte suspension medium, effective insulation must first be applied to the electrodes of the sensor to avoid electrical loss and short circuiting through the aqueous medium. The

Shih and Shih group have developed two different techniques[33,40] that both insulate piezoelectric cantilever electrodes while also allowing for subsequent functionalization with antibody.

4.2.1 Methyltrimethoxysilane (MTMS) Insulation

The first of these methods specifically applies to PMN-PT cantilevers as discussed in Section 4.1.2. These piezoelectric cantilever biosensors possess one electrode composed of platinum and one that is electroplated with tin. This variation in electrode material can, and indeed is, used advantageously to allow for insulation and subsequent bio-functionalization of the cantilever. The approach taken is to insulate just one of the electrodes and leave the other surface available for bio-conjugation, since this will sufficiently break the circuit between the two electrodes through the aqueous medium.

To insulate the non-piezoelectric layer of a PMN-PT/Sn PEMS, the PEMS is first soaked in a diluted (1:40 in water) piranha solution (one part 98% sulfuric acid (Fisher, Fair Lawn, NJ) with one part 30% hydrogen peroxide (FisherBiotech, Fair Lawn, NJ)) at 20ºC for 2 min. Methyltrimethoxysilane (MTMS) (95% Aldrich, Milwaukee, WI) is then spin coated (Headway Research, Garland, TX) on the tin surface at 2000 rpm and cross linked (pH = 9.5 for 2 hr) to form an MTMS coating on the tin surface. The step of MTMS deposition, spin coating and cross linking is then repeated to form a second insulation layer.[33-35] This procedure leaves the platinum electrode of the PMN-PT free for bio-conjugation, as will be discussed in Section 4.3.2.

4.2.2 3-MERCAPTOPROPYLTRIMETHOXYSILANE (MPS) INSULATION

The second method of piezoelectric cantilever (or cantilever array) electrode insulation used in this body of research insulates both cantilever electrodes at the same time, but allows for bio-conjugation to this insulation layer itself. This method is specifically suited for electrode surfaces that are covered by a metal oxide layer, such as exists on the nickel electrodes of commercial PZT. In this scheme, the siloxane moiety of the MPS molecules form silanol bonds with the oxide surface of the metal. This leaves the sulfhydryl groups available for antibody immobilization.

As in the procedure for MTMS insulation, the cantilever is first cleaned with dilute (1:40 v:v in water) piranha solution (1:1 v:v 98% sulfuric acid (Fisher, Fair Lawn, NJ):30% hydrogen peroxide (FisherBiotech, Fair Lawn, NJ)), at 20ºC for 2 min. It is then rinsed with excess anhydrous ethanol and submerged in a solution of 40 mM 3-mercaptopropyltrimethoxysilane (MPS) titrated with acetic acid to pH = 4.5 in ethanol for at least 4 hours. Finally, the cantilever is dried at 50^{o}C for 2 hours. This initial insulation procedure is repeated twice more so that a final MPS coating thickness of approximately 30 nM is achieved.[40]

Once a cantilever insulated in this fashion is removed from the oven after the last layer deposition, it is ready for immobilization of antibody onto its surface by means of sulfo-SMCC conjugation, as will be discussed in Section 4.3.3. Figure 4-8, displays the resonance spectra of a PZT-only cantilever after insulation by MPS. The blue trace is the spectrum of the cantilever in air while the red trace is the spectrum upon submersion in PBS. While the peak heights diminish slightly and the baseline deviates from -90^{o} marginally, the resonance peaks are still wholly monitorable for biodetection.

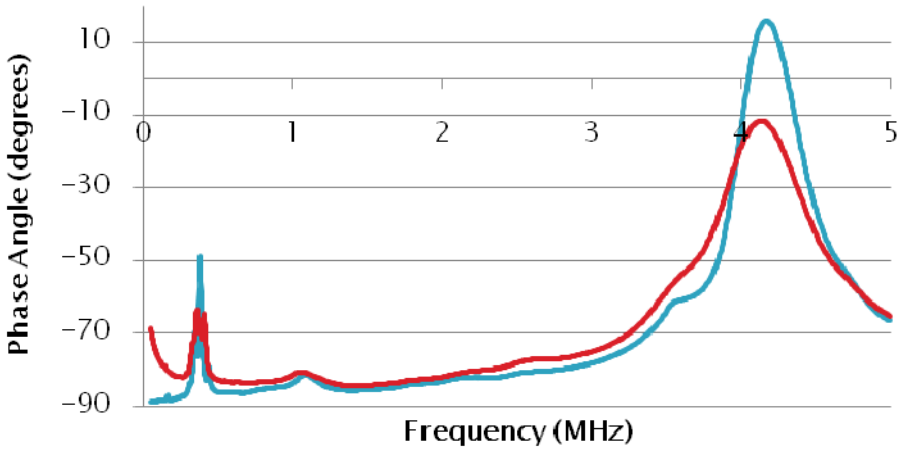

Figure 4-8: Spectra of an MPS-insulated PZT-only cantilever in air (blue) and in PBS (red)

Also, it should be noted that this insulation scheme possesses the advantage of extensive sensor reusability. Once a cantilever has been insulated, as just described, functionalized with antibody and used for detection, a re-insulation procedure (as modified from the original procedure) can be used to ready the sensor for a new round of biodetection.

First, the cantilever is rinsed with excess ethanol and dried at 50°C for at least two hours following the biodetection just performed. Then, it is cleaned with dilute piranha solution, as previously described, rinsed with ethanol, and immersed in the same MPS solution as above for at least four hours. It is then dried again and is now ready for immobilization of new antibody.

4.3 Sensor Functionalization

Once a piezoelectric cantilever biosensor (or biosensor array) is insulated according to the above protocols or if it is simply to have its tip dipped in analyte suspension, the

final step before biodetection can be commenced is the functionalization of at least one of its surfaces with antibody.

4.3.1 GOPTS TIP FUNCTIONALIZATION

When a cantilever is to be used for biodetection by dipping only its tip in the analyte solution, it is unnecessary to insulate the cantilever prior to antibody functionalization. As such, immobilization directly onto the tip of the cantilever can be accomplished using glycidoxypropyltrimethoxysilane (GOPTS). GOPTS is a bifunctional linker that does not require activation of itself or the antibody for proper conjugation. Similar to MTMS and MPS, GOPTS contains a trimethoxysilane group that readily binds to glass or metallic oxides.[37,147] By submerging a piranha cleaned tip of a PZT-glass or titanium cantilever into pure GOPTS for one hour this silane linkage is allowed to occur and leaves the glycidoxy epoxide moiety of the molecule available for covalent binding to primary amines of the antibody. The main advantage of this method is that since the glycidoxy group of GOPTS is highly reactive due to bond-angle instabilities, it serves the same purpose as the activated carbonyl group in functionalization using NHS/EDC, without the need for an additional activation step.[37]

4.3.2 NHS/EDC ACTIVATED MPA FUNCTIONALIZATION

To achieve functionalization on a noble metal surface, such as remains after insulation of a PMN-PT cantilever by MTMS, or as is present on the tip of a PZT-glass cantilever where the tip has been gold-coated, MPA (mercaptopropionic acid) is first used to carboxylate the noble metal surface. The MPA molecule forms a sulfide bond with the noble metal[148] leaving the carboxylic acid group of the compound available for subsequent activation and reaction with the antibody to be immobilized. To accomplish

this MPA coating, the cantilever, array or cantilever tip is cleaned once again with diluted piranha solution and then immersed in an aqueous 2mM MPA solution for two hours. The cantilever is then rinsed with DI water and immediately submersed in a solution of 2 mM N-hydroxysuccinimide (NHS) and 5 mM 1-ethyl-3-3-dimethylaminopropyl-carbodiimide (EDC) to activate the carboxylic acid group of the MPA for a period of forty minutes.

Once activated as such this cantilever is then again briefly rinsed with DI water, and submerged in a 0.2 mg/mL solution of antibody specific for the antigen to be detected. Immobilization is allowed to proceed for thirty minutes, after which time, the sensor is ready for biodetection.

4.3.3 SULFO-SMCC FUNCTIONALIZATION

When a cantilever or cantilever array is insulated with MPS, as in Section 4.2.2, the number of total steps needed for insulation and antibody functionalization is markedly reduced. Since the sulfhydryl groups available on the surface of such an insulated cantilever are readily reactive with other particular functional groups, it is the antibody, rather than the sensor surface, in this procedure that is activated in order to facilitate immobilization.

First, a 200 µl 1 mg/mL antibody aliquot is incubated with 1 mL of a 5 mM solution of sulfosuccinimidyl-4-N-maleimidomethylcyclohexane-1-carboxylate (sulfo-SMCC) at room temperature for a period of one hour. This step allows for conjugation of primary amines on the antibody molecule to the NHS-ester moiety of the sulfo-SMCC molecule. After this activation, excess sulfo-SMCC is removed from solution by centrifugation through a properly-sized filter (100 kDa for IgG). The MPS-insulated

cantilever is then dipped into this resulting solution of activated antibody for a period of one hour to allow the maleimide groups of the sulfo-SMMC molecule to bind to the sulfhydryl groups of the MPS.[40] After this time, the cantilever or array is ready for detection of biological pathogens.

4.3.4 Minimization of Detection Sensor Noise

When any PEMS, or indeed any real-time biosensor, is implemented for detection, some level of noise in the detection signal is always present. This noise level may be so large as to impede the observation of a resonance frequency shift, or it may be acceptably small such that detection is easily observed and signal to noise ratios (SNR) are high. Clearly, this second noise level scenario is desirable and every effort is made to attain such levels of noise.

Noise, in a plot of resonance frequency shift versus time has many sources, and it is important to address all of these sources individually to minimize their combined effects. Since our PEMS biosensors are all electrically actuated and detected, certainly electrical noise arising from poor electrical connections or insufficient shielding of wires can lead to sensor noise. Another source of electrical noise can arise from ineffective insulation. The methods for insulation described above have been shown to provide effective insulation over the course of several hours, but if these protocols are followed incorrectly, or if a sensor is used for an extended duration of time, electrical loss from one electrode, through the insulation, through the liquid medium, to the other electrode can cause increased levels of noise.

Beyond electrical noise, noise can also be of mechanical or geometric origin. In other words, a PEMS constructed with opposite sides (in the length and width direction)

that are not parallel can have poorly defined resonance frequencies, with low Q values, that in turn lead to noisier resonance frequency versus time results. Furthermore, an un-square epoxy clamp, or an epoxy clamp made of incorrectly-mixed epoxy can lead to low Q resonance peaks, and thus, increased noise.

The peak reconstruction software discussed in Appendices A and B have been developed to reduce the effects of noise, regardless of its origin, by more precisely locating resonance peaks for final generation of resonance frequency shift versus time results. While these algorithms have proven effective, it is imperative that care in the initial construction, insulation, and cleaning of PEMS and PEMS arrays be taken so as to minimize sensor noise as much as possible.

Along the path of PEMS or PEMS array construction, the main indication of future noise in detection experiments is the Q value of resonance peaks. Higher Q peaks will lead to lower noise in detection experiments. To accomplish the highest Q values possible for any PEMS construction scheme, the following steps should be followed, and checks performed, along the path of construction. First, the piezoelectric and nonpiezoelectric layers to be used in the PEMS or PEMS array should be cut such that their sides are square and parallel. For the case of PEMS array cut by wire-saw or other means, it is imperative that all cuts are made parallel. This is most easily accomplished by mounting the sample in the chuck, and ensuring that all cuts are made before the sample it de-mounted or the chuck is rotated.

With square and parallel edges of the cantilever(s) being constructed, the attention is then focused on the electrical connections to the piezoelectric electrodes. Whenever possible, neat, clean soldering should be used to connect wire leads to these electrodes. It

is currently the case that noble metals are used for at least one electrode of PMN-PT-based cantilevers. A future improvement in the production of these PEMS could incorporate nickel, or some other material that accepts solder, in this electrode. Once these electrical connections are made, if possible, testing on the impedance analyzer should be performed. Though, without a clamp in place, resonance peaks may be nonexistent or poorly defined, it is still possible to check for an acceptable baseline of the future resonance spectrum. If low-loss electrical connections have been made, this baseline will be very close to -90 degrees in the range of zero to 10 MHz.

Following this soldering check, application of a clean, straight epoxy clamp is the next critical step. This clamp serves two purposes: first, it provides the anchor point for resonance oscillations, but it also encapsulates the connections of the wire, or foil leads to the rear end of the piezoelectric electrodes. This encapsulation is critical for any subsequent in-liquid experiments. Once this clamp is applied and cured, a first check of the resonance spectrum in air is performed on the impedance analyzer. In the phase angle versus frequency spectrum, this stage of construction should provide the best spectrum that will ever be observed for this particular sensor. The most important factor in assessing this spectrum is the Q factor of the peaks. At this stage, Q values higher than 50 will likely provide fair detection results after insulation and functionalization. Q values higher than 75 at this stage are ideal. Q values below 25 at this stage will only worsen upon later processing and such a peak should be deemed un-usable.

Presuming this first Q-check is passed, the Q should be checked again after each subsequent round of insulation and functionalization. Once insulation is completed, the spectrum of the PEMS can be checked in air as well as in liquid. The Q values of peaks

in air should not deviate more than 10 from the originally measured Q, but this Q value may be lessened by as much as half once submersion in water or buffer is performed. However, as long as the Q value of a particular resonance peak remain above about 25 once submerged in liquid, this peak can be deemed a useful candidate for detection experiments.

4.4 Detection Flow System Design and Materials Considerations

4.4.1 Sample Delivery Systems

When any real-time biosensor is used for detection of a pathogen in a fluid medium, an engineered fluid flow system is a requirement. The only alternative to a flow system for sample delivery is a passive diffusion-based detection system. While, with high concentrations of analyte, this is a feasible approach[37], the brief analysis in Chapter 1 has shown that fluid flow becomes a necessity as analyte concentrations dwindle. The fluid in which a pathogen is detected can be liquid, or air, and in the case of liquid, it can be a buffered aqueous system, DI water or some other solvent. Each type of fluid presents its own design challenges and constraints, but whatever the case, the interactions of the fluid, the analyte of interest contained in the fluid and the sensor itself must be carefully considered in order to achieve optimum sensor performance. Nonetheless, rarely, if ever, has recently published biodetection research given even a cursory treatment of this topic on the length scales required for detection of biological cells, spores and oocysts. In some instances of literature, perhaps the geometry of the flow chamber in use is discussed, but treatment of the actual forces resulting from fluid interactions with the analyte and sensor surface is negletcted.[113,133,135,136,149] In other instances, it is discussed that fluid flow of the analyte suspension is used, and sometimes

even the volumetric flow rate is given, but there is no mention of flow chamber geometries and flow characteristics.[9,138,139]

In Chapter 1 of this dissertation, the need for controlled fluidics in biosensor systems was identified, and this need will be addressed in this section. First, an introductory discussion of the types of fluid flow systems is in order. There are two main implementations of flow that are possible in biosensor systems: The first is a closed-loop, recirculation system, while the second is a flow-through, one-way system. Each type of system has its own advantages and disadvantages.

4.4.1.1 Closed-Loop Recirculation System

The closed-loop recirculation system, as depicted in Figure 4-9(a), below, is much as its name indicates. It is comprised of a flow cell or chamber, a pump and tubing connecting the two. In this case, the flow cell contains a PEMS sensor for biodetection. In Figure 4-9(b)[35], a more sophisticated, and practical closed-loop flow system is depicted schematically. In this system, there are three total three-way valves, with two valves in the actual circulation loop. In normal operation, these valves, labeled V2 and V3 would be set such that the closed loop is completed. In order to fill the loop initially, in this case with PBS solution, all three valves would be set in such a way that the PBS flows in an open-loop fashion from its reservoir, through V1, through V2, through the pump and flow cell, through V3 and to the waste container. Once this section of the loop is filled, valves V2 and V3 would be turned 180 degrees, so that the flow of PBS follows from its reservoir, through V1, through V2, through V3 and to the waste container. In this way, the tubing between valves V2 and V3 is filled and the entirety of the closed loop system is primed with PBS.

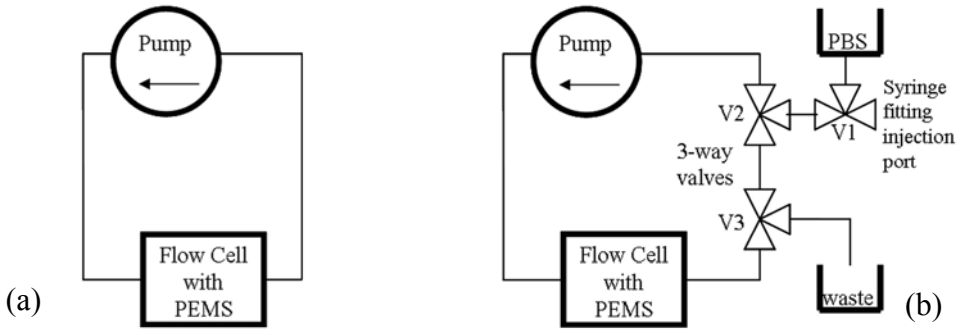

Figure 4-9: Closed-loop flow system embodiments

A further utility of this design is that analyte sample can be injected into the closed-loop system without removing the PEMS sensor from its established environment, changing the pressure of said environment, or otherwise disturbing the sensor. This is accomplished by fitting an injection syringe to the free opening of valve V1. Valves V2 and V3 are then set in the same manner as was used to fill the tubing between V2 and V3 and V1 is set so that open flow is established through itself from the syringe to valve V2. The syringe can then be used to fill the tubing between V2 and V3 with analyte suspension. Then, once the valves are set such that closed-loop flow is established, the sample in the tubing between V2 and V3 is mixed with the PBS in the rest of the system and delivered to the flow cell containing the PEMS.

In such a closed-loop flow system, the sample that has been injected into the system is then circulated *ad infinitum* until the user (or automated control system) deems it necessary to flush the whole system and begin again. This continuous delivery and re-delivery of the same analyte system has the advantage of allowing for detection of biological pathogens in very low concentrations. That is, imagine just one pathogen was

present in the entire close-loop detection system. As the pathogen passes through the flow cell and near the PEMS, depending on the properties of the fluid flow and the receptor immobilized on the sensor surface, there is a finite chance that this pathogen will be captured by the receptor on the sensor surface, thus inducing a frequency shift in the resonance of the PEMS. The key word, though, in this hypothetical situation is 'chance.' There is no guarantee that our single pathogen will be detected on its first pass over the PEMS sensor. Thus, provided the pathogen does not adhere to the walls of the tubing or valves, as will be addressed in Section 4.4.3, the closed-loop recirculation system continually passes this pathogen through the flow chamber and near the surface of the PEMS, such that, with each circulation, the chances of detection are increased.

If it is a must that this single pathogen, or perhaps more realistically, pathogens in extremely low concentrations be detected, then a detection algorithm need be implemented such that the number of recirculations is sufficiently high that sufficiently high statistical sensitivities and specificities are achieved. However, it may be the case that the number of recirculations required, far outstrips the time available for such detections. If real-time detection is a requirement and, say, 30 min is the maximum time allowed per assay, but statistics dictate that recirculations be performed for at least 1 hour for proper detection, clearly there is a disconnect. This issue can be addressed by increasing the flow rate of the system, though, as we will see shortly, this, in turn, has ramifications as to the efficiency of detection of the pathogen by the sensor surface. Another approach to decrease the total time needed for detection in a recirculation system is to decrease the total volume to be recirculated. This approach was taken by this author in the detection of BA in PBS where just 800 μl of analyte solution were circulated

through the system at a flow rate of 1 mL/min.[35] This means that one complete recirculation of analyte took only 48 seconds. Using this approach, successful detection of just thirty six total BA spores was achieved. Figure 4-10 is an image of this detection system, as modeled after Figure 4-9(b), above.

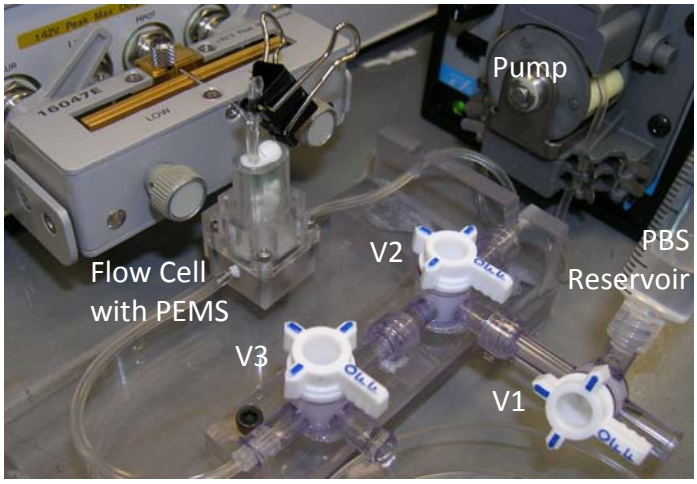

Figure 4-10: Image of recirculation system used for successful detection of 36 BA spores in PBS

It is the case, however, as required by particular types of detection, that neither faster recirculation speeds, nor smaller analyte volumes will appropriately enable highly sensitive and specific real-time detection as needed. In this case, a flow-through, one-way detection system may be necessary.

4.4.1.2 Flow-Through One-Way System

A flow-through, one-way fluid flow system is particularly well suited when processing of large volumes of analyte fluid is required. This system can also be an appropriate choice when, as dictated by the pathogen to be detected and the antibody immobilized on the sensor surface, fluid flow speeds must remain relatively slow. Figure 4-11 is a schematic representation of a typical flow-through, one way system. In this

type of system, there is just one valve which is used to select between two reservoirs leading through the pump, through the flow cell and into a waste collection container. This valve, labeled V1 in the figure, is initially set such that the PBS reservoir is selected in order to fill the tubing, pump and flow cell with buffer. Once this is accomplished, the valve is turned so that the sample reservoir is connected to the pump and analyte suspension is flowed through the flow cell.

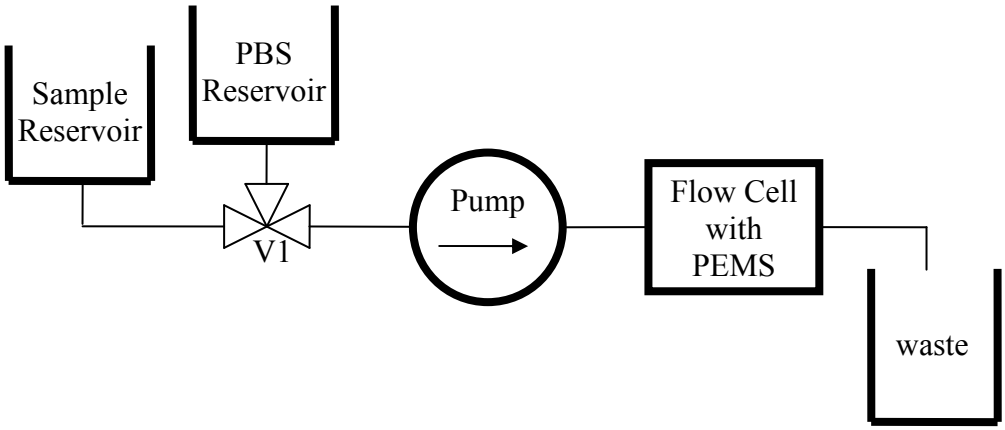

Figure 4-11: One-way flow-through detection system embodiment

The PBS reservoir in Figure 4-11 can be any analyte fluid desired, as dictated by the needed detection. Figure 4-12, below is an image of a one-way, flow-through detection system used in the detection of *Cryptosporidium* oocysts in tap water.

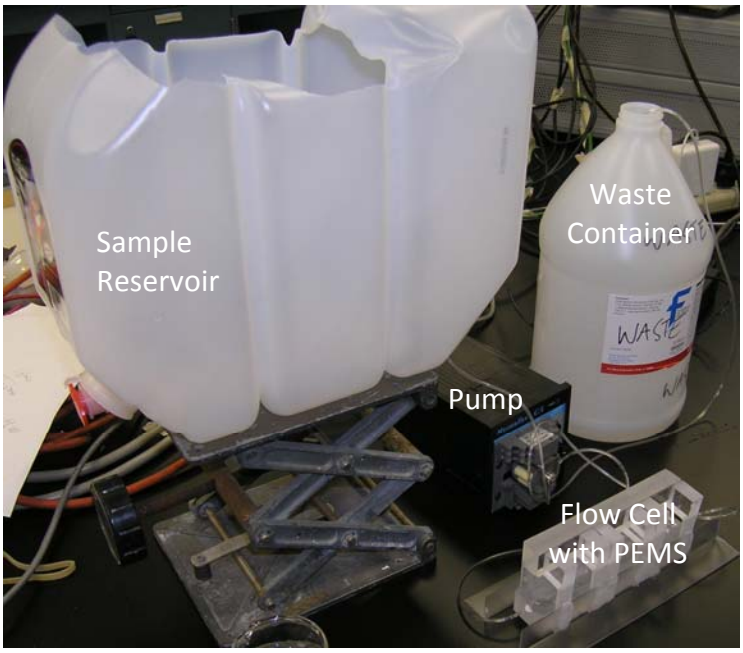

Figure 4-12: One-way, flow-through system used for detection of *Cryptosporidium* oocysts

Such a system is required for this application as oocysts are usually found in tap and surface waters in concentrations of just a few per liter of water.[20,24,27,32] Thus, if time-consuming pre-concentration of sample is to be avoided, large volumes of water must be processed in order to examine a representative sample.

4.4.2 Engineered Fluidics – Sensor Flow Cell Design

Thus far, discussion concerning pathogen-containing fluid delivery to the sensor has been focused on the entire delivery system from beginning to end. However, this discussion has not touched upon issues such as tubing size, pump speed and the actual resultant flow rates through the tubing and flow cell. The reason for this conspicuous absence is that these topics are entire areas of engineering unto themselves. The forgoing sections will detail the properties and constraints that go into designing an effective flow

chamber in which the PEMS performs its detection as well how this design affects the pump and connective tubing requirements of the entire system.

4.4.2.1 Laminar Flow and Fluid Flow Speeds

One of the most basic and important properties of any fluid in motion is its Reynolds Number, abbreviated 'Re.' The Reynolds Number is a function of the density, ρ, dynamic viscosity, μ, average velocity of the fluid, $\bar{v}$, and the characteristic length of the channel in which the fluid is flowing, D, according to the following equation[150]:

$$Re = \frac{\rho D \bar{v}}{\mu} \tag{4.4}$$

The characteristic length of a fluid flow channel is its width if it is rectangular in cross section, or its diameter if it is circular in cross-section. The average velocity of a fluid in a channel or duct is given by:

$$\bar{v} = \frac{Q}{A} \tag{4.5}$$

where Q is the volumetric flow rate of the fluid, and A is the cross-sectional area of the fluid flow channel.

It is important to know the Reynolds Number of a particular fluid flow in a channel, as knowledge of this number allows one to make further assumptions concerning the flow pattern itself. When the calculated Reynolds Number for a particular system is less than 2000, the fluid flow is termed 'laminar,' while when the Reynolds Number exceeds 2000, the flow is termed 'turbulent.'[150] Laminar flow, as the name suggests, is a type of fluid flow where the fluid in motion is characterized by nice, neat layers that share common velocities and pressures as they flow over, under or next to

adjacent layers. Of course, these layers are layers in the sense of infinitesimally small elements as in calculus, but the important aspect of laminar flow is that the properties of fluid velocity and pressure vary continuously as one moves from the wall of the flow, through the center of the channel and to the far wall. As such, concise formulae can be derived to predict the fluid flow properties at given points in space based simply on the fluid's physical properties as well as the volumetric flow rate and the geometry of the channel through which the fluid is flowing. In the case of turbulent flow, there are marked discontinuities in these flow velocity and pressure gradients such that neat mathematical formulae cannot be used to precisely ascertain values at given points in a flow – numerical approximations are the best that can be attained for such flow systems.

Fortunately, in the case of the flow systems to be discussed and designed in this dissertation, we are decidedly in the laminar regime of fluid flow. Most Reynolds numbers we will deal with will be between 0.1 and 10 with the highest value we will attain on the order of 100 - still a full order of magnitude below the laminar-to-turbulent transition. Since we know our fluid flow to be laminar in the flow channels we will design and since the depth of the channel will be at least as large as the width, the following two dimensional equation for laminar flow velocity profiles will prove immensely useful:[150]

$$v(z) = \frac{3}{2}\bar{v}\left(1 - \left(\frac{2z}{h}\right)^2\right) \tag{4.6}$$

This equation provides the fluid velocity, v, as a function of distance, z, from the centerline of the channel, where h is the total width of the flow channel and $\bar{v}$, again, is the average fluid flow speed in the channel as calculated by equation (4.5). Upon

examination of this equation, we see that the velocity profile of a fluid flowing in a channel is parabolic in nature and that it diminishes to zero at the walls of the channel. The fact that velocity diminishes to zero at the wall of a fluid flow channel holds for both laminar and turbulent flows and is referred to as the 'no-slip' condition.[150] Figure 4-13 schematically represents this two dimensional flow channel and velocity profile as viewed from above.

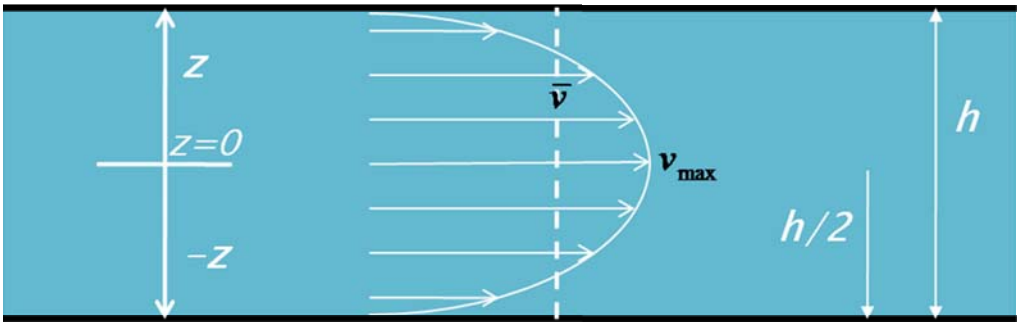

Figure 4-13: A 2-D schematic representation of a fluid flow channel with a laminar parabolic flow velocity profile

In this figure, we see that *z=0* is defined as the center of the channel and that the flow velocity profile is symmetric about this point. Additionally, we see that v_{max} occurs at this point where *z=0*, or equivalently, a distance *h/2* from the wall at the center of the channel. As such, the fluid velocity at the center of the channel is defined as:

$$v(0) = \frac{3}{2}\bar{v} = v_{max} \tag{4.7}$$

Similarly, according to equation (4.6) and the no-slip condition, the velocity at the wall of the flow channel is given as:

$$v\left(\frac{h}{2}\right) = 0 \tag{4.8}$$

A more interesting and important case, as we will see in Section 4.4.2.2, arises when we examine the velocity of fluid flow at a very small distance from the channel wall, which we will call *d*. At this distance, *d*, from the wall, the velocity of the fluid flow is defined as:

$$v\left(\frac{h}{2} - d\right) = \frac{3}{2}\bar{v}\left(\frac{4d}{h} - \frac{d^2}{h^2}\right) \tag{4.9}$$

However, since $\frac{d}{h} < 1$ and, thus $\frac{d^2}{h^2} \ll 1$, we can approximate equation (4.9) as:

$$v\left(\frac{h}{2} - d\right) \approx \frac{3}{2}\bar{v}\frac{4d}{h} \tag{4.10}$$

4.4.2.2 Forces Resultant from Laminar Flow

With knowledge of the laminar fluid velocity at various points across the breadth of a channel, it is possible to further calculate the forces imparted to particles that might be contained within this flow. To calculate these forces we look to Stokes' Law for the frictional force of fluids on a settling spherical particle:[151]

$$F = 6\pi\mu a v \tag{4.11}$$

where μ, is again, the dynamic viscosity of the fluid, *a* is the radius of the particle in motion and *v* is the velocity of the particle.

Stokes' Law is originally derived for spherical particles settling under the influence of gravity in a stationary liquid, however, the same phenomenon applies to any

sphere in a fluid where the sphere is moving relative to the fluid, or equivalently, the fluid is moving relative to the sphere. In our case, we will consider the case where the particle in question is our biological pathogen to be detected by our PEMS biosensor and the fluid is the analyte liquid suspension containing the biological pathogens. When our pathogen is adhered to our biosensor surface, or one of the walls of the flow channel, the relative velocity between the pathogen and the fluid flow is equal to the velocity of the fluid flow. When the particle is moving relative to the sensor and walls at a velocity greater than zero, the effective velocity, *v*, in equation (4.11) decreases, and thus the force on the particle decreases. Thus, the maximum force impingent on a pathogen occurs when it is bound to a stationary object in the sensor flow system. Considering this, in conjunction with the equation for the fluid flow velocity profile in our flow channel, as given by equation (4.6), we see that the force impingent on our biological pathogens when adhered to a surface is a function of the pathogen's distance, *z*, from the centerline of the channel according to:

$$F(z) = 6\pi\mu a v(z) = 9\pi\mu a\bar{v}\left(1 - \left(\frac{2z}{h}\right)^2\right) \tag{4.12}$$

Thus, considering the special cases for velocity discussed above, we can calculate the forces impingent on a stationary sphere in the center (*z=0*) of our flow channel as:

$$F(z = 0) = 9\pi\mu a\bar{v} \tag{4.13}$$

Also, since our pathogens to be detected, such as *Bacillus anthracis* spores, *Cryptosporidium* oocysts and bacterial cells have finite diameters on the order of one to six microns, the case exactly at the wall of our flow channel (*z=h/2*), becomes irrelevant

as the center of the pathogen cannot become closer than its radius to the wall. The case of fluid flow velocity only a small distance, *d*, from the wall (*z=h/2-d*), however, becomes very important, since when we consider the case where *a*, the radius of our pathogen is equal to this small distance *d*, *i.e.* our particle is in contact with the wall, we arrive at the following relation:

$$F\left(z=\frac{h}{2}-a\right)=\ 36\pi\mu\frac{a^2}{h}\bar{v} \tag{4.14}$$

This theoretical examination of fluid forces impingent on particles adhered to, or near surfaces in a laminar flow has been examined experimentally and simulated numerically for confirmation of its validity.[152-154] While the validity of this analysis was confirmed, it was determined that in close proximity to a surface in the fluid flow, a particle experiences forces greater than those predicted by derivation from Stokes' Law alone. These increased forces arise from the fluid's interaction with the surface and range from a correction factor of 1.06 at a distance of 10 times the radius of the particle (*10a*) from the wall, to a correction factor of 1.70 at the point where the particle contacts the wall. As such, we see that equations (4.13) and (4.14) become:

$$F(z=0)=(1.70)9\pi\mu a\bar{v} \tag{4.15}$$

and

$$F\left(z=\frac{h}{2}-a\right)=(1.70)36\pi\mu\frac{a^2}{h}\bar{v} \tag{4.16}$$

for the case where our pathogen is in contact with a sensor positioned in the center or wall of the flow channel.

Examining equations (4.15) and (4.16), we see that the force at the center of the flow channel is a linear function of the radius of our pathogen, while the force on a pathogen in contact with the wall is a square function of this radius. And with this radius on the order of microns as just discussed, the differences in the force on a pathogen in the center of flow versus one near the wall can be up to six orders of magnitude.

An initial reaction to this comparison might be that our PEMS biosensor should be placed at the wall of the flow channel so as to minimize the forces impingent on any potential pathogen to be detected. In this way, the fluid force counteracting the interaction force between our sensor-immobilized antibody trying to 'capture' the pathogen will be minimized and the chances of capture will be maximized. While this is true, it is also the case that non-specific interactions of other particulate matter in our analyte suspension will also be maximized, thus increasing the chances of a false positive detection.

4.4.2.3 Application-Inspired Flow Channel Design

Some biosensors, such as SPR and QCM are limited in their possible locations within a flow channel due to requirements of optical illumination on the back-side of the sensor surface in the case of SPR, or due to requirements of the sensor holder configuration in the case of QCM. Such sensors must be positioned at the wall of a flow channel with the sensing surface contacting the flow. However, our PEMS biosensor is not limited in its location in the flow channel since, as discussed in Section 4.2, effective insulation of the PEMS by means of MTMS or MPS allows the sensor to function while fully submerged in aqueous solution such that both sides of the cantilever are available for biodetection.

With this possibility of positioning the PEMS biosensor anywhere from the center of fluid flow to very close to the wall, we are able to take full advantage of the implications of equations (4.12), (4.15) and (4.16). In other words, we can use the forces impingent upon particles in a fluid flow to our advantage. Since the interaction force between an IgG antibody and its specific antigen has been determined to be on the order of 10 to 100 pN[155], we have a starting point for our flow cell design. The goal of this design is two-fold:

1. To keep the forces impingent on the pathogens to be detected sufficiently low such that detection is not hindered or prevented and;
2. To use the flow of the analyte suspension to increase the natural selectivity of antibody receptors by minimizing the interaction of non-specific particles with the sensor surface.

Flow cell design goal (1) is straightforward enough to implement. Based on the diameter of the pathogen to be detected, and the desired position of the PEMS biosensor, we perform the necessary calculations to determine the channel dimensions and corresponding volumetric flow rates in order to keep the forces acting on the pathogen at the sensor surface sufficiently low. Since this range of antibody interaction forces is just that, a range, experimentation will be required to find the conditions which give the best sensor performance. In this body of research, this is carried out by building a custom flow channel of fixed dimensions and then varying the volumetric flow rate via the speed control on the pump and the selected tubing size.

Design goal (2) is somewhat more complicated, however since we don't necessarily know the interaction forces of the nonspecific binding we are looking to

prevent. We can assume that these forces are less than the forces of interaction between the antibody and its antigen – otherwise, we should obtain a new antibody – but we do not know how much less to expect. Thus, the course of action is to first perform a survey of sensor responses to our pathogen of interest over a variety of flow rates, then perform the same survey with other particulate matter or biological entities that might be present in a real world detection situation. These two response profiles will enable quantitative comparison of the senor response at each of various flow rates explored. From this comparison, a flow rate(s) with the highest ratio of sensor response to pathogen of interest versus nonspecific sensor response can be identified. It is this flow condition that will yield the highest statistical sensitivity and specificity for a given sensor-antibody-pathogen system.

To begin to implement these design goals, appropriate dimensions for the flow channel in which cantilever biodetection will take place must be calculated. Table 4-2, below, details the resulting calculations for a flow system designed to detect BA spores. BA spores have a diameter ranging from 1 to 1.2 μm. In this table, the channel widths, h, explored are 1, 8 and 19 mm – chosen simply because they are common mill bit sizes found in any machine shop in the United States. To calculate the range of forces on a stationary spore as a result of the speed of fluid flow at the center, $F(z=0)$, and at the wall, $F(z=h/2-a)$, of the flow channel, the maximum and minimum volumetric flow rates of our laboratory pump are entered into equations (4.15) and (4.16). These maximum and minimum flow rate values are 0.36 and 14.0 mL/min, respectively. In this table, we see that the previously stated range of antibody-antigen interaction values of 10 to 100 pN are best suited for experimentation in an 8 mm wide flow channel.

Table 4-2: Fluid forces on a BA spore as a function of channel width and flow rate

Channel Width (h) [mm]	Q [mL/min]	v bar [mm/s]	F(z=0) (@ center) [pN]	F(z=(h/2-a)) (near wall) [pN]
1	.36	15.2	440	1.0
	14.0	594	17136	41.1
8	.36	0.25	7.2	0.002
	14.0	9.64	278	0.085
19	.36	0.04	1.2	.0002
	14.0	1.64	47.2	0.006

Table 4-3, below, detail these same calculations for the case of *Cryptosporidium* oocysts. As opposed to BA spores, *Cryptosporidium* oocysts range in diameter from 4 to 6 μm. For these calculations, the average radius of 5 μm was used. In the case of these biological pathogens, it appears that the channel width of 19 mm is a better choice for experimentation.

Table 4-3: Fluid forces on a *Cryptosporidium* oocyst as a function of channel width and flow rate

Channel Width (h) [mm]	Q [mL/min]	v bar [mm/s]	F(z=0) (@ center) [pN]	F(z=(h/2-a)) (near wall) [pN]
1	.36	15.2	1836	18.4
	14.0	594	71400	714
8	.36	0.25	29	0.037
	14.0	9.64	1158	1.48
19	.36	0.04	5.1	0.003
	14.0	1.64	196	0.103

4.4.3 Flow System Materials Interactions and Considerations

Once the required geometries for our flow cell have been calculated, the material for construction of this chamber, as well as all connecting tubing must be selected such that interactions with the pathogen of interest are minimized. That is, we want to ensure that

our detection is not hindered by nonspecific 'sticking' of the analyte to the walls of the chamber or tubing.

To this end, the appropriate choice of materials for our flow cell and tubing is a material with a similar surface charge to that of our pathogens to be detected. It has been shown experimentally that surface of *Bacillus* spores is highly negative in aqueous solutions at neutral pH. Average zeta potentials for these spores in water near pH=7 are -40 mV.[156] Similarly, *Cryptosporidium* oocysts have been shown to possess zeta potentials ranging from -25 to -15 mV at neutral pH in water. Thus, the choice of flow cell and tubing material must also possess negative surface charges at these aqueous pH conditions. Polycarbonate is chosen as the material from which to fabricate all flow cells as its surface is, indeed, negative at neutral pH, with zeta potential values near -100 mV.[157] Silicone resins, polyurethanes and teflons are also and appropriate choices for flow cell or tubing materials as their surface charges at pH=7 range from -8 to -25 mV depending on composition and grade.[158] As such, Tygon (Saint-Gobain, Les Miroirs, France) tubing was used as the connecting tubing in all biodetection experiments as it is a blend of polydimethylsiloxane and polyurethane compounds that possesses good flexibility.

4.5 Chapter Summary

This chapter has discussed many practical matters ranging from construction of PZT-glass, PMN-PT/tin and PZT-only cantilevers to the design and construction of cantilever array systems; from insulation and functionalization of these cantilevers to their implementation in biodetection fluidics systems. In these discussions, literally years of experience and experimentation in cantilever building has been distilled down to just a

few pages concerning the most pertinent facts of this trade. In the course of engineering and refining the construction of these types of cantilevers, a new type of resonance was identified: the length and width mode resonances. Though high frequency resonances have been used by other researchers for biodetection, the claim was made that such peaks were still flexural resonance peaks, while accompanying theory to accurately predict these frequencies was not presented.[159] An appropriate theory was developed herein, and applied to observed resonances of a PZT-only cantilever. The theory was shown to be a valid analysis of these new peaks. Such sensors have been experimentally demonstrated to possess superior limits of detection levels which will be presented in Chapters 5 and 6. The MPS and MTMS insulation schemes discussed have allowed for the transition of these highly sensitive sensors from theoretical exercises to true, real-time, *in situ* biodetection platforms.

This chapter has also opened a discussion of theoretical fluid mechanics as it relates to biosensors of biological pathogens and has used this analysis to develop some guidelines for design and fabrication of the flow chambers that will house our piezoelectric cantilever biosensors and biosensor arrays in upcoming chapters. This engineered flow over the cantilever surface, as well as the first true implementation of a real-time piezoelectric cantilever array will allow for improved limits of detection while also augmenting the statistical sensitivity and specificity of the cantilever biosensor. Limits of detection will be improved by providing greater resonance frequency shifts in response to the binding of pathogens to the sensor surface as a result of cantilevers with higher frequency and the new width and length mode detection peaks. Increased statistical sensitivity and specificity will arise from the use of engineered fluid flow to

maximize the ratio of specific pathogen detection versus nonspecific detection of other bacterial species and particulate matter. The piezoelectric cantilever array will also allow for improved real-time sensitivity and specificity since redundant biodetection assays and a determination of background interactions of the analyte suspension with a reference biosensor will be able to be performed concurrently for the first time.

CHAPTER 5: *BACILLUS ANTHRACIS* DETECTION

Chapter 5 is focused on the detection of Bacillus anthracis, first by PMN-PT biosensors, then by a PZT-glass sensor and then by means of a PZT-glass array system. The goals of the PMN-PT study are to: 1) use the higher frequency peaks available in cantilevers constructed from 8 and 20 μm PMN-PT freestanding tapes to attain high resonance frequency shift sensitivity, and thus lower limits of detection; 2) study the use of MTMS insulation for real-time, continuous biodetection of BA; 3) acquire a dose response profile of such a sensor to BA; and 4) determine the lowest limit of detection of such a sensor.

The goals of the BA detection study using the PZT-glass sensor are to: 1) systematically determine the optimal flow condition(s) for BA detection; 2) determine the optimal flow condition(s) for minimal cross reactivity of the anti-BA-functionalized cantilever with spores of the close cousins of BA such as *Bacillus thuringiensis* (BT), *B. cereus* (BC) and *B. subtilis* (BS); and 3) determine the optimal flow condition(s) where the ratio of detection of BA versus the detection of other Bacillus species is maximized. BT, BC and BS spores were chosen for these cross-reactivity studies as these are the most closely related species to BA. While these species are non-virulent, their size is the same as that of BA and their spore coats are nearly identical in chemical composition as well.[49]

The goals of the BA detection study using the PZT-glass array system are to: 1) use the higher frequency length and width modes available in these cantilevers to achieve high resonance frequency shift sensitivity; 2) study the use of MPS insulation and sulfo-SMCC functionalization for real-time, continuous array biodetection of BA with triplicate redundancy; 3) determine the lowest limit of detection of BA for these array

sensors; and 4) study the effects of 'interferant' biological species present in the analyte sample in concentrations 100 and 1000 times higher than BA.

5.1 Dose Response Detection of *Bacillus anthracis* (BA)

At the time of experimentation, real-time *in situ* detection using a piezoelectric cantilever was still a relatively new detection methodology and, as such, the work herein aimed to extol the capabilities of PMN-PT-based biosensors for continuous sample monitoring with multiple detections being performed sequentially. At this point in time, however, it was known that flow was necessary to deliver particles in low concentration to the biosensor, but it was not yet fully understood how to best optimize this flow.

5.1.1 Sensor, Flow System and Experimental Setup

A 1 mm wide by 1 mm high by 10 mm long wide flow chamber was designed with the help of Marek Swoboda and fabricated by the Drexel University machine shop. The flow speed used for detection was 1 mL/min. We now know that, as enumerated in Table 4-2, this flow system and speed may not provide optimal conditions for this detection, but at the time of experimentation, this was unknown. Nonetheless, some impressive limits of detection and mass sensitivity numbers were attained using this setup. Two PMN-PT PEMS biosensors were used in this study. PEMS A, as it will be called was fabricated from 20 μm thick freestanding PMN-PT, while PEMS B was fabricated from 8 μm thick PMN-PT tape. Both cantilevers were fabricated according to the protocol given in Section 4.1.2. Figure 5-1(a) is an image of the flow chamber used for detection, while in Figure 5-1(c)[35], we see an optical micrograph of the 8 μm PMN-PT (PEMS B) sensor used for detection in this study.

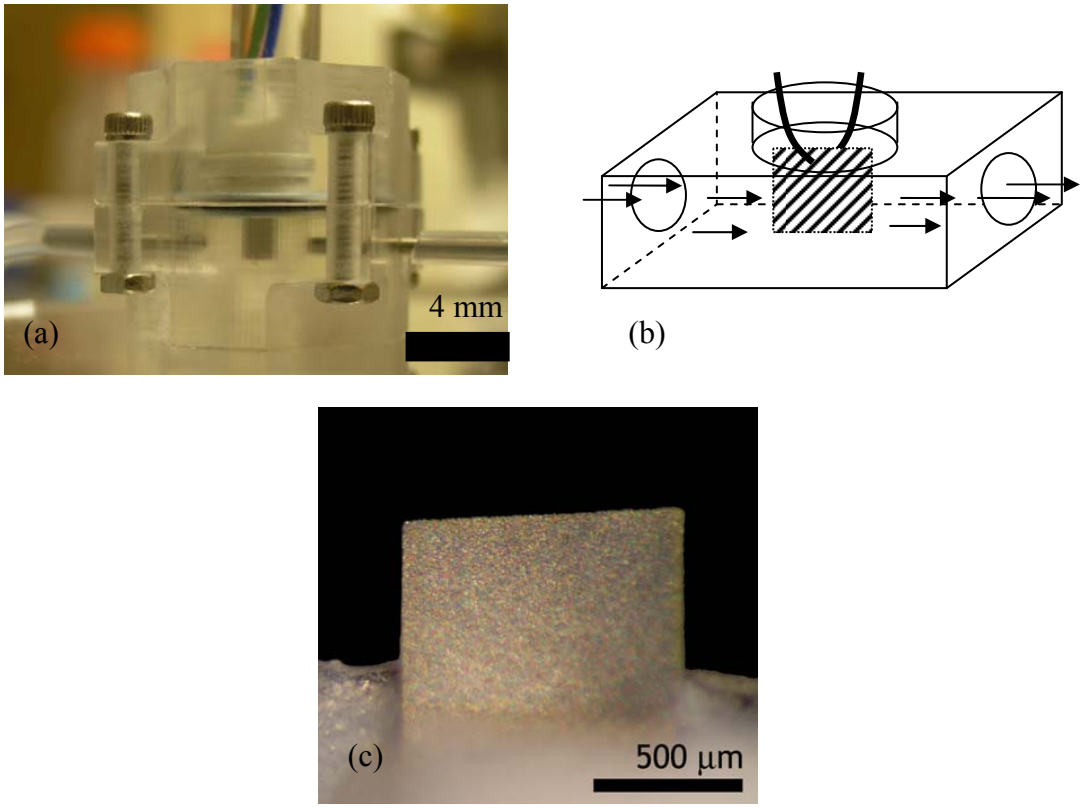

Figure 5-1: (a) 1mm wide flow chamber for detection of BA, (b) schematic representation of flow through this chamber and sensor orientation within, (c) an optical micrograph of the 8 µm PMN-PT sensor used for biodetection of BA.

In preparing the sensors for detection, MTMS was used to insulate the tin layer of the cantilevers, according to the protocol in Section 4.2.1, and MPA activated by NHS/EDS, as in Section 4.3.2, was used to prepare the platinum surface of the cantilever for antibody immobilization. The insulated PEMS with activated MPA on the platinum surface were then mounted in a specifically designed holder and vertically inserted in the center of the custom polycarbonate flow cell with its major faces parallel into the flow as schematically shown in Figure 5-1(b)[35]. The liquid in the flow cell was pumped with a Cole-Parmer Masterflex C/L pump (Model 77120-62, Vernon Hills, Illinois). The flow rate used for antibody immobilization and BA detection was 1mL/min, corresponding to

a Reynolds number of 1.6 in the laminar flow regime and a flow speed of 2.5 cm/s over the PEMS surface. A schematic of the closed-loop, recirculation flow system used for detection in these experiments was shown in Figure 4-9(b).

For antibody immobilization, first, a baseline of pure PBS solution was run for several minutes. This was accomplished by setting valves V1, V2 and V3 (see Figure 4-9(b)) such that the PBS reservoir flowed to the pump, through the flow cell and to the waste container (*i.e.* the open-loop setup). After this baseline recording, a 600 nM antibody solution was then injected into the system by setting V1 such that the syringe fitting injection port was open to V2. Once an excess of antibody solution had been used to displace all of the fluid in the pump-flow-cell system, as well as the tubing between V2 and V3, valves V2 and V3 were set such that a closed loop from pump to flow cell and back to pump was formed. The antibody solution was pumped for 40 min in this closed-loop format, after which the flow system was once again rinsed with pure PBS by setting the valves to the PBS reservoir-to-waste format, as described previously.

Subsequently, the desired concentrations of BA spores were injected into the flow system in the same fashion as the antibody solution and run for thirty minutes in the closed-loop setup followed by an induced BA spore release from the sensor surface in a mixture of glycine (Fisher Scientific, Fair Lawn, NJ) and HCl^{160} at pH=2.5 for 7 min. Only 7 min of release was allowed so as to avoid damage to the antibody from prolonged acid exposure.[72] Following this release there was a 5 min PBS rinse in the open-loop setup. It should be noted that for each change of solution, care was taken to avoid introduction of air bubbles into the system as well as to purge and rinse the tubing between V2 and V3. As a control experiment to determine non-specific BA spore

interactions with the PEMS, an anti-(*Bacillus globigii)* functionalized PEMS was exposed to a BA suspension under identical conditions.

Note that in the current study the total volume of the liquid present was only 0.8 mL. Thus, the number of spores present in solution and available for detection by the PEMS is actually only 80% of the indicated concentration value. For example, at a concentration of 100 spores/mL, there were just 80 spores present in solution for detection by the PEMS. Finally, scanning electron microscopy (SEM) (FEI XL30 ESEM, Hillsboro, Oregon) and optical microscopy (Olympus BX51, Center Valley, Pennsylvania) were used for spore detection confirmation and sensitivity calculations.

5.1.2 Real-Time Detection, Dose Response And Limit of Detection

As mentioned above, a low pH solution can be used to remove bound spores from the antibody-functionalized sensor surface such that the PEMS can be used for another spore detection instance without the need for complete regeneration of the antibody layer. As an example, Figure 5-2(a) shows the time evolution of a 404 kHz flexural resonance frequency peak of PEMS-B during antibody immobilization, BA spore detection, and spore release.

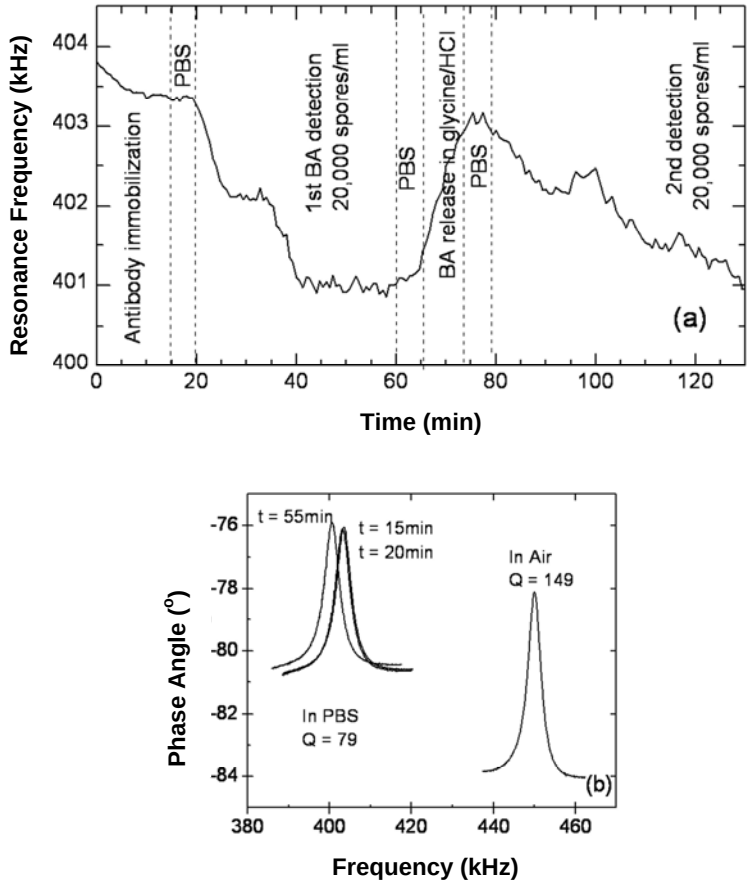

Figure 5-2: (a) Resonance frequency of PEMS-B versus time: antibody immobilization at t = 0-15 min; rinse with a phosphate buffer solution (PBS) at t =15-20 min; the first Bacillus anthracis (BA) spores detection at t = 20-60 min; rinse with PBS at t = 60-65 min; BA release by glycine/HCl at t = 65-75 min; and the second BA spores detection at t = 75-130 min, and (b) resonance peak spectra of

The antibody solution was introduced at t = 0. The resonance frequency shift during t = 0-15 min corresponds to the immobilization of the antibody to the PEMS platinum surface. The resonance frequency decreased 0.4 kHz from 403.8 kHz at t = 0 min to 403.4 kHz at t = 15 min due to the binding of the antibody to the MPA on the platinum surface. This resonance frequency shift saturated at t = 10 min and $\Delta f = -0.4$ kHz, indicating the immobilization took about 10 min, approximately the same as dipping in static solution.[98,161] This was reasonable considering the concentration of the antibody

solution was sufficiently high such that the flow had minimal effect on the binding of the antibody to the sensor surface.[39] At t = 15-20 min the antibody solution was replaced with PBS. As can be seen, there was no significant shift in that period. At t = 20 min, when 0.8 mL of a 20,000 spores/mL (16,000 total spores) BA suspension was introduced into the flow cell, the resonance frequency rapidly decreased from 403.4 kHz at t = 20 min to 401 kHz at t = 40 min with a $\Delta f = -2.4$ kHz. The resonance frequency shift during t = 20-40 min corresponded to the binding of spores to the antibody immobilized on the PEMS surface.

At t = 60-65 min, the spore suspension was replaced by PBS, again resulting in no significant resonance frequency shift in that period. From t = 65-72 min, the release of the bound spores from the sensor surface in glycine/HCl solution was performed resulting in a recovery (up-shift) to 403.1 kHz at t = 72 min, nearly the value before the detection. From t = 72-77 min, the system was once again rinsed with PBS and the second detection period with 0.8 mL of a suspension of 20,000 spores/mL (16,000 total spores) was started at t = 77 min. As can be seen, the second detection at the same concentration exhibited a resonance frequency shift similar to the first detection, though the rate of binding differed which was likely due to possible antibody damage sustained during the glycine/HCl release or incomplete antigen release[72].

In Figure 5-2(b) the resonance spectra of PEMS-B in Figure 5-2(a) at different times of detection are shown. In air, the resonance peak of PEMS-B had a peak frequency value of 449 kHz and a Q of 149. After immersion in PBS, the resonance peak frequency shifted to 403 kHz and the Q decreased to 79. The decrease in resonance frequency was a result of the mass of liquid that moves with the dipped sensor and the

decrease in Q, a result of the damping that occurs from such dipping as described previously by Shih, *et al*.[142]

After five minutes of immersion in PBS, the peak position remained unchanged, but once BA spores were introduced at t = 20 min, the peak downshifted to 401 kHz, while still retaining the Q of 79. This peak evolution showed that while liquid damping of the PEMS did result in a decrease in peak position and a decrease in Q, the peak was still of sufficient Q to be easily monitored electrically. This is in stark contrast to the silicon microcantilevers mentioned previously whose Q values decrease to unity or below when dipped in liquid media,[162] making peak position monitoring difficult, if not impossible.

The above example illustrates that the present MTMS-insulated PEMS can indeed be completely submerged in PBS and used to detect protein and spore binding to the sensor surface by monitoring the resonance frequency down-shift of a particular peak. Conversely the release of the antigen can be detected by monitoring the resonance frequency up-shift as is shown during the release of the spores by glycine/HCl solution.

In Figure 5-3, we plot the resonance frequency shift of PEMS-B versus time using a resonance peak of 285 kHz at BA spore concentrations of 20,000 spores/mL (16,000 total spores), 2000 spores/mL (1600 total spores), 100 spores/mL (80 total spores), 45 spores/mL (36 total spores) and 12 spores/mL (10 total spores). Also shown inset in Figure 5-3 are several in-PBS resonance spectra of PEMS-B during the BA spore detection at the 20,000 spores/mL concentration. The solid line, the dashed line, and the dashed-dotted line represent the resonance spectrum at t = 0, 15 and 30 min, with Q values of 75, 65 and 69 respectively. As can be seen in Figure 5-3, resonant frequency shifts of 2400±200, 1500±200, 500±160, and 300±100 Hz were observed at t = 30 min

for 16000, 1600, 80, and 36 total spores, respectively. As the concentration was reduced to 12 spores/mL (10 total spores), no discernable resonance frequency shift could be resolved from the sensor noise.

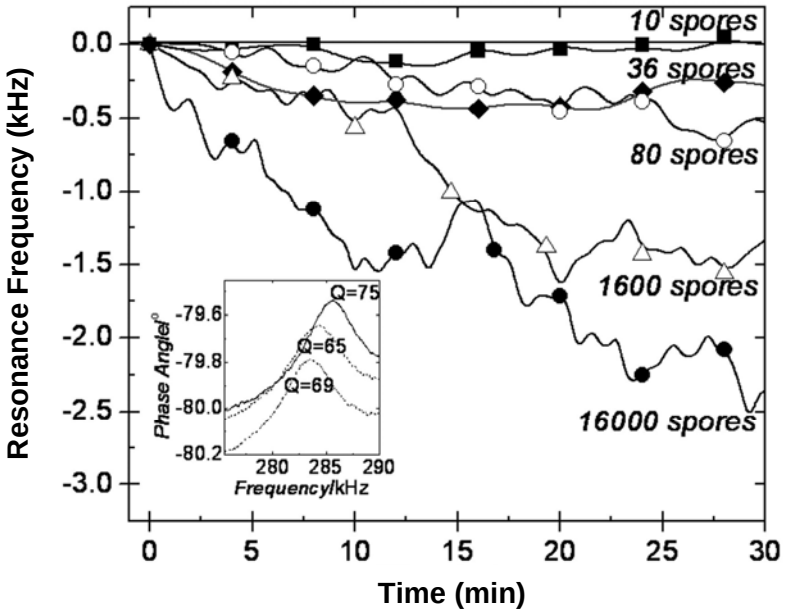

Figure 5-3: Resonance frequency of PEMS-B versus time in the presence of 16000 (full diamonds), 1600 (open up triangles), 80 (stars), 36 (full circles), and 10 (full squares) total spores. The insert shows the resonance spectra of PEMS-A in the presence of 16000 total spores at t =0 (solid line), 15 min (dashed line) and 30 min (dashed-dotted line).

PEMS-A was likewise monitored for resonance frequency shift when exposed to BA spore concentrations of 20,000 spores/mL (16,000 total spores), 2,000 spores/mL (1,600 total spores) and 200 spores/mL (160 total spores). These concentrations yielded frequency shifts of 2100 ± 200, 1100 ± 100, and 700 ± 100 Hz, respectively. For this PEMS, Q values of 62, 50 and 53 were observed at t = 0, 15, and 30 min, respectively during the detection of BA spores at 16,000 total spores. Also of note, for the lower spore levels of 160 and 1,600, the resonance frequency shift begins to level off at approximately 20 min while for the higher spore level of 16,000, the resonance frequency

continues to decrease during the entire detection period as similar to the situations with PEMS-B.

The resonance frequency shifts versus total number of BA spores of both PEMS-A and PEMS-B are summarized in Table 5-1. Meanwhile, as can be seen in Figure 5-2 and Figure 5-3, a positive detection response for all detectable BA concentrations was attained within 10 min even though all the experiments were run for a full 30 min.

Table 5-1: PEMS A and B resonant frequency shifts for tested BA spore concentrations

Total Spores Present	**16000**	**1600**	**160**	**80**	**36**
-Δf, PEMS A (Hz)	2100 ± 200	1100 ± 100	700 ± 100	-	-
-Δf, PEMS B (Hz)	2400 ± 200	1500 ± 200	-	500 ± 160	300 ± 100

Finally, to verify that the BA detected in suspension was indeed specifically bound to the sensor surface rather than simply 'sticking' to the surface by nonspecific means (e.g. electrostatic interaction), a control experiment using a PEMS functionalized with antibody to *Bacillus globigii* (BG) was performed. In this experiment, one anti-BA functionalized PEMS and one anti-BG functionalized PEMS were placed in the same flow channel under the same flow conditions described above and at 20,000 spores/mL concentration. Figure 5-4 displays the frequency response profile of these two PEMS and it can be seen that the capture of BA by the anti-BA functionalized PEMS is definitively specific.

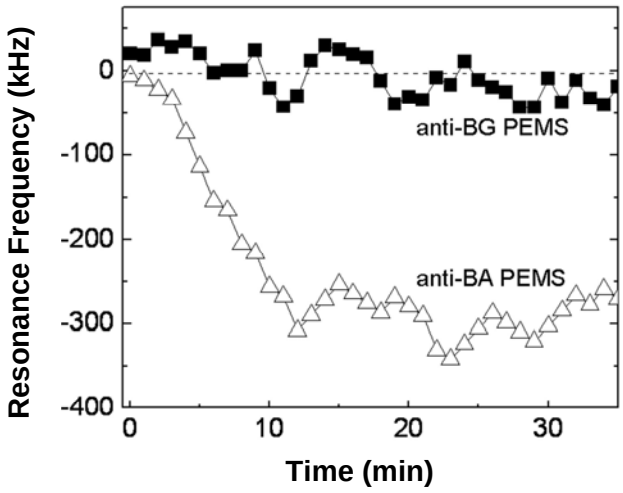

Figure 5-4: Frequency response of anti-BA and anti-BG functionalized PEMS when simultaneously immersed in BA solution.

To further verify the specific detection of BA by the PEMS sensors, the sensor surface was examined by SEM after the detections for visual verification and enumeration of spore binding to the platinum surface. As an example, an SEM micrograph of the sensor surface after 30 min of detection in 0.8 mL of a 20000 spores/mL BA suspension is shown in Figure 5-5(a). Therein, bound BA spores are seen as spheres approximately 1 μm in size indicated by arrows. Note the grain structure of the PMN-PT layer was also clearly seen in the SEM micrograph below the thin platinum electrode on the PMN-PT surface.

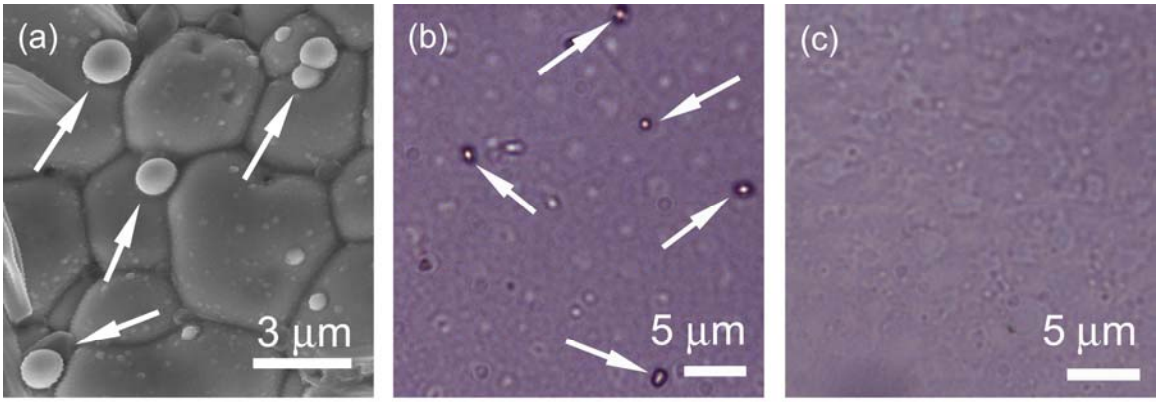

Figure 5-5: (a) Scanning electron microscopy (SEM) micrograph of BA spores captured on the sensor surface after 30 min in the flow cell with 16000 total spores (20000 spores/ml in 0.8 ml), (b) optical micrograph of BA spores bound to anti-BA on platinum surface, and (c) optical micrograph of the tin surface that showed no spore attachment. White arrows indicate the BA spores.

Using SEM micrographs to establish a surface coverage factor of BA spores on the sensor surface after detection, we obtained a mass detection sensitivity of $\Delta m/\Delta f = 3 \times 10^{-13}$ g/Hz for PEMS-B and $\Delta m/\Delta f = 1 \times 10^{-12}$ g/Hz for PEMS-A where Δf and Δm are the resonance frequency shift and the corresponding mass change. With SEM it was difficult to resolve all the spores on the sensor surface in a reasonable amount of time. To count the spores for the entire sensor surface, a separate optical microscopy enumeration of bound spores to surrogate platinum and tin surfaces of the same surface area as the PEMS was carried out. As the PMN-PT surface was not flat, platinum and tin surfaces coated on a flat glass substrate were necessary for this optical microscopy examination and enumeration. These slides were subjected to the same preparation methods, antibody immobilization procedures, and then exposed to identical flow conditions as the PEMS in BA concentrations of 20,000 and 45 spores/mL. An optical micrograph of the surrogate platinum surface and that of the surrogate tin surface after detection at 20,000 spores/mL for 30 min are shown in Figure 5-5(b) and Figure 5-5(c), respectively. As can be seen,

spore attachment on the surrogate platinum surface was evident while the surrogate tin surface did not exhibit spore attachment. After exposure to 20,000 spores/mL, by optical microscopy we counted 1083 spores adhered to the surrogate platinum surface of PEMS-A and 421 spores adhered to that of PEMS-B. Only five and two spores were adhered to the surrogate tin surface of PEMS-A and that of PEMS-B, respectively, confirming the selective binding nature of the anti-BA functionalized PEMS platinum surface. After exposure to 45 spores/mL, we counted 24 spores on the surrogate platinum surface of PEMS-B and zero spores on the tin surface. The mass detection sensitivities calculated from the number of spores on the surrogate sensor surfaces were 6×10^{-13} g/Hz for PEMS-A and 2×10^{-13} g/Hz for PEMS-B, consistent with the sensitivities of 1×10^{-12} for PEMS-A and 3×10^{-13} g/Hz for PEMS-B deduced from the SEM micrographs. Considering both of these methods for sensitivity determination, the sensitivities of PEMS A and B are given as $1 \pm 0.5 \times 10^{-12}$ and $2 \pm 1 \times 10^{-13}$ g/Hz, respectively. These mass detection sensitivities are comparable to other PMN-PT PEMS of similar dimension in chemical sensing in air.[143]

Meanwhile, the theoretical mass sensitivity by considering only the mass loading effect was calculated according to equation (3.5), where $\rho_p = 7.9$ g/cm^3, $\rho_n = 7.3$ g/cm^3 are the densities of the PMN-PT and tin layers, respectively.[41,163] The calculated theoretical mass sensitivities for PEMS-A and PEMS-B were $(\Delta m/\Delta f)_{mass} = -4 \times 10^{-11}$ g/Hz and -5×10^{-10} g/Hz, respectively. The present experimentally obtained mass detection sensitivities are more than 100 times more sensitive than the values suggested by considering simply the mass loading effect alone. This enhancement happened in air as well as in liquid, thereby it was not related to film viscoelastic properties or

perturbations in molecular slip and interfacial viscosity. Similar enhancement has also been observed in other piezoelectric cantilever detection systems[124,133,164] and was attributed to the change in the effective spring constant of the PEMS.[124,125]

5.1.3 Sensor Noise and Statistical Analysis

It is suspected that some of the noise exhibited in Figure 5-2, Figure 5-3 and Figure 5-4 was in part due to the actual binding (and sometimes unbinding) events of BA to the sensor surface, as this noise tended to decrease with a decreasing BA concentration. However direct, conclusive proof of this hypothesis is not possible, and as such, this observation, led, at least in part to an investigation of antibody-antigen interaction forces as has been discussed in Section 4.4.2. Additionally, as a reviewer of the published form of this work correctly pointed out, variations in spore distribution along the length of the sensor could lead to a somewhat different sensor response, as described by Bhalerao, *et al*.[165] These variations in distribution are unlikely to contribute to sensor noise, though, as this distribution is precisely what the factor of 0.236, in equations (3.5) and (3.6) accounts for.

Finally, to apply the statistical analysis techniques presented in Section 2.4 to the 12 total experimental BA detection results presented in this section, we first arrive at Table 5-2. The ten true positive results come from the seven positive detections listed in Table 5-1, the two positive results in Figure 5-2(a), and the positive detection in Figure 5-4. The true negative result comes from the lack of sensor response to BA when functionalized with anti-BA, as in Figure 5-4, and the false negative response comes from the missed detection of 10 spores in Figure 5-3. Based on these experimental results, a statistical sensitivity of 91% is calculated, while the specificity is calculated as 100%.

Table 5-2: Statistical characterization of BA detection test outcomes

	Known Samples ('Gold Standard' Test)		
Biosensor Test Results	**BA attack (+)**	**No BA (-)**	**Totals**
BA attack (+)	10	0	10
No BA (-)	1	1	2
Totals	11	1	12

However, with noise levels as high as 200 Hz observed in these detection data, if a signal to noise ratio (SNR) of two were required for positive detection of BA to be deemed accurate, we would not be able to say that the 36 spores was accurately detected and our statistical sensitivity would slip to 82%. If the SNR requirement were further raised to a value of three, the detection of 80 spores by PEMS B could also no longer be deemed accurate and our sensitivity would further slip to 73%. Since no instances of false positive were recorded, though, specificity remains at 100% for even these higher SNR requirements.

These hypothetical SNR requirements serve to illustrate the point that while the goal of a very low limit of detection is indeed an important aim in sensor design, an almost equally important aim is the reduction of noise in the detection signal of the sensor. Noise reduction is first and foremost achieved by careful building of sensors such that detection peaks are as sharp as possible, as calculated by the Q value. As seen in the preceding detection, this was successfully achieved as a Q of 149 in air was recorded. The second method of achieving low levels of noise in real-time aqueous detection is realized by effective insulation techniques. While our Q factor does diminish to 79 upon dipping in PBS, this is still a very good value for detection. Yet another method for decreasing noise levels in sensor response is by optimizing the algorithm by which the

actual resonant peak position of the piezoelectric cantilever biosensor is determined. Appendix A details an algorithm by which the present author has markedly reduced noise levels by an improved detection.

5.2 Specific Detection of BA among other *Bacillus* species

With Section 5.1 demonstrating the use of PMN-PT PEMS to attain an extremely low limit of detection, the next experimental area to explore was that of engineered fluidics design for improved sensitivity and specificity of detection. To accomplish this, a PZT-glass PEMS with its glass tip coated with gold was used. This sensor was millimeters long in size, which, while markedly less sensitive in terms of resonance frequency shift than the PMN-PT sensor used, provided a robust and highly reusable platform for the many experiments that would be required for this work.

The purpose of this study is to explore the use of flow as a means to minimize nonspecific binding of BT, BC, and BS spores to an anti-BA spore immunoglobulin G (IgG)-functionalized PEMS. We show that, as with the detection of BA, the nonspecific interactions of BT, BS, and BC with the anti-BA antibody functionalized sensor surface initially increase with an increasing flow speed as the fluid flow helps bring more spores to the sensor surface. However, as the flow rate (velocity) becomes larger than 5 mL/min, the nonspecific binding of BT, BS, and BC diminishes, while the binding of BA remains steady, dramatically enhancing the specificity of the detection. The observed reduction of nonspecific binding at higher flow rates is similar to the result of a recent study where flow and micrometer-size labels conjugated to a secondary receptor were used to improve specificity in DNA detection.[166]

In addition to improving the specificity of our PEMS sensor by means of controlling the fluid flow rate, the data obtained will also allow for an estimation of the interaction forces involved in the antibody-antigen interactions that take place at the sensor surface. Such force interrogation has been previously investigated by rupture event scanning (REVS) on the QCM.[73,167] The PEMS system differs from REVS in that, with PEMS detection, it is the binding of the antigen to the antibody that is probed rather than the unbinding of an antigen bound in a previous preparation step, as is the case with REVS. Additionally, the PEMS system uses fluid flow for its basic detection,[35] while the experiments presented here further probe the utility of this same fluid flow for specificity enhancement and force interrogation.

5.2.1 Sensor, Flow System, *Bacillus* Species and Experimental Setup

A PZT/gold-coated glass PEMS was constructed by bonding a 2 mm wide and 150 μm thick glass wafer (Fisher Scientific, Pittsburg, PA) to a 1.5 mm wide and 127 μm thick PZT wafer (T105-H4E-602, Piezo Systems Inc., Cambridge, MA) with insulating epoxy (Loctite Hysol 1C, Rocky Hill, CT). Prior to cantilever fabrication, a 150 nm-thick gold layer (with 10 nm-thick chromium bonding layer) was coated on both sides of the glass wafer by electron-beam evaporation (E-gun: 3 kW, 2×10^{-6} torr).

To achieve the cantilever geometry shown in Figure 5-6, the gold-coated glass wafer was bonded to the PZT wafer such that the long edges of both wafers were parallel and coincident, and on one end the gold-coated glass protruded past the PZT by 1.7 mm to serve as the cantilever tip. After attaching wire leads to the other end of the PZT, the rear end of this PZT-glass bilayer was encapsulated in a tube with the above mentioned insulating epoxy. The final PZT/gold-coated glass PEMS was 2.2 mm long; the

PZT/gold-coated glass portion was 0.5 mm long and the gold-coated glass tip was 1.7 mm long (see Figure 5-6). This tipped cantilever structure allowed the gold-coated glass tip to be dipped into an aqueous medium for in-situ biological detection while also allowing for all-electrical actuation and detection by the PZT layer which remained free from submersion.

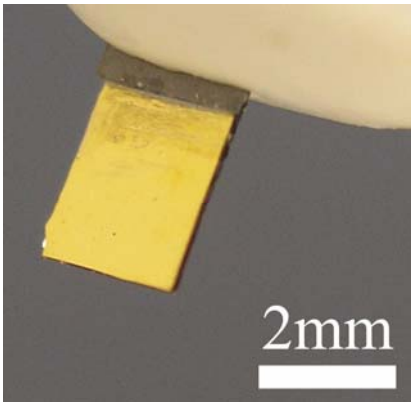

Figure 5-6: Optical micrograph of PZT-Glass PEMS used for BA selectivity studies

To determine the specificity of the anti-BA IgG functionalized cantilever, additional *Bacillus* species were chosen for study: (BS), (BC), and (BT) were all provided by Dr. Richard Rest, Drexel University College of Medicine. *Salmonella typhimurium* (ST) (Kirkegaard & Perry Laboratories Inc., Gaithersburg, MD) was used as an additional unrelated control species. Anti-BA spore was also provided by Dr. Richard Rest and was raised in rabbits by Lampire Biological Laboratories, Inc. (Pipersville, PA) against UV-killed PA medium BA Sterne strain 7702 spores. Serum was collected 7 days after a 3rd subcutaneous injection of spores in Freund's Incomplete Adjuvant. IgG was purified from the serum by protein A column chromatography.

The gold-coated tip of the PEMS was freshly immobilized with anti-BA-spore IgG according to the NHS/EDC activated MPA immobilization scheme discussed in Section 4.3.2. For continuous, real-time analyte detection, the tip of this anti-BA IgG functionalized PZT/gold-coated glass PEMS was submerged 1 mm into the center of an open flow channel 80 mm long and 8.0 mm wide as schematically shown in Figure 5-7. The flow channel was 9 mm deep with a semi-circular bottom of 4.0 mm radius. These flow channel geometry values were chosen as a result of analysis and resulting calculation presented in Section 4.4.2.

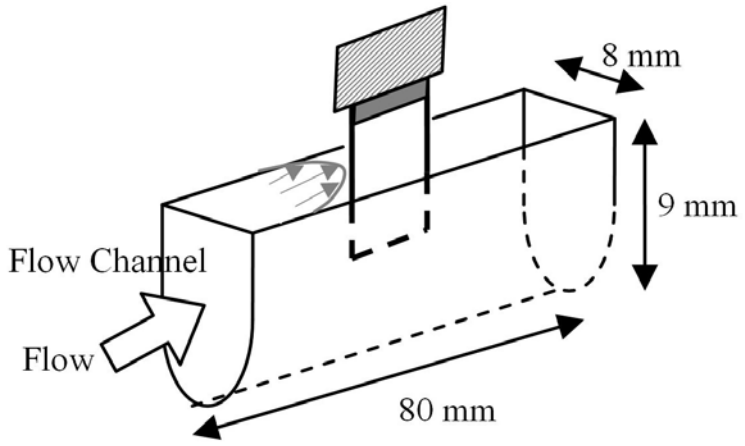

Figure 5-7: Schematic of PEMS situated in center of flow channel

As mentioned, since the present PZT/gold coated glass PEMS was to have its gold-coated glass tip only partially dipped in the liquid insulation of the PZT electrodes was not necessary. However, the humidity was controlled at 90% relative humidity in a glove box to ensure that the resonance frequency of the partially-dipped PZT-glass PEMS was stable with time.[39] The analyte suspension was circulated using a Masterflex C/L pump (Model 77120-62, Cole-Parmer, Vernon Hills, Illinois) with an adjustable

volumetric flow rate of 0 to 14 mL/min. Prior to exposure to any suspension of spores or cells, a baseline resonance frequency of the PEMS was recorded for a period of thirty minutes in pure PBS solution.

As an example, the inset in Figure 5-8 displays phase angle versus frequency spectra of the PEMS at different stages of a detection experiment. The resonance peak of the sensor shifted to lower frequencies with time. The resonance peak frequency position of such spectra versus time is shown in Figure 5-8. As can be seen, the PEMS resonance frequency remained unchanged in PBS at t<0. After the introduction of the spores at t=0, binding of spores to the PEMS surface lowered the resonance frequency. All the detection results described below were obtained using this peak at 313 kHz in PBS. As can be seen, during detection the resonance peak frequency decreased with time while the Q value remained stable around 33 throughout the detection period.

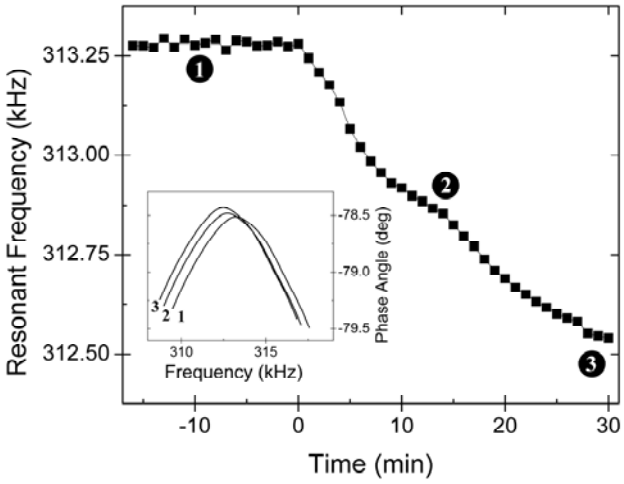

Figure 5-8: Continuous, real-time PEMS monitoring of analyte solution. BA is injected into PBS at t=0. Example resonance peaks (numbered 1 - 3) monitored during this detection are shown inset, with their peak frequencies versus time indicated by the corresponding encircled numbers.

5.2.2 Flow-Rate Dependent Sensor Response and Associated Forces on the Spores

In Figure 5-9, we plot the resonance frequency shift of the PEMS during the detection of BA spores at various flow rates from 1.3 to 14 mL/min. Also shown in Figure 5-9 is the resonance frequency of the PEMS versus time in PBS at 14 mL/min. When exposed to a BA spores suspension with no flow, a resonance frequency shift of −740 Hz was observed at 30 min. The magnitude of the resonance frequency shift was markedly increased in the presence of a flow: The resonance frequency shift at 30 min was increased from -740 Hz to -1150, -1190, -1470, and -1370 Hz at 1.3, 4.6, 10, and 14 mL/min, respectively. This result indicates that the attachment of BA spores to the sensor surface was enhanced by the presence of flow and that flow rates greater than or equal to 4.6 mL/min all enhance detection of BA over and above the conditions of no flow and 1.3 mL/min. The enhancement by flow in the detection of BA spores seems to be maximized at 10 mL/min.

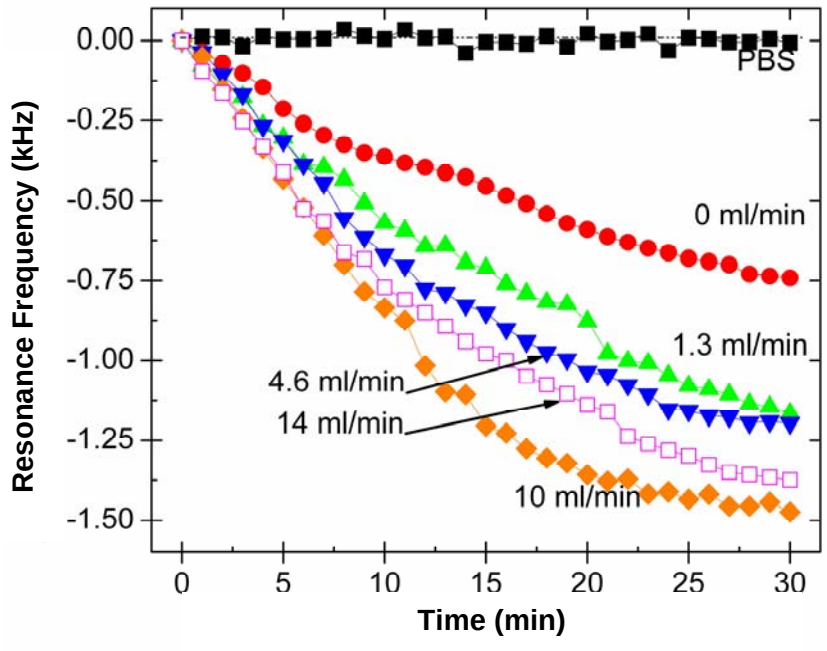

Figure 5-9:PEMS frequency shift responses of anti-BA functionalized PEMS to BA spores at flow rates of 0 (circles), 1.3 mL/min (up triangles), 4.6 mL/min (down triangles), 10 mL/min (diamonds) and 14 mL/min (open squares). A control of PBS with no spores at 14 mL/min is shown for reference (closed squares).

Subsequently, non-specific binding to the anti-BA functionalized PEMS at various flow rates was examined in BS, BC, BT and ST suspensions at the same 20,000 spores(cells)/mL concentration. As an example, Figure 5-10 shows the resonance frequency shift versus time of the anti-BA functionalized PEMS in a 20,000 spores/mL BT suspension at various flow rates, from 0 to 14 mL/min. Also shown is the background run in PBS at 10 mL/min which exhibited no discernable resonance frequency shift with a standard deviation of ±25 Hz.

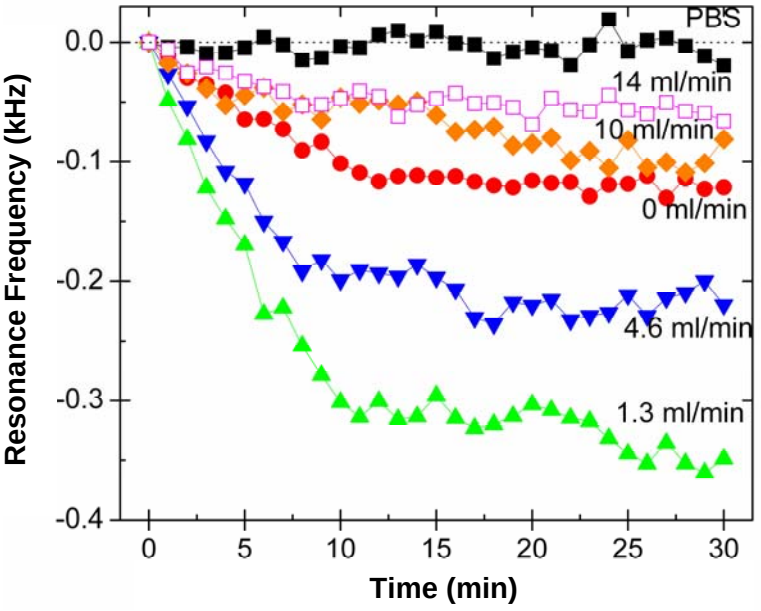

Figure 5-10: PEMS frequency shift responses of anti-BA functionalized PEMS to BT spores at flow rates of 0 (circles), 1.3 mL/min (up triangles), 4.6 mL/min (down triangles), 10 mL/min (diamonds) and 14 mL/min (open squares). A control of PBS with no spores at 10 mL/min is shown for reference (closed squares).

We can see that, initially, the magnitude of the resonance frequency shift was increased by the introduction of flow. The resonance frequency shift at 30 min was enhanced from -120 Hz with no flow to -350 Hz at 1.3 mL/min. However, as the flow rate was further increased, the magnitude of the resonance frequency shift was reduced. At 30 min, the resonance frequency shift was changed from -350 Hz at 1.3 mL/min to -210, -100, and -60 Hz at 4.6, 10, and 14 mL/min, respectively. Interestingly, the magnitude of the resonance frequency shift at 14 mL/min was even smaller than that with no flow.

In Figure 5-11, we plot the resonance frequency shift after 30 min of detection versus flow rate over the anti-BA spore IgG coated PEMS, of BA, BT, BC, BS, and ST suspensions, all at concentrations of 20,000 spores/mL. Also, plotted on the top axis of

the figure is the removal force impingent on a spore on the surface of the sensor. This will be discussed in Section 5.2.3

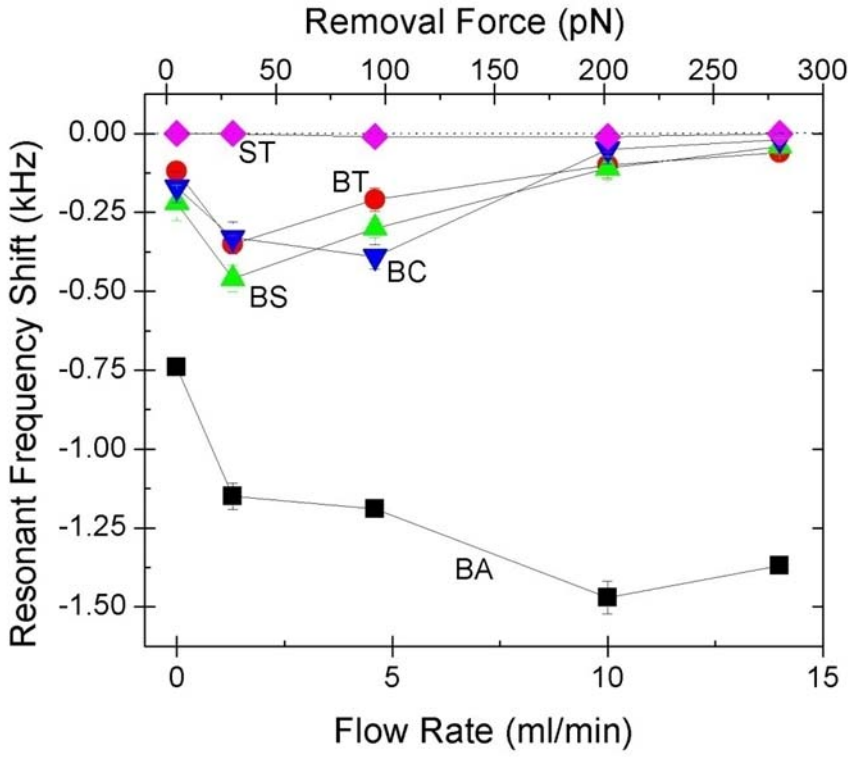

Figure 5-11: PEMS resonant frequency shift as a function of fluid flow rate and removal force for BA (squares), BS (up triangles), BC (down triangles), BT (circles) spores, and ST (diamonds).

As discussed above, we see that the magnitude of the resonance frequency shift of the anti-BA functionalized PEMS increased with flow rate in the case of the BA suspension due to flow-enhanced spore attachment. Meanwhile, the anti-BA IgG functionalized PEMS exhibited no obvious resonance frequency shift in an ST suspension at all flow rates. This indicated that there was no nonspecific binding between an unrelated species such as ST to the anti-BA IgG functionalized PEMS. Unlike ST, the genetically closely related BT, BC, and BS spore suspensions all caused the anti-BA functionalized PEMS to exhibit a resonance frequency shift, indicating weak binding to

the sensor. Similar to BT, the magnitude of the resonance frequency shift of the anti-BA functionalized PEMS exhibited a maximum shift of -460 Hz at 1.3 mL/min for BS and -390 at 4.6 mL/min for BC, both of which decreased to very low values at higher flow rates: -40 Hz at 14 mL/min for BS and -20 Hz at 14 mL/min for BC. The -40 Hz for BS and -20 Hz shift for BC at 14 mL/min was very close to or within the noise level (±30 Hz) of the PEMS in pure PBS and is thus, insignificant. Clearly, there was a specificity enhancement by the increased flow, which increased the specific binding of BA spores while suppressing the weak binding of closely related BT, BS, and BC spores.

5.2.3 The Cross-Reactivity Ratio

From the data presented in Figure 5-8 through Figure 5-10, we see that continuous, real-time monitoring of BA and its close relatives has been achieved using the PEMS. While detection experiments were run for thirty minutes in all cases, Figure 5-9 clearly shows that positive detection of BA at all flow rates was achieved in just 2 to five minutes. To more easily compare the PEMS specificity enhancement achieved by flow, a cross reactivity ratio (CRR) of BT, BS, or BC is defined as:

$$CRR = \frac{\Delta f_{Bx@t=30min}}{\Delta f_{BA@t=30min}} \tag{5.1}$$

where *Bx* can be BT, BS or BC. This CRR is the ratio of the resonance frequency shift at 30 min obtained in the BT, BS, or BC suspension at a given flow rate to that obtained in the BA suspension at the same flow rate.

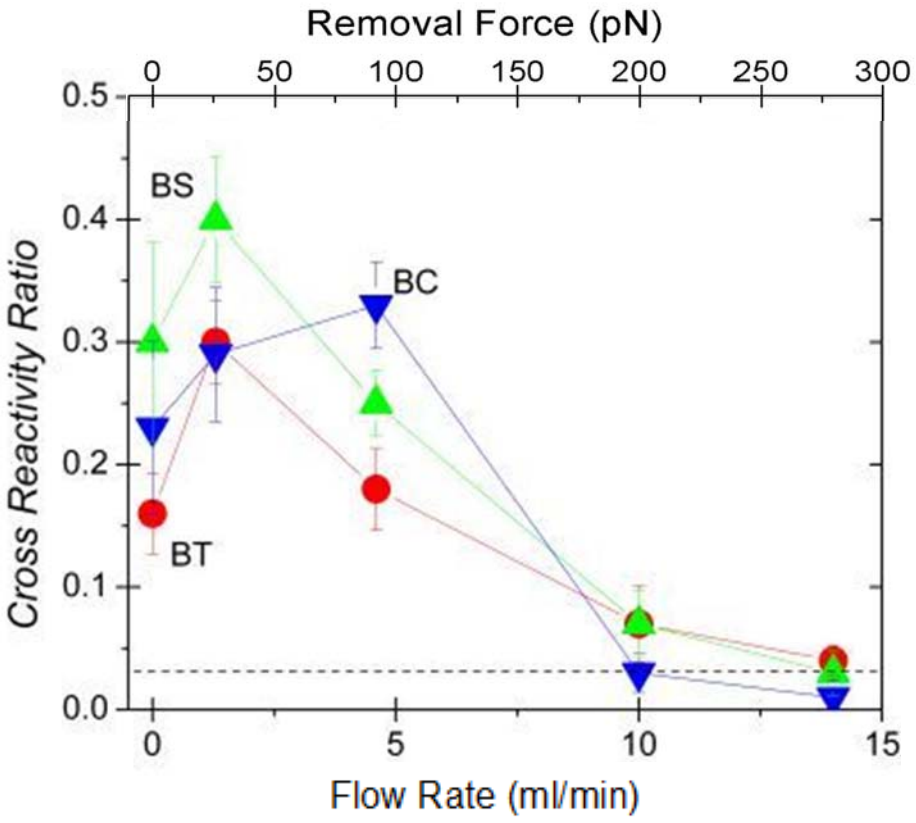

Figure 5-12: Cross reactivity ratio as a function of fluid flow rate and removal force of BT (circles), BS (up triangles), and BC (down triangles) obtained by the anti-BA antibody functionalized PEMS.

Figure 5-12 shows the calculated cross reactivity ratios versus flow rate for BT, BS and BC. Note that the cross reactivity of ST was essentially zero and for clarity, was omitted in the figure. For all cross reactive species, the cross reactivity ratios were between 0.4 and 0.15 for flow rates less than 10 mL/min and decreased to less than 0.1 at 10 mL/min and to less than 0.05 at 14 mL/min. The reduction of cross reactivity ratio at 10 and 14 mL/min was attributed to the increased force impingent on spores near or attached to the sensor surface with increasing flow velocity that eventually overcame the binding strength of the spores. The sequence of cross reactivity among the BT, BC, and BS depends on the flow rate as shown in Figure 5-12. Note that as mentioned above, the

noise level of the PEMS in pure PBS was ±50 Hz at 14 mL/min. With this noise level, one can define a cutoff cross reactivity ratio, which is depicted as the horizontal dashed line in Figure 5-12. Spores with cross reactivity ratios less than or close to the cutoff would be deemed as not detected. Clearly, BT, BS, and BC at 14 mL/min were all such cases.

Note that, according to the cross sectional area of the flow channel, the flow rates of 1.3, 4.6, 10, and 14 mL/min corresponded to average linear flow velocities, $\bar{v}$, of 0.35, 1.2, 2.7 and 3.8 mm/s, respectively. With the Reynolds number (*Re*) equal to just 34 at 14 mL/min, where ρ = 1000 kg/m^3 is the density of the fluid and η = 1 cP is the fluid's viscosity, the flow was laminar and the flow velocity profile in the width direction was parabolic, according to equation (4.6). That is, $\bar{v}$ was zero at the channel wall and maximum at the center of the flow. Thus, unlike other sensor systems where the sensor surface is actually part of a wall of the flow channel, at which point the fluid velocity diminishes to zero, the present system situates the sensor at the center of the flow where the flow velocity is at a maximum.

Applying the theory developed in Section 4.4.2.2, the deduced impingent force on the spores by the flow was about 100 pN at 14 mL/min ($\bar{v}$ = 3.8 mm/s) in the 8 mm wide flow channel. With this knowledge of force impingent on spores at the sensor surface, an estimation of forces required to prevent the detection of the other *Bacillus* species by the PEMS biosensor is possible. At the flow rate of 14 mL/min, where detection of these 'cousins' is seen to diminish drastically, forces impingent at the sensor surface are 100 pN. Although it is unclear exactly how many antibody-antigen bonds were involved in the present spore-sensor surface binding, it suffices to say that the deduced force was

consistent with the 1-500 pN range of antibody-antigen interactions as cited in literature.[168-170]

Furthermore, while current pump limitations limited the range of flow rates studied in this experiment from 0 to 14 mL/min, an estimation of BA spore interaction force with the sensor surface can be attained by analyzing the data presented in Section 5.1.2. In these experiments, detection of BA was accomplished in a 1 mm wide by 1 mm deep flow channel at a flow rate of 1 mL/min. Applying the previously developed theory for forces in fluid flow to these conditions, we see that forces on a BA spore at the senor surface are on the order of 400 pN under these conditions (where $\bar{v}$ = 16 mm/s). Thus, since successful detection was accomplished under these conditions, it can be concluded that the specific interaction force between BA spores and a sensor immobilized with anti-BA-spore IgG is equal to or greater than this value of 400 pN.

5.2.4 Statistical Analysis

In additional to the analysis of cross reactivity ratio between the binding of BA and its close cousins to an anti-BA-spore IgG functionalized sensor, the calculation of statistical sensitivity and specificity is particularly poignant here. If we define our threshold detection level at -150 Hz, which represents a signal to noise ratio (SNR) or 3, we arrive at Figure 5-13, below, detailing these statistical values at the various flow rates of detection performed.

As examples of the matrices used to perform these calculations, Table 5-3, and Table 5-4 below detail the classification of test results for the conditions of zero flow and $\bar{v}$ = 10 mL/min, respectively. In Table 5-3, we see that, since there were two instances where our piezoelectric microcantilever biosensor indicated shifts of greater than 150 (for

BS and BC), we have recorded two false positive events. This has lead to a reduction in specificity to 60%, while the sensitivity to the presence of actual BA remains at 100%.

Table 5-3: Statistical characterization of anti-BA-spore functionalized PEMS at zero flow

	Known Samples ('Gold Standard' Test)		
Biosensor Test Results	**BA present (+)**	**No BA (-)**	**Totals**
BA present (+)	1	2	3
No BA (-)	0	3	3
Totals	1	5	6

Table 5-4: Statistical characterization of anti-BA-spore functionalized PEMS at 10 mL/min

	Known Samples ('Gold Standard' Test)		
Biosensor Test Results	**BA present (+)**	**No BA (-)**	**Totals**
BA present (+)	1	0	1
No BA (-)	0	5	5
Totals	1	5	6

In Table 5-4, we see that an increase in flow rate to 10 mL/min, and equivalently, 14 mL/min has lead to just the one true positive detection event and five true negative events. As such, the sensitivity and specificity at these flow rates are both 100%. Clearly, in addition to the natural sensitivities and specificities of the BA-spore antibody, the introduction and precise control over the flow conditions to which the spore suspensions were subjected has enhanced these specificities and sensitivities, as illustrated in Figure 5-13 where sensitivities and specificities for all flow conditions are plotted.

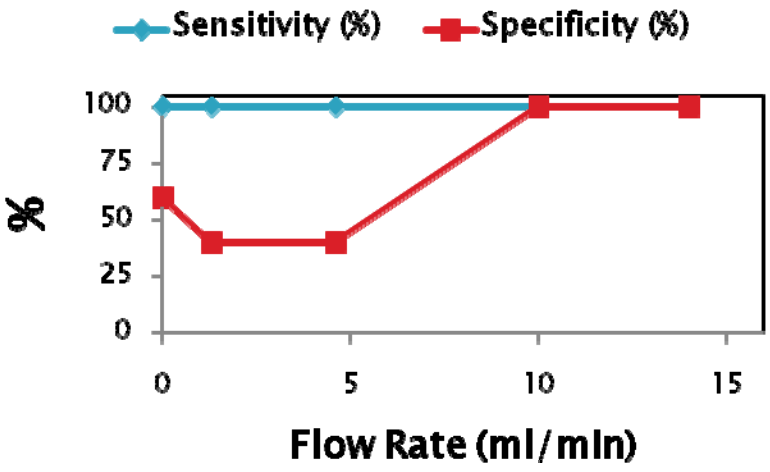

Figure 5-13: Statistical sensitivity and specificity of the anti-BA-spore functionalized PEMS

5.3 Sensitive and Selective Array Detection of BA among Bacterial 'Interferants'

With the successful demonstration of fluid flow engineering as a means to improve biological pathogen detection sensitivity and specificity, attention was focused upon the development and testing of an array of piezoelectric microcantilever sensors, as described in Section 4.1.3. The goal of using these array systems was to enable real-time redundancy, and thus confirmation, of detection as well as to allow for real-time background determination. The following experiments detailing the detection of BA spores in a wide range of concentrations and in high concentrations of background 'interferant' cells address the desire to attain redundant detection. The use of a simultaneous reference sensor will be introduced in Chapter 6.

5.3.1 Sensor Array, Flow System and Experimental Setup

The PZT-glass biosensor array used in these experiments was fabricated by bonding a 75 μm thick glass layer to a 127 μm thick square of PZT (Piezo Systems, Inc., Cambridge, MA). As described in Section 4.1.3, piece of 25 μm thick copper foil were

then soldered to the top and bottom electrode of the PZT layer in order to provide conductive leads for subsequent wire connection. This PZT-glass bilayer was then bonded onto a substrate of glass microscope slide (Fisher, Fair Lawn, NJ). The 75 μm glass layer protruded over the edge of the microscope slide by 3 mm and the PZT extended 1.5 mm over the edge of the slide, *i.e.* 1.5 mm back from the edge of the glass layer. This bimorph, layered structure was then cut with a wire-saw (WS-22, Princeton Scientific, Princeton, NJ) at spacings of 400 microns and ribbon wires were then carefully soldered to the resulting copper foil tabs attached to the top and bottom electrodes of each individual cantilever. These soldered wire connections were then embedded in non-conductive epoxy to achieve the final structure shown in Figure 5-14.

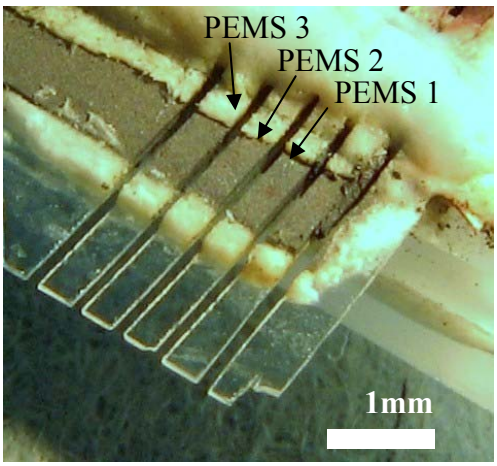

Figure 5-14: Optical micrograph of a PEMS array

A switch box (3499A, Agilent) and an impedance analyzer (4294A, Agilent), both computer controlled, were used for multiplexed, real-time detection of BA spores in suspension. However, due to limitations of the switch box, as well as cycle-time constraints, only three of the sensors shown in Figure 5-14 were monitored during

detection experiments. The spectra of these sensors are shown in Figure 5-15 and the co-location of the peaks in the different spectra is owed to the near-identical geometric dimensions of each cantilever. The peaks occurring near 410 kHz (indicated by arrows) were those monitored during detection.

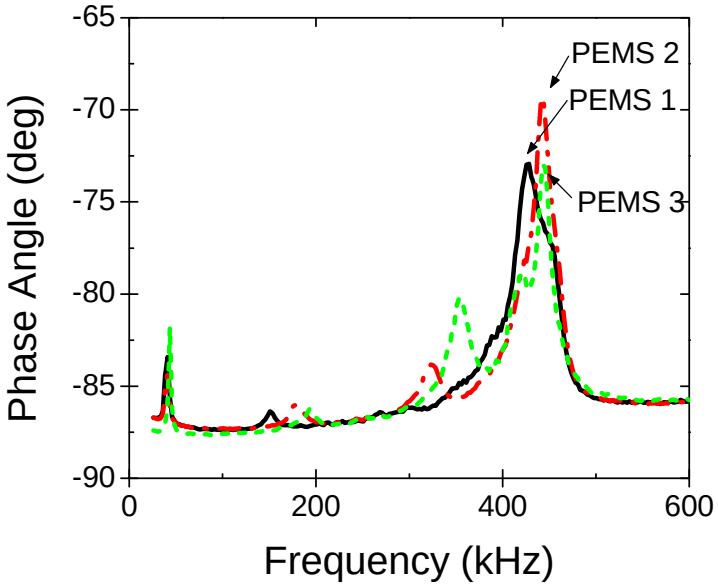

Figure 5-15: Resonance spectra of PEMS array

All PEMS detection experiments were performed in a custom-fabricated semi-circular flow chamber 4.8 mm deep with the flow entering and exiting at its diameter (15 mm). Tubing was connected to this flow chamber and the suspensions were circulated by a Masterflex C/L pump (Model 77120-62, Cole-Parmer, Vernon Hills, IL) at 1 mL/min. The total volume of the fluidics system was 3 mL. This flow system was designed such that the cartridge, together with the PEMS array were a self-contained unit and could be simply plugged into an electrical monitoring and fluidics pumping system. Several advantages exist for implementing a closed cartridge system such as this. The issue of

evaporation of aqueous analyte suspension, and the resultant precise dipping depth and humidity control requirements are rendered unnecessary and obsolete.[38,39] Since the PEMS array is completely insulated and thus can be completely submerged in analyte fluid, the cartridge system is designed and constructed such that, once filled, no analyte liquid is in contact with ambient air and subject to evaporation. This leads to improved sensor stability as well as better temperature stabilization of the PEMS array due to its complete immersion in the aqueous analyte suspension.

Figure 5-16 is an image of this cartridge system. The white arrow indicates the location of the PEMS array in the cartridge with the pins in the lower left corner of the image allowing for connection to the inlet, outlet and air bleed connections of the fluidics system. This fluidics system was fabricated entirely out of polycarbonate plastic with silicone rubber used for the gasket layers. As discussed in Section 4.4.3, the surface charge of BA spores as well as that of polycarbonate and silicone rubbers is well characterized and all are negative at neutral pH (as was the case for all experiments herein).[156-158] Thus no 'sticking' of the BA spores to the flow system walls was expected and indeed, no adverse effects from such possible 'sticking' were observed.

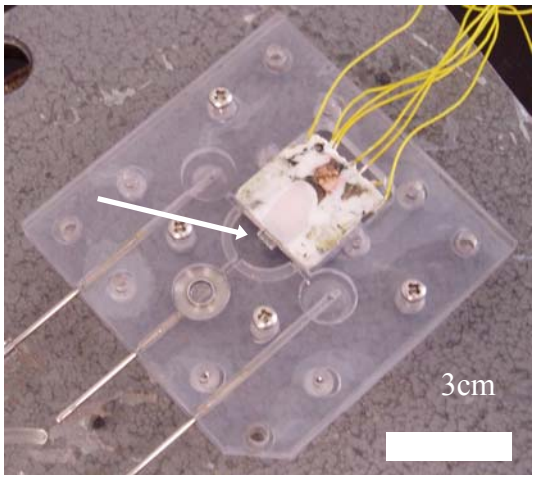

Figure 5-16: Custom designed and fabricated cartridge for BA detection

5.3.2 Anti-BA-Functionalized and BSA-Functionalized Sensor Responses

To study the PEMS array lower limit of detection, the response over a wide range of concentrations, as well as any potential nonspecific interactions of the of the PEMS array with BA and bacterial cells, two tests were run. First, the array was insulated with MPS, as described in Section 4.2.2, and was coated with anti-BA-spore IgG by means of sulfo-SMCC linking molecules, as discussed in Section 4.3.3. This sensor array was then mounted in the flow chamber and DI water was circulated for 15 min. Following this background period, 10^1 BA spores/mL were added to the system and circulated for a period of 30 min. At 30 min, 90 spores/mL were added to the system, bringing the total number of spores in the system to 100 spores/mL. Again, this concentration was circulated for 30 min. Order of magnitude additions of spores were continued in this manner up to a concentration of 10^7 spores/mL.

Following this experiment, the sensor array was then cleaned with dilute piranha solution as in the procedure for insulation by means of MPS, and coated with bovine

serum albumin (BSA) in the same fashion as anti-BA-spore, previously. This coating was chosen as a control coating for the PEMS array since BSA is also negatively charged at neutral pH.[171] Thus, nonspecific interaction between the PEMS array and the BA spores was not expected. To verify this hypothesis, the BSA-coated array was subjected to the same BA spore suspensions as was the anti-BA-spore-coated array.

Figure 5-17 shows the resonance frequency shifts versus time of the array PEMS with anti-BA-spore IgG immobilized on the surface when exposed to BA spore suspensions. Squares, circles, and triangles represent the resonance frequency shift of PEMS 1, PEMS 2, and PEMS 3, respectively. Also shown are the resonance frequency shifts versus time of the same array PEMS in the same BA suspensions when immobilized with BSA on the surface, rather than anti-BA-spore IgG. The BA spore concentrations during the various 30 min time intervals are indicated by arrows at the time of injection. As can be seen, all three PEMS exhibited no discernable resonance frequency shift when the BSA-coated array PEMS was presented with the full gamut of BA spores.

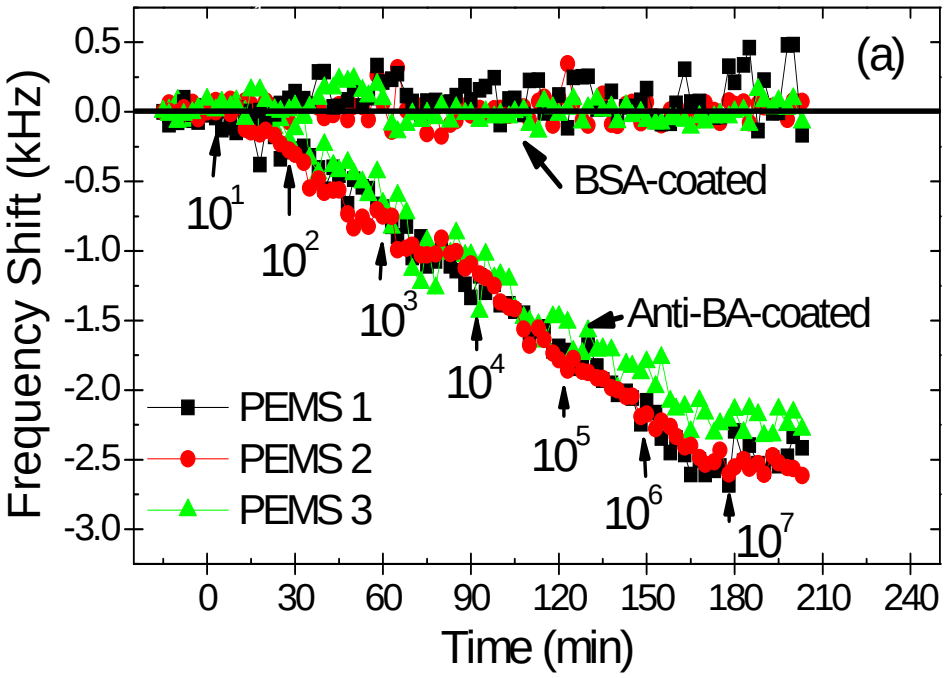

Figure 5-17: Anti-BA- and BSA-functionalized PEMS array responses to BA spore suspensions

When the anti-BA-coated array was exposed to 10 BA spores/mL, a frequency shift of approximately 300 Hz was observed on all three PEMS at t = 30 min, as seen in Figure 5-17. Then, when the concentration was increased to 100 spores/mL, the frequency shift of the three PEMS decreased another 500 Hz to a total shift of 800 Hz. After each 10-fold increase in concentration, the resonant frequencies shifted approximately 500 Hz in the ensuing 30 min up to the concentration increase to 10^6 spores/mL. It can then be seen that saturation of the sensors occurred at approximately 165 min – during the middle of the exposure to 10^6 spores/mL. No additional frequency decrease was observed upon addition of 10^7 spores/mL, probably due to the saturation of BA binding at such high concentrations.[35,37,39] For all detections at all concentrations, all three PEMS exhibited similar resonance frequency shifts with a standard deviation of

11% among the three PEMS. This clearly illustrates the repeatability and reliability of the three PEMS in the array and the utility of the system as a whole for highly sensitive, *in situ*, real-time, in-liquid bio-detection.

During the 15 min leading up to both experiments, the noise levels of the sensor in DI water were 42, 48 and 26 Hz for PEMS 1, PEMS 2, and PEMS 3, respectively. During exposure of the BSA-coated array to the BA spore concentrations, noise levels of 80, 140 and 85 were observed. The anti-BA-spore-coated sensors exhibited noise levels of 60, 75 and 53 Hz during detection of BA spores. Thus, all noise levels were at or below 140 Hz. Even with the worst-case noise level of 140 Hz, the -300 Hz resonance frequency shift for the detection of just 10 BA spores/mL allows for a signal to noise ratio (SNR) of greater than 2. Detections of all other concentrations give an SNR far larger than this, indicating that all observed resonance frequency shifts are true positive responses, when SNR=2 is defined as the threshold for positive response.

While these experiments did not yield a linear dose response of the PEMS to these concentrations of BA, which would require preparing the sensor surface after detection at each concentration (a total of 14 times), they nonetheless amply demonstrated the repeatability of the detection from sensor to sensor, which was one of the main goals of this study. This repeatability provides the redundancy needed when such a system is to be implemented in real-world usage. Without such concurrent redundancy allowed by this array system, several tests would have to be performed, one after another, in order to provide the level of confidence needed to confirm the presence of the target antigen, BA in this case. Clearly, such a one-after-another testing protocol eliminates both the real-time and continuous monitoring nature of such a system.

These sensitivity experiments showed that there was negligible, if any, non-specific binding of BA spores to the sensor surface when it was coated with BSA. That is, there were no 'false positive' responses on the BSA-coated array. Selectivity experiments were aimed to further probe this possibility, but also test for a 'false negative' response when other bacterial species (*i.e.* interferants) were added to the BA spore suspensions.

5.3.3 Selective Array Detection of BA in mixtures of *Staphylococcus aureus* (SA) and *Pseudomonas aeruginosa* (PA)

For a study of the selectivity of the PEMS array, a blind study was arranged and administered by a collaborator, Mr. Mark Mattucci. Samples labeled A through D were prepared by Ms. Mitali Purohit in Dr. Rick Rest's lab and provided for experimentation. Experiments were then carried out on the four samples in a similar fashion as in the sensitivity experiments. Namely, the PEMS array was cleaned and immobilized with anti-BA-spore IgG. The array was then mounted in the flow chamber and exposed to DI water for 15 min. Then one of the blind samples was added to the system and circulated for 25 min.

Following the testing of each sample, the PEMS array was cleaned with dilute piranha solution (as above), and re-coated with anti-BA-spore IgG in preparation for the next sample. Unknown until after experimentation, these blinded samples contained mixtures of BA, *S. aureus* (SA) and *P. aeruginosa* (PA) in DI water at varying concentrations and ratios. Table 5-5, below details the contents of these mixtures.

Table 5-5: Blinded selectivity study samples

Sample ID	BA Spores/mL	Ratio of 2 interferants (equal mixture)	Number of bacteria/mL
A	3.3×10^3	all BA	0
B	3.3×10^3	100:1	3.3×10^5
C	0	all interferants	3.3×10^6
D	3.3×10^3	1000:1	3.3×10^6

Figure 5-18 depicts the resonance frequency shift versus time obtained in these blind selectivity experiments. For clarity, the resonance frequency shifts of the three PEMS during exposure to each sample are plotted as one averaged shift with the error bars indicating the standard deviation of this average.

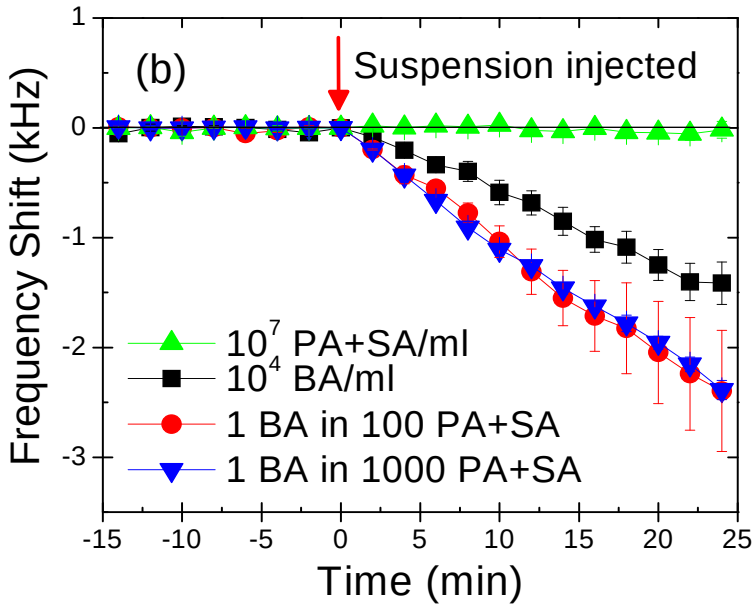

Figure 5-18: Blinded selectivity experiment PEMS array responses

In this figure, we see that Sample C produced no resonance frequency shift, Sample A produced a resonance frequency shift of 1.3 kHz at 25 min and Samples B and D produced resonance frequency shifts of 2.3 kHz at 25 min. After completion of all

testing, the compositions, as given above, of all samples were revealed to this author and the obtained PEMS responses were compared. We see that 3.3×10^6 interferants/mL produced no frequency shift in any of the PEMS. The sample containing just 3.3×10^3 BA spores/mL resulted in an average frequency shift of 1.3 kHz for all three PEMS in the array. This shift was consistent with a similar concentration in the sensitivity studies. Finally, Samples B and D, both of which contained 3.3×10^3 BA spores but also contained 3.3×10^5 and 3.3×10^6, respectively, SA and PA cells/mL, produced nearly identical resonant frequency shifts of 2.3 kHz at 25 min. Again, all three PEMS exhibited identical responses in all detections with a standard deviation of approximately 10%. The higher standard deviation of sample B was due to the formation of a bubble on one of the cantilever tips towards the latter part of the detection.

From these comparisons, it is clear that the PEMS array correctly detected the presence or absence of BA in all four blinded samples. The all-interferant mixture, Sample C, produced no 'false positive' response. Furthermore, as evident in the response to samples B and D, the presence of interferants in a suspension of BA (in ratios of 100:1 and 1000:1, interferants:BA) did not cause a 'false negative' response, *i.e.* the interferants did not prevent the positive detection of BA spores.

Interestingly, the interferants augmented the resonance frequency shift in the detection of the BA spores, as compared to Sample A. A first reaction to this observation would be to assume that the interferants were non-specifically 'sticking' to the sensor surface, thus artificially increasing the array response. However, this was clearly not the case as Sample C showed that no PEMS array response occurred when a mixture of only interferants was presented. The next conclusion to be drawn is that one or both of the

interferants was agglomerating or 'clumping' with the BA spores in suspension. Then, when the BA spore of an agglomerate contacted the anti-BA-spore-coated sensor surface, the whole agglomerate bound to the surface, and thus induced a greater resonant frequency shift than would just a lone spore. This explanation becomes plausible when it is noted that *S. aureus* possesses a more neutral[172] surface charge than that of *Bacillus* spores[156], allowing for such agglomeration.

To further examine the origin of the exaggerated resonance frequency shift in the presence of SA and PA, scanning electron microscopy (SEM) (FEI, XL30) was used to examine the PEMS surfaces after exposure to these samples. As an example, for Sample A (3.3×10^3 BA spores/mL) there is a single BA spore bound to the PEMS surface in the area of the electron micrograph shown in Figure 5-19.

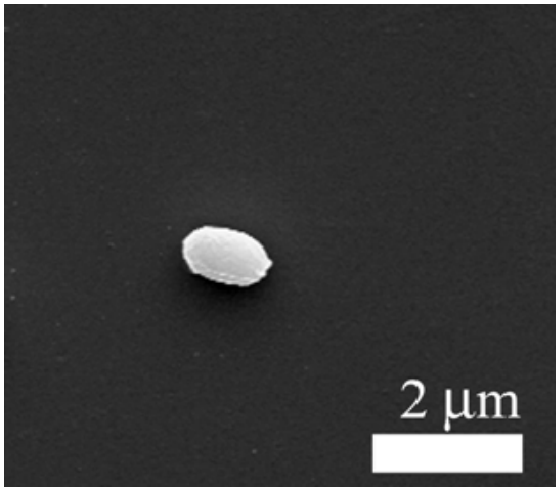

Figure 5-19: Scanning electron micrograph of a BA spore on the surface of a PEMS biosensor

This degree of surface coverage is typical of the entire sensor surface. SEM examination showed that no cells adhered to a PEMS sensor surface after exposure to Sample C (3.3×10^6 SA+PA cells/mL) (not shown), which is consistent with the

negligible resonance frequency shift exhibited by the PEMS in Sample C. After exposure to Sample D (3.3×10^3 BA spores/mL plus 3.3×10^6 SA+PA cells/mL), agglomerates of spores and cells are seen to be bound to the sensor surface as in Figure 5-20.

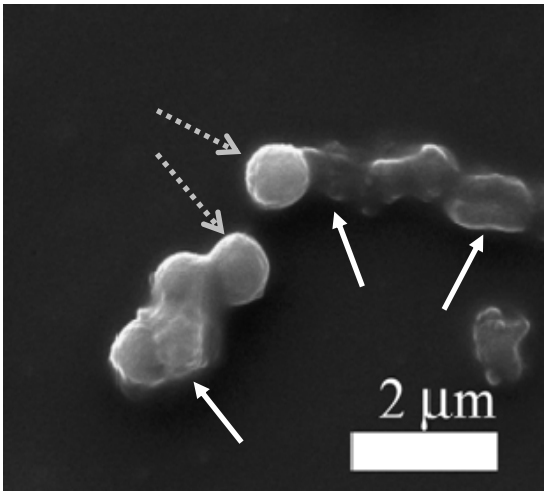

Figure 5-20: BA and SA aggolomerates on the surface of a PEMS biosensor

In this image, we see several biological entities on the sensor surface in close proximity. The geometries of the three possible cells/spores enable visual differentiation and identification. SA cells are exclusively spherical; PA cells are decidedly elongated with typical aspect ratios (the ratio of length to width) greater than 2; BA spores are slightly elongated with aspect ratios between 1.2 and 1.5. Thus, we can see in Figure 5-20, no PA is observed on the sensor surface while SA (as indicated by dashed arrows) is observed to be agglomerated with BA (as indicated by solid arrows) on the surface. Furthermore, by considering the additional resonance frequency shift associated with detection of these agglomerates and the calculated mass of an SA cell as compared to a BA spore, from 1.3 kHz to 2.3 kHz, we can say that, on average, the agglomerates detected by the PEMS were comprised of one BA spore and one SA cell.

5.3.4 Statistical Analysis

With the several different BA detection experiments performed in this particular study, we can characterize the PEMS array's detection capabilities by means of a statistical analysis, as described in Section 2.4. In characterizing our outcomes in the form of Table 2-1, and by analyzing the data only from Figure 5-18, we arrive at Table 5-6, below. In doing so, since these are laboratory experiments, we take our 'Gold Standard' test to be the known identities of Samples A through D and we say that Biosensor Test Result is positive (+) if the average sensor response is greater than twice the maximum noise level observed in the initial limit of detection trials. That is, we require a SNR of 2 where the noise level is 140 Hz.

Table 5-6: Statistical characterization of BA array detection of BA-interferant mixtures

	Known Samples ('Gold Standard' Test)		
Biosensor Test Results	**BA present (+)**	**No BA (-)**	**Totals**
BA present (+)	3	0	3
No BA (-)	0	1	1
Totals	3	1	4

From this table, according to equations (2.4) and (2.5), we can calculate both the statistical sensitivity and specificity of this detection as 100%. If we, then, include the limit of detection data presented in Figure 5-17, the addition of these 14 experiments causes Table 5-6 to become Table 5-7.

Table 5-7: Statistical characterization of BA array detection including limit of detection data

	Known Samples ('Gold Standard' Test)		
Biosensor Test Results	**BA present (+)**	**No BA (-)**	**Totals**
BA present (+)	9	0	9
No BA (-)	1	8	9
Totals	10	8	18

In this case, we see that the fact that the sensor was unresponsive when the concentration was increased from 10^6 to 10^7 spores/mL has led to the single false negative case where BA was, in fact, present, but it was not detected. The inclusion of these numbers bring our statistical sensitivity and specificity values to 90% and 100%, respectively. However, if we consider the situation where 10^7 spores/mL were added to the detection system without prior exposure to 10^6 spores/mL, we would most certainly attain a true positive response. This point illustrates the fact that while a 'yes' detection will still occur for this concentration, our sensor will not be able to quantify detected BA concentrations above 10^6 spores/mL. Additionally, it serves notice to the fact that once a BA detection is recorded, a new sensor should be used such that subsequent detections are not missed.

Another permutation of this analysis could include increasing our SNR requirement from 2 to 3. If this SNR level were the requirement for positive vs. negative detection, we would see the number of false negatives increase to two and the number of true positives decrease to eight, as the concentration of 10^1 spores/mL would have to be deemed undetectable with this new SNR requirement. As a result our statistical sensitivity value would slip to 80% while our specificity percentage would remain at 100.

5.4 Chapter and BA Detection Summary

In this Chapter, three different types of *Bacillus anthracis* (BA) detection using three distinctly different types of PEMS biosensors have been presented. In the first study, the use of a highly sensitive PMN-PT/tin PEMS was used to achieve a detection of just 36 total spores suspended in 0.8 mL PBS. Also, proven as effective was the method of MTMS insulation and MPA immobilization for this type of sensor. With this detection and the accompanying dose response elucidation, the PMN-PT PEMS was firmly established as a highly sensitive biodetection platform. Based on the 12 individual detection instances in this study, calculated statistical sensitivities were found to range from 91% to 73% depending on the signal to noise ratio (SNR) chosen as the detection threshold. As such, array detection was later explored as a means to improve this performance. Also, since no real instances of possible false positive were presented to this sensor, to further probe specificity values under various conditions, close cousins of BA and mixtures of BA with 'interferant' biological species were later presented to PEMS biosensors.

In the first of these subsequent explorations, the optimal flow conditions for detection of BA spores, reduction of nonspecific interaction of cousins of BA with the senor surface and an optimization of these two conditions were achieved. These optimal conditions were identified for an 8 mm wide flow channel and were found to occur at 10 and 14 mL/min. At these flow rate values cross reactivities of the BA spore cousins were minimized to levels below 0.1, and both the statistical sensitivity and specificity of the PZT-glass biosensor used for investigation were found to be 100%. This is opposed to the lower flow rates of 1 and 4 mL/min where cross reactivity values were as high as 0.4,

and specificity values dipped as low as 40%. This work involved the determination of spore and cell interaction with the PEMS sensor under 36 different experimental conditions.

In the final study using BA as the biological pathogen of interest, the first presentation of a piezoelectric cantilever array used for simultaneous, real-time, *in situ,* redundant biodetection was presented. First, the sensor-to-sensor reliability and repeatability of resonance frequency shift response to BA concentrations ranging from 10 to 10^7 spores/mL were demonstrated. Subsequently, the true positive detection of BA among 1000 times more bacterial interferant cells was demonstrated while false positive detection of the bacterial cells alone and false negative responses to the BA/cell mixtures were avoided. These array detection experiments lead to statistical sensitivities and specificities of 100% for the BA/interferant mixture trials, and would have led to the same values of 100% with an SNR of 2 if the sensor had not been saturated by BA spore adhesion upon addition of 10^7 spores/mL.

Thus, in this chapter, while initial BA spore detections at very low limits of detection were achieved using PMN-PT PEMS, the implementation and optimization of engineered fluidics along with true real-time, redundant piezoelectric array pathogen monitoring markedly improved the sensitivity and specificity of detection of this sporulated pathogen. Also, it was determined that the flow rate, speed and force needed to prevent detection of BS, BT, and BC spores by our PEMS biosensor was in excess of 14 mL/min, 3.8 mm/s and 100 pN, respectively. For BA spores, however, it was estimated that the interaction force with the anti-BA-spore functionalized PEMS surface was greater than or equal to 400 pN.

CHAPTER 6: *CRYPTOSPORIDIUM* OOCYST DETECTION

Following the improvements in piezoelectric cantilever biosensor performance demonstrated by the sensitive and specific detection of *Bacillus anthracis* (BA) spores in the previous chapter, this current chapter will focus on the detection of *Cryptosporidium* oocysts in water suspensions by means of two different advanced piezoelectric cantilever array systems. In Chapter 5, the detection of as few as 37 total BA spores and ten BA spores/mL was demonstrated. These values are clearly on the cusp of single pathogen detection. Thus, in addition to the technological, social and economic concerns dictating the need for a more sensitive and more rapid *Cryptosporidium* oocyst biosensor, it also makes sense from a piezoelectric cantilever development and testing standpoint to evaluate the detection of this pathogen.

Since *Cryptosporidium* oocysts range from 4 to 6 μm in diameter,[173] as compared to BA spores which are typically 1 to 1.2 μm across[9], the mass of these oocysts is more than 100 times greater than that of a BA spore. Thus, with the mass of a BA spore at approximately 0.5 pg, the mass of a *Cryptosporidium* oocyst is calculated as approximately 65 pg. Or, in terms of the frequency shift sensitivities associated with the BA detection presented in Chapter 5, we should expect a shift on the order of 500 Hz per Cryptosporidium oocyst detected by a PEMS sensor. With PEMS array noise levels in Chapter 5 at 100 Hz, this expected resonant frequency shift of 500 Hz should produce signal to noise ratios (SNR) exceeding three, thus enabling definitive detection of single *Cryptosporidium* oocysts.

Furthermore, the redundancy of the PEMS array system allows for multiple simultaneous C*ryptosporidium* biodetection assays as well as the concurrent monitoring

of a reference PEMS to continuously check for non-specific detection or 'false positives.' In our PEMS array systems, all of these advantages are available without sacrificing the real-time nature of the assay. Two types of PEMS arrays were fabricated for this study. One PEMS array consisted of cantilevers composed of a PZT layer bonded to a glass layer, as in Section 5.3, while the second type of PEMS array was comprised of cantilevers made of only a single layer of PZT, as presented in Section 4.1.1.2.

6.1 Dose Response Array Detection of *Cryptosporidium Parvum* (CP) oocysts

Similar to the experimental protocol for BA, the first systematic piezoelectric cantilever test for the detection of *Cryptosporidium* oocysts involved establishing a dose response profile and probing the lower limit of detection for this pathogen system. To perform this dose response study, the same PZT-glass array system used for detection of BA in Section 5.3 was used.

6.1.1 Sensor Array, Flow System and Experimental Setup

Cryptosporidium parvum (CP) oocysts and monoclonal IgM antibody were both purchased from Waterborne, Inc. (New Orleans, LA). Once a PEMS array is constructed, insulated and functionalized as described previously, it can be monitored continuously and in real-time using an impedance analyzer (Agilent, 4294A, Santa Clara, CA) in conjunction with a switch box (3499A, Agilent, Santa Clara, CA) and a PC-based control and data-acquisition program. Improvements to the switch box system and data acquisition program following the BA array detection experiments in Section 5.3 have allowed for the simultaneous monitoring of up to four PEMS in these *Cryptosporidium* oocyst detection experiments. Thus, the three redundant sensors comprising the array in Figure 5-14 were functionalized with anti-CP IgM and a fourth, separate cantilever was

introduced to serve as a real-time reference sensor. This reference cantilever was functionalized with antibody to *Salmonella typhimurium* to provide an immunoglobulin surface similar to the active sensors, but lacking the affinity for *Cryptosporidium* oocysts. The cantilever array and reference sensor were insulated (and subsequently re-insulated after each use) for complete submersion in aqueous suspensions by means of MPS according to the procedure in Section 4.2.2 Sulfo-SMCC immobilization of antibody was carried out according to the protocols of Section 4.3.3. Figure 6-1 is an optical micrograph of the individual PEMS used as the reference sensor and Figure 6-2 displays its resonance spectrum. The peak at 430 kHz was monitored during experimentation as it coincided in location, and height (almost 15 degrees) with the peaks monitored in the detection array, as given in Figure 5-15.

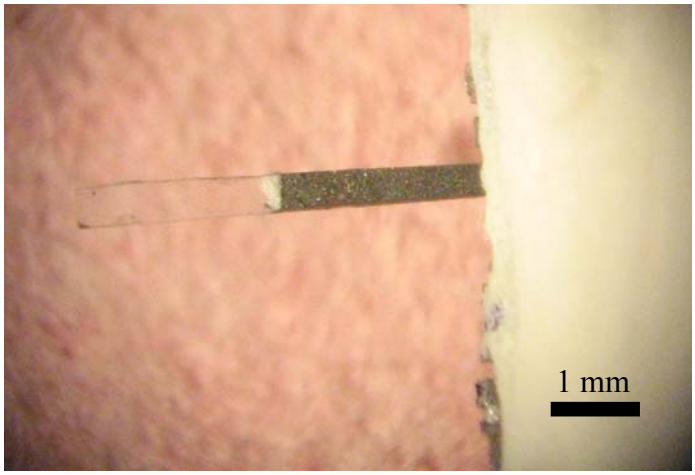

Figure 6-1: PZT-glass reference PEMS used in CP detection experiments

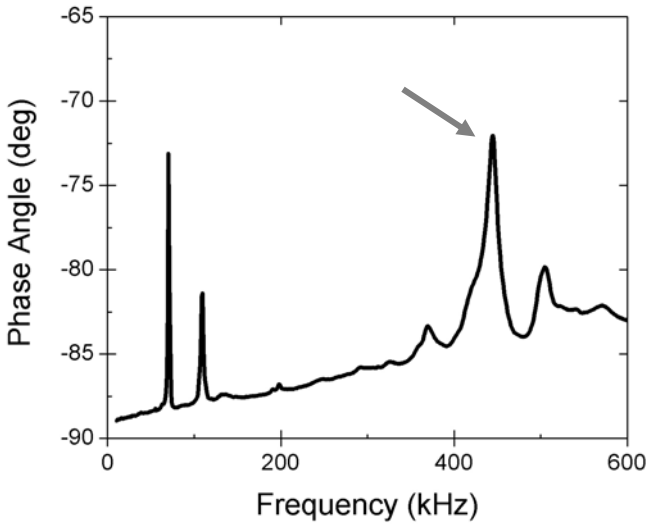

Figure 6-2: Phase angle vs. frequency spectrum of reference PEMS used in CP detection

The flow cell used for the study of *Cryptosporidium* oocyst detection by PEMS array was 19 mm in width with a semicircular cross-section (and thus, a 9.5 mm depth). These dimensions were chosen according to the engineered fluid flow analysis and the results of experimental fluid force calibration presented in Section 4.4.2, such that the predicted force impingent on the *Cryptosporidium* oocysts by the flow of the analyte fluid remains on the order of 10 to 100 pN. The Reynolds Number (*Re*) for all possible flow speeds in this channel ranged from 0.8 to 31, thus all conditions were laminar (*i.e.* $Re \ll 2000$). The channel was 130 mm long, and thus occupied a volume of 18 mL. In the dose response study of CP detection, a closed-loop, recirculation flow system was used with an additional external reservoir of 82 mL to bring the total detection volume to 100 mL. Figure 6-3, below displays three optical images of this custom designed and constructed flow cell. Side view (a), top view (b) and end-on view (c) orientations are shown so as to illustrate the placement of the sensors.

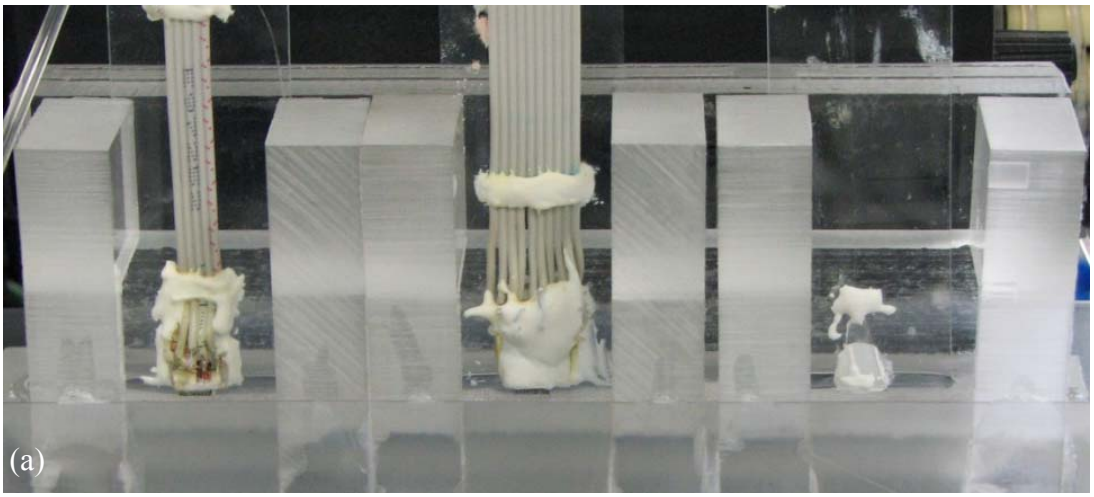

Figure 6-3: (a) Side view of *Cryptosporidium* oocyst detection flow cell with detection array inserted in center clamp, reference cantilever inserted in left clamp and glass strip inserted in right clamp, (b) top view of the same, (c) end-on view of the same

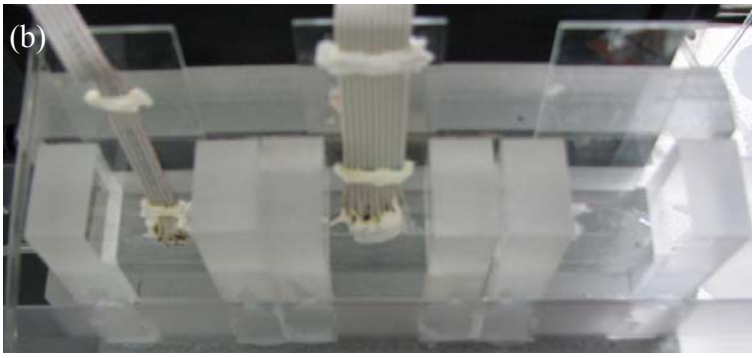

In this flow cell, the fluid flow is contained in the semicircular trough at the bottom of image (a) and is open to the surrounding environment. As the detection arrays were completely submerged, evaporation of the detection fluid was not a concern.[34,37-39] Additionally, as shown, three pairs of clamps were included in the design in order to ensure that the detection array and reference sensor were aligned in the center of the flow. This clamp design also allowed for easy sensor insertion into and removal from the

system. These separate array/sensor insertion points into the flow cell allowed for the precise positioning of both the detection array and the reference senor, while the third clamp position allowed for the insertion of a simple strip of glass mounted onto a microscope slide, as seen to the right in Figure 6-3(a). This strip of glass was identical to that used in the fabrication of the detection array and was also identically insulated and functionalized. As such, this surrogate cantilever could be used for optical and SEM imagining without risking harm to the actual PEMS cantilever array itself.

To obtain the dose response characteristics of this PEMS array system, *Cryptosporidium parvum* (CP) oocyst suspensions of 100, 10, 1 and 0.1 oocysts/mL were prepared. As a starting point, 1 mL/min (*Re* = 2) was chosen as a flow speed.

6.1.2 Detection Dose Response and Real-Time CP Detection

Figure 6-4, below displays the dose response data collected in the detection of CP oocysts. In this figure, as was the case for the array detection of BA among interferants, for each CP detection trace, each data point represents the average response of the three array cantilevers at that point in time. The errors bars represent the standard deviation of these averaged values. For the reference trace, each point in time represents the average of the five individual reference responses from all experimental trial. The error bars, though barely visible, represent the standard deviation of these five data for each point in time. Also, the concentration of 0.1 oocysts/mL (or one oocyst per ten mL) was performed twice, so that the trace as plotted represents the average of six data points instead of three.

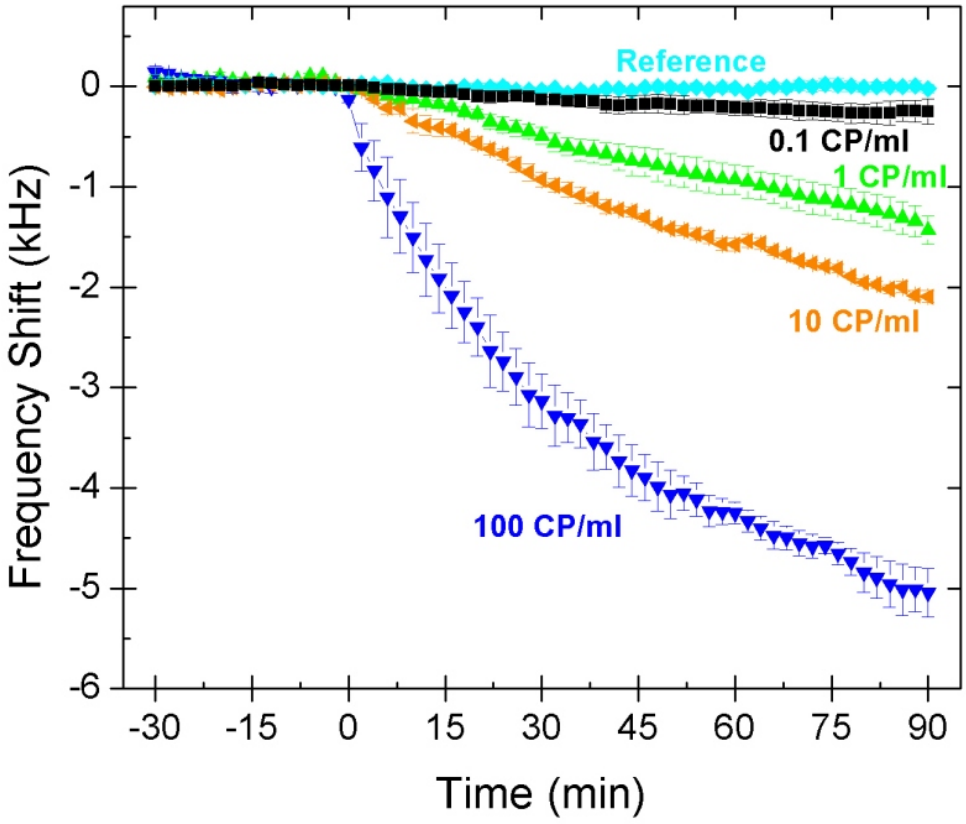

Figure 6-4: *Cryptosporidium parvum* dose response profile of PZT-glass PEMS array

In this figure, we see that the CP oocyst concentration of 100 oocysts/mL induced an average cantilever frequency shift response of -5 kHz in 1.5 hours, and that this response was -2.1 kHz in just fifteen minutes. The concentration of 10 oocysts/mL induced a response of -2.1 kHz in 1.5 hrs and a shift of -500 Hz in just fifteen minutes. One oocyst per mL induced a cantilever array response of -1.5 kHz in 1.5 hours, and a response of -500 kHz in 30 min. For the two detections of 1 oocyst per 10 mL of water, average detection shift of -200 Hz was acquired for both experiments at sixty minutes, though forthcoming analysis in Figure 6-7 will reveal further information contained in

these data. In the case of 100 oocysts/mL, the standard deviation of the average response of the three sensors is calculated to be as high as 400 Hz, while the standard deviation for the 10 CP/mL curve is only -75 Hz. However, for all concentrations of CP oocysts, each individual sensor in the array was characterized by noise levels of no higher than 50 Hz.

The reference sensor in all five detection experiments showed no frequency shift response and its noise level was between 25 and 50 Hz for all experiments. For all of these experiments, the noise reduction technique of resonance peak reconstruction, described in Appendix A, was used to achieve these very low levels of PEMS noise.

From this PEMS array dose response elucidation, we see that concentrations of 100, 10 and 1 CP oocysts/mL are easily detected in times as short as fifteen minutes. Additionally, the concentration of 0.1 oocyst/mL is also detected with a signal to noise ratio (SNR) of 4 in sixty minutes. Already, this *Cryptosporidium* oocyst limit of detection of the PEMS array has far outstripped the performance of other current real-time methodologies for oocyst detection presented in Chapter 2.

The statistical analysis of *Cryptosporidium* oocyst detection by PEMS array in DI water between the concentrations of 100 and 0.1 oocysts/per is trivial, as all concentrations were successfully detected. Thus, the specificity and sensitivity of these experiments were 100% for an SNR as high as four. While this method of calculating sensitivity is fitting for these and previous *Bacillus anthracis* detection experiments, forthcoming discussion in Section 6.3.3 will expound on further considerations that become necessary when dealing with such low concentrations of analyte in suspension.

6.1.3 Verification of Oocyst Detection by Microscopy

To verify that *Cryptosporidium* oocysts had indeed been detected by the PEMS array in concentrations as low as 0.1 oocysts/mL, both optical and scanning electron microscopy (SEM) were used to verify oocyst presence on the surface of the surrogate sensor as explained above. The images in Figure 6-5(a) and (b), below, are optical micrographs of the glass surface of the surrogate sensor immediately after detection experiments. Figure 6-5(a) shows two oocysts adhered to the top of the sensor after the detection of 1 oocyst/mL while (b) shows an oocyst adhered to the sensor surface after detection conditions of 0.1 oocysts/mL. For morphological comparison, Figure 6-5(c) is a fluorescent micrograph of CP oocysts published by the US EPA.[174]

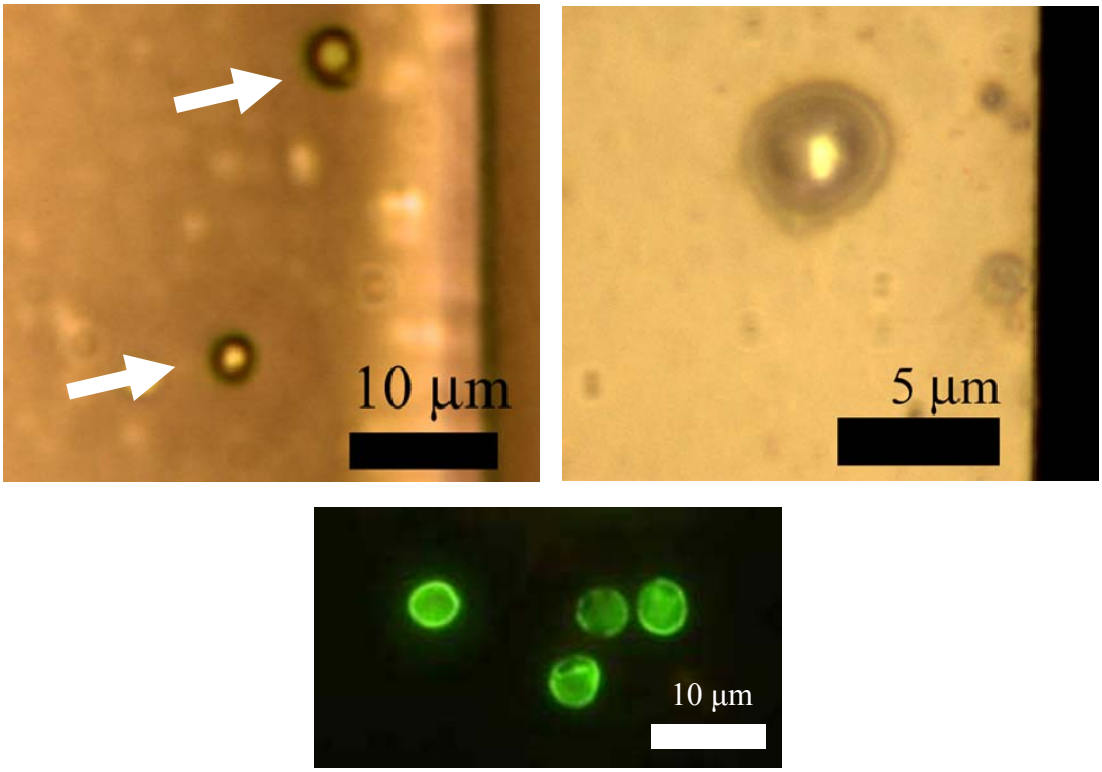

Figure 6-5: (a) Optical micrograph of CP oocysts (indicated by arrows) on sensor surface after 1 oocyst/mL detection, (b) Optical micrograph of CP oocyst on sensor surface after 0.1 oocyst/mL detection, (c) Fluorescent optical micrographs of CP oocysts (US EPA)

After these optical images were obtained, the cantilever in Figure 6-5(b) was imaged by SEM for further morphological investigation. Figure 6-6 is a micrograph obtained as a result of this investigation. Here, we see a single CP oocyst on the surface of the sensor. Additionally, it is clear that the oocyst in this image has previously excystated upon release of its sporozoites as shown in Figure 1-1. Due to bio-safety considerations, the oocysts purchased from Waterborne, Inc. were killed in formaldehyde prior to shipping. This may be the cause of excystation.

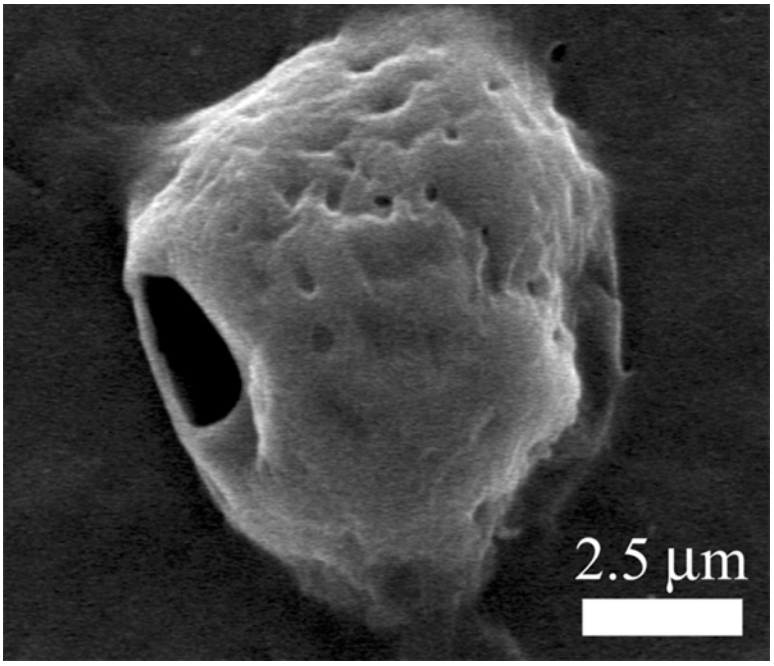

Figure 6-6: Scanning electron micrograph of CP oocyst on the surface of a sensor

6.2 Single CP Oocyst Detection in the Closed-Loop Circulation System

As discussed above, there is much more detail involved in the detection of 0.1 CP oocysts/mL than simply the average of the three PEMS resonance frequency shifts at various points in time. A closer examination of these data reveals that individual oocyst detection events can be 'seen' by the individual cantilevers in the PEMS biosensor array. As discussed in the introduction to this chapter, the large size of *Cryptosporidium* oocysts, as compared to other biological cells should lead to resonance frequency shifts as high as 500 Hz per oocyst.

6.2.1 Single CP Oocyst Detection Using PZT/Glass PEMS Arrays

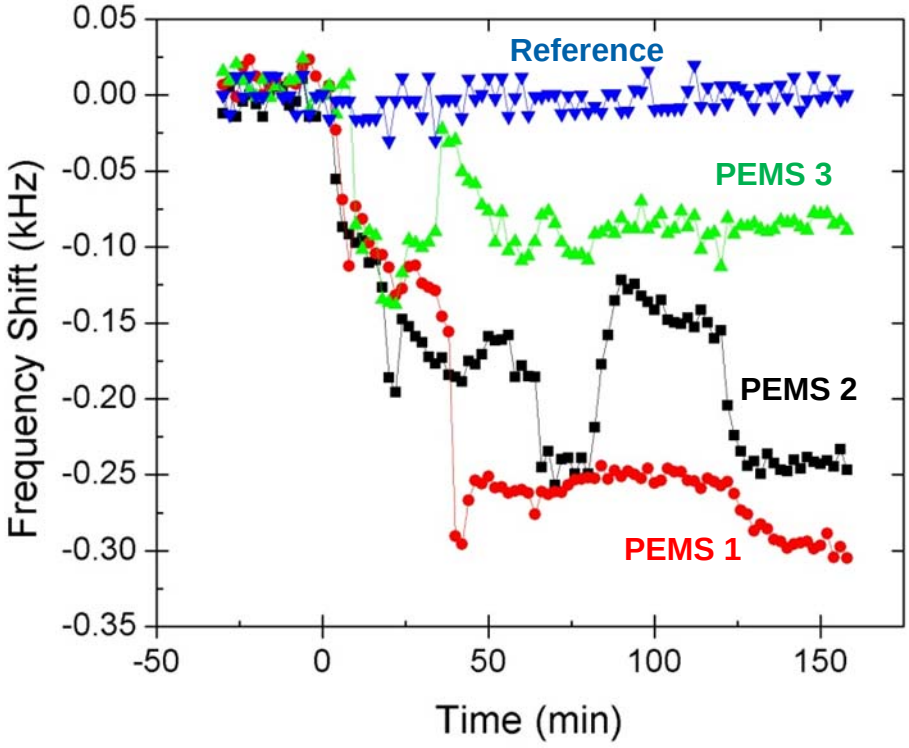

Figure 6-7: Individual PEMS array cantilever responses to 0.1 CP oocysts/ml

In Figure 6-7, the individual PEMS responses to 0.1 oocysts/mL are plotted along with the response of the reference cantilever. In this detection, the flow system was circulated with DI water for a period of thirty minutes prior to injection of the CP oocysts. These oocysts were then injected immediately upstream of the detection array, and it is seen that all cantilevers in the detection array responded to the CP oocysts closely following this injection. While each sensor response was slightly different at this point, all three showed a shift of approximately 100 Hz in the time intervening between two data points, near, or closely after t = 0.

Following this injection, over the course of the next 2.5 hours, as the 100 mL of pathogen suspension was re-circulated, additional instances of oocyst interaction and

binding to the sensor surface were observed. Also, instances of unbinding can be seen. For PEMS 1, after this initial CP oocyst detection, another step-wise resonance frequency drop of 200 Hz is observed at forty minutes, followed by a period of relative stability. In the case of PEMS 2, a drop of 100 Hz followed closely after the first 100 Hz drop. Then, another shift of approximately 80 Hz is observed, followed by an upshift of 100 Hz and another downshift of 90 Hz. In the case of PEMS 3, a resonance frequency upshift of 100 Hz, nearly back to the baseline value was observed at thirty seven minutes. Whereas the resonance frequency downshifts of approximately 100 Hz seems to correspond to the detection of an oocyst, the upshifts of these same magnitudes likely correspond to the removal of an oocyst from the sensor surface as a result of the fluid flow overcoming the force of interaction with the sensor surface. This presumption will be explored in depth at a later point in this chapter.

6.2.2 Single CP Oocyst Detection Using PZT-only Arrays

The data in Figure 6-7 and Figure 6-4 represented a promising start to the detection of *Cryptosporidium* oocysts by means of PEMS biosensors. However, a clearer detection of single CP oocysts with better signal to noise ratios was desired in order to confidently make the claim of this lowest of limits of detection. In hopes of accomplishing this goal, two particular paths of development were followed simultaneously. In one vein, a yet more sensitive PEMS array was sought, and in the other vein, improvements in the method of electronic noise reduction were developed. This method of further reducing the electronic noise reduction involved the implementation of more symmetric peak reconstruction methods for each individual detection peak scan as detailed in Appendix B.

In hopes of producing the more sensitive PEMS array biosensors, the development of the PZT-only PEMS array was initiated. The impetus for this PEMS engineering strategy was found first in the unusually high frequency and amplitude (in terms of degrees above -90^{o}) peaks found in such PZT-glass arrays as pictured in Figure 5-14 and for which the resonance spectra are show in Figure 5-15. In this figure, we see that the flexural resonance peaks located at 45 kHz is approximately 5 degrees high. However, the peaks at 410 kHz are as high as 16 degrees high. It was this observation that initially led to the theoretical investigation of length and width mode peaks as discussed in Section 4.1.1.2. The motivation was that such peaks should be more sensitive according to the general maxim that higher frequency peaks are more sensitive, but also that these peaks should be more 'monitorable' due to their high amplitude and the resulting ease of tracking by the resonance frequency acquisition program. Indeed, such was born out in the forthcoming experiments with these arrays.

When the analysis presented in Section 4.1.1.2 revealed that peaks such as this 410 kHz peak may indeed be length or width mode peaks, the logical experimental test to probe this hypothesis involved the construction of a PEMS array consisting of only PZT and no nonpiezoelectric layer. While such a cantilever would not be expected to demonstrate flexural resonance, it should retain its width and length mode peaks. We see this result demonstrated in Figure 6-8(b) where the width and length mode peaks are seen clearly, but there are no flexural mode peaks in their usual range of 100 kHz. Furthermore, it was hypothesized that such PZT-only cantilevers would be better suited for detection via these peaks due to the lack of damping experienced from the nonpiezoelectric layer in bi-layer arrays.

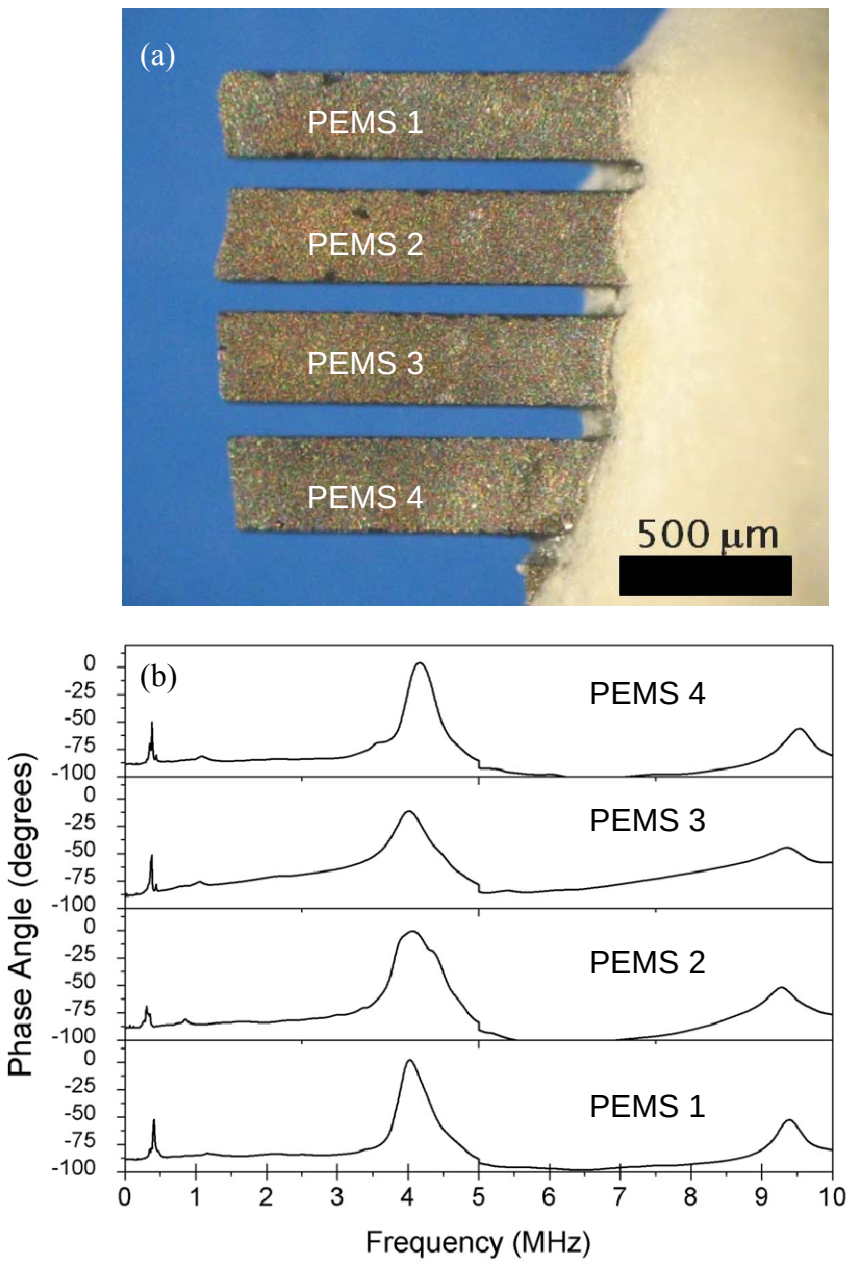

Figure 6-8: (a) A PZT-only array used for *Cryptosporidium* oocyst detection and (b) the resonance spectra of this array

Figure 6-8(a) represents a PZT-array constructed according to the method in Section 4.1.1.2, while in Figure 6-8(b) the resonance spectra of this array are shown. We see that four 400 µm wide PZT-only cantilevers have been produced, but that the clamp

on the fourth cantilever is markedly un-square. As a result this cantilever was not used for detection, but rather PEMS 1, 2 and 3 were chosen as the active array for detection of *Cryptosporidium* oocysts in subsequent experiments. The peak at 400 kHz was the detection peak used in all subsequent experiments. The peaks at 4 and 9.4 MHz have also be probed for their utility as detection peaks, but, as yet, have been found too noisy (due to their low Q) for effective biodetection. Future improvements in array production and signal processing may prove otherwise.

The reference sensor used in subsequent experiments is shown in Figure 6-9, as indicated by the arrow, and its resonance spectrum is similar to those of PEMS 1, 2 and 3 and shown in Figure 4-3.

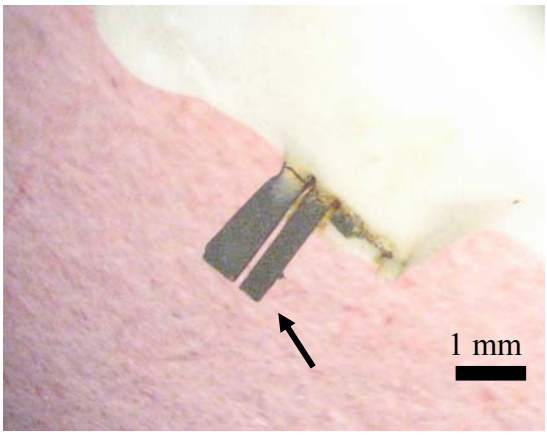

Figure 6-9: PZT-only reference cantilever

The first experiment performed with this PZT-only array involved the detection of CP oocysts in a concentration of 0.5 per milliliter in DI water (*i.e.* 5 CP oocysts per 10 mL of water). This concentration was chosen so as to increase the number of oocysts present in the 100 mL sample, thus increasing the frequency with which detections should occur. During this experiment, the flow rate at which the CP oocysts suspension

was circulated was varied through the entire range of speeds possible. The initial flow rate was 0.4 mL/min, with the final flow rate equal to 14 mL/min. This experimental protocol was designed to determine the effect of these various flow rates on the detection of CP oocysts, similar to BA experiments in Chapter 5.

Figure 6-10, below, displays the individual resonance frequency shifts of all PEMS biosensors monitored in this experiment, under the fluid flow rate conditions of 0.4, 1 and 2 mL/min. In the case of this experiment, CP oocysts were added to the external 82 mL reservoir, rather than immediately upstream of the detection array, as in Section 6.1. As a result of this, sensor response to the added oocysts was delayed at least until the oocysts could be circulated through the system and reach the PEMS detection array

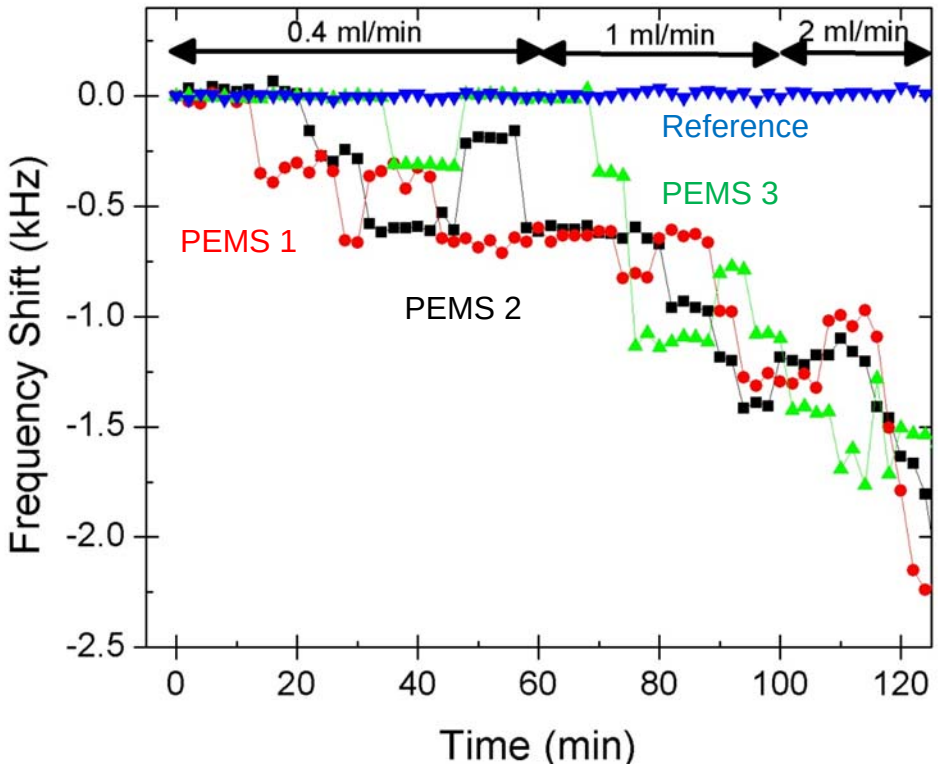

Figure 6-10: PZT-only PEMS array response to CP oocysts at flow rates of 0.4 to 2 mL/min

. In the case of this detection, PEMS 1 exhibited an initial resonance frequency step shift of -290 Hz at twelve minutes, while PEMS 2 and PEMS 3 exhibited similar shifts near twenty and forty minutes, respectively. Subsequent to these initial oocyst detections by each PEMS, instances of additional detection and removal of oocysts by the fluid flow are observed, similar to the previous detection experiment. However, compared to the previously PZT-glass array, in which -100 Hz shift was observed per oocyst detected, in the case of this new PZT-only PEMS, though the same length-mode resonance peaks are used for detection, we observe resonance frequency shifts of -290 Hz for each oocyst detected. Additionally, as the flow rate is increased from 0.4 mL/min to

1 mL/min and then to 2 mL/min, it is seen that the frequency of this binding and unbinding increases.

Throughout the entire detection presented here, the reference sensor remains unresponsive with noise levels of approximately 15 Hz. The noise levels of PEMS 2 and 3 were similar to this value, whereas the noise of PEMS 1 was slightly higher at 35 Hz. This highest noise value observed leads to a calculated SNR of 8 for the shift of -290 Hz associated with the first instance of oocyst detection. This improvement in SNR is attributed to the improved resonance peak reconstruction algorithm as well as the improved magnitude of resonance shifts associated with each oocyst detection by the PZT-only cantilever array.

6.2.3 Flow Rate Dependence of CP Oocysts Detection and CP Oocyst Binding Force Determination

To further probe and quantify the flow rate dependence of CP oocyst detection by this PEMS array, the experiment presented in the previous section was continued through the flow rates of 5, 8, 10, 12 and 14 mL/min. Figure 6-11, displays the PEMS response profiles for the entire range of flow rates probed. Again, the CP oocyst concentration during this experiment was 0.5 CP/mL and the total volume of re-circulated suspension was 100 mL.

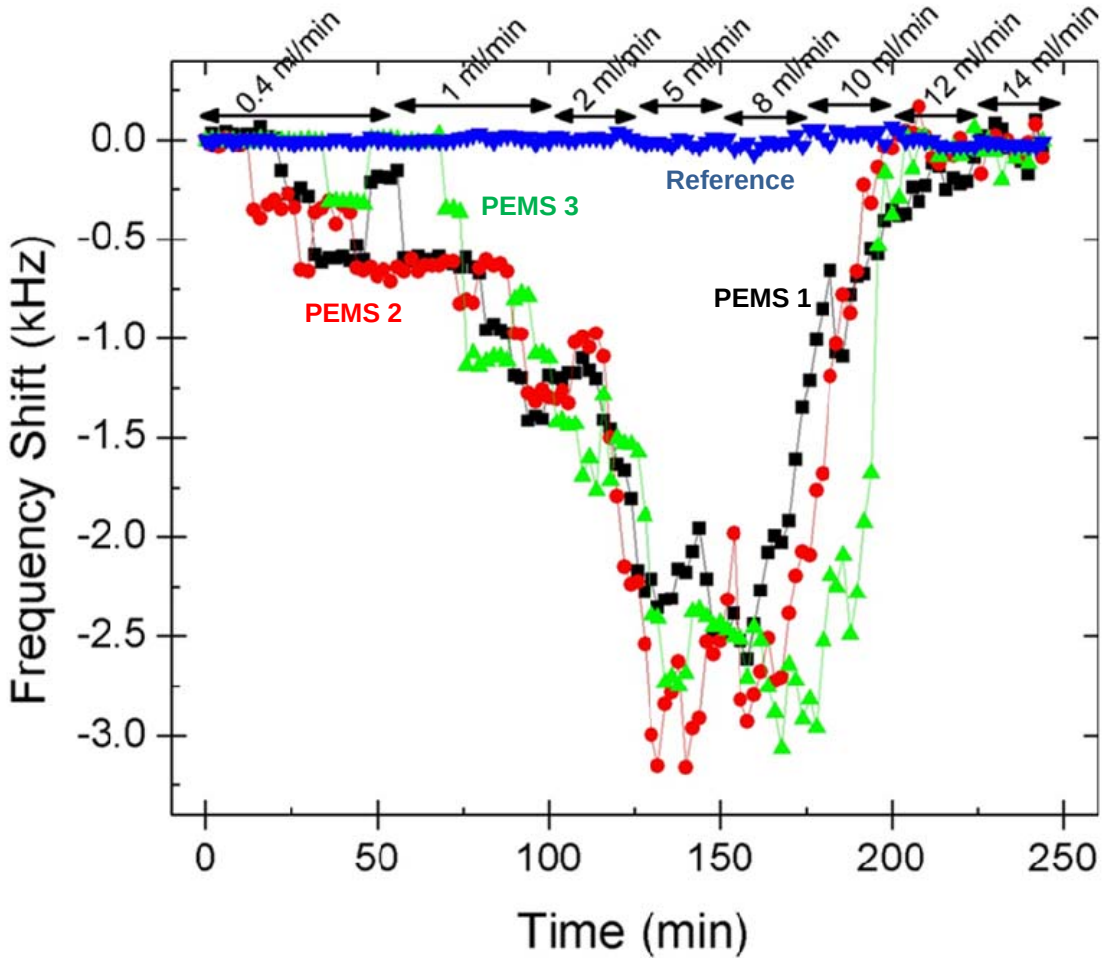

Figure 6-11: PZT-only array response profile to a CP oocyst suspension at flow rates from 0.4 to 14 mL/min

In this figure, we see that the quantum steps associated with oocyst detection under the conditions of 0.4, 1 and 2 mL/min begin to become less clearly defined as flow rates of 5 mL/min are reached and exceeded. At this flow rate of 5 mL/min, the sensor 'noise' is seen to increase to levels of hundreds of Hz and resonance frequency shifts for the detector array are seen to level off between 2.5 and 3 kHz. This 'noise,' however, is likely due to the concurrence of several instances of oocyst detection and removal from the sensor surface, rather than an actual increase in sensor noise. This is supported by the

fact that the reference sensor maintains its previous noise levels through the entire experiment and that the detector array sensor noise nearly returns to previous levels during higher flow rates.

Once the flow rate of 8 mL/min is introduced, the resonance frequency positions of each biosensor in the array begin to tend toward their initial frequency positions. This tendency is carried through the rates of 10 and 12 mL/min with all previous resonance frequency shifts being diminished to zero at the flow rate of 14 mL/min. During this fluid flow rate of 14 mL/min, the detection sensor noise for all three PEMS is approximately 75 Hz. Again, this increase in noise level is likely due to the constant delivery of oocysts to the sensor surface by the action of the fluid flow and the fleeting interactions that occur therewith, as the noise level of the reference sensor maintains at a constant level of 20 Hz throughout all flow rates.

From these CP oocyst detection data under the various flow conditions presented, an estimation of the interaction force between an oocyst and the anti-CP functionalized sensor surface is possible. However, at this point, though the neatly discernable single oocyst detection events will be lost, it is useful to average the resonance frequency shifts of the three individual cantilevers that make up the detection array in order to make a clearer determination of the flow rate at which CP oocysts are prevented from further interactions with the sensor surface. Figure 6-12, below represents this averaged data, with the reference PEMS response is shown again, for comparison.

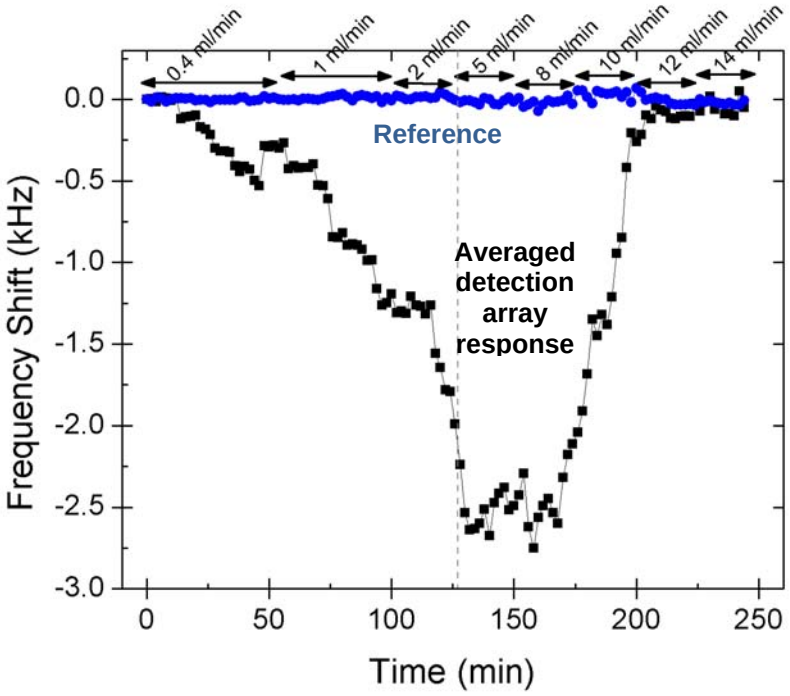

Figure 6-12: Average of the PZT-only detection array response and reference PEMS response profile to a CP oocyst suspension at flow rates from 0.4 to 14 ml/min

It is observed that the beginning of the 5 mL/min fluid flow rate, indicated by the dashed grey line, represents the point at which CP oocysts are no longer captured by the surface-immobilized antibody. Also, during this and the 8 mL/min flow rate, we see net oocysts previously on the surface begin to be removed. As such, in our 19 mm wide flow channel at 5 mL/min, which corresponds to a fluid flow speed of 0.9 mm/s over the sensor surface, according to equation (4.15), the force of CP oocyst interactions with the anti-CP immobilized on the PEMS surface is estimated at 70 pN.

6.3 Single CP oocyst Detection in the Flow-Through System

In the previous experiment, where an estimation of the binding force of CP oocysts to the surface of an anti-CP PEMS was made, it was clear to see that oocysts were detected with the best efficiency in the analyte suspension flow rate range of 1 to 5

mL/min. However, by the nature of the experiment conducted, a direct comparison of detection efficiencies among flow rates was not possible. This impossibility is due to the fact that an extremely low concentration of oocysts was circulated in a closed-loop, recirculation detection format. As such, with each instance of detection, the remaining concentration of oocysts in the system available for detection was markedly reduced, making comparisons of detection efficiencies between flow rates necessarily only qualitative in nature. In making this qualitative comparison, one might conclude that the flow rates of 2 and 5 mL/min provided the best detection efficiencies as resonance frequency downshifts of nearly -1 kHz occurred for all PEMS in the detection array during just the twenty five minutes of detection at these flow rates.

6.3.1 CP Oocyst Detection at 1, 2, 5 and 8 mL/min

In order to allow for more quantitative comparisons of the detection efficiencies of the PEMS biosensor array at various flow rates, four individual experiments were performed at the rates of 1, 2, 5 and 8 mL/min using much larger volumes of water. In these experiments, oocyst concentrations of just 0.1 oocyst/mL were prepared in 10 liters of Drexel University tap water for detection by the same PEMS array and reference as in previous experiments. The same 19 mm wide flow channel was used and all detections were performed for a period of 180 minutes (3 hours).

Figure 6-13(a) through (d) detail the results obtained in these experiments. In (a), for the flow rate of 1 mL/min we see that all three anti-CP functionalized PEMS detected CP oocysts at different points in time. PEMS 3 experienced a -290 Hz shift at twenty four minutes. PEMS 2 experienced a -260 Hz shift at seventy eight minutes and then experienced a proportional shift of +260 Hz at 102 minutes corresponding to the

unbinding of this oocyst by the fluid flow. PEMS 1, at this flow rate experienced a detection event of -280 Hz at 129 minutes. The control cantilever experienced no appreciable frequency shift during the 180 minutes of experimentation. The noise levels of PEMS 1, 2, 3 and the reference PEMS in this detection experiment were 15, 13, 16 and 20 Hz, respectively.

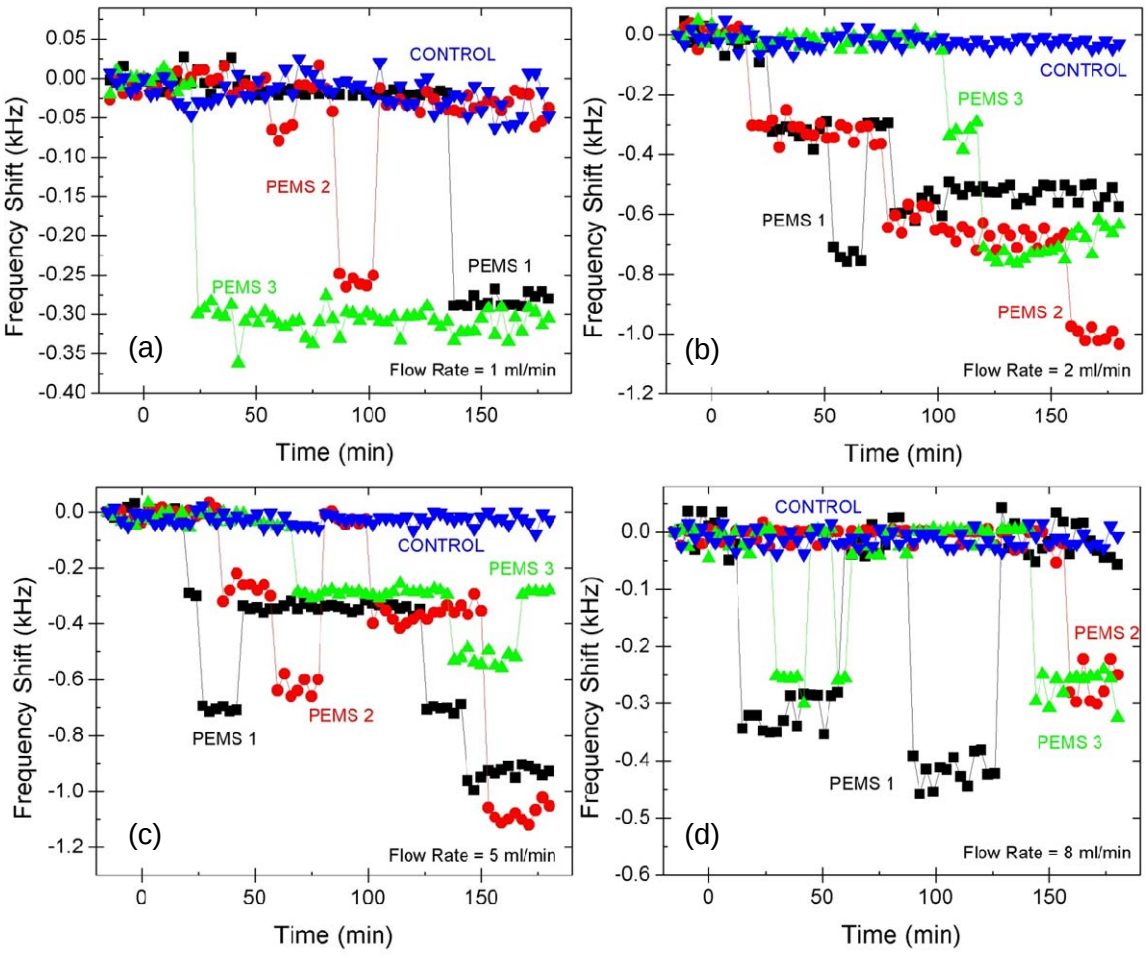

Figure 6-13: PEMS array response to 0.1 CP oocysts/mL in flow-through detection format at (a) 1 mL/min, (b) 2 mL/min, (c) 5 mL/min and (d) 8 mL/min

In the experiment where the fluid flow rate was 2 mL/min, we observe much more detection activity than that when the flow rate was 1 mL/min. In (b), we see that all

biosensors experienced at least two oocyst detection events with PEMS 1 and 2 having detected a total of three different oocysts while PEMS 1 had one of these removed from its surface at seventy two minutes. When the fluid flow rate was 5 mL/min, yet more detection activity is observed. PEMS 1 detected a total of four oocysts while having one removed; PEMS 2 detected five total oocysts with two removed; and PEMS 3 detected two oocysts and also had one removed from its surface. In Figure 6-13(d), the case of 8 mL/min, we see that the number of oocyst detections has decreased from the levels observed in the case of 2 and 5 mL/min. In this detection, PEMS 1 sees two total oocysts with both of these being removed from the surface in separate instances. PEMS 2 sees just one oocyst only after 150 minutes of detection. PEMS 3 sees three oocysts with two of these having been removed prior to detection of the third oocyst. The noise levels for these experiments did not exceed those observed with the flow rate of 1 mL/min, with the exception of the noise level of PEMS 1 which did increase to 28 Hz in the case of 8 mL/min.

Of note, in these experiments, we find that the flow rate of 5 mL/min does not completely prevent the detection of CP oocysts by the PEMS array as concluded from the experiment in Figure 6-11 and Figure 6-12. While Figure 6-11 and Figure 6-12 enabled an estimation of the interaction for of CP oocysts with the functionalized sensor surface, the number of oocysts available for detection may have significantly diminished by the time the flow rate of 5 mL/min was reached. As such, a better and more quantitative determination of CP oocyst interaction force with the functionalized PEMS detection array surfaces was ascertained using these individual flow rate experiments in Figure 6-13.

6.3.2 Oocyst Detection Efficiencies

From these data in Figure 6-13, we have seen our original observation supported, in that 2 mL/min presents excellent detection conditions for our PEMS array. However, by a simple comparison of this flow rate to the rate of 5 mL/min, it would appear that 5 mL/min produces better biosensor detection as a total of 11 oocysts were detected at this rate as compared to just 8 in the case 2 mL/min. However, as Table 6-1, below details, the actual detection efficiencies at these flow rates are quite different than they might appear.

In Table 6-1, all oocyst detection and removal events from Figure 6-13 are recorded. Also tabulated, are the total amount of oocysts available for detection at these different flow rates. That is, with a concentration of 0.1 oocyst/mL and with the flow rates of 1, 2, 5 and 8 mL/min, simple arithmetic tells us that it is not an equal number of oocysts passing through the flow chamber in the 180 minutes of detection for the different flow rates.

Table 6-1: Detection statistics for flow-through CP oocyst detection experiments

Suspension Flow Rate		**1 mL/min**	**2 mL/min**	**5 mL/min**	**8 mL/min**
available oocysts		18	36	90	144
PEMS 1	*Detected*	1	3	4	2
	Removed	0	1	1	2
PEMS 2	*Detected*	1	3	5	1
	Removed	1	0	2	0
PEMS 3	*Detected*	1	2	2	3
	Removed	0	0	1	2
Totals	*Detected*	3	8	11	6
	Removed	1	1	4	4
Fraction detected		0.17	0.22	0.12	0.04
Fraction removed		0.33	0.13	0.36	0.67

From this table, we can see that the flow rate of 2 mL/min provides the best conditions for CP oocyst detection as 22% of the 36 oocysts available for detection were seen by the array system. Also, only 13% of these captured oocysts were later removed by the force of the fluid flow during the 180 min of detection. While the 5 mL/min flow rate did capture 3 more total oocysts during the 180 min test period, this accounted for only 12% of all oocysts available for detection. Also, of these 11 captured oocysts, 36% were later removed by the fluid flow. As such, the conditions of maximum oocyst detection efficiency as well as minimal removal of detected oocysts both occur at the flow rate of 2 mL/min. At 5 mL/min, while significant detection of oocyst still occurs, we see a marked decline in oocyst detection efficiency as well as an increase in the number of detected oocysts that are later removed.

Thus, while our previous experimental result, from Figure 6-11 and Figure 6-12, that no additional oocysts are detected at 5 mL/min has been proven erroneous, the fact that ideal detection conditions for CP oocysts by our PEMS array exist at 2 mL/min has been upheld. Also, from Figure 6-13 and Table 6-1 it is clear that at 8 mL/min, with less than 5% of available oocysts detected by the PEMS array, and with two thirds of these oocysts later removed, the force of oocyst interaction with the PEMS surface has been nearly completely overcome.

As a result, we adjust our previous determination of CP oocyst interaction force with our sensor surface in our 19 mm flow channel from the flow rate of 5 mL/min, corresponding to a flow speed of 0.9 mm/s and 70 pN, to the more accurately determined flow rate of 8 mL/min. This corresponds to a fluid flow speed over the sensor surface of 1.4 mm/s and an interaction force ranging of 110 pN.

Thus, when building an online continuous CP oocyst monitoring system, based on the results herein, the device should include multiple arrays of PEMS sensors with a fluid flow speed of 2 mL/min. To achieve more rapid detection of larger volumes of liquid, rather than increasing the fluid flow rate, which would lead to lower detection efficiencies in terms of total oocysts detected, multiple sensor array flow channels can be employed such that the flow rate of total water sampled can be increased while still maintaining optimal flow conditions for each individual sensor array in the flow system. However, as will be discussed in forthcoming sections, the fluid flow rate of 5 mL/min could also be deemed an acceptable flow rate of online CP oocyst monitoring. Though slightly lower CP detection performance is observed at this flow rate, if it is the case that better discrimination between other particulate matter in real-world influent water is achieved at 5 mL/min, similar to the situation with BA in Chapter 5, the flow rate of 5 mL/min might represent the best compromise of CP oocyst detection efficiency and selectivity.

6.3.3 Statistical Analysis

In the case of the single oocyst detection data presented here, calculating the statistical sensitivities and specificities, as defined in Section 2.4, is not quite as straightforward an endeavor as it was with *Bacillus anthracis* (BA) detection. In the case of BA detection, the only *a priori* decision to be made in calculating these statistical values was the threshold frequency shift or signal to noise ratio (SNR) that would be required to deem a detection instance positive if exceeded or negative if not. However, implicit in this choice of threshold shift or SNR was the choice of timeframe in which such a shift should be observed. Though it was not explicitly stated when calculating the

statistical sensitivities and specificities of various BA detections, a timeframe of thirty minutes was generally established as the time in which the SNR of choice must be reached in order to deem the detection positive.

In the *Cryptosporidium* oocyst detection events presented thus far in this chapter, this time frame may no longer be applicable. From the dose response experiments presented above, we see that the concentrations of 100, 10 and 1 oocysts/mL led to large resonance frequency shifts for all PEMS in the detection array in only fifteen minutes. In the case of 1 oocyst/mL, resonance frequency shifts of -280, -230 and -250 Hz were recorded for PEMS 1, 2 and 3, respectively, at fifteen minutes. Even with a sensor noise level as high as 50 Hz (which is a value exceeding any single PEMS noise levels observed in CP detection in this chapter), an SNR of greater than 4 is achieved for all PEMS in the array at fifteen minutes.

However, when the case of single oocyst detection is examined, as in Figure 6-7, Figure 6-10, Figure 6-11 and Figure 6-13, the time frame of fifteen or thirty minutes may be insufficient for the detection of even one oocyst, leading to increased false negatives in the classification of results. In the case where CP oocysts are injected into the external reservoir of the system as in Figure 6-10, rather than immediately upstream of the PEMS array, PEMS 3 takes as long as forty minutes to detect its first oocyst at a flow rate of 0.4 mL/min and a concentration of 0.5 oocysts/mL. In the case of the experimentally determined optimal flow rate of 2 mL/min, in Figure 6-13(b), we see that the first oocyst response times for PEMS 1, 2 and 3 are twenty one, thirty three and sixty nine minutes, respectively, at a concentration of 0.1 oocysts/mL.

If the timeframe of thirty minutes is a requirement for detection, and the response of all four individual PEMS in the array are considered separately, then for the optimal flow rate of 2 mL/min, if a shift on the order of 300 is required for positive detection of CP oocysts in suspension, both PEMS 2 and 3 would have to be deemed false negative responses. This yields a dismal statistical sensitivity of 33% (while specificity is 100% due to the correct true negative response of the reference sensor). However, is not the goal of true, real-time array implementation to allow for redundant PEMS detection of the same analyte suspension? And does not this situation of extremely low analyte concentration beg the need for such an array? With the answer to these questions clearly, 'yes,' we see that considering each PEMS in the array individually is not the proper method of analysis. At such exceedingly low pathogen concentrations, it is more appropriate to consider the response of all of the detection PEMS together as compared to the reference PEMS. In this way, our detection is similar to dispatching three different people in different directions to search for a lost dog. If any one of the searchers finds the dog, the entire search party has succeeded.

Similarly, in the monitoring of such extremely low concentrations of *Cryptosporidium* oocysts, the real question is: Are *Cryptosporidium* oocysts present in our water sample or are they not? Thus, in the experiments detailed in Figure 6-13, we see that at the best performing flow rates of 2 and 5 mL/min, in a time frame of twenty one minutes, we see our first oocyst(s) detections and accordingly, have shown that we can answer the question of whether oocysts are present or not correctly in less than thirty minutes in concentrations of 0.1 oocyst/mL. If however, a concentration of oocysts in the tested sample is needed in addition to just a simple absence or presence test, longer

testing is required such that the number of oocysts 'seen' by the array can be used to back-calculate the entire sample concentration according to the known detection efficiency under the particular flow conditions – 22% in the case of 2 mL/min in this 19 mm flow channel.

6.4 Detection of CP Oocysts Among Background Particulate Matter

Having successfully detected *Cryptosporidium parvum* oocysts in concentrations as low as 0.1 mL/min, in volumes of 10 L of tap water, and in less than thirty minutes, the next point of investigation in this study is to probe the response of the anti-CP functionalized PEMS array when presented with various possible sample background conditions. First, a different *Cryptosporidium* species, *C. muris* will be probed for detection by our PZT-only PEMS array to determine if cross-reactivity of the CP antibody occurs between species of *Cryptosporidium*. Then, two inorganic particulate suspensions, silicon dioxide and clay, will be presented to the PEMS array system to determine what response occurs. Finally, mixtures of CP oocysts with these background particles will be tested to determine if the detection efficiency, sensitivity or specificity of the PEMS array is altered as a result of these particles.

6.4.1 Interaction Force Determination of *C. muris* Oocysts

The investigation of the PEMS biosensor array response to *Cryptosporidium muris* (CM) oocysts involved replicating the CP oocyst interaction force determination experiment detailed Section 6.2.3, whereas the CP oocyst suspension was replaced by a suspension of CM oocysts identical in concentration, *i.e.* 0.5 CM oocysts/mL. In this way, the behavior of CM oocyst interaction with the PEMS array sensor surface as a function of suspension flow rate will be elucidated. With this experimental result, in

much the same way as with *Bacillus anthracis* and its close cousins, a determination of the optimal flow rate for detection of CP oocysts among those of CM is possible.

Figure 6-14 displays the results of this experiment. We see that the overall shape of the interaction profile of CM with the anti-CP immobilized PEMS array is similar to the CP interaction profiled in Figure 6-11. However, a close examination of these data reveals that, overall, far less interaction of CM oocysts with the PEMS biosensors occurred than did CP oocysts. PEMS 3 exhibits just one instance of detection during the optimal CP detection flow rate of 2 mL/min, but PEMS 1 and 2 exhibit no discernable oocyst detection. The flow rate of 0.4 mL/min induced resonance frequency shifts near -300 Hz in all anti-CP-oocyst functionalized PEMS, corresponding to the detection of one oocyst each. At 1 mL/min, one additional oocyst was detected by PEMS 1 and 2, while the resonance frequency of PEMS 3 remained unchanged.

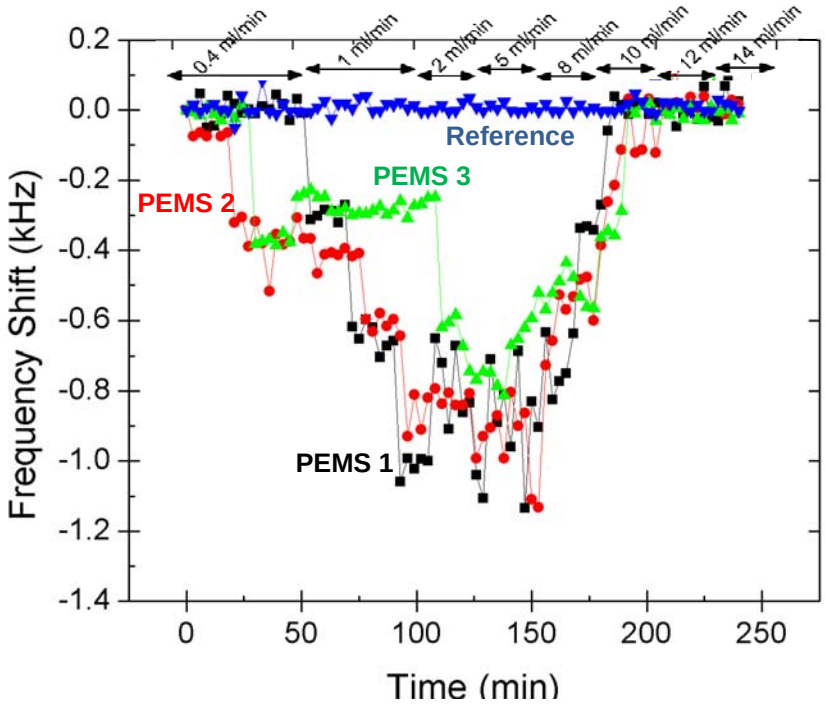

Figure 6-14: PZT-only array response profile to a CM oocyst suspension at flow rates from 0.4 to 14 mL/min

In contrast to the detection of CP oocysts where 11 oocysts were detected by the array and four were removed, a CM oocyst flow rate of 5 mL/min yielded no net frequency shift in all PEMS biosensors indicating that at least as many oocysts were removed from the surface as were detected during this period. Then, as the flow rate is increased to 8 mL/min, we see that net oocysts are removed from all three of the detection PEMS and that during the flow rate of 10 mL/min, all PEMS have reverted back to their initial resonance frequencies, indicating that all oocysts had been removed. The noise levels of PEMS 1, 2, 3 and the reference sensor were 28, 39, 25 and 21 during this experiment. Figure 6-15, below, presents an average the resonance frequency shifts of the three individual cantilevers that make up the detection array in order to make a clearer determination of the flow rate at which CM oocysts are prevented from further

interactions with the sensor surface, as was performed for CP oocysts in Figure 6-12. The reference PEMS response is shown again, unchanged, for comparison.

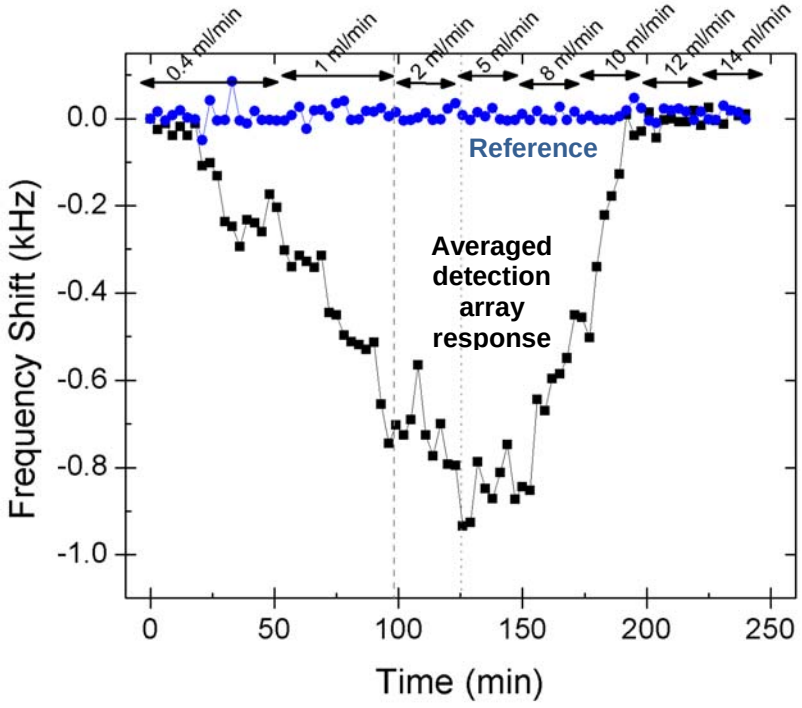

Figure 6-15: Average of the PZT-only detection array response and reference PEMS response profile to a CM oocyst suspension at flow rates from 0.4 to 14 ml/min

In analyzing this investigation of CM interaction force with the surface of our PEMS array, we see that all fluid flow rates greater than 1 mL/min in our 19 mm wide flow channel lead to an average of less than one CM interaction per PEMS. In the case of 2 mL/min, no new oocysts are detected after the introduction of this flow rate, indicated by the grey dashed line. Then, at 5 mL/min, indicated by the grey dotted line, a small amount of interaction with the detection PEMS is initially observed, but then no additional CM oocysts are detected by any PEMS in the array. As such the interaction force between CM and the anti-CP immobilized sensor surfaces is estimated to be on the

order of 30 to 70 pN, corresponding to the flow rates of 2 and 5 mL, which, in turn, correspond to fluid flow speeds of 0.4 and 0.9 mm/s over the sensor surface as calculated according to equation (4.15) and the analysis presented in Section 4.4.2. While these interaction force values are less than the experimentally determined value for the interaction force of CP oocysts with the anti-CP immobilized sensor surface of 110 pN, it is reasonable that that the two values are as close as they are. Though the anti-CP IgM antibody was specifically raised against CP oocysts[175], it is approved, and indeed recommended for use by the EPA in Method 1623 for the detection of oocysts from all *Cryptosporidium* species in water.[27] Furthermore, it is stated by the manufacturer that this anti-CP antibody "shows varying degrees of cross-reactivity with oocysts of other species of *Cryptosporidium*."[175] As such, it is not unexpected that this degree of interaction of CM oocysts with the anti-CP functionalized PEMS has been observed.

To further and more quantitatively identify the flow speed at which CM oocysts are no longer detected by the PEMS array and to determine their interaction force with the anti-CP-oocyst functionalized PEMS array, experiments similar to those in Figure 6-13 were performed where CM oocysts were used instead of CP. Aside from this substitution, all other parameters were kept constant: the concentration of CM oocysts used was 0.1 mL/min and the 10 L flow-through one-way fluid delivery system was used. Figure 6-16 details the experimental results at the flow rates of 2 and 5 mL/min. The noise levels for the detection array were between 39 and 65 and between 42 and 67 Hz for the flow rates of 2 and 5 mL/min, respectively. Reference PEMS noise levels were 47 and 58 Hz, respectively.

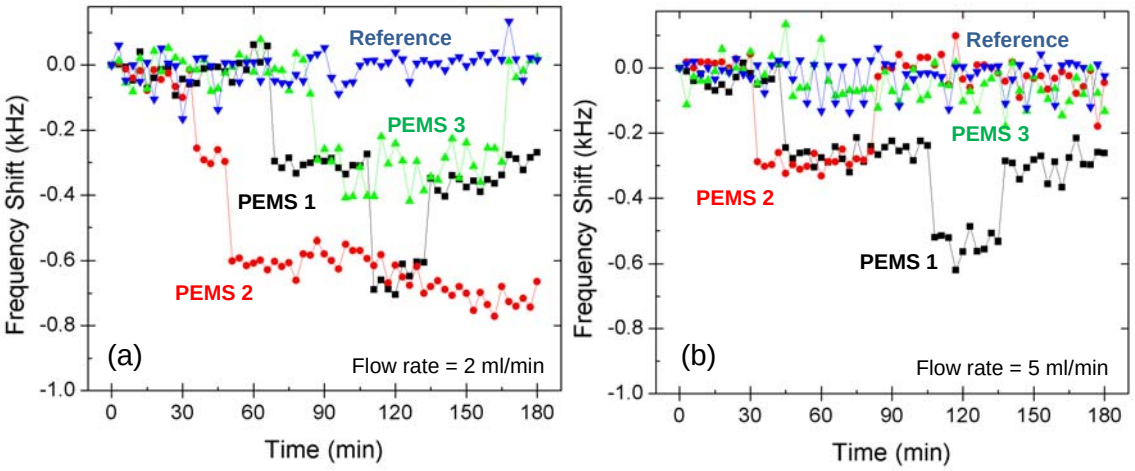

Figure 6-16: PEMS array response to 0.1 CM oocysts/mL in flow-through detection format at (a) 2 mL/min, (b) 5 mL/min

From these experiments, we see that there is significant interaction of CM oocysts with the anti-CP-oocyst functionalized PEMS at 2 mL/min, but only minimal interaction at 5 mL/min. Table 6-2, below presents the statistics associated with these experiments. Here we see that 14% of available CM oocysts are detected by the PEMS array at 2 mL/min while only 3% of such oocysts are detected at 5 mL/min. Also, the removal rates of these flow conditions are 40 and 67%, respectively. Thus, the interaction force of CM oocysts with the anti-CP-oocyst functionalized PEMS surface is identified as 5 mL/min, which corresponds to a fluid flow speeds over the sensor of 0.9 mm/s and a removal force impingent on bound oocysts of 70 pN, Again, as discussed above, it is reasonable that that the this value of removal force for CM is similar to that of CP (110 pN), as the supposed 'anti-CP-oocyst' antibody has documented cross-reactivity with oocysts of other *Cryptosporidium* species.

Table 6-2: Detection statistics for flow-through CM oocyst detection experiments

Suspension Flow Rate		**2 mL/min**	**5 mL/min**
available oocysts		36	90
PEMS 1	*Detected*	2	2
	Removed	1	1
PEMS 2	*Detected*	2	1
	Removed	0	1
PEMS 3	*Detected*	1	0
	Removed	1	0
Totals	*Detected*	5	3
	Removed	2	2
Fraction detected		0.14	0.03
Fraction removed		0.40	0.67

From an engineering standpoint, based on these results in combination with previous CP detection results, we see that if we are aiming to design a PEMS biosensor that will detect CP as well as CM oocysts, we would choose the flow rate of 2 mL/min. This would provide detection conditions that are optimal for CP detection, but also suitable for CM detection. However, if we are in the business of selectively detecting CP oocysts while trying to discriminate against the detection of CM oocysts, the flow rate of 5 mL/min is the appropriate choice. At the flow rate of 5 mL/min, we would still detect CP oocysts with an efficiency of 12%, but only 3% of CM oocysts would be 'nonspecifically' detected.

6.4.2 Selective Detection of CP Oocysts in Simulated Surface Water

Two different simulated surface water systems were used to probe the PEMS array sensor response to analyte suspensions that better approximate the make-up of actual rivers and streams influent to modern drinking water treatment plants. The first of these simulated systems was simple tap water from Drexel University, to which silica,

(aka silicon dioxide, quartz or sand), had been added. The second of these systems used the same tap water, but used clay particles as the particulate matter. These two classes of particulates make up the vast majority of particulate matter found in most rivers and streams.[176-178]

6.4.2.1 Sensor Array Response to Silica in Water

To probe the PEMS array response to silica, and its subsequent effect on the detection of CP oocysts, silica particles ranging in diameter from 0.5 μm to 10 μm (Sigma Aldrich, Milwaukee, WI) were chosen. This range approximates the sediment size distribution in which nearly all particulate matter in surface waters is found.[176,177] In this experiment, first a suspension of 0.1 mg/mL of said silica particles were suspended in 10 L of tap water by ultrasonication for fifteen minutes. Figure 6-17 is an image of a suspension of this concentration in a beaker between a silica suspension of 1 mg/mL in a flask on the left and pure tap water on the right. In this image we see that the 1 mg/mL suspension is completely opaque, while the 0.1 mg/mL suspension is translucent. An estimation of the number of silica particles in a 0.1 mg/mL suspension leads to a calculated value of 5×10^5 particles/mL of the average particle diameter, 5.25 μm. However, since the mass of these particles scales by the third power of the diameter, there are most likely many more silica particles in suspension as a 0.1 mg/mL suspension of 0.5 μm particles would contain 3.3×10^8 particles/mL. Regardless, at this concentration, there are at least 10^5 more silica particles than CP oocysts at 0.1 oocyst/mL.

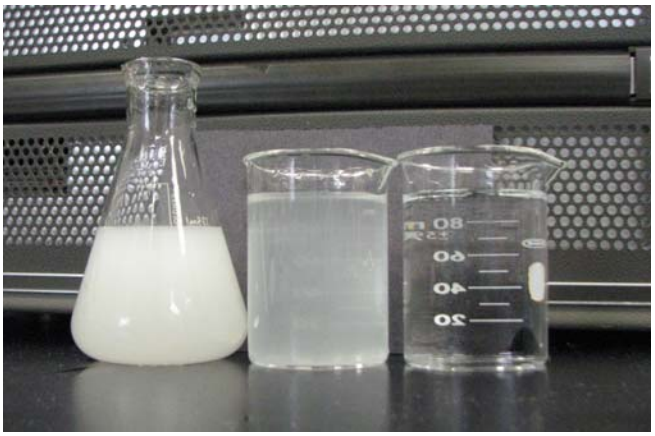

Figure 6-17: From left to right: 1 mg/mL silica suspension, 0.1 mg/mL silica suspension and pure tap water

In the experiment to determine the PEMS array response to this 0.1 mg/mL silica suspension, first, pure tap water was pumped through the flow chamber for fifteen minutes at the experimentally determined optimal flow rate for detection of CP oocysts (2 mL/min) identical to the manner explained in Section 6.3.1. Then, at fifteen minutes, the silica suspension was introduced into the flow chamber at the same flow rate and used to displace the tap water originally present. This suspension was pumped through the flow chamber for a period of 225 minutes to allow ample time for observations of any interactions that might occur between the particulate suspension and the PEMS biosensors.

Figure 6-18 details the data obtained in this experiment. In this figure, we see that upon addition of the silicon dioxide suspension, all three detection cantilevers in the flow chamber experience downward resonance frequency shifts. The detection array experiences this shift approximately six minutes after introduction of the silicon dioxide particles while the reference array remains unaffected during the entire detection period. The downward shift of the detection array proceeds at a slope of 2.4 Hz/min until it

beings to level off at 105 minutes and a total shift near 250 Hz. After this point, the resonance frequency of all three detection PEMS remains relatively stable between 200 and 300 Hz and with consistent noise levels between 30 and 38 Hz. The noise level of the reference PEMS was 41 Hz. Clearly, interaction of at least some of the silica particles has occurred with the PEMS detection array. Considering the gradual nature of the resonance frequency shift, it is reasonable to assume that only smaller silica particles nonspecifically adhered to the surface of the PEMS detection array. With the density of silica at 2.65 g/cm^3, a quartz particle of 0.6 microns in diameter is of the same mass as one BA spore. Similarly, a 3.5 micron silica particle is of the same mass as an average CP oocyst. Thus, if larger silica particles were significantly interacting with the PEMS array, we would expect stepwise resonance frequency shifts on the order of hundreds, or at least tens of hertz. Since we observe only a consistent gradual shift, similar to the shifts observed in BA detection, it is logical to conclude that only smaller silica particles are interacting with the PEMS array.

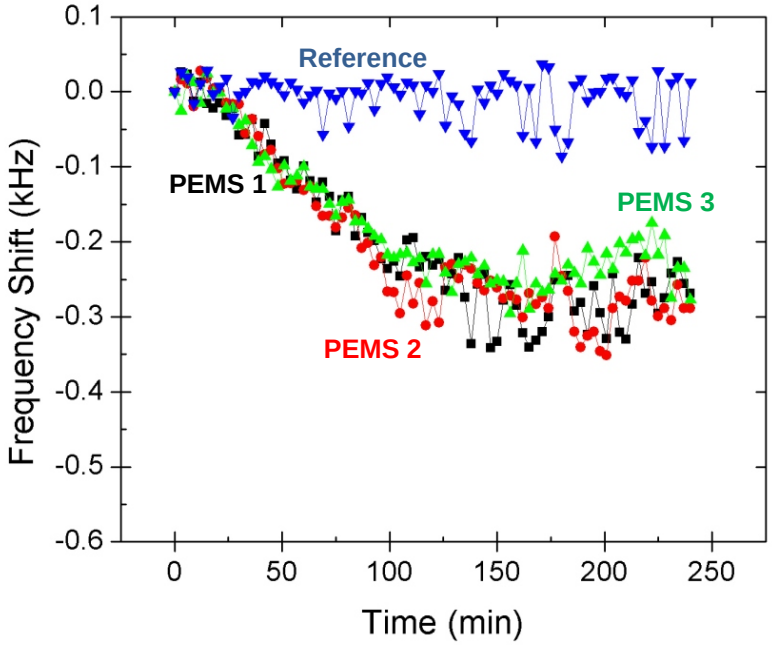

Figure 6-18: PZT-only array response profile to a 0.1 mg/mL silica suspension at a flow rate of 2 mL/min

With this response to a simple silica suspension in water characterized, the next step was to present this PEMS array system with a suspension containing the same concentration of silica particles, but also containing *Cryptosporidium* oocysts as well. Figure 6-19 displays the data acquired from such an experiment. Here, again, pure tap water was pumped through the flow chamber for fifteen minutes at 2 mL/min identical to the manner explained in Section 6.3.1. Then, at fifteen minutes, the silica suspension with 0.1 CP oocysts/mL was introduced into the flow chamber at the same flow rate and used to displace the tap water originally present.

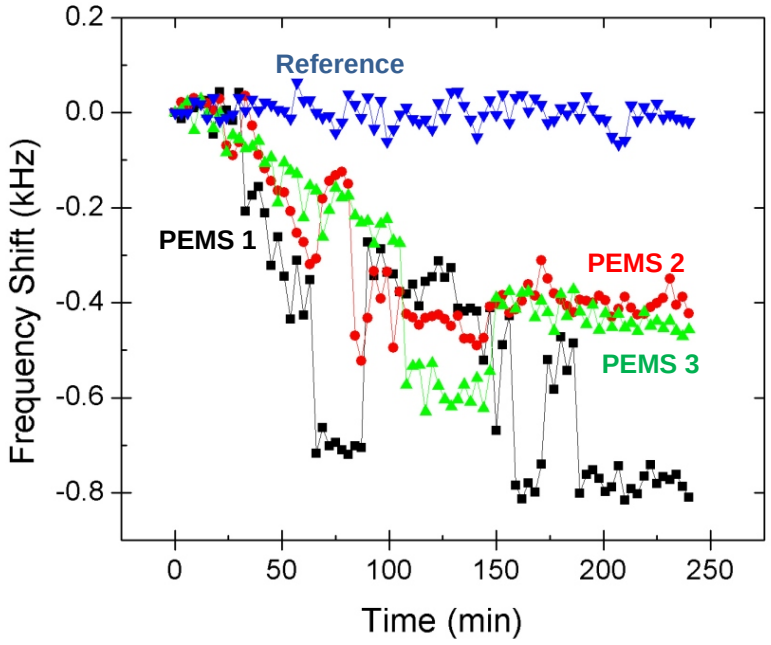

Figure 6-19: PZT-only array response profile to a 0.1 mg/mL silica suspension with 0.1 CP oocysts/ml at a flow rate of 2 mL/min

From these data we see the downward resonance frequency shift of the PEMS detection array resulting from the silica suspension manifest itself again. However, we also notice that the silica suspension has not prevented the detection of the co-suspended CP oocysts. In Table 6-3 the observed CP oocyst detection statistics are recorded. While the quantum steps associated with oocyst detection are somewhat convoluted by the concurrent downshift due to the presence of the silica particles, there are a total of 5 clearly discernable oocyst detection events by the entire array during the 225 minutes of detection. Of these 5 detected oocysts, 3 are removed by the action of the flow of the silica suspension. These values lead to calculated percentages of 11% and 60% for the fraction of total oocysts detected by the array and the number of these detected oocysts that were removed by the action of the flow of the silica suspension, respectively.

Table 6-3: Detection statistics for CP oocyst detection in a silica suspension

Suspension Flow Rate		**2 mL/min**
available oocysts		45
PEMS 1	*Detected*	3
	Removed	2
PEMS 2	*Detected*	1
	Removed	0
PEMS 3	*Detected*	1
	Removed	1
Totals	*Detected*	5
	Removed	3
Fraction detected		0.11
Fraction removed		0.60

A comparison of these percentages to those recorded for the flow rate of 2 mL/min in Table 6-1 (22% and 13%, respectively) reveals that the percentage of oocysts detected has been halved by the presence of silica particles in the suspension. Also, the fraction of these detected oocysts that were later removed by the action of the suspension fluid flow was more than quadrupled. While these reductions in detection array performance are not fatal to the real-time detection of CP oocysts in surface water applications, they do indicate the need for improved antibody performance and further correction factor consideration when attempting to quantify the numbers of oocysts present in a sample.

6.4.2.2 Sensor Array Response to Clay Particles in Water

Even more so than silica, clay is the most dominant suspended particulate matter found in the water of the world's streams and rivers.[176-179] Furthermore, due to its propensity to flocculate or agglomerate and settle to the bottom of river and stream beds,[180] clay particles are generally found suspended in surface waters only in sizes less than a few microns.[179] As such, kaolin clay particles of 30 nm diameter and lengths

ranging from 0.5 to 4 μm (Sigma Aldrich, Milwaukee, WI) were suspended in tap water in the same manner and concentration as the silica suspension, above. Figure 6-20 shows an image of this 0.1 mg/mL suspension between a suspension of 1 mg/mL in the flask to the left and pure tap water to the right. This translucent 0.1 mg/mL suspension of clay remained suspended for more than several days, while the 1 mg/mL suspension was observed to settle significantly in just a few minutes. An estimation of the number of clay particles in a 0.1 mg/mL suspension leads to a calculated value of 1×10^{10} particles/mL even if it is assumed that the entire suspension is made up of only the longest (4 μm) clay particles. Considering shorter particles of 0.5 μm in length, the number of particles increases another order of magnitude.

Figure 6-20: From left to right: 1 mg/mL clay suspension, 0.1 mg/mL clay suspension and pure tap water

As with the determination of the PEMS array response to a silica suspension, first, pure tap water was pumped through the flow chamber for fifteen minutes at 2 mL/min, identical to the manner explained in Section 6.3.1. Then, at fifteen minutes, the clay suspension was introduced into the flow chamber at the same flow rate and used to

displace the tap water originally present. This suspension was pumped through the flow chamber for a period of 225 minutes to allow ample time for observations of any interactions that might occur between the particulate suspension and the PEMS biosensors.

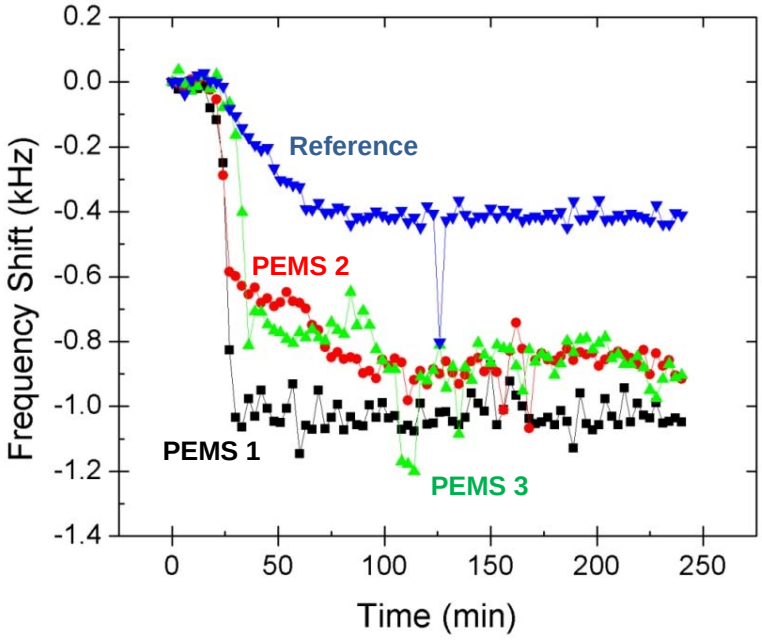

Figure 6-21: PZT-only array response profile to a 0.1 mg/mL clay suspension at a flow rate of 2 mL/min

Figure 6-21 details the data obtained in this experiment. In this figure, we see that upon addition of the clay suspension, all three detection cantilevers in the flow chamber experience marked downward resonance frequency shifts. The detection array experiences this shift approximately six to fifteen minutes after introduction of the clay suspension while the reference array begins to shift downward at 18 min after this addition. The downward shift of the detection array proceeds at a slope of 82 to 90 Hz/min until all three detection cantilever responses begin to level off between thirty and

thirty six minutes and 600 and 1000 Hz. After this point, the resonance frequency of PEMS 1 and 3 remains relatively stable at 1.1 kHz and 0.8 kHz, respectively. In contrast, after the initial rapid resonance frequency decrease to near 600 Hz, the resonance frequency of PEMS 2 continues to decline more gently at a rate of 4 Hz/min until eighty minutes and 900 Hz. The slope of the reference cantilever is 9 Hz/min between eighteen and sixty three minutes after which its resonance frequency position remains constant at 400 Hz. After each cantilevers' period of initial decline upon introduction of the clay suspension, the noise levels of PEMS 1, 2, 3 and the reference cantilever were 46, 52, 49 and 20, respectively.

Of note in this experiment are the rapid initial frequency shifts of all PEMS as well as the two instances of step-wise oocyst-detection-like frequency shift by PEMS 3 and the reference cantilever. Upon analysis of these phenomena, we find that they are interrelated. The rapid initial frequency shifts of the detection array suggest that very rapid nonspecific adhesion of clay particles or agglomerates (or both) has occurred on the sensor surfaces. Since the time between data points is three minutes, as dictated by the data acquisition program and switch box hardware (see section 4.1.3), it is impossible to determine whether many small particles or just one (or a few) large particle(s) have adhered to each PEMS between data points. However, by considering the density of the clay particles (2.53 g/cm^3)[181] and the large stepwise frequency shifts and subsequent release events in PEMS 3 and the reference array at 104 and 126 minutes, respectively, we can say that agglomerated clay particles of at least 3.5 microns in diameter are likely to exist in this suspension. This conclusion is reasonable as clay particles are well known to agglomerate and settle at neutral pH conditions.[178-180] Also, a strong agglomeration

and settling tendency of this particular type of clay was noted above at the concentration of 1 mg/mL.

Following this clay suspension experiment, a final experiment was performed where a suspension of clay, at 0.1 mg/mL, together with CP oocysts, at 0.1 oocyst/mL, was presented to the PEMS array system at a flow rate of 2 mL/min, similar to the silica/oocyst suspension described in section 6.4.2.1. Figure 6-22, below presents the data obtained in this experiment.

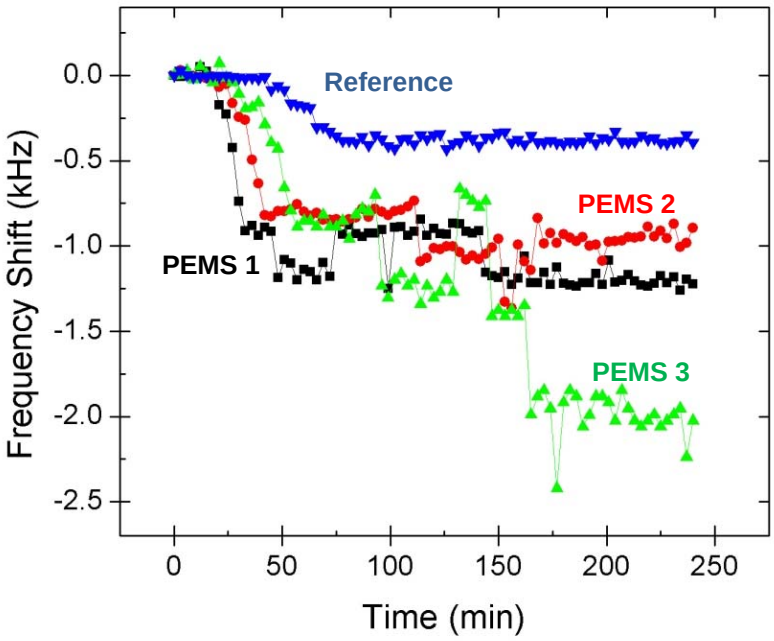

Figure 6-22: PZT-only array response profile to a 0.1 mg/mL clay suspension with 0.1 CP oocysts/mL at a flow rate of 2 mL/min

Here, we see that similar to the clay-only suspension, initial, rapid frequency shifts occur in the detection array, while a less rapid shift occurs in the reference array. Then, subsequent to this, several step-wise frequency shifts are observed in the detection array, while the reference cantilever remains unaffected by the suspended particulate matter after the seventy five minute mark. Table 6-4, below details the apparent oocyst

detection events recorded by the PEMS detection array. These detection events are termed 'apparent,' as the stepwise shifts observed in the clay-only suspension open the possibility that some of these stepwise shifts could be false positive detection events.

Table 6-4: Statistics for CP oocyst detection in a clay suspension

Suspension Flow Rate		**2 mL/min**
available oocysts		45
PEMS 1	*Detected*	2
	Removed	1
PEMS 2	*Detected*	1
	Removed	0
PEMS 3	*Detected*	2
	Removed	1
Totals	*Detected*	5
	Removed	2
Fraction detected		0.11
Fraction removed		0.40

Similar to the results of the silica/oocyst suspension, there are a total of 5 apparent oocyst detection events by the entire array during the 225 minutes of detection. Of these 5 detected oocysts, 2 are removed by the action of the flow of the clay suspension. These values lead to calculated percentages of 11% and 40% for the fraction of total oocysts detected by the array and the number of these detected oocysts later removed by the action of the flow of the suspension, respectively. A comparison of these percentages to those recorded for the flow rate of 2 mL/min in Table 6-1 (22% and 13%, respectively) reveals that, again, the percentage of oocysts detected has been halved by the presence of clay particles in the suspension. Also, the fraction of these detected oocysts that were later removed by the action of the suspension fluid flow was tripled.

6.4.3 Oocyst Detection Efficiencies in Background Suspensions

Table 6-5, below presents a compilation of CP oocyst detection results in various suspension conditions and quantifies the efficiencies of such detections. The detection conditions tabulated are all at the experimentally determined optimal flow rate of 2 mL/min and all suspensions are in Drexel University tap water. The concentrations of all oocyst suspensions is 0.1 oocyst/mL and the concentrations of silica and clay particles is 0.1 mg/mL. We see that, while dramatic background interactions with the PEMS detection system are observed in suspensions of silica and clay particles, the detection of CP oocysts is not completely precluded.

Table 6-5: Statistics for detection of 0.1 CP oocysts/mL in pure tap water and co-suspended with 0.1 mg/mL silica and 0.1 mg/mL clay particles

Suspension Conditions		**oocysts only**	**silica + oocysts**	**clay + oocysts**
available oocysts		36	45	45
PEMS 1	*Detected*	3	3	2
	Removed	1	2	1
PEMS 2	*Detected*	3	1	1
	Removed	0	0	0
PEMS 3	*Detected*	2	1	2
	Removed	0	1	1
Totals	*Detected*	8	5	5
	Removed	1	3	2
Fraction detected		0.22	0.11	0.11
Fraction removed		0.13	0.60	0.40

This table shows that the percentage of oocysts available for detection that are actually seen by the PEMS array is cut in half by the presence of the co-suspended particles. While this loss of efficiency is lamentable, it is encouraging that the ability for detection in these conditions is not lost altogether. Additionally, it is observed that the

presence of the silica and clay particles in suspension with the oocysts leads to a marked increase in the removal rate of oocysts from the PEMS surfaces.

6.5 Chapter Summary

In this chapter of *Cryptosporidium* oocyst detection of various species and in various backgrounds, much has been ascertained concerning the utility of our PEMS array biodetection system for deployed, real-time monitoring of *Cryptosporidium* oocysts in surface water. First, highly sensitive detection of *Cryptosporidium* oocysts was demonstrated via dose response determination using a novel PZT-glass PEMS array developed by this author. These experiments demonstrated positive detection at a concentration of 0.1 CP oocysts/mL. This represents a limit of detection 3×10^7 times better than SPR[31], which is the only other reported real-time method for *Cryptosporidium* oocyst monitoring. These initial CP oocyst detection experiments were carried out at a flow rate of 1 mL/min in a 19 mm wide semi-circular flow channel as designed according to the engineered fluid flow discussion presented in Section 4.4.2.

Subsequent analysis of these PZT-glass array detection data, as well as optical and SEM microscopy, revealed that the step-wise resonance frequency shifts of approximately 100 Hz were associated with instances of single CP oocyst detection. Theoretical vibrational analysis of the cantilever array that initially enabled this highly sensitive detection led to the development of the more-sensitive-yet PZT-only PEMS arrays. These arrays utilized the length-mode vibrations of the cantilever (see Section 4.1.1.2) and, together with advanced noise reduction techniques discussed in Appendices A and B, allowed for single CP oocyst detections where each oocyst induced a resonance frequency shift of 290 Hz. This PZT-only PEMS array was also used to determine the

interaction force between the CP oocysts and the anti-CP-oocyst functionalized PEMS surface, much the same as was performed with *Bacillus anthracis* spores in Chapter 5.

It was determined that the force of CP oocyst interaction with the functionalized PEMS surface is 110 pN, and that the optimal flow rate for detection of CP oocysts in this 19 mm wide flow channel is 2 mL/min. At this flow rate, 22% of all available oocysts were detected during the course of 180 minutes, while only 13% of these detected oocysts were later removed. At 1 mL/min, only 17% of all oocysts were detected, and at 5 mL/min, only 12% were detected with 33% and 36% of these detected oocysts later removed, respectively. Thus, for online, continuous real-time monitoring of *Cryptosporidium* oocysts in water, the flow rate of 2 mL/min in this 19 mm wide flow channel should be used. Then, if higher volumes of water need be processed, multiple arrays in identical, parallel flow channels can be used to enhance capacity.

Using the same PZT-only array, functionalized with the same anti-CP-oocyst antibody, in the same flow channel, revealed that the interaction force between such a sensor surface and *C. muris* (CM) oocysts was 70 pN. These experiments showed that our array also detects CM oocysts with a detection efficiency of 14% at 2 mL/min. This is not unexpected as the anti-CP-oocyst IgM used for functionalization of the PEMS detection array is known to cross-react with other *Cryptosporidium* species.[175] However, at 5 mL/min, only 3% of available CM oocysts were detected. As such, the flow rate of 2 mL/min could be used for a PEMS array biosensor designed to detect CP and CM oocysts, while the flow rate of 5 mL/min can be used to selectively detected CP oocysts from those of CM.

Furthermore, significant interaction of the PEMS detection array was observed with 0.1 mg/mL suspensions of both silica and clay particles. The silica particles used for experimentation ranged in diameter from 0.5 to 10 μm and led to a total nonspecific resonance frequency shift of 250 Hz in just under two hours. As a result of the gradual nature of this interaction, it was concluded that only the smaller of these silica particles (<1 μm) were interacting with the PEMS surfaces. The clay particles used for experimentation were tubular in nature and were 30 nm in diameter and ranged in length from 0.5 to 4 μm. The interaction of these suspended particles, at 0.1 mg/mL, was much more rapid and induced total resonance frequency shifts between 0.8 and 1.1 kHz in less than thirty minutes. Also, two instances of step-wise resonance frequency shifts on the order of hundreds of hertz were observed, indicating the presence of agglomerated clay particles on the order of 3.5 μm.

These nonspecific interactions of the functionalized PEMS array with silica and clay suspensions again indicate the need for more specific anti-CP-oocyst immunoglobulin, but notwithstanding this observed nonspecificity, detection of CP oocysts was achieved amongst these simulated surface water suspensions. In both suspensions, 11% of all available oocysts were detected during a period of 225 minutes. However, it was found that in the silica suspension, 60% of these detected oocysts were removed, while in the presence of the clay suspension, only 40% were removed. Again, these reductions in performance of the PEMS detection array are unfortunate, but the fact that detection is possible in these conditions is encouraging.

As a result of its single *Cryptosporidium* oocyst detection capability in simulated surface water on the order of hours, the PEMS array system has been demonstrated as a

viable real-time, continuous monitoring system for the presence of *Cryptosporidium* influent and effluent to drinking water treatment plants. This result is achieved by the synergistic combination of advanced PEMS array design and fabrication as well as the implementation of engineered fluidics for sample delivery. Moreover, by determining the detection efficiencies of our PEMS array in the various types of suspensions presented, in addition to simply ascertaining the presence or absence of oocysts in a given sample, it is possible to use our system to quantify the amount of this pathogen present. Since not all oocysts are detected by this system, however, this would require precise *a priori* knowledge of the water suspension in which the *Cryptosporidium* oocysts are to be found.

CHAPTER 7: CONCLUSIONS

This dissertation has presented the piezoelectric microcantilever sensor (PEMS) and the PEMS array as a highly sensitive biosensor platform for real-time detection of biological pathogens. Upon review of published literature in the field of biodetection, it was found that while methods for single pathogen detection exist in the realm of methodologies requiring many hours or days for detection, at present, there is no method for real-time detection of *Cryptosporidium* oocysts in concentrations less than 10^6 oocysts/mL of water, and that the real-time limit of detection for *Bacillus* spores is 10^3 spores/mL. With these and other biological pathogens, a clear and present risk to the health of citizens of this country as well as the world on the whole is identified, and the need for more rapid, real-time detection of such pathogens in concentrations at or near their lethal infectivity dosages is painfully apparent.

7.1 Piezoelectric Microcantilever Embodiments

With initial instances of PEMS biodetection already demonstrated,[37] this research dissertation focused on the development, iteration and optimization of PEMS in four embodiments:

1) Lead Magnesium Niobate – Lead Titantate (PMN-PT) unimorph cantilevers
2) Lead Zirconate Titanate (PZT)/glass millimeter sized cantilevers
3) PZT/glass arrays
4) PZT-only arrays

This first embodiment, the PMN-PT unimorph cantilever, utilized a highly piezoelectric free-standing PMN-PT tape,[143] previously developed in the Ceramics

Sensors and Processing Lab of Drexel University, onto which a tin non-piezoelectric layer was deposited. Two different tape thicknesses of 8 and 20 μm were used. The cantilever constructed from the 8 μm tape, insulated with methyltrimethoxysilane (MTMS) and functionalized with anti-BA IgG via N-hydroxysuccinimide/1-ethyl-3-3-dimethylaminopropyl-carbodiimide (NHS/EDC) activated mercaptopropionic acid (MPA) immobilization was demonstrated to detect just 36 total *Bacillus anthracis* (BA) spores in 0.8 mL of PBS (*i.e.* 45 spores/mL). The flow channel used for this detection was 1 mm wide by 1 mm deep and the recirculation flow rate used was 1 mL/min.

Encouraged by this highly sensitive detection of BA spores in fluid flow, anti-BA functionalized PZT/glass cantilevers were used to explore enhancements in selective detection that could be achieved by engineered fluid flow. Subsequently, the first true PZT-glass array for multiplexed, real-time monitoring was developed, tested and demonstrated for detection of BA spores and *Cryptosporidium parvum* CP oocysts. Analysis of these results and the resonance frequencies used for detection led to the development of a theoretical understanding of length and width vibrational modes in piezoelectric cantilevers. The PZT-only PEMS array is the current culmination of this understanding and exploits the high degree of experimental detection sensitivity realized by the length mode vibrational resonance near 400 kHz.

7.2 Engineered Fluid Flow for Enhanced PEMS Biodetection

As mentioned above, the first highly sensitive detection of BA spores, using PMN-PT cantilevers utilized a flow channel 1 mm wide by 1 mm deep with a fluid flow rate of 1 mL/min. These channel geometry and flow rate values were chosen with the knowledge that fluid flow is needed for biodetection in extremely low concentrations to

prevent settling of the biological pathogens and to enhance delivery of said analyte to the sensor surface, as presented in Chapter 1. However, the detailed fluidics analysis presented in Section 4.4 had not yet been developed, and thus did not dictate this design.

Nonetheless, this positive detection of just 36 total BA spores provided the impetus needed for the detailed exploration of fluidics optimization. Thus, the theory presented and derived in equations (4.4) through (4.16) was applied to the next extensive set of experiments aimed at further improving the detection of BA by means of PEMS cantilevers. These derivations of the force impingent on a sphere suspended in fluid flow revealed that placement of the PEMS biosensor in the center of the fluid flow channel is ideal for biodetection as the this force can actually be used to enhance the natural selectivity of the antibody functionalized PEMS. This enhancement arises from the fact that interactions of the biosensor surface with particles other then the pathogen of interest will necessarily be prevented provided this interaction force is less than that of the functionalized sensor surface with the pathogen of interest.

Of importance here is that the various PEMS insulation schemes presented in Chapter 4 allow for this completely submerged, center-of-channel placement, whereas other real-time systems such as QCM and SPR must be situated at the wall of their respective flow systems and thus, cannot benefit from this flow-enhanced sensor selectivity. With our PEMS sensor positioned in the center of the flow, and with its top and bottom surfaces (as in Figure 3-3) positioned parallel to the flow direction, as long as the fluid flow rate remains near, but below the rate required to prevent interaction of the pathogen of interest with the sensor surface, this enhanced selectivity can be achieved

and was shown to lead to improved statistical sensitivity and specificity performance of the sensor.

From these developed equations and the tabulation of their results in Table 4-2, we see that the calculated optimal flow channel for detection of BA using our laboratory pump is 8 mm wide by 9 mm deep, with a round bottom of 4 mm radius. The multitude of experiments aimed at determining the exact flow rate that optimizes the PEMS performance in this flow channel involved presenting the PZT-glass bimorph cantilever with 20,000 spores/mL suspensions of BA, *B. subtilis, B. cereus, B. thuringiensis* and *Salmonella typhimurium* (BS, BC, BT and ST, respectively), all at flow rates ranging from 0 to 14 mL/min. As a result of this extensive experimentation, it was determined that, in this flow channel, the flow rate of 14 mL/min provided the lowest levels of cross-reactivity between the PEMS sensor surface and the non-BA species, and also provided statistical sensitivities and specificities of 100%. In contrast, at flow rates of 1 and 4 mL/min the nonspecific interactions of BS, BC and BT with the PEMS were actually found to increase above values obtained at the conditions of no flow. Thus, for specific detection of BA among even its closes relatives, the flow conditions of 14 mL/min should be used in our 8 mm wide flow channel.

The forces associated with the volumetric flow rate of 14 mL/min in this channel correspond to the linear fluid flow speed over the sensor surface of 3.8 mm/s and forces impingent on stationary spores of 110 pN. Thus, the interaction force between BC, BT and BS spores and the anti-BA-spore functionalized PEMS sensor surface is greater than 110 pN, while the interaction force of BA with this same surface is estimated on order of 400 pN.

After the optimization of flow conditions for the detection of BA via PEMS biosensors, attention was turned to the real-time detection of the intestinal parasite, *Cryptosporidium.* In fluid force determinations involved in the detection of *Cryptosporidium parvum* (CP) oocysts by means of a PZT-only PEMS array, in a 19 mm wide flow channel, the flow rate of 8 mL/min and corresponding flow speed of 1.4 mm/s over the sensor surface was found to prevent detection of the CP oocysts by the PEMS biosensor array. This flow speed corresponds to a force 110 pN, as calculated by equation (4.15). When the same analysis was performed regarding the detection of *C. muris* (CM), it was determined that a flow rate of 5 mL/min, corresponding a flow speed 0.9 mm/s and a force of 70 pN was sufficient to prevent detection. As such, the flow speed of 5 mL/min in our 19 mm wide flow channel was identified as ideal for the specific discriminatory detection of CP from CM. If, however, a determination of *Cryptosporidium* oocysts in general is sought, the flow rate of 2 mL/min is ideal.

7.3 PEMS Array Engineering for Sensitive and Specific Detection of BA and CP

With this achieved enhancement in PEMS biodetection performance by means of fluid flow engineering, the second major focus of this dissertation was the design, implementation and iteration of a PEMS array system for true multiplexed, real-time array biodetection. The motivation for this development process was to further improve the reliability, *i.e.* statistical sensitivity and specificity, of our PEMS platform. This improved reliability was to be accomplished by the array system in two ways. First, multiple, identical PEMS biosensors were to allow for simultaneous redundant confirmatory biodetection assays. Secondly, the incorporation of a ‘reference’ PEMS sensor, functionalized with an immunoglobulin not designed to detect our pathogen of

interest allowed for a real-time, concurrent determination of false positive detection events.

In Section 4.1.3, the current method for production of PEMS cantilever arrays was presented in detail. Using a wire-saw and incorporating copper foil soldered to the PZT nickel electrodes for minimal-loss electrical connections prior to wire-saw cutting, cantilevers as narrow as 150 μm were produced. However, it was found that the best compromise of efficiency of production and resulting array performance was in making cantilevers with widths between 375 and 400 μm. These dimensions are approaching the length scales achieved by some microfabrication techniques, but are affected by much more simple and inexpensive means.

A PZT-glass cantilever array of experimentally determined ideal width, with a 1.5 mm long PZT layer and a 1.5 mm glass tip on each cantilever, as shown in Figure 5-14 was used for detection of BA in a concentration as low as 10 BA spores/mL of water in thirty minutes. This spore concentration was then increased by orders of magnitude at thirty minute intervals. The PEMS array continued its response to these additions up to the concentration of 10^6 spores/mL. This same type of experiment was then repeated, but the PEMS array was functionalized with Bovine Serum Albumin (BSA) instead of anti-BA-spore IgG. In this experiment, a correct response of zero resonance frequency shift was observed for all concentrations of spores. Also, four mixtures of BA spores among combinations of bacterial interferants (*S. aureus* and *P. aeruginosa*), where the ratio of bacterial interferants to BA spores was as high as 1000 to 1 were presented to this PEMS array system. In all four blinded trials, the PEMS array correctly identified the presence or absence of BA spores.

Following this proof of function of the PZT-glass PEMS array for detection of BA, the same array was applied as a means to accomplish the aim of detecting *Cryptosporidium* oocysts in concentrations of less than one oocyst per mL of water. In these experiments, a reference cantilever was also introduced with similar dimensions as the detection array. Per the calculation results shown in Table 4-3, a 19 mm wide flow channel with a semicircular cross-section was used in this detection experiment since *Cryptosporidium* oocysts are five times larger in diameter than BA spores, and thus more than one hundred times more voluminous. Initial dose response determination experiments showed that *Cryptosporidium parvum* (CP) oocysts were successfully detected with average detection array resonance frequency shifts of 200 Hz, and signal to noise ratios (SNR) of 4. Further investigation into the these data as well as optical and scanning electron microscopy revealed that single instances of oocyst binding were 'seen' by the individual PEMS in the array with approximately 100 Hz stepwise shifts corresponding to each oocyst detected.

Encouraged by this result, an in depth analysis of the 400 kHz resonance peak used for these CP and the BA array detection experiments was initiated. The presence of this peak was not predicted by theoretical flexural resonance calculations and peaks of such high frequency and Q values had not been observed prior to fabrication of PEMS by means of wire saw cutting (*i.e.*, by hand dicing of PZT and glass wafers). The analysis of this peak led to the realization that this and other higher frequency peaks are not flexural modes of vibration, but rather result from length and width mode oscillations of the piezoelectric layer of the cantilever (see Section 4.1.1.2). As such, the first PZT-only PEMS array for biodetection was conceived and constructed in order to exploit these

length and width mode resonances and perhaps increase detection sensitivity and resolution further.

Section 6.2.2 detailed this first successful experiment using a PZT-only cantilever and it was shown that the magnitude of the step-wise resonance frequency shift associate with CP oocyst detection increased in magnitude to 290 Hz as a result of this new cantilever array design. Furthermore, advanced noise reduction techniques, presented in Appendix B, were used in this and all following CP detection experiments where noise levels as low as 13 Hz were achieved and all subsequent PEMS noise levels were between this value and 60 Hz. Thus, these -290 Hz step-wise shifts associate with oocyst detection provided SNRs better than 5.

Further utilization of this PZT-only detection array and complementary reference PEMS involved the determination of the optimal flow rate for CP detection and exploration of the effects of co-suspended particulate matter common in the waters of rivers and streams. An initial estimation of the fluid flow rate and associated force at which CP oocysts are prevented from being detected by the PEMS array was achieved by circulating a 0.5 oocyst/mL suspension through the flow system for a period of 240 minutes and gradually increasing the flow rate of the suspension. It was determined that the flow rates of 2 and 5 mL/min presented the best detection conditions while all previously detected CP oocysts were removed from the sensor surface at a flow rate of 12 mL/min.

Based on this result, a more quantitative determination of the optimal conditions for CP detection was achieved by finding the flow rate that provided the most efficient detection of oocysts, in terms of percent of available oocysts in a one-way, flow-through

detection setup at a concentration of 0.1 oocyst/mL. By this series of experiments, it was found that the flow rate of 2 mL/min allowed for 22% of all available oocysts to be detected while 1, 5 and 8 mL/min allowed for only 17, 12 and 4%, respectively. Thus, in our 19 mm flow channel, 2 mL/min was determined as the ideal flow rate for ascertaining the presence of *Cryptosporidium parvum* oocysts in a water suspension. Additionally, for the range of CP oocyst diameters of 4 to 6 microns, the interaction force range of 70 to 110 pN was ascertained, as discussed in the previous section.

Similar to the investigations surrounding the use of PEMS biosensors and arrays for detection of BA, the next logical step in the exploration of PEMS utility for *Cryptosporidium* detection was to probe the system's selectivity. The first of these experiments involved determining if, and to what degree, *Cryptosporidium muris* (CM) oocysts interact with the surface of an anti-CP-oocyst functionalized PEMS array. In this work, it was found that CM oocysts are indeed 'seen' by our PEMS array, but to a lesser degree than CP oocysts. This result was reasonable as the manufacturer of the antibody does concede some interaction of these antibodies with other *Cryptosporidium* species. It was found that the fluid flow rates of 2 and 5 mL/min represented the transition range from consistent detection of CM oocysts to the regime where detection was prevented by increasing fluid flow rates. As such, experiments similar to those for CP, where a one-way, flow-through detection setup at a concentration of 0.1 oocyst/mL was used to determine detection efficiencies at various flow rates were performed with CM oocysts. The flow rate of 2 mL/min was found to allow a detection efficiency of 14% of available CM oocysts by the anti-CP-oocyst functionalized PEMS array. In contrast, only 3% of available CM oocysts were detected at 5 mL/min. Thus, the interaction force between CP

oocysts and the PEMS array was determined to be 70 pN. Also concluded from these experiments was that for a PEMS biosensor designed to detect both species of *Cryptosporidium* oocyst, the flow rate of 2 mL/min should be used, whereas if specific CP oocyst detection is desired, the flow rate of 5 mL/min is ideal.

Finally, the performance of the sensor system when presented with suspensions approximating actual surface waters as well as mixtures of these particles and oocysts was tested. In these experiments, at 2 mL/min, it was found that both silica and clay particles at concentrations of 0.1 mg/mL (or approximately 10^5 and 10^{10} particles/mL respectively) interact with the anti-CP-oocyst functionalized PEMS array. Silica particles induced a total resonance frequency shift of -250 Hz gradually over the course of two hours. The clay particles induced a rapid -1 kHz shift in just a few minutes after addition to the system. However, while silica had no effect on the reference PEMS, clay induced a resonance frequency shift of -410 Hz over the course of sixty five minutes after which time the resonance frequency position of this PEMS stabilized.

After determining these baseline interactions with the PEMS array, mixtures of silica with CP oocysts and clay with CP oocysts were then presented to the PEMS array to determine if detection of CP oocysts is still possible under these conditions. The first mixture consisted of 0.1 mg/mL silica particles together with 0.1 CP oocysts/mL in suspension. The clay mixture consisted of 0.1 mg/mL clay particles co-suspended with 0.1 CP oocysts/mL. In both cases, though the previously described silica and clay interactions with the PEMS array were again observed, positive detection of CP oocysts was observed still observed with frequency shifts of -290 Hz per stepwise shift. Compared to the detection efficiency and removal rates of 22 and 13%, respectively for

CP oocyst detection in unaltered tap water, detection rates of 11% were observed for both CP mixtures and removal rates of 60 and 40% for the silica and clay mixtures, respectively were observed. This result indicates that the PEMS array, as engineered and constructed here is capable of CP detection at concentrations of less than one oocyst per mL of surface water.

When we compare these results of CP mixtures with clay and silica to the results of BA mixtures with SA and PA 'interferant' cells, as in Section 5.3.3, we see a distinct difference in the obtained results. In the case of the BA mixtures with SA and PA cells, it was found that the bacterial 'interferant' cells were not nonspecifically detected by the PEMS array, but that SA cells did aggregate with the BA spores in suspension. By contrast, in the case of CP mixtures with clay and silica particles, we find that both clay and silica particles did interact nonspecifically with the anti-CP-oocyst functionalized PEMS surface. However, since stepwise detection shifts corresponding to instances of oocyst detection were still found to be -290 Hz, and were not observed to be significantly larger than this value, it is concluded that neither inorganic species agglomerated with detected CP oocysts in appreciable amounts.

7.4 Recommendations for Future Work and Binding Force Comparisons

In addition to the engineering and development of the various PEMS and PEMS array embodiments detailed in this dissertation, as described above, the other major area of focus has been the use of engineered fluidics for enhanced limits of detection, specificity and selectivity of the PEMS array in biodetection applications. The implementation of the theory developed in Section 4.4.2 has certainly lead to such enhancements, but the actual values of interaction forces of *Bacillus* spores and

Cryptosporidium oocysts with the surface of functionalized PEMS sensors has, as yet, not been compared to other methods for quantifying these interactions.

We can begin to make some of these comparisons here, but largely, this discussion will be confined to a recommendation for future work as the experiments required to make such comparisons are highly sophisticated and represent an entirely new body of work. Nonetheless, the groundwork for such experimental comparisons can be laid here.

As discussed previously, typical antibody-antigen interaction forces have been estimated to be on the order of 10 to 100 pN per interaction.[43] Furthermore, the distance range that these interactions are estimated to operate over is between 2 nm and up to a few microns. These longer range interactions are generally non-specific electrostatic double layer forces that initially draw dissimilarly charged particles together, and are rather weak in nature.[42,43] The interaction distance on the order of a few nanometers is that associated with typical 'lock and key' antibody-antigen interactions and is the strongest of immunoglobulin interaction forces. With the known diameter of our BA spores and CP oocysts and this 2 nm interaction distance, we can estimate a contact area between our pathogens and the antibody functionalized PEMS surfaces. For Bacillus spores, this contact area is estimated as 0.013 square microns while for *Cryptosporidium* oocysts, which are much larger, the contact area is estimated as 0.031 square microns. The reader is directed to Appendix D for a detailed description of the attainment of these values.

This contact area is an important parameter when comparisons with shear stress values, as developed by Garcia in his extensive work with the spinning disc apparatus,[182] are sought. This apparatus is applied to the determination of adhesion strengths of bone

and other mammalian somatic cells by first allowing the cells to adhere to a surface and then by spinning that surface in a vat of aqueous solution. Microscopic determination of the radius of spinning that cells are removed allows for said adhesion strength determinations. These strengths are typically on the order of hundreds of dynes/cm^2 and extensive cell spreading associated with adhesion to the disc surface is the norm.[182,183]

The situation with our biological pathogens is markedly different, in that: 1) our pathogens are not allowed to first adhere to the PEMS surface, but rather are dynamically presented to the surface by the same flow that provides the discrimination of interaction forces; and 2) both *Bacillus* spores and *Cryptosporidium* oocysts are rigid entities when compared to somatic cells. As such, calculated shear stresses of interaction are expected to be much lower than have been obtained for somatic cells. Nonetheless, with the estimate of contact area described above, and the theory developed by Garcia and Boettiger,[182-184] as described in detail in Appendix C, we can translate our experimentally determined BA and CP interaction forces into interaction shear stresses. Table 7-1, below, summarizes the results of the calculations detailed in the Appendix.

Table 7-1: Summary of pathogen removal flow speeds and calculated interaction parameters

Pathogen	**Experimentally Determined Fluid Flow Speed of Removal (mm/s)**	**Calculated Interaction Force with PEMS (pN)**	**Interaction Area (microns^2)**	**Calculated Interaction Shear Stress (dynes/cm^2)**
B. anthracis spores	25 +	400 +	0.013	14 +
Other Bacillus spores	3.8	100	0.013	7.3
C. Parvum oocysts	1.4	110	0.031	1.2
C. muris oocysts	0.9	70	0.031	1.0

Here, we see that, as expected, our interaction shear stresses are much lower than the typically obtained values of several hundred dynes/cm^2 in spinning disc experiments. As such, use of this apparatus with the sporulated and oocyst pathogens and accompanying antibody systems discussed in this dissertation would be difficult at best. However, these results indicate that the PEMS and PEMS array biosensors can be useful in the determination of cell-surface interactions on smaller shear stress scales than those possible with traditional techniques. As such, future work stemming from the results presented herein could entail the use of the spinning disc apparatus to verify the interaction forces determined in this work, or perhaps the PEMS biosensor could be applied as a highly sensitive alternative to the spinning disc for the probing of cell-surface interactions in the laboratory.

Beyond these basic science studies, the advances in PEMS array production as well as fluidics engineering presented in this dissertation have allowed for highly sensitive and specific detection of BA spores and CP oocysts. The future work required to bring these promising results toward implementation in real-world applications necessarily now involves mass production of these sensors and extensive statistical characterization. While the wire-saw did allow for precise fabrication of the PEMS arrays, many hands on production steps remained. In order to attain the production numbers and yields required for testing that would lead to real-world implementation, the next step in mass production of PEMS biosensors and biosensor arrays, on the order of hundreds of units, must be taken. Only once consistent production of identical sensors and arrays is achieved can the detailed statistical analysis needed for verification of function by government agencies be achieved.

List of References

1. Glossary for chemists of terms used in biotechnology Volume 64: International Union of Pure and Applied Chemistry (IUPAC); 1992.
2. Definition of Pathogen. www.medicinenet.com: MedicineNet, Inc., 2008.
3. Taco Bell supplier halts green onion production over E. Coli link. Philadelphia Business Journal 2006 December 7, 2006.
4. Ackerman J. Salmonella outbrak plagues University. The Daily Princetonian 2008 May 7, 2008.
5. Prevention CfDCa. Bioterrorism Agents/Diseases. Centers for Disease Control and Prevention, 2008.
6. Ireland J, Hanna P. Anthrax Spores Use Failsafe Germination System. Medicine at Michigan. 2002;4(2).
7. Barun K. De SLB, Gary N. Sanden, Kathy E. Wilson, Lois A. Diem, Chung K. Marston, Alex R. Hoffmaster, Gwen A. Barnett, Robbin S. Weyant, Teresa G. Abshire, John W. Ezzell, Tanja Popovic Two-Component Direct Fluorescent-Antibody Assay for Rapid Identification of Bacillus Anthracis. Emerging Infectious Diseases. 2002;8(10):1060 - 5.
8. Branch DW, Brozik S. Low-Level Detection of a Bacillus Anthracis Simulant Using Love-Wave Biosensors on 36° YX LiTaO3. In: Labs SN (ed). Albuquerque, New Mexico, 2003.
9. Davila AP, Jang J, Gupta AK, Walter T, Aronson A, Bashir R. Microresonator mass sensors for detection of Bacillus anthracis Sterne spores in air and water. Biosensors and Bioelectronics. 2007;22(12):3028-35.
10. Edwards K, Clancy H, Baeumner A. Bacillus anthracis : toxicology, epidemiology and current rapid-detection methods. Analytical and Bioanalytical Chemistry. 2006;384(1):73-84.
11. Kline CR. High-Speed Advanced Sensors for Bioterror Weapons. IEEE Engineering in Medicine and Biology. 2002;Sept/Oct:43-7.
12. Skottman T, Piiparinen H, Hyytiäinen H, Myllys V, Skurnik M, Nikkari S. Simultaneous real-time PCR detection of Bacillus anthracis , Francisella tularensis and Yersinia pestis. European Journal of Clinical Microbiology & Infectious Diseases. 2007;26(3):207-11.
13. Tims TB, Lim DV. Rapid detection of Bacillus anthracis spores directly from powders with an evanescent wave fiber-optic biosensor. Journal of Microbiological Methods. 2004;59(1):127-30.
14. Peters CJ, Hartley DM. Anthrax inhalation and lethal human infection. The Lancet. 2002;359(9307):710-1.
15. Tyzzer E. A sporozoon found in the peptic glands of the common mouse. Proc Soc Exp Med. 1907;5:12-3.
16. Tyzzer E. An extracellular coccidium, Cryptosporidium muris (gen. & sp. nov.), of the gastric glands of the common mouse. J Med Res. 1910;18:487-509.
17. MacKenzie WR, Hoxie NJ, Proctor ME, et al. A massive outbreak in Milwaukee of cryptosporidium infection transmitted through public water supply. New England Journal of Medicine. 1994;331:161-7.

18. Casemore DP, Sands RL, Curry A. Cryptosporidium species a 'new' human pathogen. J Clin Pathol. 1985;38:1321-36.
19. Xiao L, Ryan UM. Cryptosporidiosis: an update in molecular epidemiology. Curr Opin Infect Dis. 2004;17:483-90.
20. Sunnotel O, Lowery CJ, Moore JE, et al. Cryptosporidium. Letters in Applied Microbiology. 2006;43(1):7-16.
21. Doganci T, Araz E, Ensari A, Tanyuksel M, Doganci L. Detection of Cryptosporidium Parvum infection in childhood using various techniques. Med Sci Monit. 2002;8:223-6.
22. Cryptosporidium parvum. In: Administration USFaD (ed). Foodborne Pathogenic Microorganisms and Natural Toxins Handbook, 2006.
23. Fayer RJ, Trout M, Jenkins MC. Infectivity of Cryptosporidium parvum oocysts stored in water at environmental temperatures. J Parasitology. 1998;84:1165-9.
24. Betancourt WQ, Rose JB. Drinking water treatment processes for removal of Cryptosporidium and Giardia. Vet Parasitology. 2004;126:219-34.
25. Thurston-Enriquez JA, Haas CN, Jacangelo J, Gerba CP. Inactivation of enteric adenovirus and feline calicivirus by ozone. Water Research. 2005;39(15):3650-6.
26. Method 1604: Total Coliforms and Escherichia coli in Water by Membrane Filtration Using a Simultaneous Detection Technique (MI Medium). In: Water UEOo (ed). Washington, DC, 2002.
27. Method 1623: *Cryptosporidium* and *Giardia* in Water by Filtration/IMS/FA. In: Agency USEP (ed). Cincinanati, OH, 2005.
28. Xiao L, Alderisio K, Limor J, Royer M, Lal AA. Identification of species and sources of Cryptosporidium oocysts in storm waters with a small-subunit rRNA-based diagnostic and genotyping tool. Applied and Environmental Microbiology. 2000;66:5492-8.
29. Xiao L, Singh A, Limor J, Graczyk TK, Gradus S, Lal A. Molecular Characterization of Cryptosporidium Oocysts in Samples of Raw Surface Water and Wastewater. Appl Environ Microbiol. 2001 March 1, 2001;67(3):1097-101.
30. Brook EJ, Christley RM, French NP, Hart CA. Detection of Cryptosporidium oocysts in fresh and frozen cattle faeces: comparison of three methods. Letters in Applied Microbiology. 2008;46:26-31.
31. Kang CD, Lee SW, Park TH, Sim SJ. Performance enhancement of real-time detection of protozoan parasite, Cryptosporidium oocyst by a modified surface plasmon resonance (SPR) biosensor. Enzyme and Microbial Technology. 2006;39(3):387-90.
32. LT2ESWTR Source Water Monitoring for Systems Serving At Least 10,000 People Factsheet. In: Water UEOo (ed). Washington, DC, 2006.
33. Capobianco JA, Shih WY, Shih W-H. Methyltrimethoxysilane-insulated piezoelectric microcantilevers for direct, all-electrical biodetection in buffered aqueous solutions. Review of Scientific Instruments. 2006;77(12):125105-6.
34. McGovern J-P, Shih WY, Rest R, Purohit M, Pandya Y, Shih W-H. Label-free flow-enhanced specific detection of Bacillus anthracis using a piezoelectric microcantilever sensor. Analyst. 2008;133:649-54.

35. McGovern J-P, Shih WY, Shih W-H. In situ detection of Bacillus anthracis spores using fully submersible, self-exciting, self-sensing PMN-PT/Sn piezoelectric microcantilevers. Analyst. 2007;132:777-83.
36. McGovern JP, Shih WY, Mattiucci M, et al. Array PZT/Glass Piezoelectric Microcantilevers for real-time detection of BA with 10 spores/ml sensitivity and 1/1000 selectivity in bacterial mixtures.
37. McGovern J-P, Shih WY, Shih W-H, Sergi M, Chaiken I. Real-Time Salmonella Detection Using Lead Zirconate Titanate-Titanium Microcantilevers. Materials Research Society. Boston, MA, 2005:AA3.8.1 - AA3.8.6.
38. Zhu Q, Shih WY, Shih W-H. In situ, in-liquid, all-electrical detection of Salmonella typhimurium using lead titanate zirconate/gold-coated glass cantilevers at any dipping depth. Biosensors and Bioelectronics. 2007;22(12):3132-8.
39. Zhu Q, Shih WY, Shih W-H. Real-time, label-free, all-electrical detection of Salmonella typhimurium using lead titanate zirconate/gold-coated glass cantilevers at any relative humidity. Sensors and Actuators B: Chemical. 2007;125(2):379-88.
40. Capobianco JA, Shih WY, Shih W-H. 3-mercaptopropyltrimethoxysilane as insulating coating and surface for protein immobilization for piezoelectric microcantilever sensors. Review of Scientific Instruments. 2007;78(4):046106-3.
41. Yi JW, Shih WY, Shih W-H. Effect of length, width, and mode on the mass detection sensitivity of piezoelectric unimorph cantilevers. Journal of Applied Physics. 2002;91(3):1680-6.
42. Leckband D, Israelachvili J. Intermolecular Forces in Biology. Quarterly Reviews of Biophysics. 2001;34(2):105-276.
43. Leckband DE, Kuhl TL, Wang HK, Müller W, Herron J, Ringsdorf H. Force Probe Measurements of Antibody-Antigen Interactions. Methods. 2000;20(3):329-40.
44. Leckband DE, Schmitt FJ, Israelachvili JN, Knoll W. Direct Force Measurements of Specific and Nonspecific Protein Interactions. Biochemistry. 1994;33(15):4611-24.
45. Kulkarni P, Dutari G, Biswas P, Haught R. Gravity settling characteristics of Cryptosporidium parvum oocysts in aqueous suspension using in situ static light scattering. Colloids and surfaces A. 2004;233:1-10.
46. Hart A, Edwards C. Buoyant density fluctuations during the cell cycle of Bacillus subtilis. Archives of Microbiology. 1987;147(1):68-72.
47. Loong T-W. Understanding sensitivity and specificity with the right side of the brain. BMJ. 2003 September 27, 2003;327(7417):716-9.
48. Whipple SJ, Patten BC, Verity PG. Colony growth and evidence for colony multiplication in Phaeocystis pouchetii (Prymnesiophyceae) isolated from mesocosm blooms. Journal of Plankton Research. 2005:fbi026.
49. Todar K. Todar's Online Textbook of Bacteriology. In: Todar K (ed). Madison, WI: University of Wisconsin, 2005.
50. Brown RC. Air Filtration: An Integrated Approach to the Theory and Applications of Fibrous Filters: Pergamon; 1993.

51. Vicsek T, Cserzo, Miklós, Horváth VK. Self-affine growth of bacterial colonies. Physica A: Statistical Mechanics and its Applications. 1990;167(2):315-21.
52. Kiel JL, Parker JE, Alls JL, et al. Rapid Recovery and Identification of Anthrax Bacteria from the Environment. Annals of the New York Academy of Sciences. 2000;916(1):240-52.
53. Basic Diagnostic Testing Protocols for Level A Laboratories for the Presumptive Identification of Bacillus anthracis In: Prevention CfDCa (ed). Atlanta, GA 2002:22.
54. Wang SH, Zhang JB, Zhang ZP, et al. Construction of Single Chain Variable Fragment (ScFv) and BiscFv-Alkaline Phosphatase Fusion Protein for Detection of Bacillus Anthracis. Anal Chem. 2006;78(4):997-1004.
55. Immunology, Infection, and Immunity. 1 ed. Washington, DC: ASM Press; 2004. 718 p.
56. Immunology <http://www.biology.arizona.edu/immunology/tutorials/antibody/prob_set/01t.html>. Accessed 2008 6/23/08. The Univerisity of Arizona.
57. Nolte DD. Antibody Molecule <http://www.physics.purdue.edu/people/faculty/nolte.shtml>. Accessed 2008 6/23/2008. Purdue University, Dept. of Physics.
58. Gervay J, McReynolds KD. Utilization of ELISA technology to measure biological activities of carbohydrates relevant in disease states. Current Medical Chemistry. 1999;6:129 - 53.
59. EnVision Multilabel Plate Readers. Waltham, MA: PerkinElmer, Inc.
60. Jones JB, Somodi GC, Scott JW, Jones B. Increased ELISA sensitivity using a modified extraction buffer for detection of Xanthomonas campestris pv. vesicatoria in leaf tissue. Journal of Applied Microbiology. 1997;83:397-401.
61. Tsuchiya K, d'Ursel CCM. Development of a sensitive ELISA using three monoclonal antibodies against lipopolysaccharides to detect Xanthomonas campestris pv. vesicatoria, the causal agent of bacterial spot of tomato and pepper. Journal of General Plant Pathology. 2004;70(1):21-6.
62. Kleppe K, Ohtsuka E, Kleppe R, Molineux I, Khorana HG. Studies on Polynucleotides XCVI. Repair Replication of Short Synthetic DNA's as catalyzed by DNA Polymerases. Journal of Molecular Biology. 1971;56:341-61.
63. Fields YEKHA. Artificial DNA: Methods and Applications. Boca Raton, FL: CRC Press; 2002. 420 p.
64. Saiki RK, Gelfand DH, Stoffel S, et al. Primer-directed enzymatic amplification of DNA with a thermostable DNA polymerase. Science. 1988 January 29, 1988;239(4839):487-91.
65. Bartlett JM, Stirling D. PCR Protocols. 2 ed. Totowa, NJ: Humana Press, Inc.; 2003.
66. Miyazaki Y, Koga H, Kohno S, Kaku M. Nested polymerase chain reaction for detection of Mycobacterium tuberculosis in clinical samples. Journal of Clinical Microbiology. 1993;31:2228-32.
67. Nolan T, Hands RE, Bustin SA. Quantification of mRNA using real-time RT-PCR. Nat Protocols. 2006;1(3):1559-82.

68. Method 1623 Giardia and Cryptosporidium Microscopy Training Module <http://www.epa.gov/lt2/training/module_microscopy/crypto/gandcrypto/index.html>. Accessed 2008. US EPA.
69. Sauerbrey GZ. Use of a quartz vibrator for weighing thin layers on a microbalace. Zeitschrift für Physik. 1959;155:206-22.
70. IEEE Standard on Piezoelectricity: Institute of Electrical and Electronic Engineers, 1988.
71. Liu F, Li Y, Su X-L, Slavik M, Ying Y, Wang J. QCM immunosensor with nanoparticle amplification for detection of Escherichia coli O157:H7. Sensing and Instrumentation for Food Quality and Safety. 2007;1(4):161-8.
72. Fung YS, Wong YY. Self-Assembled Monolayers as the Coating in a Quartz Piezoelectric Crystal Immunosensor To Detect Salmonella in Aqueous Solution. Anal Chem. 2001;73(21):5302-9.
73. Dultsev FN, Ostanin VP, Klenerman D. "Hearing" Bond Breakage. Measurement of Bond Rupture Forces Using a Quartz Crystal Microbalance. Langmuir. 2000;16(11):5036-40.
74. Sang-Hun L, Stubbs DD, Cairney J, Hunt WD. Real-time detection of bacteria spores using a QCM based immunosensor. Sensors, 2003 Proceedings of IEEE, 2003:1194-8 Vol.2.
75. Quartz Crystal Microbalance Unit. Millinocket , ME Brim Ness Corporation.
76. Su X-L, Li Y. A QCM immunosensor for Salmonella detection with simultaneous measurements of resonant frequency and motional resistance. Biosensors and Bioelectronics. 2005;21(6):840-8.
77. Mori T, Naito M, Irimoto Y, Okahata Y. Nucleobase molecular recognition in supercritical carbon dioxide by using a highly sensitive 27 MHz quartz-crystal microbalance. Chemical Communications. 2000:45-6.
78. Biacore Life Sciences <http://www.biacore.com/lifesciences/index.html>. Accessed. GE Healthcare, General Electric Company, Fairfield, CT.
79. Chinowsky TM, Soelberg SD, Baker P, et al. Portable 24-analyte surface plasmon resonance instruments for rapid, versatile biodetection. Biosensors and Bioelectronics. 2007;22(9-10):2268-75.
80. Lakowicz J. Plasmonics in Biology and Plasmon-Controlled Fluorescence. Plasmonics. 2006;1(1):5-33.
81. Hanken D, Jordan C, Frey B, Corn R. Surface plasmon resonance measurements of ultrathin organic films at electrode surfaces. Electroanalytical Chemistry. Boca Raton, FL: CRC Press, 1998.
82. Scofield RH, Kurien BT, Zhang F, et al. Protein-protein interaction of the Ro-ribonucleoprotein particle using multiple antigenic peptides. Molecular Immunology. 1999;36(15-16):1093-106.
83. Karlsson R, Michaelsson A, Mattsson L. Kinetic analysis of monoclonal antibody-antigen interactions with a new biosensor based analytical system. Journal of Immunological Methods. 1991;145(1-2):229-40.
84. Maillart E, Brengel-Pesce K, Capela D, et al. Versatile analysis of multiple macromolecular interactions by SPR imaging: application to p53 and DNA interaction. Oncogene. 2004;23(32):5543-50.

85. Barlen B, Mazumdar SD, Lezrich O, Kämpfer P, Keusgen M. Detection of *Salmonella* by Surface Plasmon Resonance. Sensors. 2007;7:1427-46.
86. Zourob M, Mohr S, Brown BJT, Fielden PR, McDonnell MB, Goddard NJ. Bacteria detection using disposable optical leaky waveguide sensors. Biosensors and Bioelectronics. 2005;21(2):293-302.
87. Leung A, Shankar PM, Mutharasan R. A review of fiber-optic biosensors. Sensors and Actuators B: Chemical. 2007;125(2):688-703.
88. Ogert RA, Edward Brown J, Singh BR, Shriver-Lake LC, Ligler FS. Detection of Clostridium botulinum toxin A using a fiber optic-based biosensor. Analytical Biochemistry. 1992;205(2):306-12.
89. Wadkins RM, Ligler FS. Immunobiosensors Based on Evanescent Wave Excitation. Volume 7, 1998:77-87.
90. Lim DV. Detection of microorganisms and toxins with evanescent wave fiber-optic biosensors. Proceedings of the IEEE. 2003;91(6):902-7.
91. Bakaltcheva IB, Ligler FS, Patterson CH, Shriver-Lake LC. Multi-analyte explosive detection using a fiber optic biosensor. Analytica Chimica Acta. 1999;399(1-2):13-20.
92. Jung CC, Saaski EW, McCrae DA, Lingerfelt BM, Anderson GP. RAPTOR: a fluoroimmunoassay-based fiber optic sensor for detection of biological threats. Sensors Journal, IEEE. 2003;3(4):352-60.
93. Tang L, Ren Y, Hong B, Kang KA. Fluorophore-mediated, fiber-optic, multi-analyte, immunosensing system for rapid diagnosis and prognosis of cardiovascular diseases. Journal of Biomedical Optics. 2006;11(2):021011-10.
94. Geng T, Uknalis J, Tu S-I, Bhunia AK. Fiber-Optic Biosensor Employing Alexa-Fluor Conjugated Antibody for Detection of Escherichia coli O157:H7 from Ground Beef in Four Hours. Sensors. 2006;6:796-807.
95. Sapsford KE, Taitt CR, Loo N, Ligler FS. Biosensor Detection of Botulinum Toxoid A and Staphylococcal Enterotoxin B in Food. Appl Environ Microbiol. 2005 September 1, 2005;71(9):5590-2.
96. DeMarco DR, Saaski EW, McCrae DA, Lim DV. Rapid Detection of Escherichia coli O157:H7 in Ground Beef Using a Fiber-Optic Biosensor. Journal of Food Protection. 1999;62:711-6.
97. Jung C, McCrae DA, Saaski EW, DeMarco DR, Lim DV. RAPTOR: a fluoroimmunoassay-based fiber optic sensor for detection of food pathogens. Optical Fiber Sensors Conference Technical Digest, 2002 OFS 2002, 15th, 2002:249-52 vol.1.
98. Dhayal B, Henne WA, Doorneweerd DD, Reifenberger RG, Low PS. Detection of Bacillus subtilis Spores Using Peptide-Functionalized Cantilever Arrays. J Am Chem Soc. 2006;128(11):3716-21.
99. Lavrik NV, Sepaniak MJ, Datskos PG. Cantilever transducers as a platform for chemical and biological sensors. Review of Scientific Instruments. 2004;75(7):2229-53.
100. Wu G, Datar RH, Hansen KM, Thundat T, Cote RJ, Majumdar A. Bioassay of prostate-specific antigen (PSA) using microcantilevers. Nat Biotech. 2001;19(9):856-60.

101. Vashist SK. A Review of Microcantilevers for Sensing Applications. Journal of Nanotechnology Online. 2007;3:1-15.
102. Shu W, Laue ED, Seshia AA. Investigation of biotin-streptavidin binding interactions using microcantilever sensors. Biosensors and Bioelectronics. 2007;22(9-10):2003-9.
103. McKendry R, Zhang J, Arntz Y, et al. Multiple label-free biodetection and quantitative DNA-binding assays on a nanomechanical cantilever array. Proceedings of the National Academy of Sciences. 2002 July 23, 2002;99(15):9783-8.
104. Gfeller KY, Nugaeva N, Hegner M. Micromechanical oscillators as rapid biosensor for the detection of active growth of Escherichia coli. Biosensors and Bioelectronics. 2005;21(3):528-33.
105. Nugaeva N, Gfeller KY, Backmann N, Lang HP, Düggelin M, Hegner M. Micromechanical cantilever array sensors for selective fungal immobilization and fast growth detection. Biosensors and Bioelectronics. 2005;21(6):849-56.
106. Ilic B, Czaplewski D, Craighead HG, Neuzil P, Campagnolo C, Batt C. Mechanical resonant immunospecific biological detector. Applied Physics Letters. 2000;77(3):450-2.
107. Lavrik NV, Datskos PG. Femtogram mass detection using photothermally actuated nanomechanical resonators. Applied Physics Letters. 2003;82(16):2697-9.
108. Ilic B, Czaplewski D, Zalalutdinov M, et al. Single cell detection with micromechanical oscillators. The 45th international conference on electron, ion, and photon beam technology and nanofabrication. Washington, DC (USA): AVS, 2001:2825-8.
109. Arakawa ET, Lavrik NV, Datskos PG. Detection of anthrax simulants with microcalorimetric spectroscopy: Bacillus subtilis and Bacillus cereus spores. Applied Optics. 2003;42(10):1757-62.
110. Velu H, Soulie P, Bellocq B. PULMONARY ANTHRAX AND CHLORINE POISONING: MINIMUM INFECTIOUS DOSE OF SPORES. In: Center DTI (ed). JOINT PUBLICATIONS RESEARCH SERVICE. Arlington, VA, 1962.
111. Altman DG, Bland JM. Statistics Notes: Diagnostic tests 1: sensitivity and specificity. BMJ. 1994 June 11, 1994;308(6943):1552-.
112. Zhang B, Mao Q, Zhang X, et al. A novel piezoelectric quartz micro-array immunosensor based on self-assembled monolayer for determination of human chorionic gonadotropin. Biosensors and Bioelectronics. 2004;19:711-20.
113. Yao C, Chen Q, Chen M, et al. A Novel Piezoelectric Quartz Micro-Array Immunosensor for Detection of ImmunoglobulinE. Journal of Nanoscience and Nanotechnology. 2006;6:3828-34.
114. Zeng H, Wang H, Chen F, et al. Development of quartz-crystal-microbalance-based immunosensor array for clinical immunophenotyping of acute leukemias. Analytical Biochemistry. 2006;351(1):69-76.
115. Kramer MF, Lim DV. A Rapid and Automated Fiber Optic-Based Biosensor Assay for the Detection of Salmonella in Spent Irrigation Water Used in the Sprouting of Sprout Seeds. Journal of Food Protection. 2004;67:46-52.

116. Bosch ME, Sánchez AJR, Rojas FS, Ojeda CB. Recent Development in Optical Fiber Biosensors. Sensors. 2007;7:797-859.
117. Nanduri V, Kim G, Morgan MT, et al. Antibody Immobilization on Waveguides Using a Flow–Through System Shows Improved Listeria monocytogenes Detection in an Automated Fiber Optic Biosensor: RAPTOR™. Sensors. 2006;6:808-22.
118. Hindson BJ, McBride MT, Makarewicz AJ, et al. Autonomous Detection of Aerosolized Biological Agents by Multiplexed Immunoassay with Polymerase Chain Reaction Confirmation. Anal Chem. 2005;77(1):284-9.
119. McBride MT, Masquelier D, Hindson BJ, et al. Autonomous Detection of Aerosolized Bacillus anthracis and Yersinia pestis. Anal Chem. 2003;75(20):5293-9.
120. SASS 2000 <http://www.resrchintl.com/sass2000-air-sampler.html>. Accessed. Research International.
121. Veeco Instruments Accessed, Plainview, NY.
122. Shen Z. Synthesis, fabrication, and characterization of self-exciting, self-sensing PZT/SiO2 piezoelectric micro-cantilever sensors. Philadelphia, PA: Drexel University, 2007. 222 p.
123. Lee JH, Hwang KS, Park J, Yoon KH, Yoon DS, Kim TS. Immunoassay of prostate-specific antigen (PSA) using resonant frequency shift of piezoelectric nanomechanical microcantilever. Biosensors and Bioelectronics. 2005;20(10):2157-62.
124. Lee JH, Kim TS, Yoon KH. Effect of mass and stress on resonant frequency shift of functionalized Pb(Zr[sub 0.52]Ti[sub 0.48])O[sub 3] thin film microcantilever for the detection of C-reactive protein. Applied Physics Letters. 2004;84(16):3187-9.
125. Chen GY, Thundat T, Wachter EA, Warmack RJ. Adsorption-induced surface stress and its effects on resonance frequency of microcantilevers. Journal of Applied Physics. 1995;77(8):3618-22.
126. Ramos D, Tamayo J, Mertens J, Calleja M, Zaballos A. Origin of the response of nanomechanical resonators to bacteria adsorption. Journal of Applied Physics. 2006;100(10):106105-3.
127. Ren Q, Zhao YP. Influence of surface stress on frequency of microcantilever-based biosensors. Microsystem Technologies. 2004;10(4):307-14.
128. Zhu Q, Shih WY, Shih W-H. Mechanism of the flexural resonance frequency shift of a piezoelectric microcantilever sensor in a dc bias electric field. Applied Physics Letters. 2008;92(3):033503-3.
129. Zhu Q, Shih WY, Shih W-H. Mechanism of flexural resonance frequency shift of a piezoelectric microcantilever sensor during humidity detection. Applied Physics Letters. 2008;92(18):183505-3.
130. Algueró M, Jiménez B, Pardo L. Rayleigh type behavior of the Young's modulus of unpoled ferroelectric ceramics and its dependence on temperature. Applied Physics Letters. 2003;83:2641-3.
131. Lee Y, Lim G, Moon W. A self-excited micro cantilever biosensor actuated by PZT using the mass micro balancing technique. Sensors and Actuators A: Physical. 2006;130-131:105-10.

132. Zurn S, Hsieh M, Smith G, et al. Fabrication and structural characterization of a resonant frequency PZT microcantilever. Smart Materials and Structures. 2001;10(2):252-63.
133. Hwang KS, Lee JH, Park J, Yoon DS, Park JH, Kim TS. In situ quantitative analysis of a prostate-specific antigen (PSA) using a nanomechanical PZT cantilever. Lab on a Chip. 2004;4:547-52.
134. Campbell GA, Mutharasan R. Sensing of liquid level at micron resolution using self-excited millimeter-sized PZT-cantilever. Sensors and Actuators A: Physical. 2005;122(2):326-34.
135. Campbell GA, Mutharasan R. Detection and quantification of proteins using self-excited PZT-glass millimeter-sized cantilever. Biosensors and Bioelectronics. 2005;21(4):597-607.
136. Campbell GA, Mutharasan R. Use of Piezoelectric-Excited Millimeter-Sized Cantilever Sensors To Measure Albumin Interaction with Self-Assembled Monolayers of Alkanethiols Having Different Functional Headgroups. Anal Chem. 2006;78(7):2328-34.
137. Maraldo D, Rijal K, Campbell G, Mutharasan R. Method for Label-Free Detection of Femtogram Quantities of Biologics in Flowing Liquid Samples. Anal Chem. 2007;79(7):2762-70.
138. Campbell GA, Mutharasan R. PEMC sensor's mass change sensitivity is 20 pg/Hz under liquid immersion. Biosensors and Bioelectronics. 2006;22(1):35-41.
139. Campbell GA, Mutharasan R. Piezoelectric-excited millimeter-sized cantilever (PEMC) sensors detect Bacillus anthracis at 300 spores/mL. Biosensors and Bioelectronics. 2006;21(9):1684-92.
140. Shih WY, Shih W-H, Aksay lA. Scaling Analysis for the Axial Displacement and Pressure of Flextensional Transducers. Journal of the American Ceramic Society. 1997;80(5):1073-8.
141. Li X, Shih WY, Aksay IA, Shih W-H. Electromechanical Behavior of PZT-Brass Unimorphs. Journal of the American Ceramic Society. 1999;82(7):1733-40.
142. Shih WY, Li X, Gu H, Shih W-H, Aksay IA. Simultaneous liquid viscosity and density determination with piezoelectric unimorph cantilevers. Journal of Applied Physics. 2001;89(2):1497-505.
143. Luo H. Colloidal Processing of PMN-PT Thick Films for Piezoelectric Sensor Applications. Philadelphia, PA: Drexel University, 2005. 167 p.
144. Everest FA. Master Handbook of Acoustics. Columbus, OH: McGraw-Hill Publishing Co; 2000.
145. Bouzid A, Bourim EM, Gabbay M, Fantozzi G. PZT phase diagram determination by measurement of elastic moduli. Journal of the European Ceramic Society. 2005;25(13):3213-21.
146. WS-22 High Precision Wire Saw. Princeton, NJ: Princeton Scientific Corp.
147. Piehler J, Brecht A, Valiokas R, Liedberg B, Gauglitz G. A high-density poly(ethylene glycol) polymer brush for immobilization on glass-type surfaces. Biosensors and Bioelectronics. 2000;15(9-10):473-81.
148. Jung SK, Wilson GS. Polymeric Mercaptosilane-Modified Platinum Electrodes for Elimination of Interferants in Glucose Biosensors. Anal Chem. 1996;68(4):591-6.

149. Detzel AJ, Campbell GA, Mutharasan R. Rapid assessment of Escherichia coli by growth rate on piezoelectric-excited millimeter-sized cantilever (PEMC) sensors. Sensors and Actuators B: Chemical. 2006;117(1):58-64.
150. Smits AJ. A Physical Introduction to Fluid Mechanics. New York: Wiley and Sons, Inc.; 1999.
151. Stokes GG. On the effect of internal friction of fluids on the motion of pendulums. Trans Cambridge Philos. 1851;9.
152. Goldman AJ, Cox RG, Brenner H. Slow viscous motion of a sphere parallel to a plane wall - I Motion through a quiescent fluid. Chemical Engineering Science. 1967;22:637-51.
153. Goldman AJ, Cox RG, Brenner H. Slow viscous motion of a sphere parallel to a plane wall - II Couette flow. Chemical Engineering Science. 1967;22:653-60.
154. Masako S-S. Flow around cells adhered to a microvessel wall II: Comparison to flow around adherent cells in channel flow. Biorheology. 2001;38(1):3-13.
155. Leckband DE, Kuhl TL, Wang HK, et al. Force Probe Measurements of Antibody-Antigen Interactions. Methods: A Companion to Methods in Enzymology. 2000;20:329-40.
156. Mamane-Gravetz H, Linden KG. Relationship between physiochemical properties, aggregation and u.v. inactivation of isolated indigenous spores in water. Journal of Applied Microbiology. 2005;98(2):351-63.
157. Beattie JK. The intrinsic charge on hydrophobic microfluidic substrates. Lab on a Chip. 2006;6:1409-11.
158. Khorasani MT, MoemenBellah S, Mirzadeh H, Sadatnia B. Effect of surface charge and hydrophobicity of polyurethanes and silicone rubbers on L929 cells response. Colloids and Surfaces B: Biointerfaces. 2006;51(2):112-9.
159. Campbell GA, Mutharasan R. Method of Measuring Bacillus anthracis Spores in the Presence of Copious Amounts of Bacillus thuringiensis and Bacillus cereus. Anal Chem. 2007;79(3):1145-52.
160. Kandimalla VB, Neeta NS, Karanth NG, et al. Regeneration of ethyl parathion antibodies for repeated use in immunosensor: a study on dissociation of antigens from antibodies. Biosensors and Bioelectronics. 2004;20(4):903-6.
161. Yi JW, Shih WY, Mutharasan R, Shih W-H. In situ cell detection using piezoelectric lead zirconate titanate-stainless steel cantilevers. Journal of Applied Physics. 2003;93(1):619-25.
162. Thundat T, Wachter EA, Sharp SL, Warmack RJ. Detection of mercury vapor using resonating microcantilevers. Applied Physics Letters. 1995;66(13):1695-7.
163. Shen Z, Shih WY, Shih W-H. Mass detection sensitivity of piezoelectric cantilevers with a nonpiezoelectric extension. Review of Scientific Instruments. 2006;77(6):065101-10.
164. McFarland AW, Poggi MA, Doyle MJ, Bottomley LA, Colton JS. Influence of surface stress on the resonance behavior of microcantilevers. Applied Physics Letters. 2005;87(5):053505-3.
165. Bhalerao KD, Mwenifumbo SC, Soboyejo ABO, Soboyejo WO. Biomedical Microdevices. Volume 6. The Netherlands: Kluwer Academic Publishers, 2004:23-31.
166. International Patent Application Number: WO 2005/005951 A2.

167. Cooper MA. Biosensing using rupture event scanning (REVS)&trade. Measurement Science and Technology. 2003;14(11):1888-93.
168. Sulchek TA, Friddle RW, Langry K, et al. Dynamic force spectroscopy of parallel individual Mucin1â€“antibody bonds. Proceedings of the National Academy of Sciences of the United States of America. 2005 November 15, 2005;102(46):16638-43.
169. Heymann B, Grubmuller H. Molecular Dynamics Force Probe Simulations of Antibody/Antigen Unbinding: Entropic Control and Nonadditivity of Unbinding Forces. Biophys J. 2001 September 1, 2001;81(3):1295-313.
170. Dammer U, Hegner M, Anselmetti D, et al. Specific antigen/antibody interactions measured by force microscopy. Biophys J. 1996 May 1, 1996;70(5):2437-41.
171. Watanabe N, Shirakawa T, Iwahashi M, Seimiya T. Effect of surface charge on adsorption of bovine serum albumin 2. Interaction of protein molecules with an anionic monolayer, as studied by ellipsometry, radiotracer and surface tension measurements. Colloid & Polymer Science. 1988;266(3):254-60.
172. Dickson JS, Koohmaraie M. Cell surface charge characteristics and their relationship to bacterial attachment to meat surfaces. Appl Environ Microbiol. 1989 April 1, 1989;55(4):832-6.
173. Mercado R, Santander F. Size of *Cryptosporidium* oocysts excreted by symptomatic children of Santiago, Chile. Revista do Instituto de Medicina Tropical de São Paulo. 1995;37(5):473-4.
174. Lindquist HDA. Cryptosporidium Image Sequence 1 <http://www.epa.gov/nerlcwww/cpt_seq1.htm>. Accessed 8/28/08. United States Environmental Protection Agency, 2007.
175. "A400FLK. Crypt-a-Glo Comprehensive Kit" Data Sheet. New Orleans, LA: Waterborne, Inc.
176. Xu J. Grain-size characteristics of suspended sediment in the Yellow River, China. CATENA. 2000;38(3):243-63.
177. Walling DE, Owens PN, Waterfall BD, Leeks GJL, Wass PD. The particle size characteristics of fluvial suspended sediment in the Humber and Tweed catchments, UK. The Science of The Total Environment. 2000;251-252:205-22.
178. Stone M, Saunderson H. Particle size characteristics of suspended sediment in Southern Ontario rivers tributary to the great lakes. Hydrological Processes. 1992;6(2):189-98.
179. Ren J, Packman AI. Changes in fine sediment size distributions due to interactions with streambed sediments. Sedimentary Geology. 2007;202(3):529-37.
180. Hongjun Li JLZXJHM. Flocculation of kaolinite clay suspensions using a temperature-sensitive polymer. AIChE Journal. 2007;53(2):479-88.
181. Halloysite nanoclay. Sigma-Aldrich, 2008.
182. Catherine D. Reyes AJG. A centrifugation cell adhesion assay for high-throughput screening of biomaterial surfaces. Journal of Biomedical Materials Research Part A. 2003;67A(1):328-33.
183. Gallant ND, Michael KE, Garcia AJ. Cell Adhesion Strengthening: Contributions of Adhesive Area, Integrin Binding, and Focal Adhesion Assembly. Mol Biol Cell. 2005 September 1, 2005;16(9):4329-40.

184. Boettiger D. Quantitative Measurements of Integrin-Mediated Adhesion to Extracellular Matrix. Methods in Enzymology. 2007;426:1-25.

Appendix A: Resonance Peak Reconstruction – Visual Basic Implementation

The Agilent 4294A impedance analyzer is the primary piece of equipment used to acquire phase angle versus frequency data of the various types of piezoelectric microcantilever sensors (PEMS) and PEMS arrays discussed in this dissertation. While this piece of equipment is indeed quite sophisticated, significant noise in such data does remain. Some of this noise can be reduced by increasing the point averaging of the frequency scan or expanding the bandwidth of the impedance analyzer. However, both of these methods necessarily require increases in data acquisition times that are often deemed incompatible with the goal of maintaining real-time biodetection. Furthermore, whilst this type of noise reduction will certainly increase the accuracy with which peak location is determined, full reduction of noise along the entirety of the resonance peak, from baseline to baseline may not be necessary, and thus would entail superfluous effort. In other words, it is possible to acquire the shape of the peak and then just focus on the apex of the peak to pinpoint its location.

As the HP VEE computer-side software (which controls the function of the Agilent 4294A and records the data obtained) currently functions, a particular phase angle value associated with a particular frequency value is stored in a matrix for a maximum of 801 points between the user-specified begin and end points of the chosen frequency scan range. This program then searches the phase angle values in the matrix to locate the maximum value, looks up the frequency value associated with this maximum phase value, and returns this frequency as the 'position' of the peak. With a clean, noise-free signal, this algorithm is perfectly acceptable, however, when noise levels in this

phase angle spectrum are just a few tenths of a degree, as is often the case, significant noise levels in the resonance frequency peak position versus time figure can result. Practically speaking, these noise levels in resonance peak position versus time results leads to lower signal to noise ratios (SNR) and a lessened ability to confidently assess detection of pathogens where very small resonance shifts have occurred.

For instance, if a noise level of 150 Hz exists in the resonance peak versus time plot of a particular detection sequence, but the total resonance frequency shift observed is only 200 Hz, an SNR of just over one results, and such an experimenter would have difficulty convincing any reviewer, advisor or colleague that detection has actually occurred. The blue lines in Figures A-1 and A-2, respectively represent a 'raw' resonance frequency peak as acquired by the Impedance Analyzer and the tracking of this peak over the course of eighty minutes of a detection experiment. In Figure A-1, we see the random noise that exists in the peak as monitored by the Impedance Analyzer. When the simple 'find the maximum' algorithm is executed on this data by the HP VEE program, the blue line in Figure A-2 results. The noise level of this curve is 153 Hz, and if any downshift has occurred, it is certainly not significantly greater than this noise level.

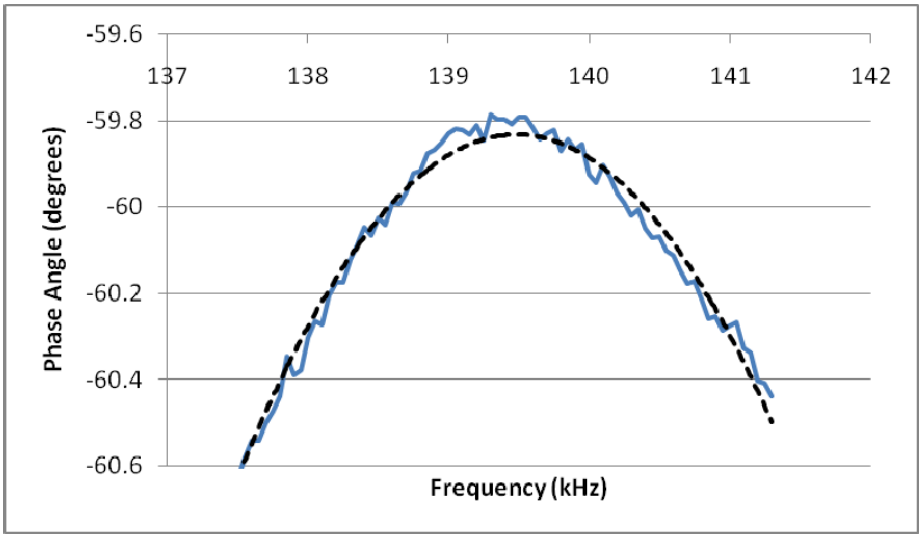

Figure A-1: Resonance peak as acquired by the Impedance Analyzer (blue curve) and the associated reconstructed peak (black dashed curve)

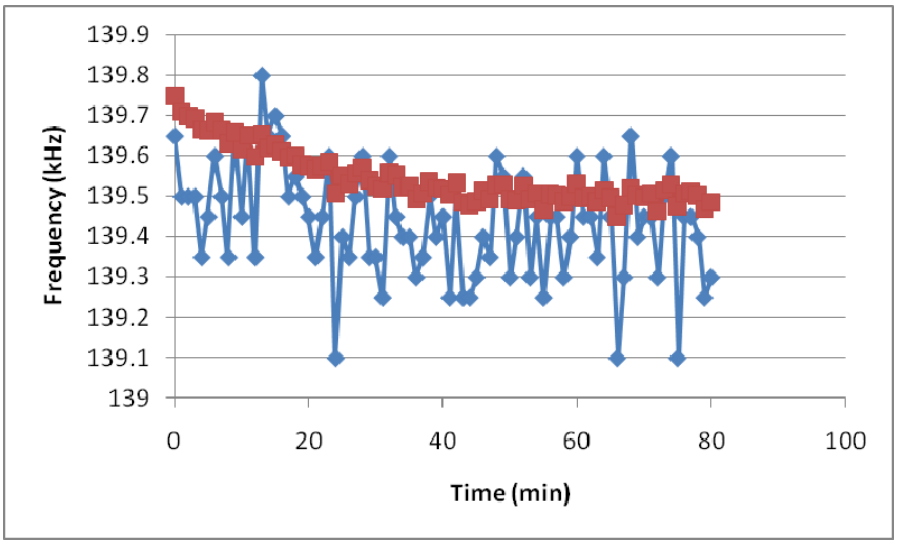

Figure A-2: Raw resonance peak position versus time graph (blue) and resonance peak position versus time graph after resonance peak reconstruction (red)

With these high levels of noise typical of just about all detection peaks and all PEMS, this author has developed a software algorithm aimed to significantly increase the accuracy with which resonance peak positions are determined. The rationale behind this algorithm is to ascertain a precise location of the resonance peak by looking past random

noise inherent in the original phase angle versus frequency scan. With this increased accuracy in determining the actual position of the resonance peak, noise levels in the final resonance peak position versus time graphs can be drastically reduced. By examining only the upper portion of a resonance curve, as shown in Figure A-1, we can assume that this shape is well approximated by a second order polynomial function. Utilizing the Visual Basic programming language available within Microsoft Excel, a program was written to examine each resonance peak, fit a second order polynomial to it and then take the derivative of this polynomial equation to pinpoint its location. The most recent embodiment of this program is transcribed below.

The red trace in Figure A-2 represents the application of this program to a particular data set. From a comparison of this curve to the original 'raw data' curve, we can see that resonance peak reconstruction has reduced the level of noise in the experimental results from 153 Hz to just 22 Hz. This has allowed for distinct recognition of the 250 Hz resonance frequency shift that occurred during the eighty minutes of this experiment and has increased the SNR from just great than unity to greater than 10.

Visual Basic Code (Excel Macro)

```
Sub CurveFit()
' Keyboard Shortcut: Ctrl+j
' DataMoveRoutine

d = 1
c = 0

For y = 1 To 82
d = d + 1

    For x = 2 To 802
    Cells(x - 1, d + 4) = Cells(x + c, 4)
    If Cells(x + c, 4) = Empty Then Exit For
    Next x
```

```
If Cells(x + c + 1, 4) = Empty Then Exit For
c = c + 802
Next y

For x = 2 To 802
Cells(x - 1, 4) = Cells(x, 2)
Next x

Range("A803:D65536").ClearContents
Range("A1:C802").ClearContents
Range("D802").ClearContents
Cells(1, 1).Select

' RawMax and CurveFitMax Routine Below

For t = 6 To 256
Dim Peak As Range
Set Peak = Range(Cells(1, t), Cells(801, t))
q = Application.WorksheetFunction.Max(Peak)
maxrow = Application.WorksheetFunction.Match(q, Peak, 0)
Cells(t - 4, 2) = Cells(maxrow, 4)

    For i = 1 To 80
    Cells(i, 5) = Cells(maxrow - 40 + i, t)
    Cells(i + 80, 5) = Cells(maxrow - 40 + i, 4)
    Next i

Cells(804, 5).Formula =
"=INDEX(LINEST(E1:E80,E81:E160^{1,2}, True, False), 1, 1)"
Cells(804, 6).Formula =
"=INDEX(LINEST(E1:E80,E81:E160^{1,2}, True, False), 1, 2)"

a0 = Cells(804, 5)
a1 = Cells(804, 6)

Cells(t - 4, 3) = -1 * a1 / (2 * a0)

Range("E804:I804").ClearContents
If Cells(1, t + 1) = Empty Then Exit For
Next t

Cells(1, 2) = "RawMax"
Cells(1, 3) = "CFMax"
Cells(1, 1) = "Time (min)"
interval = Application.InputBox("Enter Detection Time
Interval (in min)")

For h = 0 To 255
Cells(h + 2, 1) = h * interval
If Cells(h + 3, 2) = Empty Then Exit For
Next h

End Sub
```

Appendix B: Resonance Peak Reconstruction – LabView Implementation

Though impressive results in resonance peak position versus time noise reduction had been achieved by implementing a peak reconstruction algorithm in the Visual Basic programming language, as discussed Appendix A, shortcomings of this algorithm were soon observed. It was found that only mildly noisy peaks, such as the example given in Appendix A, responded well to treatment by means of this Visual Basic algorithm, but when peaks with significantly more noise (on the order of a degree) were used for detection, little to no improvement in noise could be achieved. Furthermore, errors in the execution of the program itself would arise when detection peaks became asymmetric. The largest shortcoming of this resonance peak reconstruction implementation, however, was its inflexibility of parameters.

The main parameter that would control the function of the program was that of the number of raw data points to which the polynomial would be fit. This parameter is denoted as '`i`' in the previous code, and, as a result of the '`LINEST`' function called from excel, this parameter could not be updated dynamically for each instance in the succession of peaks over time. Thus for a given data set, the user would essentially pick a value for `i` between 1 and 801 (in the example above, 80 was chosen), examine the results and choose a different value in an attempt to further reduce noise levels.

With the goal of negating this trial and error means of determining the number of data points from the original 801 to fit the polynomial to, this same algorithm was translated into LabView. Though this was the motivation for the migration to LabView, many other advantages of this robust programming environment soon became apparent

and further aided in noise reduction by means of resonance peak reconstruction for all types of PEMS biosensors and all degrees of initial noise. Upon implementation of this LabView algorithm (which is shown at the terminus of this appendix), a method was devised where the user would guess at a first value for the number of points to which the polynomial would be fit and then the program would automatically adjust this value for each individual peak in the array so as to obtain the best fit for each. The results of this process would then be displayed (in a matter of milliseconds) and the user could then further tailor this initial guess to achieve better noise reduction. All the while, the first and last resonance peaks and their polynomial reconstructions were displayed so that the user could verify that accurate peak reconstruction was taking place. Figure B-1, below is a screenshot of the front panel of this program.

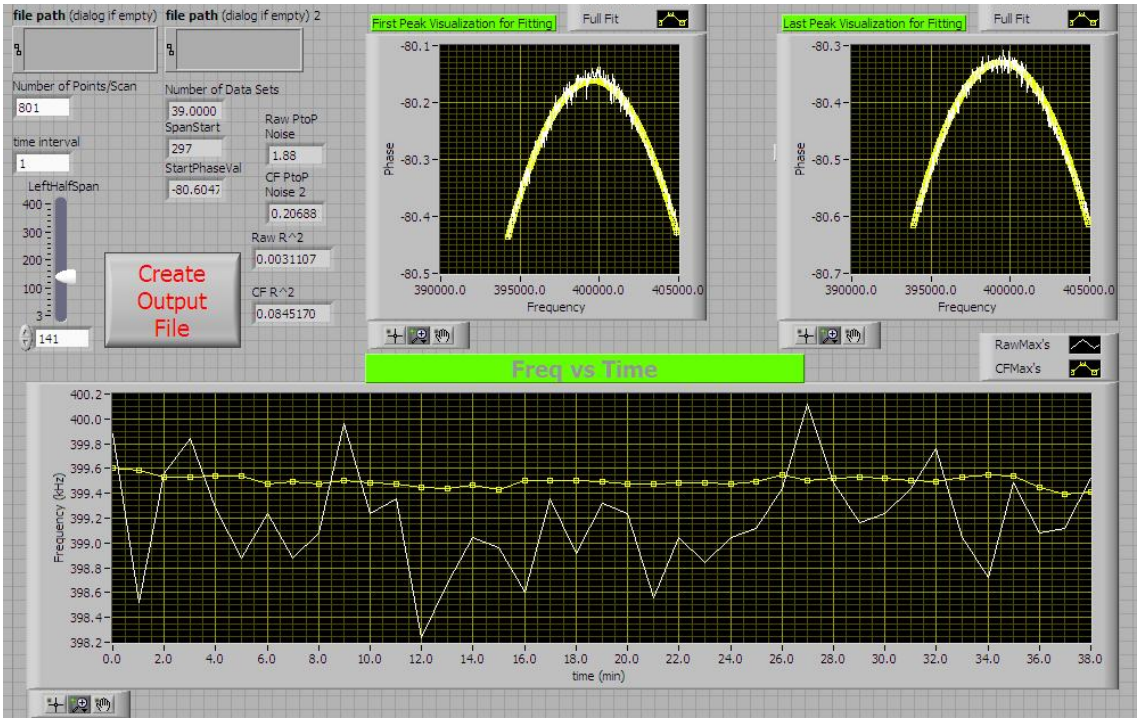

Figure B-1: Front panel of LabView resonance peak reconstruction implementation

In this figure, we see that the noise level of this particular resonance peak position versus time curve prior to peak reconstruction is nearly 2 kHz, but that effective reconstruction has reduced this noise level to less than 50 Hz. Also, we can confirm, in the 'Visualization for Fitting' windows that both the first and the last peaks are being accurately reconstructed by the fitted polynomial.

This embodiment of resonance peak reconstruction represents this author's most recent contribution to this area of PEMS biodetection noise reduction and has facilitated the highly sensitive detections of single *Cryptosporidium* oocysts as presented in Chapter 6.

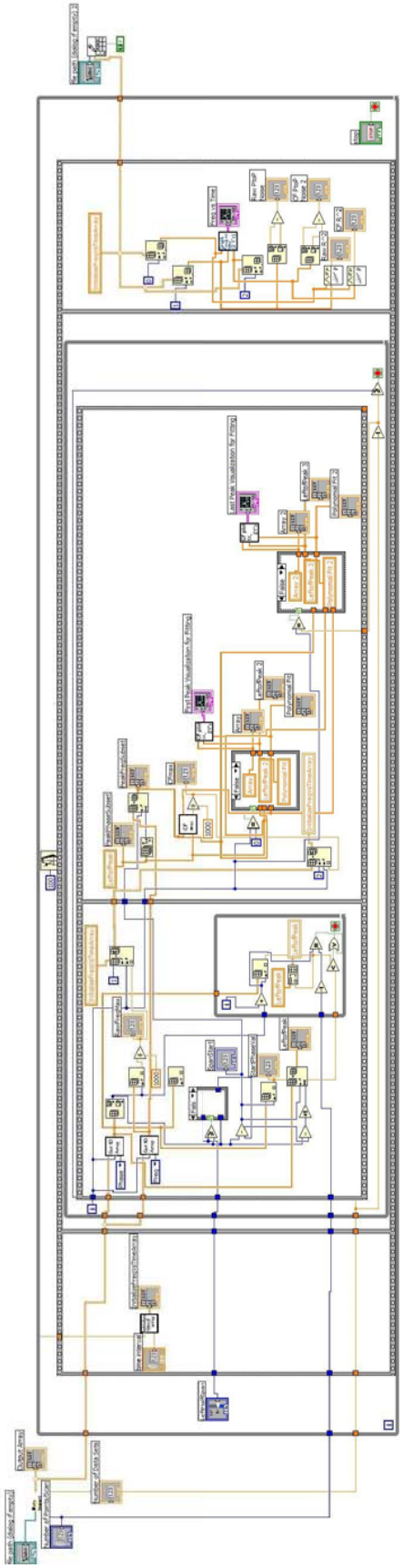

Figure B-2: LabView block diagram implementation of resonance peak reconstruction

Appendix C: Calculation of Antibody Surface Coverage Density

An estimation of antibody surface coverage density can be achieved by using the resonance frequency shift value associated with an instance of antibody immobilization onto a PEMS surface, the mass per frequency shift sensitivity of said sensor, the surface area of the sensor and the mass of the antibody molecules in question. This appendix will estimate the antibody surface coverage density of anti-BA IgG on the platinum surface of a PMN-PT PEMS described in Section 4.1.2 by means EDC/NHS activated MPA immobilization as described in Section 4.3.2.

The particular instance of antibody immobilization to be studied here occurs from zero to fifteen minutes in Figure 5-2(a). PEMS B from Chapter 5 is the biosensor to which the antibody is being immobilized and its length, width and detection sensitivity were given as 500 μm, 800 μm and 3×10^{-13} g/Hz, respectively. The resonance frequency shift associated with this instance of antibody immobilization was 400 Hz. By virtue of this value multiplied by the mass detection sensitivity given above, we see that 1.2×10^{-10} g of antibody were deposited onto the sensor surface. With the mass of an IgG antibody known as 160 kDa, or 2.65×10^{-19} g, we calculate that the total number of antibody molecules immobilized onto this particular sensor surface as 4.5×10^{8}. Thus, with a sensor surface area of 400,000 μm^2, the calculated surface coverage density of antibody molecules on the sensor surface is 1.1×10^{3} molecules/μm^2.

Appendix D: Conversion of Interaction Force to Shear Stress

Though the derivation and analyses presented in Section 4.4.2.2, 'Forces Resultant from Laminar Flow,' is useful in transforming fluid flow rates and speeds into forces impingent upon particulate matter, such as biological pathogens, it is also useful to discuss the shear stresses associated with these interactions of pathogens with biosensor surfaces. As the term 'stress' indicates, and according to the simple equation for shear stress, $\tau = {}^{F}/_{A}$, where is F is the applied force, in order to obtain a value for shear stress (τ), an area of interaction (A) must be defined over which the force will act. In the case of *Bacillus* spores and *Cryptosporidium* oocysts detection, this interaction area will be delineated by the region of the spherical (or at least roughly so) spore or oocyst surface that comes in close enough contact with the flat sensor surface to allow for significant antibody interaction. For this derivation and resulting calculations, and according to Leckband, et al,[43] significant antibody interaction will be deemed to occur when the pathogen surface is within 2 nm of the PEMS sensor surface.

In Figure D-1, below we see how this knowledge of interaction distance between an antibody molecule and a possible surface antigen of a spore or oocyst dictates the interaction area of the pathogen with the sensor surface. By simple geometric manipulations we arrive at the radius of the circle which delineates this interaction area as $a = \sqrt{2rd - d^2}$, where r is the radius of the spore or oocyst and d is the interaction distance of 2 nm. This radius, a, then allows for the calculation of the interaction area according to the formula for the area of a circle.

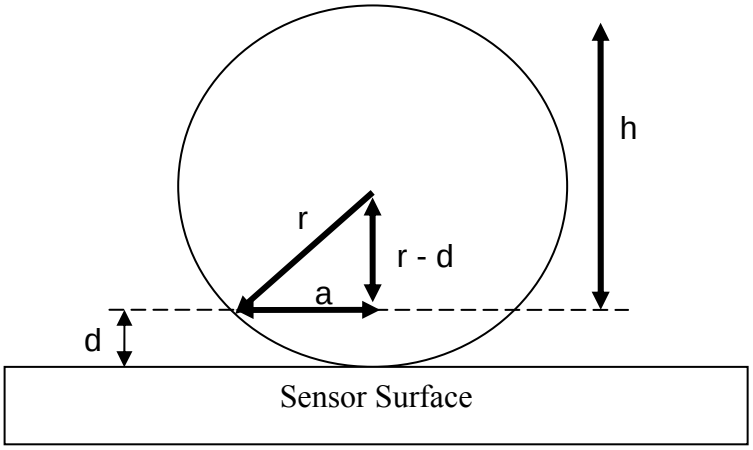

Figure D-1: Geometrical schematic of spherical spore or oocyst on a PEMS sensor surface

With this calculation of interaction area in hand, the analysis presented by Boettiger to transform shear stress into adhesion force[184] can be algebraically manipulated to perform just the opposite transformation. This original analysis was intended to enable comparisons of adhesion strength among varying cell types as ascertained in spinning disc experiments.[182-184] Combining Boettiger's four equations into one, we arrive at:

$$F = (4.33\pi r^2\tau)^2 + \left(\frac{0.75}{(2.44a + 4.33)\pi h r^2 \tau}\right)^2 \qquad \text{(D.1)}$$

where F is the calculated adhesion force, r is the radius of the spore or oocyst, a is as described above, $h = 2r - d$, as shown in Figure D-1, and τ is again, the shear stress as would be determined by spinning disc experiments. Performing our algebraic manipulations, we arrive at:

$$\tau = \left(\frac{F}{2(4.33\pi r^2)^2} + \frac{\left(F^2 - \frac{9}{4}\left(\frac{4.33\pi r^2}{(2.44a + 4.33)\pi h r^2} \right)^2 \right)^{1/2}}{2(4.33\pi r^2)^2} \right)^{1/2} \qquad \text{(D.2)}$$

By applying this equation to the spore and oocysts systems described in this dissertation and at the flow rates, flow speeds and resulting forces acting upon the suspended pathogens, we arrive at Table 7-1, as discussed in Chapter 7. The highest calculated shear stress studied in this dissertation is that of *Bacillus anthracis* spore interaction with an anti-BA-spore functionalized PEMS, as discussed in Chapter 5. This value is calculated as just 11 dynes/cm^2, however, which is a full order of magnitude less than typical shear stresses probed by the spinning disc apparatus.[182-184]

Appendix E: FTIR Verification of Antibody Immobilization

This appendix uses the vibrational technique of fourier transform infrared (FTIR) spectroscopy to study the efficacy of the EDC/NHS activated MPA surface immobilization technique used for bio-functionalization of the platinum sensor surface of PMN-PT PEMS. For FTIR characterization a DIGILAB Excalibur Series was used with an FTS 3000 MX light source. A UMA 600 microscope attachment was used to perform External Reflectance spectroscopy measurements on the Pt samples. Three separate samples were prepared for FTIR characterization and comparison.

First, three clean glass slides were sputter coated (Denton Vacuum Systems, Centralized Materials Characterization Facility, Drexel University) with platinum for four minutes each in order approximate the platinum sensor surface while enabling microscopic external reflectance FTIR measurements to be obtained. The three slides were then cleaned with a 1:100 piranha etch solution (1:1 v:v Sulfuric Acid:Hydrogen Peroxide) in deionized (DI) water, and then rinsed with DI water. One of the Pt coated slides was then set aside to be used as a background sample. The two remaining slides were immersed in a 1 mM solution of MPA in DI water for 24 hours and then rinsed with DI water. One of these two slides was then set aside for later characterization. The remaining slide was then immersed in an aqueous solution of 1-ethyl-3-(3-dimethylaminopropyl) carbodiimide (EDC) and N-hydrosuccinimide (NHS) at concentrations of 0.4 mg/ml and 0.6 mg/ml, respectively, for one hour. This slide was then rinsed with DI water, and immersed in a 500 mM solution of monoclonal antibody to Salmonella typhimurium (KPL, inc, California, USA) for one hour. Finally, this last

slide was rinsed with DI water and all three slides were allowed to dry under ambient conditions.

The method for analysis of these samples is to obtain a baseline FTIR absorbance spectrum of the un-functionalized platinum-only sample. This spectrum is then subtracted from the spectrum obtained upon analysis of the MPA functionalized sample and the antibody functionalized sample. By virtue of such analysis, it was found herein that the MPA monolayer yielded no discernable protein-specific FTIR peaks (figure not shown). However, when the FTIR spectrum of the sample with the antibody monolayer bound to the MPA layer is analyzed after baseline removal, several peaks indicative of antibody presence are noted.

The two protein-specific FTIR bands of interest in figure xx, below are the peaks located at 1753 and 1402 cm^{-1}. The peak at 1753 cm^{-1} is representative of a secondary amine vibrating in the bending mode, while the peak at 1402 cm^{-1} is indicative of a carbon-oxygen double bond. This amine vibration is necessarily attributed to the presence of a protein (in this case, our antibody) on the sample surface since there is no amine functionality in MPA. Another point of interest is the fact that the though the C=0 moiety exists in the carbonyl group of MPA, the peak was not observed in the sample with just MPA on the surface, but only in the sample with the antibody bound to the MPA. The additional peaks observed in Figure E-1 are artifacts of incomplete baseline removal. The broad peak at 1210 cm^{-1} results from incomplete platinum coverage on the glass slide samples and the resulting FTIR resonance of the SiO_2 substrate. The peak at 2362 cm^{-1} can also be identified as 'environmental' as it is that of atmospheric CO_2, resulting from the fact that the spectrometer used was not sealed or filled with inert gas.

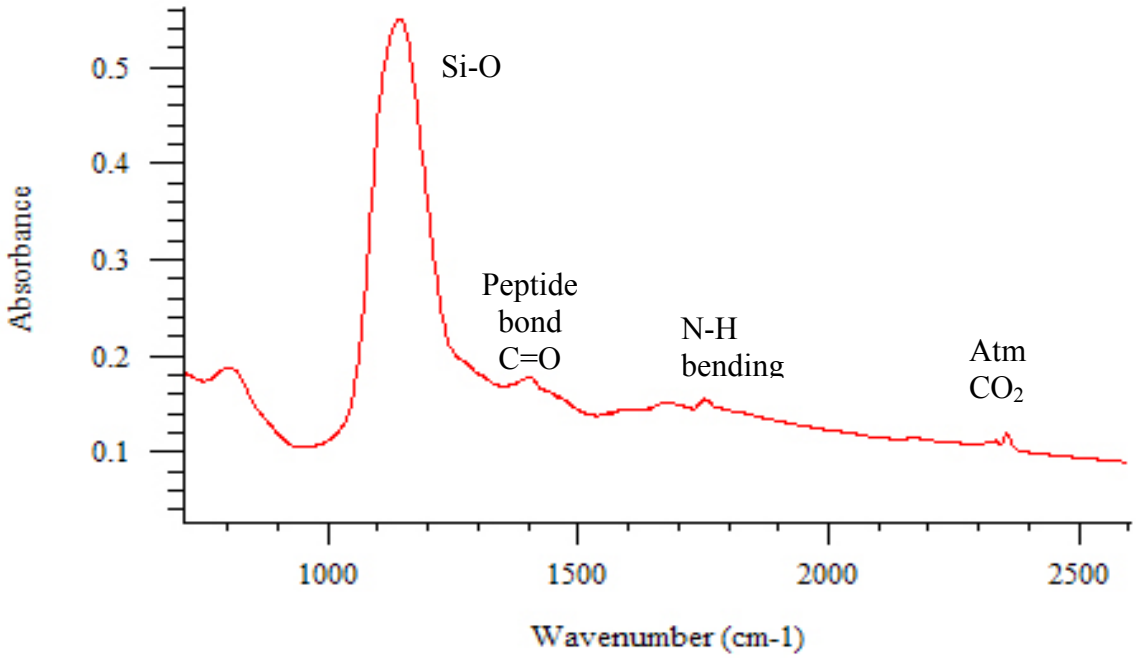

Figure E-1: Absorbance spectrum of antibody functionalized Pt surface after removal of un-functionalized Pt surface baseline

Vita

John-Paul McGovern was born on February 1, 1981 in Woodbury, NJ, USA. He attended St. Margaret's Elementary School, and graduated from West Deptford High School in West Deptford, NJ in 1999 as a member of the National Honor Society, a National Merit Scholar and New Jersey Blaustein Scholarship recipient. He attended Princeton University in Princeton, NJ and received a Bachelor of Science in Engineering degree in Mechanical Engineering as well as a Certificate in Materials Science in 2003. His undergraduate thesis title was "The effects of microgroove contact guidance on the adhesion of human osteoblasts on Ti-6Al-4V," and was advised by Dr. Wole Soboyejo. He was a recipient of the Donald Jansen Dike Award for excellence in undergraduate research. He interned at the Rothman Institute, Jefferson Hospital, Philadelphia, PA during the summer of 2002.

He began his doctoral research in the Ceramics Sensor and Processing Laboratory in the Department of Materials Science in the College of Engineering at Drexel University, Philadelphia, PA in 2003. He was a teaching assistant for the undergraduate course 'Advanced Ceramics Processing,' in the Department of Materials Science and Engineering during 2006. His publications to date are listed below:

- J.P. McGovern, W.Y. Shih, R. Rest, M. Purohit, Y. Pandya and W.H. Shih. Label-free flow-enhanced specific detection of Bacillus anthracis using a piezoelectric microcantilever sensor. Analyst, 2008, 133, 649-54.
- J.P. McGovern, W.Y. Shih, W.H. Shih. In-situ Detection of Bacillus Anthracis Spores Using Fully Submersible, Self-Exciting, Self-Sensing PMN-PT/Sn Piezoelectric Microcantilevers. Analyst, 2007, 132, 777–783.
- J. Chen, S. Mwenifumbo, C. Langhammer, J.-P. McGovern, M. Li, A. Beye, W. O. Soboyejo. Cell/Surface Interactions and Adhesion on Ti-6Al-4V: Effects of Surface Texture. Journal of Biomedical Materials Research Part B: Applied Biomaterials. 2007, 82B, 2, 360-373.
- J.P. McGovern, W.Y. Shih, W.H. Shih, M. Sergi and I. Chaiken. Real-Time Salmonella Detection Using Lead Zirconate Titanate-Titanium Microcantilevers. AA3.8.1, Mater. Res. Soc. Symp. Proc. Vol. 845